On the Numerical Stability of Co-Simulation Methods

Institut für Angewandte Dynamik
Fachbereich Maschinenbau
Technische Universität Darmstadt

Zur
Erlangung des Grades eines Doktor-Ingenieurs (Dr. -Ing.)
genehmigte

Dissertation

Vorgelegt von

Pu Li, M.Eng.

aus Shaanxi, China

Berichterstatter:	Prof. Dr.-Ing. Bernhard Schweizer
Mitberichterstatter:	Prof. Dr.-Ing. Alfons Ams
Tag der Einreichung:	02.05.2017
Tag der mündlichen Prüfung:	05.07.2017

Darmstadt 2017

D17

Erklärung

Hiermit erkläre ich, dass ich die vorliegende Arbeit, abgesehen von den in ihr ausdrücklich genannten Hilfen, selbständig verfasst habe.

Darmstadt, den 12.07.2017

Pu Li

Acknowledgements

First and foremost, I would like to express my sincere gratitude to my supervisor Professor Schweizer for the trust and guidance in the past four years. Thank you very much for the continuous support and encouragement throughout the whole time.

I am very grateful to Professor Ams for the takeover as my co-referent. Thank you so much for reviewing my thesis and valuable discussions.

My sincere thanks go to all the colleagues at Institute of Applied Dynamics at Technical University of Darmstadt for the company during my doctor study. Especially I want to express my gratitude to Daixing for kindly help at the beginning of my research. Thanks to Ioannis for interesting discussions and advices.

Last but not least, I want to take the opportunity to thank my parents for their continuous love. Particular gratitude to my wife Xiayin for intensive support and taking care of our daughter Zhiyi.

Darmstadt, den 12.07.2017

Pu Li

Contents

Abstract

To couple two or more subsystem solvers in time domain, co-simulation methods are used in many fields of application. In the framework of mechanical systems, there exist mainly two ways to couple different subsystems, namely coupling either by constitutive laws or by algebraic constraint equations.

In this work, the numerical stability and the convergence behavior of co-simulation methods is analyzed. For the stability analysis, a test model has to be defined. Following the stability definition for numerical time integration schemes, namely Dahlquist's stability theory, a linear test model is used. The co-simulation test model applied here is a two-mass oscillator, where the two masses are connected by a spring-damper element or by a rigid link. Discretizing the test model with a co-simulation method, recurrence equations can be derived, which describe the time discrete co-simulation solution.

Applying an applied-force coupling approach, the stability behavior of the linear two-mass oscillator is characterized by 7 independent parameters. In order to compare different co-simulation approaches, 2D stability plots are convenient. Therefore, 5 of the 7 parameters are fixed so that the spectral radius can be depicted as a function of the remaining 2 parameters. The results presented show that implicit coupling schemes exhibit a significantly better numerical stability behavior than explicit schemes. Furthermore, enhanced stability behavior can be achieved by extending the coupling conditions, i.e., by taking into account derivatives and integrals of the constitutive equations. Especially, a very good stability behavior may be obtained with the D-extended force/force-coupling approach in combination with quadratic approximation functions.

The analysis of the numerical stability of co-simulation methods with algebraic constraints is the second subject of this work. 5 independent parameters have to be introduced for the corresponding test model. The dimensionless real and imaginary part of the eigenvalue of subsystem 1 are used as axes in 2D stability plots; the other 3 parameters are held constant. Three classical methods for constraint stabilization, namely the Baumgarte stabilization technique, the weighted multiplier approach and the projection technique, are discussed for different approximation orders. Alternatively, co-simulation approaches on index-2 and on index-1 level are discussed, where the Lagrange multiplier is discretized between the macro-time points (extended multiplier approach). As a result, the coupling conditions and their time derivatives can simultaneously be fulfilled at the macro-time points. Different multibody models are used in order to demonstrate the application of the above mentioned co-simulation techniques.

Kurzfassung

Co-Simulation wird in vielen Bereichen verwendet, um zwei oder mehrere Subsystem-Solver im Zeitbereich zu koppeln. Bei mechanischen Systemen gibt es im Wesentlichen zwei Kopplungsarten, nämlich Kopplungsverfahren auf der Basis von Konstitutivgleichungen und Kopplungsansätze basierend auf algebraischen Bedingungsgleichungen.

In dieser Dissertation werden die numerische Stabilität und das Konvergenzverhalten von verschiedenen Co-Simulationsverfahren analysiert. Für die Stabilitätsanalyse muss ein Testmodell definiert werden. In Anlehnung an die Stabilitätsdefinition für numerische Zeitintegrationsschemata (Dahlquistsche Stabilitätstheorie) werden lineare Co-Simulationstestmodelle definiert. Als Co-Simulationstestmodelle werden hier Zweimassenschwinger eingesetzt, wobei die Massen über ein Feder-Dämpfer-Element oder über ein starres Gelenk verbunden sind. Durch Diskretisierung des Testmodells mit einem Co-Simulationsverfahren können Rekurrenzen-Gleichungen abgeleitet werden, die die zeitdiskrete Co-Simulationslösung beschreiben.

Das Stabilitätsverhalten des linearen Zweimassenschwingers ist bei Anwendung von Kopplungsverfahren auf Basis eingeprägter Kopplungskräfte/-momente durch 7 unabhängige Parameter charakterisiert. Um verschiedene Co-Simulationsansätze zu vergleichen, sind 2D-Stabilitätsplots praktikabel. Daher werden 5 der 7 Parameter fixiert, so dass der Spektralradius als Funktion der verbleibenden 2 Parameter dargestellt werden kann. Die Ergebnisse zeigen erwartungsgemäß, dass implizite Kopplungsschemata eine wesentlich bessere numerische Stabilität als explizite Methoden aufweisen. Darüber hinaus kann ein verbessertes Stabilitätsverhalten durch Erweiterungen der Kopplungsbedingungen erreicht werden, d.h. durch Berücksichtigung von Ableitungen und Integralen der konstitutiven Gleichungen. Ein sehr gutes Stabilitätsverhalten ist mit dem D-erweiterten Kraft/Kraft-Kopplungsansatz in Verbindung mit quadratischen Approximationsfunktionen erreichbar.

Die Analyse der numerischen Stabilität von Co-Simulationsverfahren mit algebraischen Bedingungen ist das zweite zentrale Thema dieser Arbeit. Hier müssen 5 unabhängige Parameter für das lineare Testmodell definiert werden. Der dimensionslose Real- und Imaginärteil des Eigenwerts von Subsystem 1 werden als Achsen in 2D-Stabilitätsplots verwendet; die anderen 3 Parameter werden konstant gehalten. Drei klassische Stabilisierungsmethoden, nämlich Baumgarte-Stabilisierung, Methode der gewichteten Multiplikatoren und Koordinatenprojektion, werden für unterschiedliche Approximationsordnungen diskutiert. Alternativ kann der Lagrange-Multiplikator zwischen den Makrozeitpunkten diskretisiert werden (erweiterter Multiplikatorenansatz), um Co-Simulationsansätze auf Index-2 und auf Index-1-Ebene zu erhalten. Dadurch können gleichzeitig die Kopplungsbedingungen und deren Zeitableitungen an den Makrozeitpunkten erfüllt werden. Es werden mehrere Mehrkörpermodelle verwendet, um die praktische Anwendung der erwähnten Co-Simulationsverfahren aufzuzeigen.

1. Introduction

Computer-Aided Engineering (CAE) has seen an increasing usage in the last decades. It can be used to analyze complicated systems accurately and time-efficiently. Practical information for the industrial product design can be obtained in an early development stage in order to shorten the circle time of production development. Nowadays, it is indispensable to describe complex technical systems by numerical models. The models are usually very complex and consist of different components, which are represented by different submodels that are connected by appropriate coupling conditions. As a consequence, co-simulation of distributed systems is one main trend of CAE development [64].

To couple different subsystem solvers of multidisciplinary systems or in order to parallelize dynamic models, co-simulation (also called simulator coupling) is becoming an increasingly important tool in different fields of application, for instance in the area of mechatronic systems, where interfaces between mechanical and electronical subsystems have to be defined [36, 37]. MBS-FEM coupling plays an important role in the analysis of flexible multibody systems [20, 63]. Until now, co-simulation has been successfully used in vehicle systems [28, 61], railway systems [1-3], in connection with fluid-structure interaction (FSI) problems [22, 29, 57], etc..

1.1. Literature Review

1.1.1. Fields of Application

Starting from the visionary contribution of parallel simulation by Nievergelt [62], co-simulation has experienced great interest over the last decades [39]. Multirate-step approaches for different components in ODE systems were firstly introduced in the pioneer work of Gear and Wells [42]. In multibody systems, a gluing algorithm was presented in [82, 85] that can be used to couple distributed submodels by introducing gluing matrices to keep the compatibility conditions at the interfaces. Based on this algorithm, FEM/MBS coupling problems have been analyzed [64, 76]. However, some researchers pointed out that the method may cause some artificial chattering and oscillations [81]. Divide and conquer algorithms (DCA), based on recursive assembly and disassembly phases, may also be applied to parallelize dynamical models, see for instance [23, 33, 34, 53]. Automatic generation of the equations of motion in the assembly part may, however, be problematic for system with loops [50, 53]. A modular co-simulation approach for constraint coupling problems was proposed in [48, 49]. It was pointed out that stable results are in general only obtained, if an iterative scheme is applied. Following the idea of modular simulation, a master-slave concept was utilized in [37] for the parallelization of multidisciplinary problems.

A detailed explanation of different decomposition methods for FSI systems is given in [31, 35], where also numerical errors and stability behavior are analyzed. A weak coupling strategy based on staggered time schemes is presented in [57]. An interface-Jacobian-based co-simulation algorithm (IJCSA) was introduced in [77, 86] and used

in connection with wind turbine simulations.

A numerical technique called “subcycling”, firstly presented in the work of Belytschko [12], is basically an explicit co-simulation approach in the field of parallel finite element simulation [25-27]. More recently, the Finite-Element Tearing and Interconnecting (FETI) method has been the focus of research in connection with parallel finite element analyses [32, 43, 44]. Different algorithms have been proposed to decompose systems and impose continuity at the interfaces. A detailed review of subcycling methods and applications for flexible multibody systems can be found in [58, 59]. It should be mentioned that waveform relaxation is another iterative co-simulation method that is commonly utilized in integrated circuit simulation [51] or in connection with field/circuit analysis [68].

1.1.2. Classification of Co-Simulation Methods

To solve coupled multidisciplinary systems or in order to parallelize monolithic dynamical systems, there basically exist two techniques, namely strong coupling and weak coupling [66, 83]. In the framework of strong coupling, the subsystems are solved with only one single solver. Strong coupling is, for instance, carried out, if software tools like Modelica [60] are applied to simulate multidisciplinary systems. In contrast to strong coupling methods, co-simulation represents a typical weak coupling technique. That means, each subsystem is solved by its specific numerical integrator and coupling variables are exchanged at some user-defined macro-time points only. With co-simulation methods, several simulators can be coupled without specific information on the subsystems and their solvers. In the following, only weak coupling (co-simulation) will be discussed.

With respect to the coupling algorithm, one can distinguish between explicit, semi-implicit and full-implicit methods. Applying a co-simulation, we have to define coupling variables (input variables) for the subsystem integration from the macro-time point T_N to T_{N+1}. When the integration from T_N to T_{N+1} is only performed once, i.e. if an explicit approach is applied, it is possible to use controllers – e.g. an PI controller – to compensate the error introduced by the co-simulation [13, 14, 16, 17, 80]. If the numerical integration between the macro-steps is repeated, we are faced with implicit coupling methods. In [73, 74], a semi-implicit coupling technique is presented based on a predictor-corrector approach, where the macro-time integration has to be repeated only once. For example, we consider two subsystems, which are integrated from T_N to T_{N+1}, where i terms the number of iterations carried out in each macro-step, see Figure 1.1. $i = 0$, $i = 1$ and $i > 1$ represent explicit, semi-implicit and implicit approaches, respectively. In the framework of an explicit co-simulation algorithm, the macro-step is not repeated, which reduces the computational effort significantly. However, due to the error introduced by the extrapolated coupling variables, the numerical stability of the co-simulation may become a problem. Implicit and semi-implicit algorithms exhibit a better numerical stability behavior; implementation of such methods is, however, more involved.

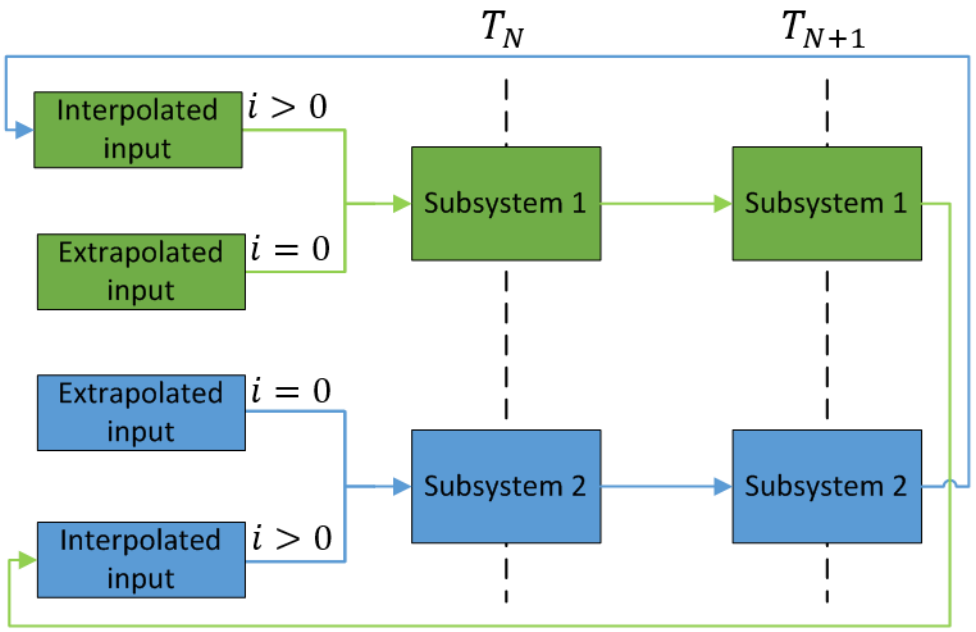

Figure 1.1 Explicit ($i = 0$), semi-Implicit ($i = 1$) and implicit ($i > 1$) coupling schemes

Considering mechanical subsystems, we have to distinguish between solver coupling approaches based on algebraic constraints (i.e. coupling by reaction forces/torques) [6, 45, 48, 49, 72, 74] and solver coupling methods on the basis of constitutive laws (i.e. based on applied force/torques) [2, 3, 21, 37, 47, 67, 73]. To illustrate the two approaches, we regard the two mass oscillator, where the two masses are coupled by a spring-damper element or by a rigid link, see Figure 1.2.

Applying an applied-force coupling approach, both subsystems are coupled by constitutive laws, for instance by the coupling force $F_c = c_c \cdot (x_2 - x_1) + d_c \cdot (v_2 - v_1)$ representing a linear spring-damper element. The decomposed system has two degrees of freedom. In the framework of a constraint coupling approach, the subsystems are coupled by algebraic constraint equations, for instance by a rigid link to be described by the implicit coupling condition $g(x_1, x_2) = x_2 - x_1 = 0$. Introduction algebraic constraints entails reaction forces/torques (Lagrange multipliers) and a reduction of the degree of freedom of the overall system.

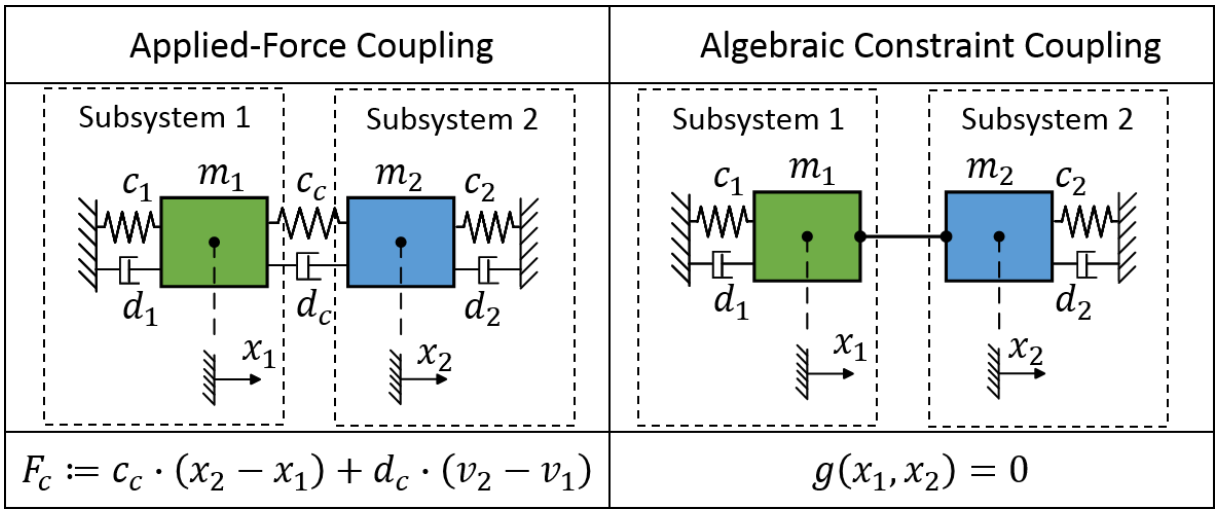

Figure 1.2 Two fundamental coupling approaches: applied-force coupling and algebraic constraint coupling

Concerning the decomposition technique of the global system into subsystems, basically three decomposition approaches may be distinguished, namely the force/force, the force/displacement, and the displacement/displacement decomposition approach [21, 37, 67, 70, 71]. In the framework of a force/force coupling technique, both subsystems are force-driven oscillators, where the coupling force is calculated either by the constitutive laws or by the constraint equations. Applying a force/displacement coupling technique, subsystem 1 will be a force-driven oscillator and subsystem 2 a base-point excited oscillator. Making use of a displacement/displacement decomposition technique, both subsystems are base-point excited oscillators. The three decomposition techniques will be discussed in detail in the following sections for both cases, applied-force coupling and algebraic constraint coupling.

Furthermore, we have to distinguish between parallel and sequential co-simulation approaches [4, 6]. If the subsystems are integrated in parallel (Jacobi type), both subsystems exchange coupling data simultaneously. If the integration of the subsystems is carried out sequentially (Gauss-Seidel type), information is exchanged between the subsystems at different macro-time points [6, 65].

The different co-simulation methods are summarized in Figure 1.3. In the following sections, the numerical stability and convergence behavior of these approaches will be discussed in detail.

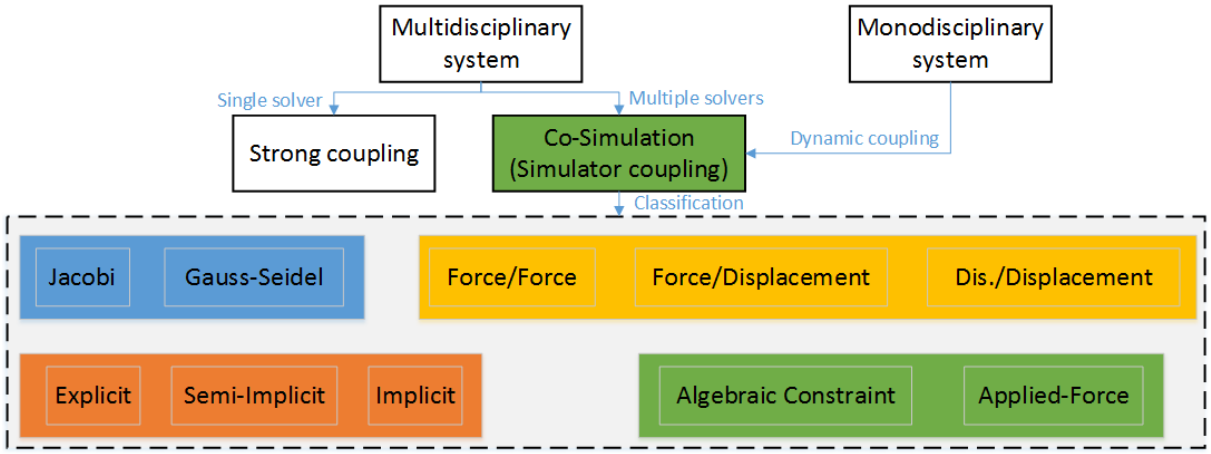

Figure 1.3 Classification of co-simulation approaches

1.2. Numerical Stability of Co-Simulation

Within a co-simulation approach, the subsystems are integrated by specific solvers. Data exchange is accomplished at certain user-defined macro-time points only. Therefore, it is possible to apply different and optimized subsystem integrators, so that the computational efficiency of the overall simulation may be significantly increased. Due to the approximation of the coupling variables by polynomials and as a result of the data exchange between the subsystems, numerical errors are produced, which may entail severe stability problems. Especially in connection with explicit co-simulation approaches, numerical instabilities will be introduced by the coupling scheme, in spite of the fact that the subsystems are integrated with stable subsystem solvers. Hence, the development of stabilized coupling techniques is of special interest.

In order to define and investigate the numerical stability of co-simulation methods, it is useful to adopt and extend the theory developed for time integration schemes. The stability of time integration schemes is defined by Dahlquist's test equation

$$\dot{y} = \Lambda \cdot y(t), \tag{1.1}$$

where $y(t)$ is a scalar function of time and $\Lambda \in \mathbb{C}$ an arbitrary complex constant. Note that $\dot{y} = dy/dt$ terms the derivative of y with respect to time t. Dahlquist's test equation may – from the mechanical point of view – be interpreted as the complex representation of the equations of motion for the linear single-mass oscillator, see Figure 1.4.

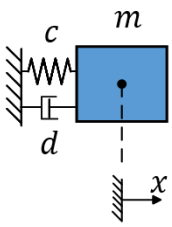

Figure 1.4 Linear single-mass oscillator

This can be easily seen by considering the linear homogenous mass-spring-damper oscillator, which is mathematically described by

$$\begin{pmatrix} \dot{x} \\ \dot{v} \end{pmatrix} = \begin{pmatrix} 0 & 1 \\ -\frac{c}{m} & -\frac{d}{m} \end{pmatrix} \begin{pmatrix} x \\ v \end{pmatrix} , \tag{1.2}$$

where x and v denote the position and the velocity of the mass m. c and d term the spring constant and the damping coefficient.

The eigenvalues of Eq. (1.2) are given by

$$\Lambda_{1,2} = \Lambda_r \pm i \cdot \Lambda_i = -\frac{d}{2m} \pm i \cdot \frac{\sqrt{4mc - d^2}}{2m} . \tag{1.3}$$

With these eigenvalues, Eq. (1.2) can easily be transformed into the two decoupled equations

$$\begin{gathered} \begin{pmatrix} \dot{y}_1 \\ \dot{y}_2 \end{pmatrix} = \begin{pmatrix} \Lambda_1 & 0 \\ 0 & \Lambda_2 \end{pmatrix} \begin{pmatrix} y_1 \\ y_2 \end{pmatrix} \\ \text{with } \begin{pmatrix} y_1 \\ y_2 \end{pmatrix} = \boldsymbol{Q}^{-1} \begin{pmatrix} x \\ v \end{pmatrix}, \ \boldsymbol{Q} = \begin{pmatrix} 1 & 1 \\ \Lambda_1 & \Lambda_2 \end{pmatrix}. \end{gathered} \tag{1.4}$$

Discretizing the Dahlquist equation (1.1) with a linear single-step (e.g., Runge-Kutta method) or a linear multistep method (e.g., Adams-Bashforth method) and assuming a constant step size yields a recurrence equation for the discretized values $y_n (n = 0, 1, 2, \dots)$, which approximate the analytical solution $y(t_n)$ at the time points t_n. Provided that $m, c, d > 0$ (i.e., assuming that the system is stable from the mechanical point of view), a numerical time integration method is called numerically stable, if the discretized Dahlquist equation yields a sequence of exponentially decaying values y_n. This will be the case if the spectral radius of the recurrence equation is smaller than 1.

1.3. Organization of this Dissertation

The main objective of this dissertation is to introduce a linear stability analysis (according to the Dahlquist theory for time integration schemes) for different coupling approaches and to investigate the influence of the subsystem and coupling parameters on the stability behavior of the co-simulation. Of special interest are implicit co-simulation methods, since they usually show a better stability behavior than explicit algorithms. Moreover, the convergence behavior of the coupling approaches will be analyzed. Also, different multibody models are used in order to demonstrate the applicability and accuracy of the presented methods. The structure of the thesis is depicted in Figure 1.5.

In Chapter 2, a two-mass oscillator model is introduced to build up the framework for the stability analysis. Furthermore, the equations of motion for the test models that are used in connection with the applied-force and the constraint coupling methods will be derived. In addition, the governing system of recurrence equations will be formulated.

Chapter 3 contains a detailed stability analysis with respect to the applied-force coupling methods. We consider explicit and semi-implicit algorithms and discuss the force/force-, the force/displacement- and the displacement/displacement decomposition approaches. Taking into account derivatives and integrals of the coupling equations (constitutive equations), the stability of the co-simulation approach may be significantly improved.

In Chapter 4, the stability analysis is presented for different constraint coupling approaches: a co-simulation approach based on Baumgarte stabilization, a method on the basis of a weighted multiplier approach and a coupling technique on the basis of a projection approach. In this chapter, only semi-implicit coupling methods are discussed. Also, an improved coupling approach is presented, where the Lagrange multipliers are discretized between the macro-step so that the constraint equations and also the hidden constraints can be enforced simultaneously at the macro-time points. Again, different multibody models are used to demonstrate the practical usage of the presented coupling methods.

The thesis is summarized in Chapter 5.

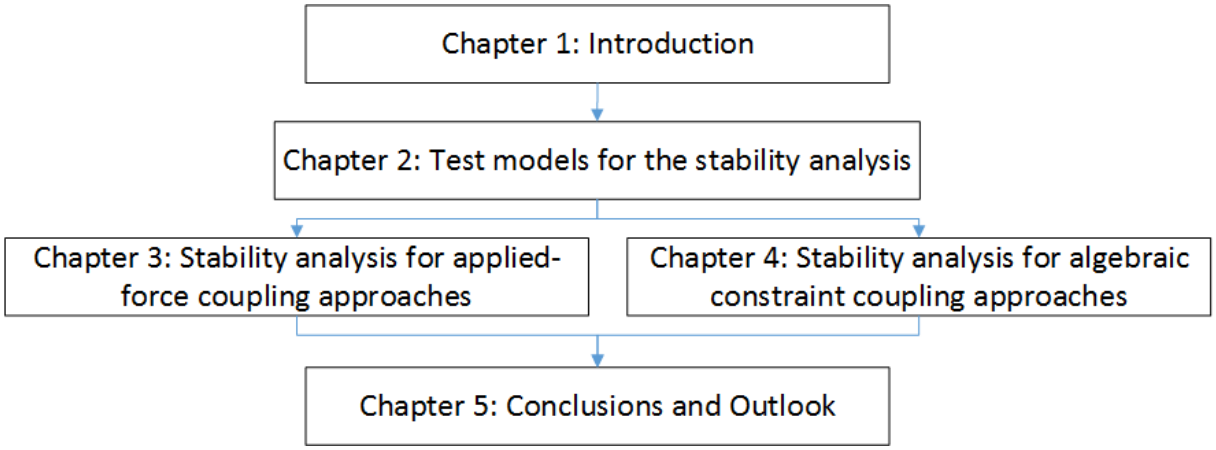

Figure 1.5 Organization of the thesis

2. Test Models for Stability Analysis

To examine the numerical stability of co-simulation methods, appropriate test models for applied force coupling and algebraic constraint coupling co-simulation methods are introduced. Based on the discretized equations of motion of these test models, the corresponding recurrence equations will be derived for the stability analysis. All three decomposition approaches are considered, i.e. force/force-, force/displacement- and displacement/displacement-decomposition.

2.1. Test Models for Applied Force Coupling Approach

We consider again the two-mass oscillator shown in Figure 1.2. The two-mass oscillator can be interpreted as two single-mass oscillators (masses m_1 / m_2, spring constants c_1 / c_2, damping coefficients d_1 / d_2), which are coupled by the coupling spring c_c and the coupling damper d_c. Hence, the two-mass oscillator can be regarded as two Dahlquist equations, which are coupled by a linear spring/damper system.

The equations of motion for the coupled oscillator read as

$$\begin{aligned}
\dot{x}_1 &= v_1 \\
\dot{v}_1 &= -\frac{c_1}{m_1} x_1 - \frac{d_1}{m_1} v_1 + \frac{c_c}{m_1} \cdot (x_2 - x_1) + \frac{d_c}{m_1} \cdot (v_2 - v_1) \\
\dot{x}_2 &= v_2 \\
\dot{v}_2 &= -\frac{c_2}{m_2} x_2 - \frac{d_2}{m_2} v_2 - \frac{c_c}{m_2} \cdot (x_2 - x_1) - \frac{d_c}{m_2} \cdot (v_2 - v_1),
\end{aligned} \tag{2.1}$$

where x_1/x_2 and v_1/v_2 describe position and velocity of the two masses.

For the stability analysis of co-simulation methods, it is useful to introduce dimensionless variables. We assume that $\bar{x}_1, \bar{x}_2$ are properly chosen dimensionless position coordinates. The variables $\bar{v}_1 = H \cdot d\bar{x}_1/dt$ and $\bar{v}_2 = H \cdot d\bar{x}_2/dt$ denote dimensionless velocities, where H denotes the macro-step size of the co-simulation approach. The dimensionless time is defined by $\bar{t} = t/H$. Furthermore, it is suitable to define the following 7 parameters:

$$\begin{gathered}
\bar{c}_1 = \frac{c_1 \cdot H^2}{m_1}, \quad \bar{d}_1 = \frac{d_1 \cdot H}{m_1}, \quad \alpha_{m21} = \frac{m_2}{m_1}, \quad \alpha_{c21} = \frac{c_2}{c_1}, \quad \alpha_{d21} = \frac{d_2}{d_1}, \\
\alpha_{cc1} = \frac{c_c}{c_1}, \quad \alpha_{dc1} = \frac{d_c}{d_1}.
\end{gathered} \tag{2.2}$$

With these parameters, Eq. (2.1) can be rewritten as

$$
\begin{aligned}
\bar{x}_1' &= \bar{v}_1 \\
\bar{v}_1' &= -\bar{c}_1 \cdot \bar{x}_1 - \bar{d}_1 \cdot \bar{v}_1 + \alpha_{cc1} \cdot \bar{c}_1 \cdot (\bar{x}_2 - \bar{x}_1) + \alpha_{dc1} \cdot \bar{d}_1 \cdot (\bar{v}_2 - \bar{v}_1) \\
\bar{x}_2' &= \bar{v}_2 \\
\bar{v}_2' &= -\frac{\alpha_{c21}}{\alpha_{m21}} \cdot \bar{c}_1 \cdot \bar{x}_2 - \frac{\alpha_{d21}}{\alpha_{m21}} \cdot \bar{d}_1 \cdot \bar{v}_2 - \frac{\alpha_{cc1}}{\alpha_{m21}} \cdot \bar{c}_1 \cdot (\bar{x}_2 - \bar{x}_1) - \frac{\alpha_{dc1}}{\alpha_{m21}} \cdot \bar{d}_1 \\
&\quad \cdot (\bar{v}_2 - \bar{v}_1) \ .
\end{aligned}
\tag{2.3}
$$

Alternatively written in compact form, we have

$$
\boldsymbol{z}' = \boldsymbol{A} \cdot \boldsymbol{z}
$$

$$
\text{with } \boldsymbol{z} = (\bar{x}_1 \quad \bar{v}_1 \quad \bar{x}_2 \quad \bar{v}_2)^T \in \mathbb{R}^4 \text{ and}
$$

$$
\boldsymbol{A} = \begin{pmatrix}
0 & 1 & 0 & 0 \\
-(1+\alpha_{cc1}) \cdot \bar{c}_1 & -(1+\alpha_{dc1}) \cdot \bar{d}_1 & \alpha_{cc1} \cdot \bar{c}_1 & \alpha_{dc1} \cdot \bar{d}_1 \\
0 & 0 & 0 & 1 \\
\frac{\alpha_{cc1}}{\alpha_{m21}} \cdot \bar{c}_1 & \frac{\alpha_{dc1}}{\alpha_{m21}} \cdot \bar{d}_1 & -\frac{\alpha_{c21}+\alpha_{cc1}}{\alpha_{m21}} \cdot \bar{c}_1 & -\frac{\alpha_{d21}+\alpha_{dc1}}{\alpha_{m21}} \cdot \bar{d}_1
\end{pmatrix}. \tag{2.4}
$$

Obviously, the two-mass oscillator is a mechanically stable system, if $m_1, m_2, c_1, c_2, d_1, d_2 > 0$.

Regarding the two-mass oscillator as two coupled single-mass oscillators, the equations of motion can alternatively be written in a modular manner, i.e.

$$
\begin{aligned}
\boldsymbol{z}' &= \boldsymbol{A} \cdot \boldsymbol{z} + \boldsymbol{B} \cdot \boldsymbol{u} \\
\boldsymbol{g} &= \boldsymbol{C} \cdot \boldsymbol{z} + \boldsymbol{D} \cdot \boldsymbol{u} = \boldsymbol{0} \ .
\end{aligned}
\tag{2.5}
$$

The vector $\boldsymbol{z} = (\bar{x}_1 \quad \bar{v}_1 \quad \bar{x}_2 \quad \bar{v}_2)^T \in \mathbb{R}^4$ collects the dimensionless state variables, while the vector $\boldsymbol{u} = (\tilde{\bar{x}}_1 \quad \tilde{\bar{v}}_1 \quad \tilde{\bar{x}}_2 \quad \tilde{\bar{v}}_2 \quad \bar{\lambda}_c)^T \in \mathbb{R}^5$ contains the coupling variables required for the three decomposed test models. $\bar{\lambda}_c = \lambda_c \cdot H^2/m_1$ terms the dimensionless coupling force, which is a function of the state variables of the subsystems. $\boldsymbol{A}, \boldsymbol{B}, \boldsymbol{C}$ and $\boldsymbol{D}$ are corresponding coefficient matrices or vectors.

Applying the applied force coupling approach, we can distinguish three decomposed models, namely force/force-, force/displacement-, displacement/displacement test models that will be discussed in the following sections.

In the framework of a force/force coupling approach, the basic idea is to divide the two-mass oscillator into two single-mass oscillators, i.e. into two subsystems that are driven by the coupling force λ_c, see Figure 2.1.

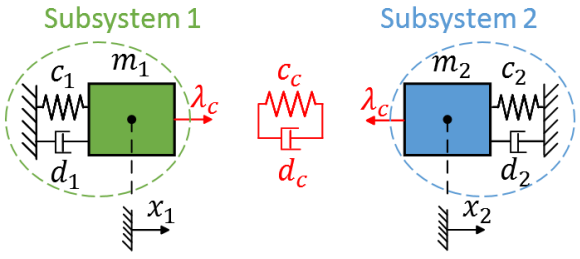

Figure 2.1 Co-simulation test model for force/force coupling approach

For the test models, the coupling force is calculated by the implicit coupling condition $g_c := \lambda_c - c_c \cdot (x_2 - x_1) - d_c \cdot (v_2 - v_1) = 0$ with the help of state variables of both subsystems. Based on the general Eq. (2.5), it is straightforward to derive the coefficient matrices for the force/force coupling approach:

$$\boldsymbol{A}_{FF} = \begin{pmatrix} 0 & 1 & 0 & 0 \\ -\bar{c}_1 & -\bar{d}_1 & 0 & 0 \\ 0 & 0 & 0 & 1 \\ 0 & 0 & -\dfrac{\alpha_{c21}}{\alpha_{m21}} \cdot \bar{c}_1 & -\dfrac{\alpha_{d21}}{\alpha_{m21}} \cdot \bar{d}_1 \end{pmatrix},$$

$$\boldsymbol{B}_{FF} = \begin{pmatrix} 0 & 0 & 0 & 0 & 0 \\ 0 & 0 & 0 & 0 & 1 \\ 0 & 0 & 0 & 0 & 0 \\ 0 & 0 & 0 & 0 & -\dfrac{1}{\alpha_{m21}} \end{pmatrix}, \tag{2.6}$$

$$\boldsymbol{C}_{FF} = (\alpha_{cc1} \cdot \bar{c}_1 \quad \alpha_{dc1} \cdot \bar{d}_1 \quad -\alpha_{cc1} \cdot \bar{c}_1 \quad -\alpha_{dc1} \cdot \bar{d}_1), \quad \boldsymbol{D}_{FF} = (0 \quad 0 \quad 0 \quad 0 \quad 1).$$

For the case that the co-simulation test model is decomposed by a force/displacement-coupling approach, subsystem 1 will be a force-driven and subsystem 2 a base-point excited single-mass oscillator as illustrated in Figure 2.2.

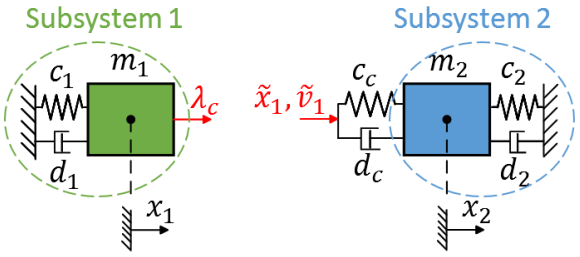

Figure 2.2 Co-simulation test model for force/displacement coupling approach

Applying a force/displacement decomposition, the coupling force λ_c is replaced in subsystem 2 with the help of the coupling condition $g_c := \lambda_c - c_c \cdot (x_2 - x_1) - d_c \cdot (v_2 - v_1) = 0$. Due to the fact that the state variables x_1 and v_1 are unknown in subsystem 2, they are replaced by two additional coupling variables, which are denoted by $\tilde{x}_1$ and $\tilde{v}_1$. The introduction of two additional coupling variables entails the definition of two additional coupling conditions, namely, $g_{cx1} := \tilde{x}_1 - x_1 = 0$ and $g_{cv1} := \tilde{v}_1 - v_1 = 0$. Then, the decomposed system is described by the following dimensionless coefficient matrices:

$$\boldsymbol{A}_{FD} = \begin{pmatrix} 0 & 1 & 0 & 0 \\ -\bar{c}_1 & -\bar{d}_1 & 0 & 0 \\ 0 & 0 & 0 & 1 \\ 0 & 0 & -\dfrac{\alpha_{c21}+\alpha_{cc1}}{\alpha_{m21}}\cdot\bar{c}_1 & -\dfrac{\alpha_{d21}+\alpha_{dc1}}{\alpha_{m21}}\cdot\bar{d}_1 \end{pmatrix},$$

$$\boldsymbol{B}_{FD} = \begin{pmatrix} 0 & 0 & 0 & 0 & 0 \\ 0 & 0 & 0 & 0 & 1 \\ 0 & 0 & 0 & 0 & 0 \\ \dfrac{\alpha_{cc1}}{\alpha_{m21}}\cdot\bar{c}_1 & \dfrac{\alpha_{dc1}}{\alpha_{m21}}\cdot\bar{d}_1 & 0 & 0 & 0 \end{pmatrix}, \tag{2.7}$$

$$\boldsymbol{C}_{FD} = \begin{pmatrix} \alpha_{cc1}\cdot\bar{c}_1 & \alpha_{dc1}\cdot\bar{d}_1 & -\alpha_{cc1}\cdot\bar{c}_1 & -\alpha_{dc1}\cdot\bar{d}_1 \\ -1 & 0 & 0 & 0 \\ 0 & -1 & 0 & 0 \end{pmatrix},$$

$$\boldsymbol{D}_{FD} = \begin{pmatrix} 0 & 0 & 0 & 0 & 1 \\ 1 & 0 & 0 & 0 & 0 \\ 0 & 1 & 0 & 0 & 0 \end{pmatrix}.$$

When a displacement/displacement coupling approach is used to decompose the two-mass oscillator, each subsystem is described by a base-point excited single-mass oscillator, see Figure 2.3.

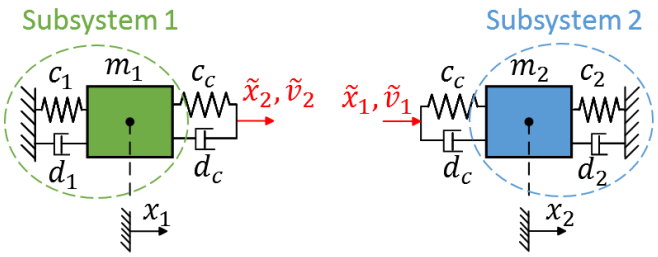

Figure 2.3 Co-simulation test model for displacement/displacement coupling approach

For this purpose, the coupling spring/damper system has to be duplicated, i.e., the coupling variable λ_c is replaced in both subsystems and four additional coupling variables are introduced, namely $\tilde{x}_1, \tilde{x}_2$ and $\tilde{v}_1, \tilde{v}_2$. The corresponding coefficient matrices characterizing the decomposed system read as

$$\boldsymbol{A}_{DD} = \begin{pmatrix} 0 & 1 & 0 & 0 \\ -(1+\alpha_{cc1})\bar{c}_1 & -(1+\alpha_{dc1})\bar{d}_1 & 0 & 0 \\ 0 & 0 & 0 & 1 \\ 0 & 0 & -\dfrac{\alpha_{c21}+\alpha_{cc1}}{\alpha_{m21}}\bar{c}_1 & -\dfrac{\alpha_{d21}+\alpha_{dc1}}{\alpha_{m21}}\bar{d}_1 \end{pmatrix},$$

$$\boldsymbol{B}_{DD} = \begin{pmatrix} 0 & 0 & 0 & 0 & 0 \\ 0 & 0 & \alpha_{cc1}\cdot\bar{c}_1 & \alpha_{dc1}\cdot\bar{d}_1 & 0 \\ 0 & 0 & 0 & 0 & 0 \\ \dfrac{\alpha_{cc1}}{\alpha_{m21}}\cdot\bar{c}_1 & \dfrac{\alpha_{dc1}}{\alpha_{m21}}\cdot\bar{d}_1 & 0 & 0 & 0 \end{pmatrix}, \tag{2.8}$$

$$\boldsymbol{C}_{DD} = \begin{pmatrix} -1 & 0 & 0 & 0 \\ 0 & -1 & 0 & 0 \\ 0 & 0 & -1 & 0 \\ 0 & 0 & 0 & -1 \end{pmatrix}, \quad \boldsymbol{D}_{DD} = \begin{pmatrix} 1 & 0 & 0 & 0 & 0 \\ 0 & 1 & 0 & 0 & 0 \\ 0 & 0 & 1 & 0 & 0 \\ 0 & 0 & 0 & 1 & 0 \end{pmatrix}.$$

2.2. Test Models for Algebraic Constraint Coupling

For defining and investigating the numerical stability of co-simulation methods with algebraic constraints, we use the linear two-mass oscillator depicted in Figure 1.2. The oscillator consists of two single-mass oscillators (masses m_1, m_2, spring constants c_1, c_2, damping coefficients d_1, d_2), which are connected by a rigid link. Hence, the two-mass oscillator may be interpreted as two Dahlquist equations, which are coupled by the algebraic constraint equation $x_2 - x_1 = 0$.

The equations of motion for the coupled oscillator are given by the index-3 DAE system

$$\begin{aligned} \dot{x}_1 &= v_1 \\ \dot{v}_1 &= -\frac{c_1}{m_1} x_1 - \frac{d_1}{m_1} v_1 + \frac{1}{m_1} \cdot \lambda_c \\ \dot{x}_2 &= v_2 \\ \dot{v}_2 &= -\frac{c_2}{m_2} x_2 - \frac{d_2}{m_2} v_2 - \frac{1}{m_2} \cdot \lambda_c \\ 0 &= x_2 - x_1 \,. \end{aligned} \tag{2.9}$$

For the stability analysis, it is convenient to define the 5 subsequent parameters:

$$\bar{c}_1 = \frac{c_1 \cdot H^2}{m_1}, \quad \bar{d}_1 = \frac{d_1 \cdot H}{m_1}, \quad \alpha_{m21} = \frac{m_2}{m_1}, \quad \alpha_{c21} = \frac{c_2}{c_1}, \quad \alpha_{d21} = \frac{d_2}{d_1}. \tag{2.10}$$

Making use of these parameters and using dimensionless state variables, we can rewrite Eq. (2.9) according to

$$\begin{aligned} \bar{x}_1' &= \bar{v}_1 \\ \bar{v}_1' &= -\bar{c}_1 \cdot \bar{x}_1 - \bar{d}_1 \cdot \bar{v}_1 + \bar{\lambda}_c \\ \bar{x}_2' &= \bar{v}_2 \\ \bar{v}_2' &= -\frac{\alpha_{c21}}{\alpha_{m21}} \cdot \bar{c}_1 \cdot \bar{x}_2 - \frac{\alpha_{d21}}{\alpha_{m21}} \cdot \bar{d}_1 \cdot \bar{v}_2 - \frac{\bar{\lambda}_c}{\alpha_{m21}} \\ 0 &= \bar{x}_2 - \bar{x}_1 \,. \end{aligned} \tag{2.11}$$

The above equations of motion can be rewritten in a compact manner, namely

$$\begin{aligned} \boldsymbol{z}' &= \widetilde{\boldsymbol{A}} \cdot \boldsymbol{z} + \widetilde{\boldsymbol{B}}\, \bar{\lambda}_c \\ \boldsymbol{g} &= \widetilde{\boldsymbol{C}} \cdot \boldsymbol{z} = \boldsymbol{0} \,. \end{aligned} \tag{2.12}$$

The vector $\boldsymbol{z} = (\bar{x}_1 \quad \bar{v}_1 \quad \bar{x}_2 \quad \bar{v}_2)^T \in \mathbb{R}^4$ collects the dimensionless state variables, $\bar{\lambda}_c$ terms the dimensionless Lagrange multiplier. The coefficient matrices/vectors $\widetilde{\boldsymbol{A}}, \widetilde{\boldsymbol{B}}, \widetilde{\boldsymbol{C}}$ are given by

$$\widetilde{\boldsymbol{A}} = \begin{pmatrix} 0 & 1 & 0 & 0 \\ -\bar{c}_1 & -\bar{d}_1 & 0 & 0 \\ 0 & 0 & 0 & 1 \\ 0 & 0 & -\dfrac{\alpha_{c21}}{\alpha_{m21}} \cdot \bar{c}_1 & -\dfrac{\alpha_{d21}}{\alpha_{m21}} \cdot \bar{d}_1 \end{pmatrix}, \quad \widetilde{\boldsymbol{B}} = \begin{pmatrix} 0 \\ 1 \\ 0 \\ -\dfrac{1}{\alpha_{m21}} \end{pmatrix}, \tag{2.13}$$

$$\widetilde{\boldsymbol{C}} = (-1 \quad 0 \quad 1 \quad 0).$$

The above system characterizes a force/force decomposition approach. Corresponding test models and equations of motion for the case of force/displacement and displacement/displacement decomposition will be derived in Chapter 4.

3. Stability Analysis of Co-Simulation Approaches with Applied Force Coupling

In this chapter, the numerical stability of different co-simulation methods based on applied force coupling are analyzed. We consider explicit and implicit coupling schemes with different approximation orders and discuss the three decomposition techniques (force/force-, force/displacement- and displacement/displacement decomposition). Discretizing the co-simulation test model with a co-simulation method, recurrence equations can be derived, which describe the time discrete co-simulation solution. The stability of the recurrence equations systems represents the stability behavior of the co-simulation approach and can easily be determined by an eigenvalue analysis. The classical implicit methods only take the coupling equations into account. In addition to these methods, we also present implicit co-simulation methods with improved stability properties. Enhanced stability behavior can be achieved by extending the coupling conditions, i.e., by taking into account derivatives and integrals of the constitutive equations. Finally, the convergence behavior of the different coupling methods is analyzed.

3.1. Original Co-Simulation Methods: Explicit and Implicit Algorithms

Applying a co-simulation approach, the overall system is split into two (or more) subsystems by using a force/force-, a force/displacement- or a displacement/displacement-decomposition technique. To simulate the decoupled system in the framework of a co-simulation approach, coupling variables (subsystem input and output variables) have to be specified and a macro-time grid (macro-time points $T_0, T_1, \dots, T_N$) has to be defined. Within this work, an equidistant macro-time grid is used so that the macro-step size $H = T_{N+1} - T_N$ is constant. Making use of a co-simulation method (weak coupling approach), the two subsystems integrate independently between the macro-time points. The coupling variables are only exchanged between the subsystems at the macro time points. For integrating the subsystems from one to the next macro-time point ($T_N \rightarrow T_{N+1}$), the coupling variables have to be approximated using extrapolation/interpolation techniques. In this work, Lagrange polynomials are used for approximating the coupling variables.

In the following sections, we investigate implicit and explicit coupling approaches for the 3 decomposition techniques. Here, we assume that the subsystems are integrated in parallel (Jacobi type). Serial integration schemes (Gauss-Seidel type) are not discussed, but may be treated in a very similar manner.

3.1.1. Implicit Force/Force Co-Simulation Approach

By applying a force/force-decomposition technique, the co-simulation test model is split into two subsystems in such a way that both subsystems are force-driven single-mass oscillators, see Figure 2.1.

The two masses are driven by the coupling force λ_c. The coupling force is a function of the state variables of the subsystems and can be defined by the implicit coupling condition $g_c := \lambda_c - c_c \cdot (x_2 - x_1) - d_c \cdot (v_2 - v_1) = 0$.

Using the modified (dimensionless) state variables and the parameters from Eq. (2.2), the decomposed system described by Eq. (2.5) can be rewritten by the following system:

Subsystem 1:

$$\begin{aligned} \bar{x}_1' &= \bar{v}_1 \\ \bar{v}_1' &= -\bar{c}_1 \cdot \bar{x}_1 - \bar{d}_1 \cdot \bar{v}_1 + \bar{\lambda}_c \end{aligned} \tag{3.1a}$$

Subsystem 2:

$$\begin{aligned} \bar{x}_2' &= \bar{v}_2 \\ \bar{v}_2' &= -\frac{\alpha_{c21}}{\alpha_{m21}} \cdot \bar{c}_1 \cdot \bar{x}_2 - \frac{\alpha_{d21}}{\alpha_{m21}} \cdot \bar{d}_1 \cdot \bar{v}_2 - \frac{1}{\alpha_{m21}} \bar{\lambda}_c \end{aligned} \tag{3.1b}$$

Coupling condition:

$$\bar{g}_{c\lambda} := \bar{\lambda}_c - \alpha_{cc1} \cdot \bar{c}_1 \cdot (\bar{x}_2 - \bar{x}_1) - \alpha_{dc1} \cdot \bar{d}_1 \cdot (\bar{v}_2 - \bar{v}_1) = 0. \tag{3.1c}$$

Note that $\bar{\lambda}_c = \lambda_c \cdot H^2/m_1$ represents the modified (dimensionless) coupling force. To derive the recurrence equations system for the discretized test-model, we consider the general macro-step from $\bar{T}_N$ to $\bar{T}_{N+1}$, where $\bar{T}_N = T_N/H$ terms the dimensionless macro-time point. For integrating the subsystems from $\bar{T}_N$ to $\bar{T}_{N+1}$, the coupling variable $\bar{\lambda}_c\ (t)$ has to be approximated in the time interval $[\bar{T}_N, \bar{T}_{N+1}]$. Therefore, Lagrange polynomials of degree k are used, which are specified by $k+1$ sampling points. Using for instance the $k+1$ sampling points $(\bar{T}_N, \bar{\lambda}_{c,N}), (\bar{T}_{N-1}, \bar{\lambda}_{c,N-1}), \dots, (\bar{T}_{N-k}, \bar{\lambda}_{c,N-k})$, we get a polynomial of degree k, which we abbreviate by $P_{\bar{\lambda}_c}[(\bar{T}_N, \bar{\lambda}_{c,N}), (\bar{T}_{N-1}, \bar{\lambda}_{c,N-1}), \dots, (\bar{T}_{N-k}, \bar{\lambda}_{c,N-k}); \bar{t}]$.

At the beginning of the macro-time step, the state variables and the coupling variable are assumed to be known

$$\begin{aligned} \bar{x}_1(\bar{t} = \bar{T}_N) &= \bar{x}_{1,N}\,, \qquad \bar{v}_1(\bar{t} = \bar{T}_N) = \bar{v}_{1,N}\,, \\ \bar{x}_2(\bar{t} = \bar{T}_N) &= \bar{x}_{2,N}\,, \qquad \bar{v}_2(\bar{t} = \bar{T}_N) = \bar{v}_{2,N}\,, \end{aligned} \tag{3.2a}$$

$$\bar{\lambda}_c(\bar{t} = \bar{T}_N) = \bar{\lambda}_{c,N}. \tag{3.2b}$$

For higher order approximation ($k > 0$), we further assume that the coupling variable is known at the previous k macro-time step points $\bar{T}_{N-1}, \dots, \bar{T}_{N-k}$.

The implicit co-simulation approaches considered here are predictor/corrector approaches, which can be subdivided into three steps. Below, predicted variables are indicated with an upper index p (e.g. $\bar{x}_{1,N+1}^p$). Variables without upper index are assumed to be corrected variables (e.g. $\bar{x}_{1,N+1}$). For the following analysis, it is useful to define the vector $z_N = \left(\bar{x}_{1,N}, \bar{v}_{1,N}, \bar{x}_{2,N}, \bar{v}_{2,N}\right)^T, z_{N-1} =$

$\left(\bar{x}_{1,N-1}, \bar{v}_{1,N-1}, \bar{x}_{2,N-1}, \bar{v}_{2,N-1}\right)^T, \ldots,\ z_{N-k} = \left(\bar{x}_{1,N-k}, \bar{v}_{1,N-k}, \bar{x}_{2,N-k}, \bar{v}_{2,N-k}\right)^T$ that collect the state variables of both subsystems at the macro-time points $\bar{T}_N, \bar{T}_{N-1}, \ldots, \bar{T}_{N-k}$.

Step 1: Predictor Step

An analytical integration of subsystem 1 and subsystem 2 from $\bar{T}_N$ to $\bar{T}_{N+1}$ with initial conditions (3.2a) and with the predictor (extrapolation) polynomial

$$\bar{\lambda}_c^p(\bar{t}) = P_{\bar{\lambda}_c}^p\left[\left(\bar{T}_N, \bar{\lambda}_{c,N}\right), \left(\bar{T}_{N-1}, \bar{\lambda}_{c,N-1}\right), \ldots, \left(\bar{T}_{N-k}, \bar{\lambda}_{c,N-k}\right); \bar{t}\right] \tag{3.3}$$

yields predicted state variables at the macro-time point $\bar{T}_{N+1}$

$$\begin{aligned}
\bar{x}_{1,N+1}^p &= \bar{x}_{1,N+1}^p\left(\bar{\lambda}_{c,N}, \bar{\lambda}_{c,N-1}, \ldots, \bar{\lambda}_{c,N-k}, \boldsymbol{z}_N\right),\\
\bar{v}_{1,N+1}^p &= \bar{v}_{1,N+1}^p\left(\bar{\lambda}_{c,N}, \bar{\lambda}_{c,N-1}, \ldots, \bar{\lambda}_{c,N-k}, \boldsymbol{z}_N\right),\\
\bar{x}_{2,N+1}^p &= \bar{x}_{2,N+1}^p\left(\bar{\lambda}_{c,N}, \bar{\lambda}_{c,N-1}, \ldots, \bar{\lambda}_{c,N-k}, \boldsymbol{z}_N\right),\\
\bar{v}_{2,N+1}^p &= \bar{v}_{2,N+1}^p\left(\bar{\lambda}_{c,N}, \bar{\lambda}_{c,N-1}, \ldots, \bar{\lambda}_{c,N-k,}\boldsymbol{z}_N\right).
\end{aligned} \tag{3.4}$$

Step 2: Calculation of Corrected Coupling Force

By analytically integrating subsystem 1 and subsystem 2 from $\bar{T}_N$ to $\bar{T}_{N+1}$ with initial conditions (3.2a) and using the interpolation polynomial

$$\bar{\lambda}_c^*(\bar{t}) = P_{\bar{\lambda}_c}^*\left[\left(\bar{T}_{N+1}, \bar{\lambda}_{c,N+1}^*\right), \left(\bar{T}_N, \bar{\lambda}_{c,N}^*\right), \ldots, \left(\bar{T}_{N-k+1}, \bar{\lambda}_{c,N-k+1}^*\right); \bar{t}\right], \tag{3.5}$$

we get the following state variables at the macro-time point $\bar{T}_{N+1}$:

$$\begin{aligned}
\bar{x}_{1,N+1}^* &= \bar{x}_{1,N+1}^*\left(\bar{\lambda}_{c,N+1}^*, \bar{\lambda}_{c,N}, \ldots, \bar{\lambda}_{c,N-k+1}, \boldsymbol{z}_N\right),\\
\bar{v}_{1,N+1}^* &= \bar{v}_{1,N+1}^*\left(\bar{\lambda}_{c,N+1}^*, \bar{\lambda}_{c,N}, \ldots, \bar{\lambda}_{c,N-k+1}, \boldsymbol{z}_N\right),\\
\bar{x}_{2,N+1}^* &= \bar{x}_{2,N+1}^*\left(\bar{\lambda}_{c,N+1}^*, \bar{\lambda}_{c,N}, \ldots, \bar{\lambda}_{c,N-k+1}, \boldsymbol{z}_N\right),\\
\bar{v}_{2,N+1}^* &= \bar{v}_{2,N+1}^*\left(\bar{\lambda}_{c,N+1}^*, \bar{\lambda}_{c,N}, \ldots, \bar{\lambda}_{c,N-k+1}, \boldsymbol{z}_N\right).
\end{aligned} \tag{3.6}$$

Note that $\bar{\lambda}_{c,N+1}^*$ represents an arbitrary coupling force at the macro-time point $\bar{T}_{N+1}$.

Differentiating the state variables of Eq. (3.6) with respect to $\bar{\lambda}_{c,N+1}^*$, we obtain the partial derivatives

$$\begin{aligned}
\frac{\partial \bar{x}_{1,N+1}^*}{\partial \bar{\lambda}_{c,N+1}^*} &= \text{const.}, \qquad & \frac{\partial \bar{v}_{1,N+1}^*}{\partial \bar{\lambda}_{c,N+1}^*} &= \text{const.}\\
\frac{\partial \bar{x}_{2,N+1}^*}{\partial \bar{\lambda}_{c,N+1}^*} &= \text{const.}, \qquad & \frac{\partial \bar{v}_{2,N+1}^*}{\partial \bar{\lambda}_{c,N+1}^*} &= \text{const.}
\end{aligned} \tag{3.7}$$

The partial derivatives are constant, because the state variables of Eq. (3.7) only depend linearly on $\bar{\lambda}_{c,N+1}^*$.

Making use of the partial derivatives, a corrected coupling force $\bar{\lambda}_{c,N+1}$ can be computed, which fulfills the coupling conditions (3.1c) at the macro-time point $\bar{T}_{N+1}$. Regarding the fixed time point $\bar{T}_{N+1}$, $\bar{g}_{c\lambda,N+1}$ may be considered as a function of the coupling force $\bar{\lambda}_{c,N+1}^*$

$$\bar{g}_{c\lambda,N+1}\left(\bar{\lambda}^*_{c,N+1}\right) := \bar{\lambda}^*_{c,N+1} - \alpha_{cc1}\cdot\bar{c}_1\cdot\left(\bar{x}^*_{2,N+1}\left(\bar{\lambda}^*_{c,N+1}\right) - \bar{x}^*_{1,N+1}\left(\bar{\lambda}^*_{c,N+1}\right)\right) - \alpha_{dc1}\cdot\bar{d}_1\cdot\left(\bar{v}^*_{2,N+1}\left(\bar{\lambda}^*_{c,N+1}\right) - \bar{v}^*_{1,N+1}\left(\bar{\lambda}^*_{c,N+1}\right)\right). \tag{3.8}$$

Since the state variables $\bar{x}^*_{1,N+1}$, $\bar{x}^*_{2,N+1}$, $\bar{v}^*_{1,N+1}$ and $\bar{v}^*_{2,N+1}$depend only linearly on $\bar{\lambda}^*_{c,N+1}$, Eq. (3.8) can be rewritten as

$$\begin{aligned}
\bar{g}_{c\lambda,N+1}\left(\bar{\lambda}^*_{c,N+1}\right) &:= \bar{g}_{c\lambda,N+1}\left(\bar{\lambda}^p_{c,N+1}\right) + \left.\frac{\partial\bar{g}_{c\lambda,N+1}}{\partial\bar{\lambda}^*_{c,N+1}}\right|_{\bar{\lambda}^p_{c,N+1}}\cdot\left(\bar{\lambda}^*_{c,N+1} - \bar{\lambda}^p_{c,N+1}\right)\\
&= \bar{\lambda}^p_{c,N+1} - \alpha_{cc1}\cdot\bar{c}_1\cdot\left(\bar{x}_{2,N+1}\left(\bar{\lambda}^p_{c,N+1}\right) - \bar{x}_{1,N+1}\left(\bar{\lambda}^p_{c,N+1}\right)\right)\\
&\quad - \alpha_{dc1}\cdot\bar{d}_1\cdot\left(\bar{v}_{2,N+1}\left(\bar{\lambda}^p_{c,N+1}\right) - \bar{v}_{1,N+1}\left(\bar{\lambda}^p_{c,N+1}\right)\right)\\
&\quad + \left[1 - \alpha_{cc1}\cdot\bar{c}_1\cdot\left(\frac{\partial\bar{x}^*_{2,N+1}}{\partial\bar{\lambda}^*_{c,N+1}} - \frac{\partial\bar{x}^*_{1,N+1}}{\partial\bar{\lambda}^*_{c,N+1}}\right)\right.\\
&\quad \left. - \alpha_{dc1}\cdot\bar{d}_1\cdot\left(\frac{\partial\bar{v}^*_{2,N+1}}{\partial\bar{\lambda}^*_{c,N+1}} - \frac{\partial\bar{v}^*_{1,N+1}}{\partial\bar{\lambda}^*_{c,N+1}}\right)\right]\cdot\left(\bar{\lambda}^*_{c,N+1} - \bar{\lambda}^p_{c,N+1}\right),
\end{aligned} \tag{3.9}$$

where $\bar{\lambda}^p_{c,N+1} = \bar{\lambda}^p_c(\bar{T}_{N+1})$ terms the predicted coupling force at $\bar{T}_{N+1}$.

By setting $\bar{g}_{c\lambda,N+1}\left(\bar{\lambda}^*_{c,N+1}\right) = 0$, we get the corrected coupling force

$$\bar{\lambda}_{c,N+1} = \bar{\lambda}^p_{c,N+1} - \frac{\bar{\lambda}^p_{c,N+1} - \alpha_{cc1}\bar{c}_1\left(\bar{x}^p_{2,N+1} - \bar{x}^p_{1,N+1}\right) - \alpha_{dc1}\bar{d}_1\left(\bar{v}^p_{2,N+1} - \bar{v}^p_{1,N+1}\right)}{\left[1 - \alpha_{cc1}\bar{c}_1\left(\frac{\partial\bar{x}^*_{2,N+1}}{\partial\bar{\lambda}^*_{c,N+1}} - \frac{\partial\bar{x}^*_{1,N+1}}{\partial\bar{\lambda}^*_{c,N+1}}\right) - \alpha_{dc1}\bar{d}_1\left(\frac{\partial\bar{v}^*_{2,N+1}}{\partial\bar{\lambda}^*_{c,N+1}} - \frac{\partial\bar{v}^*_{1,N+1}}{\partial\bar{\lambda}^*_{c,N+1}}\right)\right]}. \tag{3.10}$$

Note that for the reason of a clear representation, different variables have been used for the general coupling force $\bar{\lambda}^*_{c,N+1}$ at the time point $\bar{T}_{N+1}$ and the corrected coupling force $\bar{\lambda}_{c,N+1}$, which represents the root of Eq. (3.10).

Step 3: Corrector Step

Using an interpolation polynomial with the corrected coupling force $\bar{\lambda}_{c,N+1}$ from Eq. (3.10), an analytical integration of subsystem 1 and subsystem 2 from $\bar{T}_N$ to $\bar{T}_{N+1}$ with initial conditions (3.2a) gives the corrected states

$$\begin{aligned}
\bar{x}_{1,N+1} &= \bar{x}_{1,N+1}\left(\bar{\lambda}_{c,N+1}, \bar{\lambda}_{c,N}, \dots, \bar{\lambda}_{c,N-k+1}, \boldsymbol{z}_N\right),\\
\bar{v}_{1,N+1} &= \bar{v}_{1,N+1}\left(\bar{\lambda}_{c,N+1}, \bar{\lambda}_{c,N}, \dots, \bar{\lambda}_{c,N-k+1}, \boldsymbol{z}_N\right),\\
\bar{x}_{2,N+1} &= \bar{x}_{2,N+1}\left(\bar{\lambda}_{c,N+1}, \bar{\lambda}_{c,N}, \dots, \bar{\lambda}_{c,N-k+1}, \boldsymbol{z}_N\right),\\
\bar{v}_{2,N+1} &= \bar{v}_{2,N+1}\left(\bar{\lambda}_{c,N+1}, \bar{\lambda}_{c,N}, \dots, \bar{\lambda}_{c,N-k+1}, \boldsymbol{z}_N\right).
\end{aligned} \tag{3.11}$$

With the help of the corrected state variables from Eq. (3.11), it is straightforward to derive recurrence equations, which only contain the state variables at the current and previous macro-time points. Evaluating the coupling condition at the $k+1$ macro-time points $\bar{T}_{N+1}, \dots, \bar{T}_{N-k+1}$ yields

$$\bar{\lambda}_{c,N+1} = \alpha_{cc1} \cdot \bar{c}_1 \cdot \left(\bar{x}_{2,N+1} - \bar{x}_{1,N+1}\right) + \alpha_{dc1} \cdot \bar{d}_1 \cdot \left(\bar{v}_{2,N+1} - \bar{v}_{1,N+1}\right)$$

$$\vdots \tag{3.12}$$

$$\bar{\lambda}_{c,N-k+1} = \alpha_{cc1}\bar{c}_1\left(\bar{x}_{2,N-k+1} - \bar{x}_{1,N-k+1}\right) + \alpha_{dc1}\bar{d}_1\left(\bar{v}_{2,N-k+1} - \bar{v}_{1,N-k+1}\right).$$

Making use of Eq. (3.12), the coupling forces $\bar{\lambda}_{c,N+1}, \dots, \bar{\lambda}_{c,N-k+1}$ can be eliminated in Eq. (3.11), which results in relationships of the form

$$\begin{aligned} \bar{x}_{1,N+1} &= \bar{x}_{1,N+1}(\boldsymbol{z}_{N+1}, \boldsymbol{z}_N, \dots, \boldsymbol{z}_{N-k+1}), \\ \bar{v}_{1,N+1} &= \bar{v}_{1,N+1}(\boldsymbol{z}_{N+1}, \boldsymbol{z}_N, \dots, \boldsymbol{z}_{N-k+1}), \\ \bar{x}_{2,N+1} &= \bar{x}_{2,N+1}(\boldsymbol{z}_{N+1}, \boldsymbol{z}_N, \dots, \boldsymbol{z}_{N-k+1}), \\ \bar{v}_{2,N+1} &= \bar{v}_{2,N+1}(\boldsymbol{z}_{N+1}, \boldsymbol{z}_N, \dots, \boldsymbol{z}_{N-k+1}). \end{aligned} \tag{3.13}$$

Eq. (3.13) represents a system of 4 coupled linear recurrence equations. This system can symbolically be written as

$$\boldsymbol{A}_{N+1} \cdot \boldsymbol{z}_{N+1} + \boldsymbol{A}_N \cdot \boldsymbol{z}_N + \cdots + \boldsymbol{A}_{N-k+1} \cdot \boldsymbol{z}_{N-k+1} = \boldsymbol{0}. \tag{3.14}$$

The real-valued matrices $\boldsymbol{A}_{N+1}, \dots, \boldsymbol{A}_{N-k+1} \in \mathbb{R}^{4\times4}$ are constant and only depend on the seven parameters of the co-simulation test model.

Since the subsystem integration is carried out analytically, the stability behavior of the co-simulation approach is directly determined by the stability of the linear recurrence equations system (3.14). This system can easily be solved by the exponential approach $\boldsymbol{z}_N = \hat{\boldsymbol{z}} \cdot \Lambda^N$, where Λ denotes the Eigenvalue and $\hat{\boldsymbol{z}}$ the Eigenvector of the system. Since the recurrence system (3.14) is of order k, there generally exist $j = 1, \dots, 4 \cdot k$ Eigenvalues and corresponding Eigenvectors. If the spectral radius $\rho = \max\{|\Lambda_j|\}$, i.e. the magnitude of the largest Eigenvalue is larger than 1, the co-simulation becomes unstable. Since the matrices $\boldsymbol{A}_{N+1}, \dots, \boldsymbol{A}_{N-k+1}$ only depend on the seven parameters of the co-simulation test model, ρ is also only a function of these seven parameters.

It should finally be stressed that the implicit coupling scheme presented above does only require one corrector step, since the gradients are constant due to the linearity of the problem, see Eq. (3.7). For nonlinear problems, the predictor/corrector approach described above would be semi-implicit and a corrector iteration with several corrector steps would be necessary in order to obtain a full-implicit method.

3.1.2. Explicit Force/Force Co-Simulation Approach

For the explicit coupling approach only one explicit integration step is required, which is identical with the predictor step in Section 3.1.1, while Step 2 and Step 3 of Section 3.1.1 are omitted.

Step 1: Explicit Integration Step

An analytical integration of subsystem 1 and subsystem 2 from $\bar{T}_N$ to $\bar{T}_{N+1}$ with initial conditions (3.2a) and with the extrapolation polynomial

$$\bar{\lambda}_c^p(\bar{t}) = P_{\bar{\lambda}_c}^p\left[\left(\bar{T}_N, \bar{\lambda}_{c,N}\right), \left(\bar{T}_{N-1}, \bar{\lambda}_{c,N-1}\right), \dots, \left(\bar{T}_{N-k}, \bar{\lambda}_{c,N-k}\right); \bar{t}\right] \tag{3.15}$$

yields the following state variables at the macro-time point $\bar{T}_{N+1}$

$$\begin{aligned}
\bar{x}_{1,N+1} &= \bar{x}_{1,N+1}\left(\bar{\lambda}_{c,N}, \bar{\lambda}_{c,N-1}, \dots, \bar{\lambda}_{c,N-k}, \boldsymbol{z}_N\right),\\
\bar{v}_{1,N+1} &= \bar{v}_{1,N+1}\left(\bar{\lambda}_{c,N}, \bar{\lambda}_{c,N-1}, \dots, \bar{\lambda}_{c,N-k}, \boldsymbol{z}_N\right),\\
\bar{x}_{2,N+1} &= \bar{x}_{2,N+1}\left(\bar{\lambda}_{c,N}, \bar{\lambda}_{c,N-1}, \dots, \bar{\lambda}_{c,N-k}, \boldsymbol{z}_N\right),\\
\bar{v}_{2,N+1} &= \bar{v}_{2,N+1}\left(\bar{\lambda}_{c,N}, \bar{\lambda}_{c,N-1}, \dots, \bar{\lambda}_{c,N-k,}\, \boldsymbol{z}_N\right).
\end{aligned} \tag{3.16}$$

Making use of the coupling conditions at the macro-time points $\bar{T}_N, \dots, \bar{T}_{N-k}$, see Eq. (3.12), the coupling forces $\bar{\lambda}_{c,N}, \bar{\lambda}_{c,N-1}, \dots, \bar{\lambda}_{c,N-k}$ in Eq. (3.16) can be substituted, which yields relationships of the form

$$\begin{aligned}
\bar{x}_{1,N+1} &= \bar{x}_{1,N+1}(\boldsymbol{z}_N, \boldsymbol{z}_{N-1}, \dots, \boldsymbol{z}_{N-k}),\\
\bar{v}_{1,N+1} &= \bar{v}_{1,N+1}(\boldsymbol{z}_N, \boldsymbol{z}_{N-1}, \dots, \boldsymbol{z}_{N-k}),\\
\bar{x}_{2,N+1} &= \bar{x}_{2,N+1}(\boldsymbol{z}_N, \boldsymbol{z}_{N-1}, \dots, \boldsymbol{z}_{N-k}),\\
\bar{v}_{2,N+1} &= \bar{v}_{2,N+1}(\boldsymbol{z}_N, \boldsymbol{z}_{N-1}, \dots, \boldsymbol{z}_{N-k}).
\end{aligned} \tag{3.17}$$

As in the case of the implicit approach, Eq. (3.17) represents a system of 4 coupled linear recurrence equations of order $k+1$. According to Section 3.1.1, this system can symbolically be written as

$$\boldsymbol{Z_{N+1}} + \boldsymbol{A}_N \cdot \boldsymbol{z}_N + \boldsymbol{A}_{N-1} \cdot \boldsymbol{z}_{N-1} + \cdots + \boldsymbol{A}_{N-k} \cdot \boldsymbol{z}_{N-k} = \boldsymbol{0}\ . \tag{3.18}$$

Like in the case of implicit solver coupling, the real-valued matrices $\boldsymbol{A}_N, \dots, \boldsymbol{A}_{N-k} \in \mathbb{R}^{4\times 4}$ are constant and only depend on the seven parameters of the co-simulation test model. However, it should be mentioned that the matrices are not identical with the corresponding matrices in the case of implicit approach.

3.1.3. Implicit Force/Displacement Co-Simulation Approach

When the test model is decomposed by a force/displacement approach, subsystem 1 is represented by a force driven one mass oscillator while subsystem 2 is described by a base-point excited oscillator, see Figure 2.2. Note that it is also possible to describe the system using a displacement/force approach and hence the stability behavior might be different for unsymmetrical test models. Here, we only consider force/displacement decomposition.

The equation of motion can be rewritten in the dimensionless according to

Subsystem 1:

$$\begin{aligned}
\bar{x}_1' &= \bar{v}_1\\
\bar{v}_1' &= -\bar{c}_1 \cdot \bar{x}_1 - \bar{d}_1 \cdot \bar{v}_1 + \bar{\lambda}_c
\end{aligned} \tag{3.19a}$$

Subsystem 2:

$$\begin{aligned}
\bar{x}_2' &= \bar{v}_2\\
\bar{v}_2' &= -\frac{\alpha_{c21}}{\alpha_{m21}}\bar{c}_1\bar{x}_2 - \frac{\alpha_{d21}}{\alpha_{m21}}\bar{d}_1\bar{v}_2 - \frac{\alpha_{cc1}}{\alpha_{m21}}\bar{c}_1(\bar{x}_2 - \tilde{\bar{x}}_1) - \frac{\alpha_{dc1}}{\alpha_{m21}}\bar{d}_1(\bar{v}_2 - \tilde{\bar{v}}_1)
\end{aligned} \tag{3.19b}$$

Coupling conditions:

$$\begin{aligned}\bar{g}_{c\lambda} &:= \bar{\lambda}_c - \alpha_{cc1}\cdot\bar{c}_1\cdot(\bar{x}_2-\bar{x}_1) - \alpha_{dc1}\cdot\bar{d}_1\cdot(\bar{v}_2-\bar{v}_1) = 0\\ \bar{g}_{cx1} &:= \tilde{\bar{x}}_1 - \bar{x}_1 = 0\\ \bar{g}_{cv1} &:= \tilde{\bar{v}}_1 - \bar{v}_1 = 0\,.\end{aligned} \tag{3.19c}$$

Like in Section 3.1.1, we consider the general macro-step from $\bar{T}_N$ to $\bar{T}_{N+1}$ to derive the governing recurrence equations system for the force/displacement-coupling approach. Again, we assume that at the beginning of the macro-time step, the state and the coupling variables are known

$$\begin{aligned}\bar{x}_1(\bar{t}=\bar{T}_N) &= \bar{x}_{1,N}\,, \qquad \bar{v}_1(\bar{t}=\bar{T}_N) = \bar{v}_{1,N}\,,\\ \bar{x}_2(\bar{t}=\bar{T}_N) &= \bar{x}_{2,N}\,, \qquad \bar{v}_2(\bar{t}=\bar{T}_N) = \bar{v}_{2,N}\,,\end{aligned} \tag{3.20a}$$

$$\begin{aligned}\bar{\lambda}_c(\bar{t}=\bar{T}_N) &= \bar{\lambda}_{c,N}\\ \tilde{\bar{x}}_1(\bar{t}=\bar{T}_N) = \tilde{\bar{x}}_{1,N}\,, &\qquad \tilde{\bar{v}}_1(\bar{t}=\bar{T}_N) = \tilde{\bar{v}}_{1,N}\,.\end{aligned} \tag{3.20b}$$

For higher order approximation $(k>0)$, the coupling variables at the previous macro-time points are also assumed to be known.

Step 1: Predictor Step

If we analytically integrate subsystem 1 and subsystem 2 from $\bar{T}_N$ to $\bar{T}_{N+1}$ with initial condition (3.20a) and with the predictor (extrapolation) polynomials $\bar{\lambda}_c^p(\bar{t})$, $\tilde{\bar{x}}_1^p(\bar{t})$ and $\tilde{\bar{v}}_1^p(\bar{t})$

$$\begin{aligned}\bar{\lambda}_c^p(\bar{t}) &= P^p_{\bar{\lambda}_c}\left[\left(\bar{T}_N,\bar{\lambda}_{c,N}\right),\left(\bar{T}_{N-1},\bar{\lambda}_{c,N-1}\right),\dots,\left(\bar{T}_{N-k},\bar{\lambda}_{c,N-k}\right);\bar{t}\right],\\ \tilde{\bar{x}}_1^p(\bar{t}) &= P^p_{\tilde{\bar{x}}_1}\left[\left(\bar{T}_N,\tilde{\bar{x}}_{1,N}\right),\left(\bar{T}_{N-1},\tilde{\bar{x}}_{1,N-1}\right),\dots,\left(\bar{T}_{N-k},\tilde{\bar{x}}_{1,N-k}\right);\bar{t}\right],\\ \tilde{\bar{v}}_1^p(\bar{t}) &= P^p_{\tilde{\bar{v}}_1}\left[\left(\bar{T}_N,\tilde{\bar{v}}_{1,N}\right),\left(\bar{T}_{N-1},\tilde{\bar{v}}_{1,N-1}\right),\dots,\left(\bar{T}_{N-k},\tilde{\bar{v}}_{1,N-k}\right);\bar{t}\right],\end{aligned} \tag{3.21}$$

we get the following predicted state variables at the macro-time point $\bar{T}_{N+1}$

$$\begin{aligned}\bar{x}^p_{1,N+1} &= \bar{x}^p_{1,N+1}\left(\bar{\lambda}_{c,N},\bar{\lambda}_{c,N-1},\dots,\bar{\lambda}_{c,N-k},\boldsymbol{z}_N\right),\\ \bar{v}^p_{1,N+1} &= \bar{v}^p_{1,N+1}\left(\bar{\lambda}_{c,N},\bar{\lambda}_{c,N-1},\dots,\bar{\lambda}_{c,N-k},\boldsymbol{z}_N\right),\\ \bar{x}^p_{2,N+1} &= \bar{x}^p_{2,N+1}\left(\tilde{\boldsymbol{u}}_{2,N},\tilde{\boldsymbol{u}}_{2,N-1},\dots,\tilde{\boldsymbol{u}}_{2,N-k},\boldsymbol{z}_N\right),\\ \bar{v}^p_{2,N+1} &= \bar{v}^p_{2,N+1}\left(\tilde{\boldsymbol{u}}_{2,N},\tilde{\boldsymbol{u}}_{2,N-1},\dots,\tilde{\boldsymbol{u}}_{2,N-k},\boldsymbol{z}_N\right),\end{aligned} \tag{3.22}$$

where the vectors $\tilde{\boldsymbol{u}}_{2,N} = \left(\tilde{\bar{x}}_{1,N}\ \tilde{\bar{v}}_{1,N}\right)^T$, $\tilde{\boldsymbol{u}}_{2,N-1} = (\tilde{\bar{x}}_{1,N-1}\ \tilde{\bar{v}}_{1,N-1})^T$,…, $\tilde{\boldsymbol{u}}_{2,N-k} = (\tilde{\bar{x}}_{1,N-k}\ \tilde{\bar{v}}_{1,N-k})^T$ collect the coupling variables for subsystem 2 at the current and previous macro-time points.

Step 2: Calculation of Corrected Coupling Variables

An analytical integration of subsystem 1 and subsystem 2 from $\bar{T}_N$ to $\bar{T}_{N+1}$ with initial conditions (3.20a) and with the interpolation polynomials $\bar{\lambda}_c^*(\bar{t})$, $\tilde{\bar{x}}_1^*(t)$ and $\tilde{\bar{v}}_1^*(t)$

$$
\begin{aligned}
\bar{\lambda}_c^*(\bar{t}) &= P_{\bar{\lambda}_c}^* \left[\left(\bar{T}_{N+1}, \bar{\lambda}_{c,N+1}^*\right), \left(\bar{T}_N, \bar{\lambda}_{c,N}\right), \dots, \left(\bar{T}_{N-k+1}, \bar{\lambda}_{c,N-k+1}\right); \bar{t} \right], \\
\tilde{\bar{x}}_1^*(t) &= P_{\tilde{\bar{x}}_1}^* \left[\left(\bar{T}_{N+1}, \tilde{\bar{x}}_{1,N+1}^*\right), \left(\bar{T}_N, \tilde{\bar{x}}_{1,N}\right), \dots, \left(\bar{T}_{N-k+1}, \tilde{\bar{x}}_{1,N-k+1}\right); \bar{t} \right], \\
\tilde{\bar{v}}_1^*(\bar{t}) &= P_{\tilde{\bar{v}}_1}^* \left[\left(\bar{T}_{N+1}, \tilde{\bar{v}}_{1,N+1}^*\right), \left(\bar{T}_N, \tilde{\bar{v}}_{1,N}\right), \dots, \left(\bar{T}_{N-k+1}, \tilde{\bar{v}}_{1,N-k+1}\right); \bar{t} \right]
\end{aligned}
\tag{3.23}
$$

yields the following state variables at the macro-time point $\bar{T}_{N+1}$

$$
\begin{aligned}
\bar{x}_{1,N+1}^* &= \bar{x}_{1,N+1}^* \left(\bar{\lambda}_{c,N+1}^*, \bar{\lambda}_{c,N}, \dots, \bar{\lambda}_{c,N-k+1}, \boldsymbol{z}_N \right), \\
\bar{v}_{1,N+1}^* &= \bar{v}_{1,N+1}^* \left(\bar{\lambda}_{c,N+1}^*, \bar{\lambda}_{c,N}, \dots, \bar{\lambda}_{c,N-k+1}, \boldsymbol{z}_N \right), \\
\bar{x}_{2,N+1}^* &= \bar{x}_{2,N+1}^* \left(\widetilde{\boldsymbol{u}}_{2,N+1}^*, \widetilde{\boldsymbol{u}}_{2,N}, \dots, \widetilde{\boldsymbol{u}}_{2,N-k+1}, \boldsymbol{z}_N \right), \\
\bar{v}_{2,N+1}^* &= \bar{v}_{2,N+1}^* \left(\widetilde{\boldsymbol{u}}_{2,N+1}^*, \widetilde{\boldsymbol{u}}_{2,N}, \dots, \widetilde{\boldsymbol{u}}_{2,N-k+1}, \boldsymbol{z}_N \right),
\end{aligned}
\tag{3.24}
$$

where $\bar{\lambda}_{c,N+1}^*$, $\tilde{\bar{x}}_{1,N+1}^*$ and $\tilde{\bar{v}}_{1,N+1}^*$denote arbitrary coupling variables at the macro-time point $\bar{T}_{N+1}$.

Inserting the state variables of Eq. (3.24) into the coupling conditions (3.19c) results in a linear equations system for the coupling variables, since the state vectors of Eq. (3.24) only linearly depend on the coupling variables and since the coupling conditions are linear. Solving this equations system for the coupling variables yields the corrected variables $\bar{\lambda}_{c,N+1}$, $\tilde{\bar{x}}_{1,N+1}$ and $\tilde{\bar{v}}_{1,N+1}$.

Step 3: Corrector Step

Using interpolation polynomials with the corrected coupling variables $\bar{\lambda}_{c,N+1}$, $\tilde{\bar{x}}_{1,N+1}$ and $\tilde{\bar{v}}_{1,N+1}$, an analytical integration of the decomposed systems from $\bar{T}_N$ to $\bar{T}_{N+1}$ with initial conditions (3.20a) gives the corrected states

$$
\begin{aligned}
\bar{x}_{1,N+1} &= \bar{x}_{1,N+1} \left(\bar{\lambda}_{c,N+1}, \bar{\lambda}_{c,N}, \dots, \bar{\lambda}_{c,N-k+1}, \boldsymbol{z}_N \right), \\
\bar{v}_{1,N+1} &= \bar{v}_{1,N+1} \left(\bar{\lambda}_{c,N+1}, \bar{\lambda}_{c,N}, \dots, \bar{\lambda}_{c,N-k+1}, \boldsymbol{z}_N \right), \\
\bar{x}_{2,N+1} &= \bar{x}_{2,N+1} \left(\widetilde{\boldsymbol{u}}_{2,N+1}, \widetilde{\boldsymbol{u}}_{2,N}, \dots, \widetilde{\boldsymbol{u}}_{2,N-k+1}, \boldsymbol{z}_N \right), \\
\bar{v}_{2,N+1} &= \bar{v}_{2,N+1} \left(\widetilde{\boldsymbol{u}}_{2,N+1}, \widetilde{\boldsymbol{u}}_{2,N}, \dots, \widetilde{\boldsymbol{u}}_{2,N-k+1}, \boldsymbol{z}_N \right).
\end{aligned}
\tag{3.25}
$$

By evaluating the coupling conditions (3.19c) at the $k+1$ macro-time points $\bar{T}_{N+1}, \bar{T}_N$, ..., $\bar{T}_{N-k+1}$, the coupling variables in Eq. (3.25) can be eliminated, which gives a linear recurrence equations system of the form (3.13) and (3.14), respectively.

3.1.4. Explicit Force/Displacement Co-Simulation Approach

In order to perform an explicit coupling approach, only one explicit integration step has to be carried out. This explicit step is equivalent with the predictor step in Section 3.1.3. Replacing the coupling variables in Eq. (3.22) yields a linear system of recurrence equations of the form (3.17) and (3.18).

3.1.5. Implicit Displacement/Displacement Co-Simulation Approach

When a displacement/displacement-coupling approach is used to decompose the two-mass oscillator, each subsystem is described by a base-point excited single-mass

oscillator, see Figure 2.3. The equations of motion characterizing the decomposed system reads as

Subsystem 1:

$$\begin{aligned} \bar{x}_1' &= \bar{v}_1 \\ \bar{v}_1' &= -\bar{c}_1 \cdot \bar{x}_1 - \bar{d}_1 \cdot \bar{v}_1 + \alpha_{cc1} \cdot \bar{c}_1 \cdot (\tilde{\bar{x}}_2 - \bar{x}_1) + \alpha_{dc1} \cdot \bar{d}_1 \cdot (\tilde{\bar{v}}_2 - \bar{v}_1) \end{aligned} \tag{3.26a}$$

Subsystem 2:

$$\begin{aligned} \bar{x}_2' &= \bar{v}_2 \\ \bar{v}_2' &= -\frac{\alpha_{c21}}{\alpha_{m21}} \bar{c}_1 \bar{x}_2 - \frac{\alpha_{d21}}{\alpha_{m21}} \bar{d}_1 \bar{v}_2 - \frac{\alpha_{cc1}}{\alpha_{m21}} \bar{c}_1 (\bar{x}_2 - \tilde{\bar{x}}_1) - \frac{\alpha_{dc1}}{\alpha_{m21}} \bar{d}_1 (\bar{v}_2 - \tilde{\bar{v}}_1) \end{aligned} \tag{3.26b}$$

Coupling conditions:

$$\begin{aligned} \bar{g}_{cx_1} &:= \tilde{\bar{x}}_1 - \bar{x}_1 = 0 \\ \bar{g}_{cv_1} &:= \tilde{\bar{v}}_1 - \bar{v}_1 = 0 \\ \bar{g}_{cx_2} &:= \tilde{\bar{x}}_2 - \bar{x}_2 = 0 \\ \bar{g}_{cv_2} &:= \tilde{\bar{v}}_2 - \bar{v}_2 = 0\,. \end{aligned} \tag{3.26c}$$

The corresponding initial conditions for the state variables as well as the coupling variables at the beginning of the macro-step are given by

$$\begin{aligned} \bar{x}_1(\bar{t} = \bar{T}_N) &= \bar{x}_{1,N}\,, \qquad \bar{v}_1(\bar{t} = \bar{T}_N) = \bar{v}_{1,N}\,, \\ \bar{x}_2(\bar{t} = \bar{T}_N) &= \bar{x}_{2,N}\,, \qquad \bar{v}_2(\bar{t} = \bar{T}_N) = \bar{v}_{2,N}\,, \end{aligned} \tag{3.27a}$$

$$\begin{aligned} \tilde{\bar{x}}_1(\bar{t} = \bar{T}_N) &= \tilde{\bar{x}}_{1,N}\,, \qquad \tilde{\bar{v}}_1(\bar{t} = \bar{T}_N) = \tilde{\bar{v}}_{1,N}\,, \\ \tilde{\bar{x}}_2(\bar{t} = \bar{T}_N) &= \tilde{\bar{x}}_{2,N}, \qquad \tilde{\bar{v}}_2(\bar{t} = \bar{T}_N) = \tilde{\bar{v}}_{2,N}\,. \end{aligned} \tag{3.27b}$$

Step 1: Predictor Step

Using the initial conditions (3.27a) and the predictor (extrapolation) polynomials $\tilde{\bar{x}}_1^p(\bar{t})$, $\tilde{\bar{v}}_1^p(\bar{t})$, $\tilde{\bar{x}}_2^p(\bar{t})$ and $\tilde{\bar{v}}_2^p(\bar{t})$, an analytical integration of the two subsystems from $\bar{T}_N$ to $\bar{T}_{N+1}$ yields the predicted state variables at the macro-time point $\bar{T}_{N+1}$

$$\begin{aligned} \bar{x}_{1,N+1}^p &= \bar{x}_{1,N+1}^p\big(\widetilde{\boldsymbol{u}}_{1,N}, \widetilde{\boldsymbol{u}}_{1,N-1}, \dots, \widetilde{\boldsymbol{u}}_{1,N-k}, \boldsymbol{z}_N\big), \\ \bar{v}_{1,N+1}^p &= \bar{v}_{1,N+1}^p\big(\widetilde{\boldsymbol{u}}_{1,N}, \widetilde{\boldsymbol{u}}_{1,N-1}, \dots, \widetilde{\boldsymbol{u}}_{1,N-k}, \boldsymbol{z}_N\big), \\ \bar{x}_{2,N+1}^p &= \bar{x}_{2,N+1}^p\big(\widetilde{\boldsymbol{u}}_{2,N}, \widetilde{\boldsymbol{u}}_{2,N-1}, \dots, \widetilde{\boldsymbol{u}}_{2,N-k}, \boldsymbol{z}_N\big), \\ \bar{v}_{2,N+1}^p &= \bar{v}_{2,N+1}^p\big(\widetilde{\boldsymbol{u}}_{2,N}, \widetilde{\boldsymbol{u}}_{2,N-1}, \dots, \widetilde{\boldsymbol{u}}_{2,N-k}, \boldsymbol{z}_N\big). \end{aligned} \tag{3.28}$$

Note that the vectors $\widetilde{\boldsymbol{u}}_{1,N} = \big(\tilde{\bar{x}}_{2,N}\ \tilde{\bar{v}}_{2,N}\big)^T$, $\widetilde{\boldsymbol{u}}_{1,N-1} = (\tilde{\bar{x}}_{2,N-1}\ \tilde{\bar{v}}_{2,N-1})^T$, $\widetilde{\boldsymbol{u}}_{1,N-k} = (\tilde{\bar{x}}_{2,N-k}\ \tilde{\bar{v}}_{2,N-k})^T$ and $\widetilde{\boldsymbol{u}}_{2,N} = \big(\tilde{\bar{x}}_{1,N}\ \tilde{\bar{v}}_{1,N}\big)^T$, $\widetilde{\boldsymbol{u}}_{2,N-1} = (\tilde{\bar{x}}_{1,N-1}\ \tilde{\bar{v}}_{1,N-1})^T$, $\widetilde{\boldsymbol{u}}_{2,N-k} = \big(\tilde{\bar{x}}_{1,N-k}\ \tilde{\bar{v}}_{1,N-k}\big)^T$ collect the coupling variables at the current and previous macro-time points.

Step 2: Calculation of Corrected Coupling Variables

By making use of the interpolation polynomials $\tilde{\bar{x}}_1^*(\bar{t})$, $\tilde{\bar{v}}_1^*(\bar{t})$, $\tilde{\bar{x}}_2^*(\bar{t})$ and $\tilde{\bar{v}}_2^*(\bar{t})$, an integration from $\bar{T}_N$ to $\bar{T}_{N+1}$ with initial conditions (3.27a) gives the following state variables at the macro-time point $\bar{T}_{N+1}$

$$
\begin{aligned}
\bar{x}^*_{1,N+1} &= \bar{x}^*_{1,N+1}\left(\tilde{\boldsymbol{u}}^*_{1,N+1}, \tilde{\boldsymbol{u}}_{1,N}, \dots, \tilde{\boldsymbol{u}}_{1,N-k+1}, \boldsymbol{z}_N\right),\\
\bar{v}^*_{1,N+1} &= \bar{v}^*_{1,N+1}\left(\tilde{\boldsymbol{u}}^*_{1,N+1}, \tilde{\boldsymbol{u}}_{1,N}, \dots, \tilde{\boldsymbol{u}}_{1,N-k+1}, \boldsymbol{z}_N\right),\\
\bar{x}^*_{2,N+1} &= \bar{x}^*_{2,N+1}\left(\tilde{\boldsymbol{u}}^*_{2,N+1}, \tilde{\boldsymbol{u}}_{2,N}, \dots, \tilde{\boldsymbol{u}}_{2,N-k+1}, \boldsymbol{z}_N\right),\\
\bar{v}^*_{2,N+1} &= \bar{v}^*_{2,N+1}\left(\tilde{\boldsymbol{u}}^*_{2,N+1}, \tilde{\boldsymbol{u}}_{2,N}, \dots, \tilde{\boldsymbol{u}}_{2,N-k+1}, \boldsymbol{z}_N\right),
\end{aligned}
\tag{3.29}
$$

where $\tilde{\bar{x}}^*_{1,N+1}$, $\tilde{\bar{v}}^*_{1,N+1}$, $\tilde{\bar{x}}^*_{2,N+1}$ and $\tilde{\bar{v}}^*_{2,N+1}$ denote arbitrary coupling variables at the macro-time point $\bar{T}_{N+1}$.

Inserting the state variables of Eq. (3.29) into the coupling conditions (3.26c) results in a linear equations system for the coupling variables, the solution of which yields the corrected variables $\tilde{\bar{x}}_{1,N+1}$, $\tilde{\bar{v}}_{1,N+1}$, $\tilde{\bar{x}}_{2,N+1}$ and $\tilde{\bar{v}}_{2,N+1}$.

Step 3: Corrector Step

Using interpolation polynomials with the corrected coupling variables $\tilde{\bar{x}}_{1,N+1}$, $\tilde{\bar{v}}_{1,N+1}$, $\tilde{\bar{x}}_{2,N+1}$ and $\tilde{\bar{v}}_{2,N+1}$, a subsystem integration from $\bar{T}_N$ to $\bar{T}_{N+1}$ with initial conditions (3.27a) yields the corrected states

$$
\begin{aligned}
\bar{x}_{1,N+1} &= \bar{x}_{1,N+1}\left(\tilde{\boldsymbol{u}}_{1,N+1}, \tilde{\boldsymbol{u}}_{1,N}, \dots, \tilde{\boldsymbol{u}}_{1,N-k+1}, \boldsymbol{z}_N\right),\\
\bar{v}_{1,N+1} &= \bar{v}_{1,N+1}\left(\tilde{\boldsymbol{u}}_{1,N+1}, \tilde{\boldsymbol{u}}_{1,N}, \dots, \tilde{\boldsymbol{u}}_{1,N-k+1}, \boldsymbol{z}_N\right),\\
\bar{x}_{2,N+1} &= \bar{x}_{2,N+1}\left(\tilde{\boldsymbol{u}}_{2,N+1}, \tilde{\boldsymbol{u}}_{2,N}, \dots, \tilde{\boldsymbol{u}}_{2,N-k+1}, \boldsymbol{z}_N\right),\\
\bar{v}_{2,N+1} &= \bar{v}_{2,N+1}\left(\tilde{\boldsymbol{u}}_{2,N+1}, \tilde{\boldsymbol{u}}_{2,N}, \dots, \tilde{\boldsymbol{u}}_{2,N-k+1}, \boldsymbol{z}_N\right).
\end{aligned}
\tag{3.30}
$$

By evaluating the coupling conditions (3.26c) at the $k+1$ macro-time points $\bar{T}_{N+1}$, $\bar{T}_N$, …, $\bar{T}_{N-k+1}$, the coupling variables in Eq. (3.30) can be eliminated, which gives again a linear recurrence equations system of the form (3.13) and (3.14), respectively.

3.1.6. Explicit Displacement/Displacement Co-Simulation Approach

Performing the predictor step in Section 3.1.5, only, an explicit co-simulation scheme is obtained. Using the coupling conditions (3.26c) in order to replace the coupling variables in Eq. (3.28), one gets a linear recurrence equations system of the form (3.17) and (3.18), respectively.

3.2. Stability and Convergence Plots for Original Co-Simulation Methods

As shown in the previous sections, performing a predictor-corrector approach in connection with implicit co-simulation algorithms or only a predictor step in the framework of explicit methods, we end up with a linear system of recurrence equations described by Eq. (3.14) and Eq. (3.18) respectively. In order to display the stability behavior in 2D plots, it is mandatory to calculate the spectral radius of the recurrence equations system, which characterize the stability properties of the underlying co-simulation method.

Since the coefficient matrices of the linear system of recurrence equations depend on the 7 dimensionless parameters defined in (2.2), the spectral radius can be plotted as

the function of two parameters with the other five fixed. In accordance with the 2D stability plots for time integration schemes, where the spectral radius of the recurrence equation is plotted as a function of $h\Lambda_r$ and $h\Lambda_i$, an alternative set of parameters are introduced for representing 2D co-simulation stability plots, namely

$$\bar{\Lambda}_{r1} = -\frac{\bar{d}_1}{2}, \quad \bar{\Lambda}_{i1} = \frac{1}{2}\sqrt{4 \cdot \bar{c}_1 - \bar{d}_1^2}, \tag{3.31a}$$

$$\alpha_{m21} = \frac{m_2}{m_1}, \alpha_{\Lambda r21} = \frac{\bar{\Lambda}_{r2}}{\bar{\Lambda}_{r1}} = \frac{\alpha_{d21}}{\alpha_{m21}},$$
$$\alpha_{\Lambda i21} = \frac{\bar{\Lambda}_{i2}}{\bar{\Lambda}_{i1}} = \frac{1}{\alpha_{m21}} \frac{\sqrt{4\alpha_{m21}\alpha_{c21}\bar{c}_1 - \alpha_{d21}^2\bar{d}_1^2}}{\sqrt{4 \cdot \bar{c}_1 - \bar{d}_1^2}} \tag{3.31b}$$

$$\alpha_{\Lambda rc1} = \frac{\alpha_{dc1}}{\alpha_m^*}, \quad \alpha_{\Lambda ic1} = \frac{1}{\alpha_m^*} \frac{\sqrt{4\alpha_m^*\alpha_{cc1}\bar{c}_1 - \alpha_{dc1}^2\bar{d}_1^2}}{\sqrt{4 \cdot \bar{c}_1 - \bar{d}_1^2}} \quad \text{with} \quad \alpha_m^* = 2\frac{\alpha_{m21}}{1+\alpha_{m21}}. \tag{3.31c}$$

The physical interpretation of these parameters is straightforward. $\bar{\Lambda}_{r1}$ and $\bar{\Lambda}_{i1}$ in Eq. (3.31a) describe the real and imaginary part of the eigenvalue of subsystem 1. The dimensionless parameters in Eq. (3.31b) characterize subsystem 2: α_{m21}, $\alpha_{\Lambda r21}$ and $\alpha_{\Lambda i21}$ describe the ratio of the subsystem masses as well as the ratio of the real and the imaginary part of the eigenvalue of subsystem 2 with respect to subsystem 1. To characterize the coupling element of the subsystem, the two parameters $\alpha_{\Lambda rc1}$ and $\alpha_{\Lambda ic1}$ are introduced. The physical meaning of these parameters can be explained with the unfixed two-mass oscillator ($c_1 = c_2 = d_1 = d_2 = 0$), see Figure 3.1.

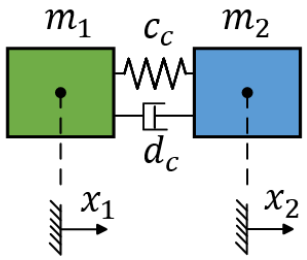

Figure 3.1 Unfixed two-mass oscillator ($c_1 = c_2 = d_1 = d_2 = 0$)

To determine the eigenvalues, we have to calculate the roots of the characteristic polynomial

$$P(\Lambda) = \Lambda^2[m_1m_2\Lambda^2 + (m_1+m_2)d_c\Lambda + (m_1+m_2)c_c]. \tag{3.32}$$

Apparently, the eigenvalues $\Lambda_{1/3} = 0$ define a rigid body motion. With $m_1 = 1$ and with the parameters of Eq. (2.2), the other two eigenvalues are given by

$$\Lambda_{2/4} = -\frac{\alpha_{dc1} \cdot \bar{d}_1}{\alpha_m^*} \pm i \cdot \frac{\sqrt{2 \cdot \alpha_m^* \cdot \alpha_{cc1} \cdot \bar{c}_1 - \alpha_{dc1}^2 \cdot \bar{d}_1^2}}{\alpha_m^*}. \tag{3.33}$$

Hence, the two parameters $\alpha_{\Lambda rc1}$ and $\alpha_{\Lambda ic1}$ characterize the ratio of the real and imaginary part of this eigenvalue with respect to $\overline{\Lambda}_{r1}$ and $\overline{\Lambda}_{i1}$. However, the factor two has artificially been introduced so that for the symmetric case (i.e. $m_1 = m_2, c_1 = c_2 = c_c$ and $d_1 = d_2 = d_c$) the parameters α_{m21}, $\alpha_{\Lambda r21}$, $\alpha_{\Lambda i21}$, $\alpha_{\Lambda rc1}$ and $\alpha_{\Lambda ic1}$ become 1.

To examine the stability properties of the different coupling approaches, we consider here the symmetric test model ($\alpha_{m21} = \alpha_{\Lambda r21} = \alpha_{\Lambda i21} = \alpha_{\Lambda rc1} = \alpha_{\Lambda ic1} = 1$). The parameters $\overline{\Lambda}_{r1}$ and $\overline{\Lambda}_{i1}$ are varied in the range $[-2, 0]$ and $[0, 10]$ for the implicit co-simulation schemes and in the range $[-1, 0]$ and $[0, 2]$ for the explicit case. Note that the spectral radius can only be calculated numerically. The solid points in the plots indicate stable cases, i.e. points for which $\rho \leq (1 + 10^{-10})$ holds. In order to reduce floating point errors, the numerical calculation has been carried out with 128 digit.

3.2.1. Stability Plots for Implicit Co-Simulation Approach

Stability plots for the implicit coupling schemes are collected in Figure 3.2 - Figure 3.4 for the force/force-, the force/displacement-, and the displacement/displacement-coupling approach. Plots have been generated for constant ($k = 0$), linear ($k = 1$), quadratic ($k = 2$) and cubic ($k = 3$) approximation polynomials. Except for the case $k = 0$, we observe that the region of instability will be increased if the polynomial degree is increased.

Since the spectral radius can only be calculated numerically, it cannot be proven that the implicit schemes are $A(\alpha)$-stable. However, further simulations, which are not shown here, indicate that the implicit schemes are also stable for very large values of $\overline{\Lambda}_{r1}$ and $\overline{\Lambda}_{i1}$.

Figure 3.3 and Figure 3.4 also exhibit that for the force/displacement- and especially for the displacement/displacement-coupling approach the region of instability for $k = 0$ is larger than for $k = 1$, which will not be the case if force/force-decomposition is applied.

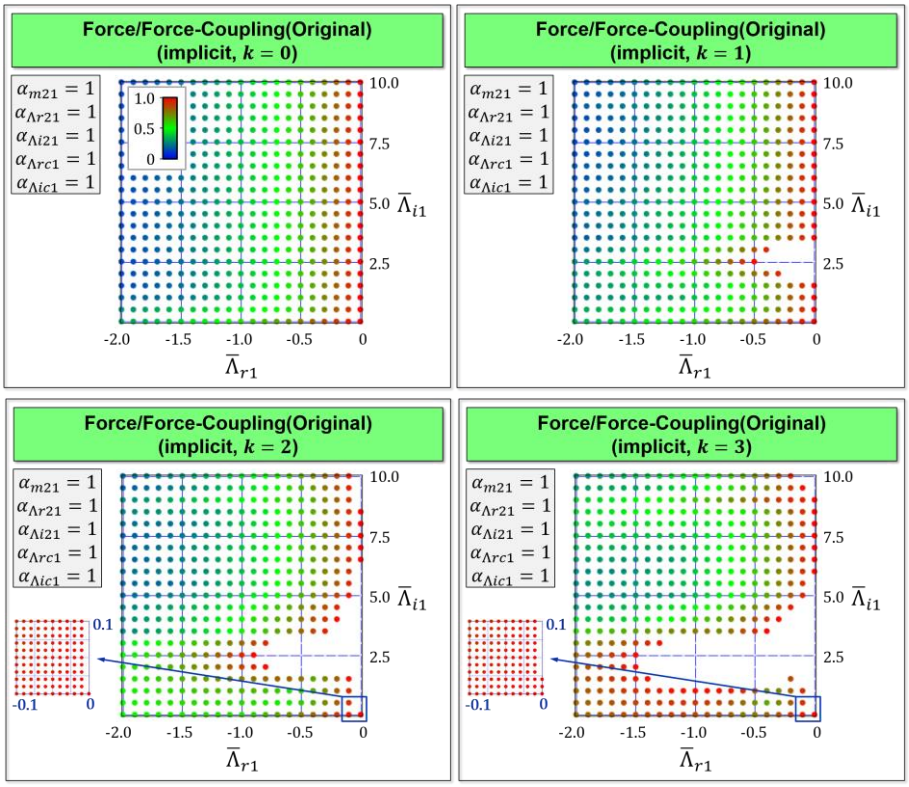

Figure 3.2 Stability plots for the implicit co-simulation approach (force/force-decomposition)

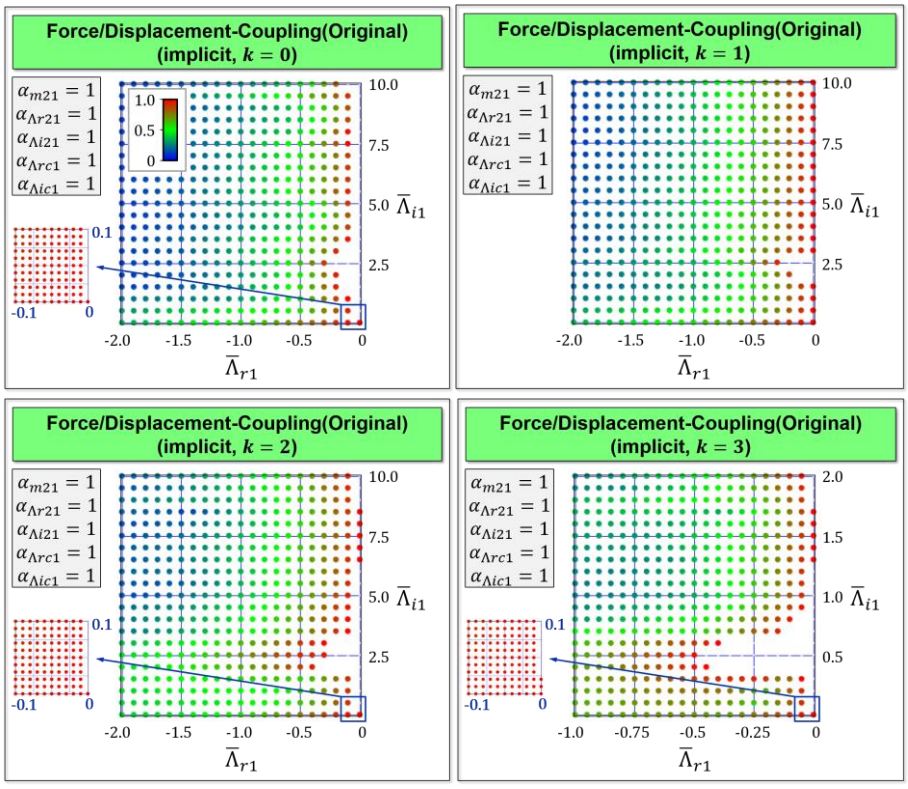

Figure 3.3 Stability plots for the implicit co-simulation approach (force/displacement-decomposition)

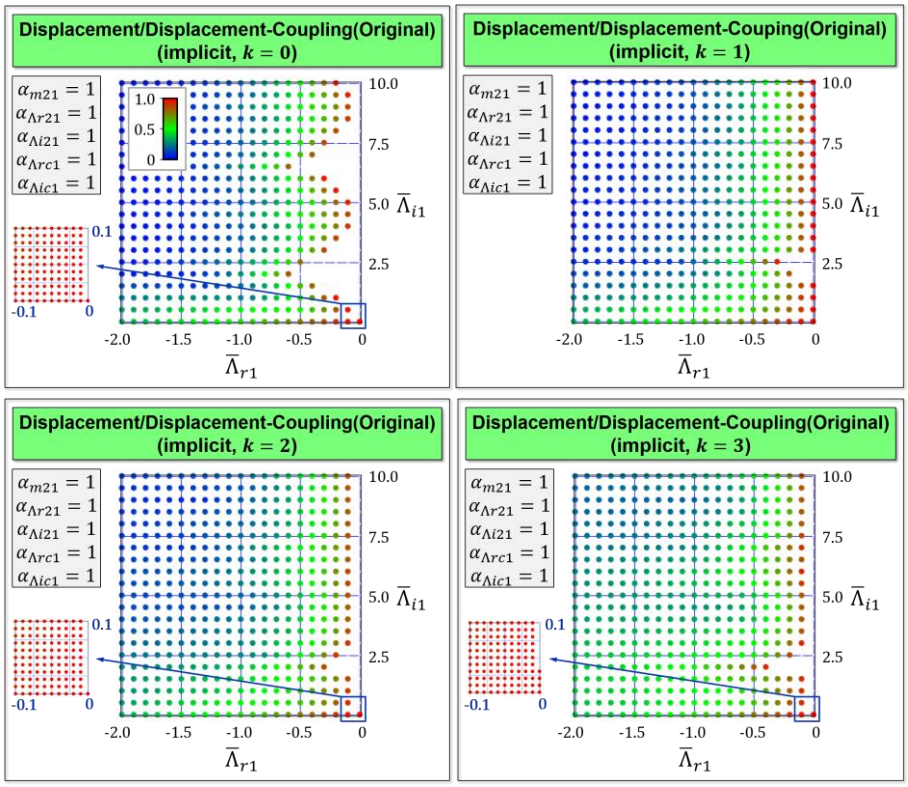

Figure 3.4 Stability plots for the implicit co-simulation approach (displacement/displacement-decomposition)

3.2.2. Stability Plots for Explicit Co-Simulation Approach

Figure 3.5 - Figure 3.7 collect 2D stability diagrams for the explicit co-simulation schemes. As shown in the previous section, plots for different approximation polynomials ($k = 0,1,2,3$) are presented for the 3 decomposition techniques. The reduced stability of the explicit schemes compared with their implicit counterparts is obvious. The higher the order of approximation is, the more the stable region is reduced. For the considered set of parameters, the displacement/displacement-coupling approach exhibits the best stability behavior.

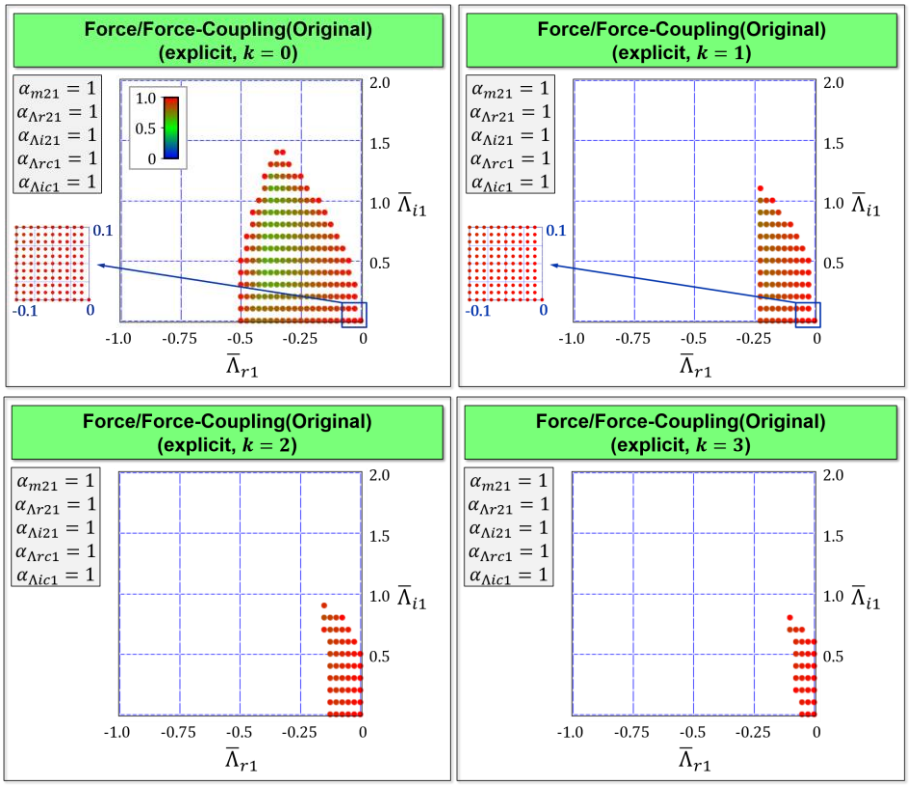

Figure 3.5 Stability plots for the explicit co-simulation approach (force/force-decomposition)

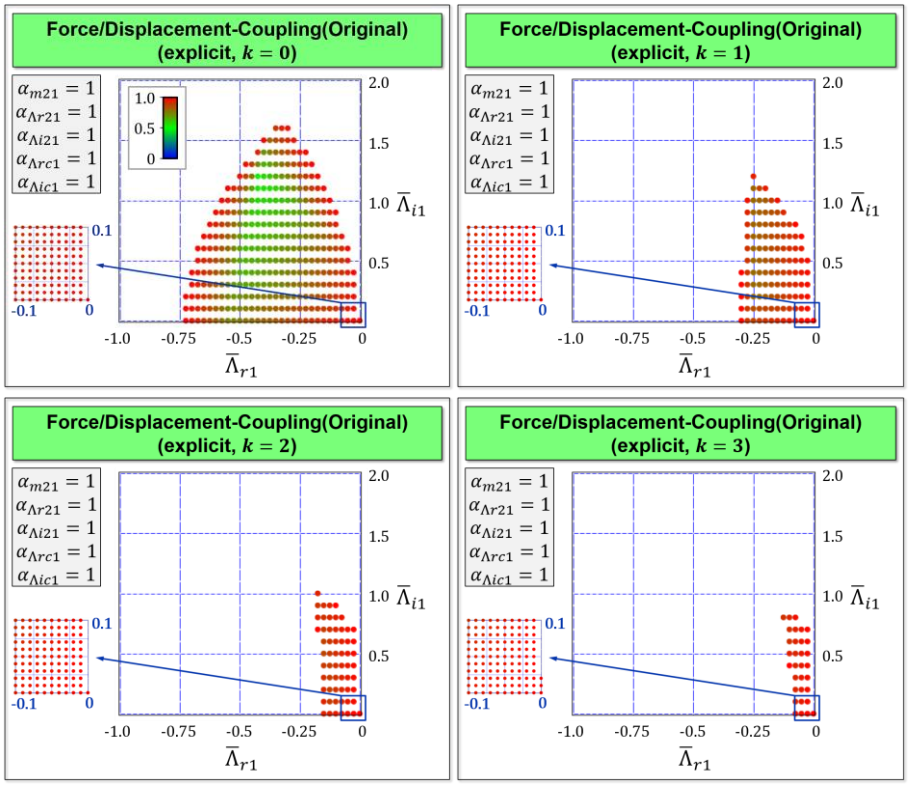

Figure 3.6 Stability plots for the explicit co-simulation approach (force/displacement-decomposition)

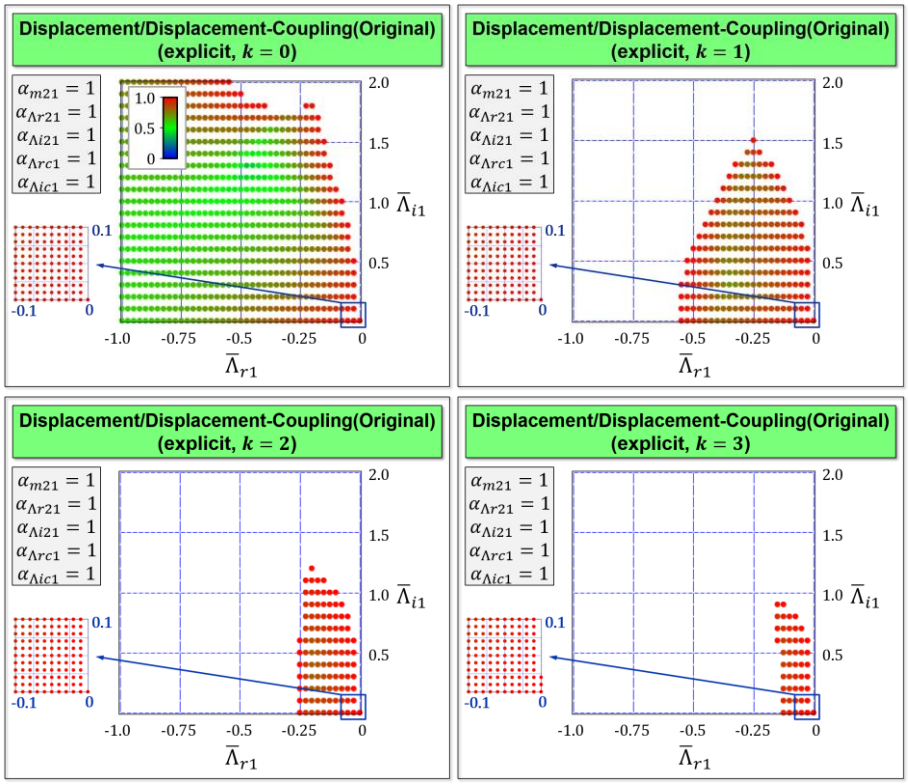

Figure 3.7 Stability plots for the explicit co-simulation approach (displacement/displacement-decomposition)

The above collected stability plots were generated with the symmetrical co-simulation test model. Further studies – which are not presented here – show that the 5 parameters $\alpha_{m21}, \alpha_{\Lambda r21}, \alpha_{\Lambda i21}, \alpha_{\Lambda rc1}$ and $\alpha_{\Lambda ic1}$, which characterize the asymmetry of the co-simulation test model, may have a significant influence on the stability behavior of the explicit and the implicit co-simulation approaches.

3.2.3. Convergence Plots

In this section, convergence plots are collected for the symmetrical co-simulation test model $(m_1 = m_2 = 1, c_1 = c_2 = c_c = 1000, d_1 = d_2 = d_c = 10)$. These plots may especially be interesting and helpful for the implementation of co-simulation methods with variable macro-step sizes, since therefore an error estimator for the local error is required. In this work, the relative global error for the position variables x_1/x_2 is calculated according to the normalized root mean square error (NRMSE)

$$\varepsilon_{pos,glo} = \sqrt{\frac{\sum_N \left(x_{1,glo}(T_N) - x_{1,N}\right)^2}{\sum_N \left(x_{1,glo}(T_N) - x_{1,mean}\right)^2} + \frac{\sum_N \left(x_{2,glo}(T_N) - x_{2,N}\right)^2}{\sum_N \left(x_{2,glo}(T_N) - x_{2,mean}\right)^2}}$$

$$\text{with } x_{1,glo}(T_N) = \int_{T_0}^{T_N} v_1(t)dt + x_1(T_0), \quad x_{2,glo}(T_N) = \int_{T_0}^{T_N} v_2(t)dt + x_2(T_0),$$

$$x_{1,mean} = \sum_N \frac{x_{1,glo}(T_N)}{N_{total}}, \quad x_{2,mean} = \sum_N \frac{x_{2,glo}(T_N)}{N_{total}} \quad . \tag{3.34}$$

In the above equation, the values $x_{1,N}, x_{2,N}$ denote the co-simulation results at the macro-time point T_N (solution of the governing recurrence system) and $x_{1,glo}(T_N), x_{2,glo}(T_N)$ the values of the analytical solution, which are integrated analytically from T_0 to T_N. N_{total} represents the total number of macro-steps. The global error $\varepsilon_{vel,glo}$ of the velocity variables v_1, v_2 are computed in a similar manner.

The local error for the position variables x_1/x_2 is calculated by

$$\varepsilon_{pos,loc} = \sqrt{\frac{\sum_N \left(x_{1,loc}(T_N) - x_{1,N}\right)^2}{\sum_N \left(x_{1,loc}(T_N) - x_{1,mean}\right)^2} + \frac{\sum_N \left(x_{2,loc}(T_N) - x_{2,N}\right)^2}{\sum_N \left(x_{2,loc}(T_N) - x_{2,mean}\right)^2}} \tag{3.35}$$

$$\text{with } x_{1,loc}(T_N) = \int_{T_{N-1}}^{T_N} v_1(t)dt + x_{1,N-1},\ x_{2,loc}(T_N) = \int_{T_{N-1}}^{T_N} v_2(t)dt + x_{2,N-1},$$

$$x_{1,mean} = \sum_N \frac{x_{1,loc}(T_N)}{N_{total}}, \qquad x_{2,mean} = \sum_N \frac{x_{2,loc}(T_N)}{N_{total}}.$$

where $x_{1,loc}(T_N), x_{2,loc}(T_N)$ term the values of the reference solution. The related local errors for the velocity variables $\varepsilon_{vel,loc}$ are calculated in a similar manner.

Figure 3.8 shows the global errors $\varepsilon_{pos,glo}$, $\varepsilon_{vel,glo}$ for the position and velocity variables with respect to the implicit force/force co-simulation approach for $k = 0, 1, 2, 3$. We can see that the global errors $\varepsilon_{pos,glo}$, $\varepsilon_{vel,glo}$ converge with $\mathcal{O}(h^{k+1})$ and that the magnitudes of position and velocity are almost on the same level.

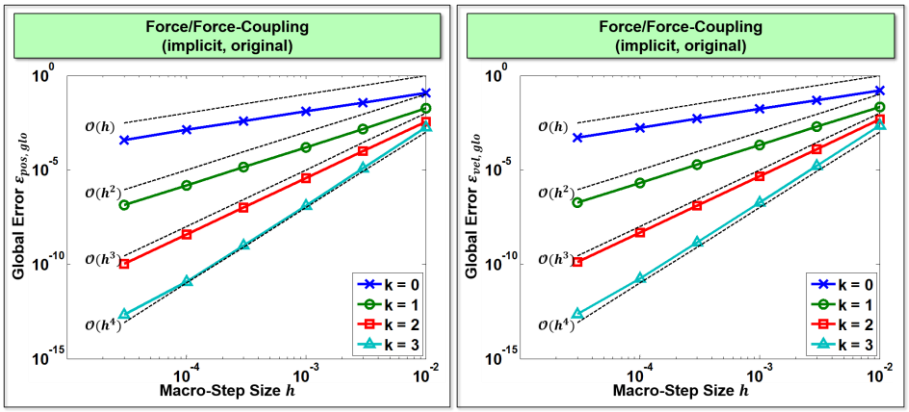

Figure 3.8 Global error plots for the implicit co-simulation approach (force/force-decomposition)

The local errors $\varepsilon_{pos,loc}$, $\varepsilon_{vel,loc}$ for the implicit force/force co-simulation approach are shown in Figure 3.9. $\varepsilon_{pos,loc}$, $\varepsilon_{vel,loc}$ converge with $\mathcal{O}(h^{k+3})$ and $\mathcal{O}(h^{k+2})$, respectively.

The convergence plots for the force/displacement- and the displacement/displacement coupling approach (not shown here) exhibit a quite similar behavior with the same convergence order and similar magnitudes.

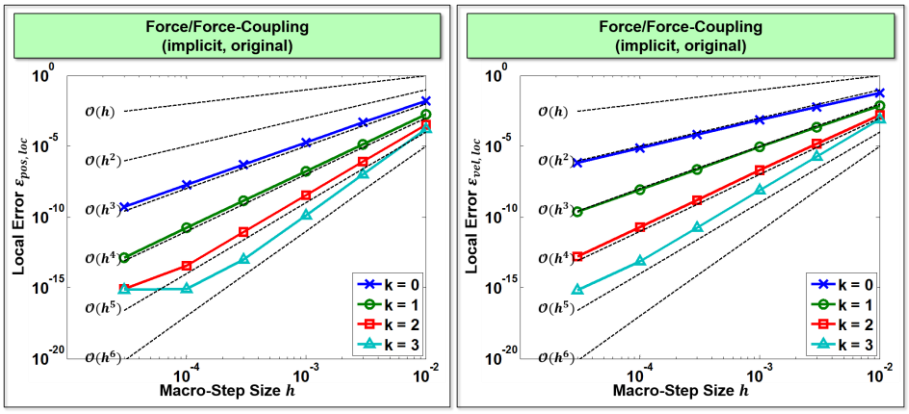

Figure 3.9 Local error plots for the implicit co-simulation approach using force/force-decomposition

A study on the convergence of the explicit co-simulation approaches (not presented here) has shown that the convergence behavior is very similar to the implicit case. However, larger error magnitudes are observed, especially for higher approximation polynomials.

3.3. Nonlinear Example: Planar Four-Bar Mechanism

In the previous sections, co-simulation methods have been investigated with respect to their numerical stability and convergence behavior. For investigating the numerical stability, Dahlquist´s stability theory based on a linear test model has been applied and extended to co-simulation approaches. In order to demonstrate the applicability of the presented co-simulation methods to more complicated problems, we now analyze a nonlinear model. The investigated system can be considered as a planar four-bar mechanism, see Figure 3.10. The middle bar is split into two parts, which are connected by a 3-DOF bushing element (stiffnesses $c_{cx}, c_{cy}, c_{c\varphi}$; damping coefficients $d_{cx}, d_{cy}, d_{c\varphi}$). The first subsystem contains bar 1 ($m_1 = 1\,\mathrm{kg}, J_1 = 1/12\,\mathrm{kg}\cdot\mathrm{m}^2, l_1 = 1\,\mathrm{m}$) and the left part of the middle bar ($m_2 = 1\,\mathrm{kg}, J_2 = 1/12\,\mathrm{kg}\cdot\mathrm{m}^2, l_2 = 1\,\mathrm{m}$). The second subsystem is represented by the right part of the middle bar ($m_3 = 1\,\mathrm{kg}, J_3 = 1/12\,\mathrm{kg}\cdot\mathrm{m}^2, l_3 = 1\,\mathrm{m}$) and by bar 4 ($m_4 = 2\,\mathrm{kg}, J_4 = 2/3\,\mathrm{kg}\cdot\mathrm{m}^2, l_4 = 2\,\mathrm{m}$). A linear viscous damping force is applied at the center of mass of all four bars (damping coefficients $d_x = d_y = 0.1\,\mathrm{Ns/m}$). Gravity is acting in positive y-direction ($g = 9.81\,\mathrm{m/s}^2$). Subsystem 1 and 2 are both mathematically described by a DAE system, which has been integrated numerically with an implicit Runge-Kutta integrator. As initial conditions, $\varphi_{1,0} = \frac{\pi}{4}\,\mathrm{rad}$ and $\dot{\varphi}_{1,0} = 0\,\mathrm{rad/s}$ have been chosen.

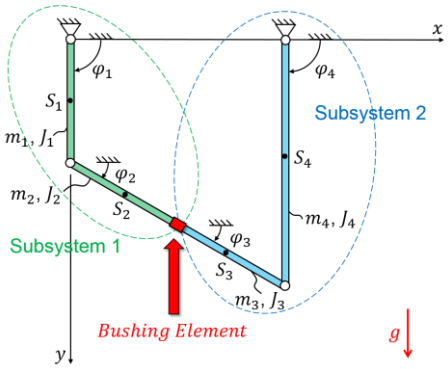

Figure 3.10 Planar four-bar mechanism: Interpretation as two double pendulums coupled by a bushing element

Simulation results for the three decomposition approaches (force/force-, force/displacement- and displacement/displacement decomposition; semi-implicit) with constant $(k = 0)$, linear $(k = 1)$ and quadratic $(k = 2)$ approximation polynomials are collected in Figure 3.11.

Depicted are the rotation angles $\varphi_2(t)$ and $\varphi_4(t)$ of bar 2 and bar 4, the corresponding angular velocities $\dot{\varphi}_2(t)$ and $\dot{\varphi}_4(t)$, the coupling force $\lambda_{cx}(t) = c_{cx} \cdot \big((x_3 - 0.5 \cdot l_3 \cdot \cos\varphi_3) - (x_2 + 0.5 \cdot l_2 \cdot \cos\varphi_2)\big) + d_{cx} \cdot \big((\dot{x}_3 + 0.5 \cdot l_3 \cdot \sin\varphi_3 \cdot \dot{\varphi}_3) - (\dot{x}_2 - 0.5 \cdot l_2 \cdot \sin\varphi_2 \cdot \dot{\varphi}_2)\big)$ acting in the bushing element in x-direction as well as the coupling torque $\lambda_{c\varphi}(t) = c_{c\varphi} \cdot (\varphi_3 - \varphi_2) + d_{c\varphi} \cdot (\dot{\varphi}_3 - \dot{\varphi}_2)$. It should be mentioned that the bushing stiffnesses have been set to $c_{cx} = c_{cy} = 1E3\ N/m$ and $c_{c\varphi} = 1E3\ Nm/rad$, the damping parameters of the bushing have assumed to be $d_{cx} = d_{cy} = 10\ Ns/m$ and $d_{c\varphi} = 10\ Nms/rad$. The co-simulations have been carried out with the constant macro-step size $H = 1E-4\ s$. The reference solution has been calculated numerically with a monolithic model. As can be seen, all semi-implicit co-simulation results show a good agreement with the reference solution.

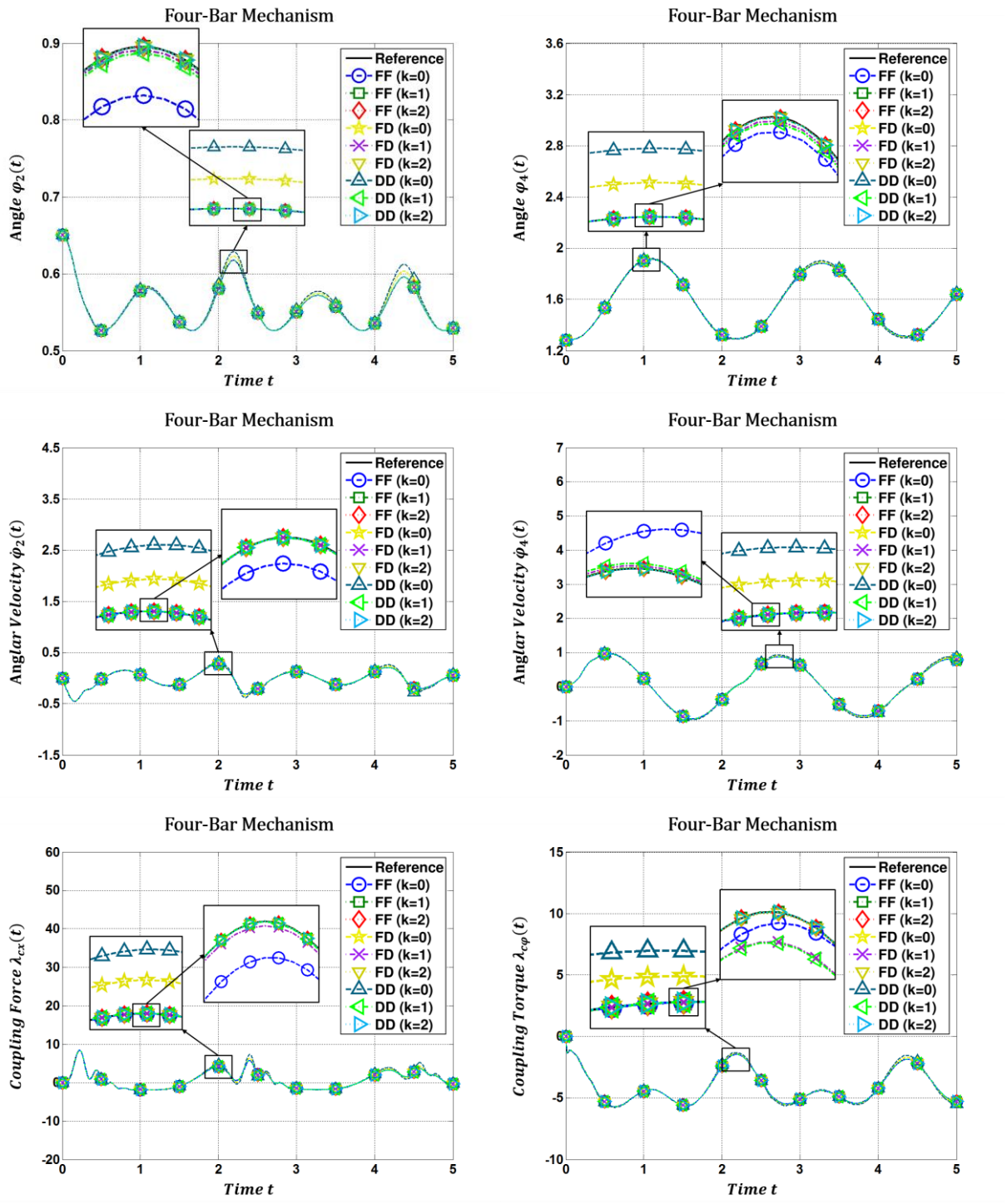

Figure 3.11 Simulation results for the four-bar mechanism based on force/force-decomposition (original methods, semi-implicit): Rotation angles $\varphi_2(t), \varphi_4(t)$ and angular velocities $\dot{\varphi}_2(t), \dot{\varphi}_4(t)$; coupling force $\lambda_{cx}(t)$ and coupling torque $\lambda_{c\varphi}(t)$

3.4. Implicit Co-Simulation Approaches with Improved Numerical Stability

The numerical stability of implicit co-simulation approaches (here called original methods, based on standard Lagrange approximation techniques) have been fully analyzed in the previous sections. We have observed that the region of stability is significantly larger compared with the explicit methods. Nevertheless, unstable regions are also observed for the original implicit methods, especially for unsymmetrical models (i.e. for the case $\alpha_{m21}, \alpha_{\Lambda r21}, \alpha_{\Lambda i21}, \alpha_{\Lambda rc1}, \alpha_{\Lambda ic1} \neq 1$). In this section, we will present implicit co-simulation methods with improved stability properties. Enhanced stability behavior can be achieved by extending the coupling conditions, i.e. by taking into account derivatives and integrals of the constitutive equations. As a consequence, additional coupling variables have to be taken into account. Results are presented for all three possible decomposition approaches.

3.4.1. Implicit Force/Force Co-Simulation Approach: D-Extension

For the original (non-extended) co-simulation method, only the coupling condition $\bar{g}_{c\lambda}$ is required and the coupling force $\bar{\lambda}_c$ is only discretized at the macro-time points $\bar{T}_N$, $\bar{T}_{N+1}$, etc.. The key idea of the D-extended co-simulation approach is to consider not only the coupling condition $\bar{g}_{c\lambda}$, but also its time derivative $\bar{g}'_{c\lambda}$. Therefore, the coupling force $\bar{\lambda}_c$ is also discretized at the time points $\bar{T}_{N+1/2}$, $\bar{T}_{N+3/2}$, etc. by introducing the additional variables $\bar{\lambda}_{c,N+1/2}$, $\bar{\lambda}_{c,N+3/2}$, etc.. As a consequence of this approach, both $\bar{g}_{c\lambda}$ and $\bar{g}'_{c\lambda}$ can be enforced at the macro-time points $\bar{T}_N$, $\bar{T}_{N+1}$, etc..

Based on the dimensionless formulation of the co-simulation test model, the decomposed D-extended system is mathematically defined by

Subsystem 1:

$$\begin{aligned} \bar{x}_1' &= \bar{v}_1 \\ \bar{v}_1' &= -\bar{c}_1 \cdot \bar{x}_1 - \bar{d}_1 \cdot \bar{v}_1 + \bar{\lambda}_c \end{aligned} \tag{3.36a}$$

Subsystem 2:

$$\begin{aligned} \bar{x}_2' &= \bar{v}_2 \\ \bar{v}_2' &= -\frac{\alpha_{c21}}{\alpha_{m21}} \cdot \bar{c}_1 \cdot \bar{x}_2 - \frac{\alpha_{d21}}{\alpha_{m21}} \cdot \bar{d}_1 \cdot \bar{v}_2 - \frac{1}{\alpha_{m21}} \bar{\lambda}_c \end{aligned} \tag{3.36b}$$

Coupling conditions:

$$\begin{aligned} \bar{g}_{c\lambda} &:= \bar{\lambda}_c - \alpha_{cc1} \cdot \bar{c}_1 \cdot (\bar{x}_2 - \bar{x}_1) - \alpha_{dc1} \cdot \bar{d}_1 \cdot (\bar{v}_2 - \bar{v}_1) = 0 \\ \bar{g}'_{c\lambda} &:= \bar{\lambda}'_c - \alpha_{cc1} \cdot \bar{c}_1 \cdot (\bar{v}_2 - \bar{v}_1) - \alpha_{dc1} \cdot \bar{d}_1 \cdot (\bar{v}_2' - \bar{v}_1') = 0 \ . \end{aligned} \tag{3.36c}$$

In the following analysis, we consider the general macro-step from $\bar{T}_N$ to $\bar{T}_{N+1}$ to derive the recurrence equations system for the discretized co-simulation test model. In order to accomplish the subsystem integration from $\bar{T}_N$ to $\bar{T}_{N+1}$, the coupling variable $\bar{\lambda}_c(\bar{t})$ has to be approximated in the time interval $[\bar{T}_N,\ \bar{T}_{N+1}]$. With respect to the approximation order, we discuss three cases, namely constant $(k = 0)$, linear $(k = 1)$, and quadratic $(k = 2)$ approximation. Therefore, it is useful to define the three functions $C(\bar{t})$, $L(\bar{t})$ and $Q(\bar{t})$. Firstly, we consider the Lagrange polynomial P of degree

k, which is specified by $k+1$ sampling points. By using the $k+1$ sampling points $(\bar{T}_{N+1}, \bar{\lambda}_{c,N+1})$, $(\bar{T}_N, \bar{\lambda}_{c,N})$, …, $(\bar{T}_{N-k+1}, \bar{\lambda}_{c,N-k+1})$, for instance, we obtain a polynomial of degree k, which is abbreviated by $P_{\bar{\lambda}_c}[(\bar{T}_{N+1}, \bar{\lambda}_{c,N+1}), (\bar{T}_N, \bar{\lambda}_{c,N}), \ldots, (\bar{T}_{N-k+1}, \bar{\lambda}_{c,N-k+1}); \bar{t}]$. For the case of constant approximation, it is useful to define the piecewise constant function $C_{\bar{\lambda}_c}(\bar{t})$ in the time interval $[\bar{T}_N, \bar{T}_{N+1}]$ according to

$$C_{\bar{\lambda}_c}[\bar{\lambda}_{c,N+1}, \bar{\lambda}_{c,N+1/2}; \bar{t}] = \begin{cases} \bar{\lambda}_{c,N+1/2} & \text{for} \quad \bar{t} \in [\bar{T}_N, \bar{T}_{N+1/2}] \\ \bar{\lambda}_{c,N+1} & \text{for} \quad \bar{t} \in [\bar{T}_{N+1/2}, \bar{T}_{N+1}] \end{cases}, \tag{3.37}$$

where $\bar{\lambda}_{c,N+1}$ and $\bar{\lambda}_{c,N+1/2}$ denote the values of the coupling variable at the time points $\bar{T}_{N+1}$ and $\bar{T}_{N+1/2}$. Using linear approximation, definition of the piecewise linear function $L_{\bar{\lambda}_c}(\bar{t})$ in the time interval $[\bar{T}_N, \bar{T}_{N+1}]$ according to

$$\begin{aligned} &L_{\bar{\lambda}_c}[\bar{\lambda}_{c,N+1}, \bar{\lambda}_{c,N+1/2}, \bar{\lambda}_{c,N}; \bar{t}] \\ &= \begin{cases} P_{\bar{\lambda}_c}[(\bar{T}_{N+1/2}, \bar{\lambda}_{c,N+1/2}), (\bar{T}_N, \bar{\lambda}_{c,N}); \bar{t}] & \text{for} \quad \bar{t} \in [\bar{T}_N, \bar{T}_{N+1/2}] \\ P_{\bar{\lambda}_c}[(\bar{T}_{N+1}, \bar{\lambda}_{c,N+1}), (\bar{T}_{N+1/2}, \bar{\lambda}_{c,N+1/2}); \bar{t}] & \text{for} \quad \bar{t} \in [\bar{T}_{N+1/2}, \bar{T}_{N+1}]' \end{cases} \end{aligned} \tag{3.38}$$

is helpful, where $\bar{\lambda}_{c,N+1}, \bar{\lambda}_{c,N+1/2}$ and $\bar{\lambda}_{c,N}$ denote the values of the coupling variable at the time points $\bar{T}_{N+1}, \bar{T}_{N+1/2}$ and $\bar{T}_N$, see Figure 3.12. For the case of quadratic approximation, three sampling points $(\bar{T}_{N+1}, \bar{\lambda}_{c,N+1})$, $(\bar{T}_{N+1/2}, \bar{\lambda}_{c,N+1/2})$ and $(\bar{T}_N, \bar{\lambda}_{c,N})$ are used to generate the quadratic approximation polynomial

$$\begin{aligned} &Q_{\bar{\lambda}_c}[\bar{\lambda}_{c,N+1}, \bar{\lambda}_{c,N+1/2}, \bar{\lambda}_{c,N}; \bar{t}] \\ &= P_{\bar{\lambda}_c}[(\bar{T}_{N+1}, \bar{\lambda}_{c,N+1}), (\bar{T}_{N+1/2}, \bar{\lambda}_{c,N+1/2}), (\bar{T}_N, \bar{\lambda}_{c,N}); \bar{t}] \quad \text{for} \quad \bar{t} \in [\bar{T}_N, \bar{T}_{N+1}] \ . \end{aligned} \tag{3.39}$$

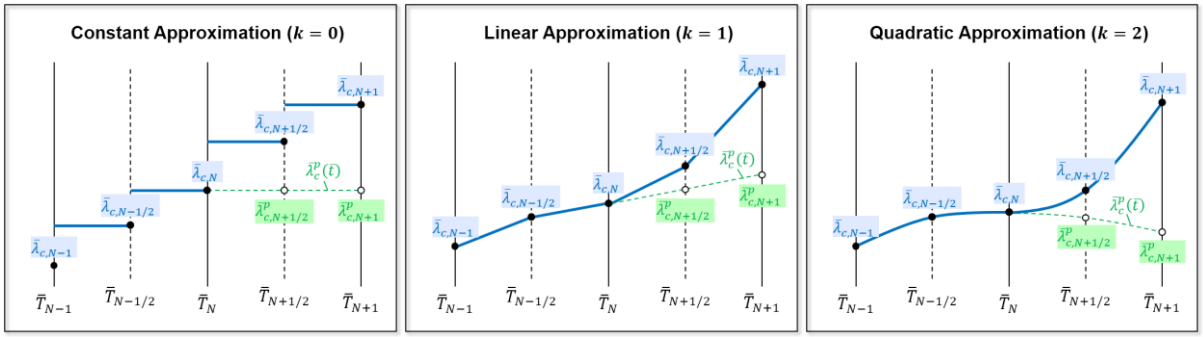

Figure 3.12 Extrapolation and interpolation functions for constant, linear and quadratic approximation.

At the macro-time point $\bar{T}_N$, we assume again that the state variables and the coupling variable are known

$$\begin{aligned} \bar{x}_1(\bar{t} = \bar{T}_N) &= \bar{x}_{1,N}\,, \qquad \bar{v}_1(\bar{t} = \bar{T}_N) = \bar{v}_{1,N}\,, \\ \bar{x}_2(\bar{t} = \bar{T}_N) &= \bar{x}_{2,N}\,, \qquad \bar{v}_2(\bar{t} = \bar{T}_N) = \bar{v}_{2,N}\,, \end{aligned} \tag{3.40a}$$

$$\bar{\lambda}_c(\bar{t} = \bar{T}_N) = \bar{\lambda}_{c,N}. \tag{3.40b}$$

The implicit (semi-implicit) extended co-simulation methods investigated here are based on a predictor/corrector approach to be accomplished in 3 steps.

Step 1: Predictor Step

By analytically integrating subsystem 1 and subsystem 2 from $\bar{T}_N$ to $\bar{T}_{N+1}$ using the initial conditions (3.40a) and the predictor (extrapolation) function

$$\bar{\lambda}_c^p(\bar{t}) = \begin{cases} \bar{\lambda}_{c,N} & (k=0) \\ P_{\bar{\lambda}_c}\left[\left(\bar{T}_N, \bar{\lambda}_{c,N}\right), \left(\bar{T}_{N-1/2}, \bar{\lambda}_{c,N-1/2}\right); \bar{t}\right] & (k=1) \\ Q_{\bar{\lambda}_c}\left[\bar{\lambda}_{c,N}, \bar{\lambda}_{c,N-1/2}, \bar{\lambda}_{c,N-1}; \bar{t}\right] & (k=2) \end{cases} \tag{3.41}$$

we get the predicted state variables at the macro-time point $\bar{T}_{N+1}$

$$\begin{aligned} \bar{x}_{1,N+1}^p &= \bar{x}_{1,N+1}^p\left(\bar{\lambda}_{c,N}, \bar{\lambda}_{c,N-1/2}, \bar{\lambda}_{c,N-1}, \boldsymbol{z}_N\right), \\ \bar{v}_{1,N+1}^p &= \bar{v}_{1,N+1}^p\left(\bar{\lambda}_{c,N}, \bar{\lambda}_{c,N-1/2}, \bar{\lambda}_{c,N-1}, \boldsymbol{z}_N\right), \\ \bar{x}_{2,N+1}^p &= \bar{x}_{2,N+1}^p\left(\bar{\lambda}_{c,N}, \bar{\lambda}_{c,N-1/2}, \bar{\lambda}_{c,N-1}, \boldsymbol{z}_N\right), \\ \bar{v}_{2,N+1}^p &= \bar{v}_{2,N+1}^p\left(\bar{\lambda}_{c,N}, \bar{\lambda}_{c,N-1/2}, \bar{\lambda}_{c,N-1}, \boldsymbol{z}_N\right). \end{aligned} \tag{3.42}$$

Note that for the case of constant approximation, the predicted states only depend on $\bar{\lambda}_{c,N}$ and for linear approximation only on $\bar{\lambda}_{c,N}$ and $\bar{\lambda}_{c,N-1/2}$. In the following representation, we generally use the arguments for the case of quadratic approximation.

It should be stressed that alternative approaches might be used for extrapolating the coupling variable. For $k=0$, the extrapolation function $C_{\bar{\lambda}_c}\left[2\,\bar{\lambda}_{c,N} - \bar{\lambda}_{c,N-1/2}, \bar{\lambda}_{c,N};\, \bar{t}\right]$ may be used, for instance. For $k=1$, the linear function $P_{\bar{\lambda}_c}\left[\left(\bar{T}_N, \bar{\lambda}_{c,N}\right), \left(\bar{T}_{N-1}, \bar{\lambda}_{c,N-1}\right);\, \bar{t}\right]$ could alternatively be applied. For $k=2$, the quadratic polynomial $Q_{\bar{\lambda}_c}\left[\bar{\lambda}_{c,N}, \bar{\lambda}_{c,N-1}, \bar{\lambda}_{c,N-2};\, \bar{t}\right]$ might also be chosen. For nonlinear problems, the usage of different extrapolation functions may affect the accuracy of a semi-implicit co-simulation approach.

Step 2: Calculation of Corrected Coupling Forces

An analytical integration of subsystem 1 and subsystem 2 from $\bar{T}_N$ to $\bar{T}_{N+1}$ with the initial conditions (3.40a) and the interpolation polynomials

$$\bar{\lambda}_c^*(\bar{t}) = \begin{cases} C_{\bar{\lambda}_c}\left[\bar{\lambda}_{c,N+1}^*, \bar{\lambda}_{c,N+1/2}^*; \bar{t}\right] & (k=0) \\ L_{\bar{\lambda}_c}\left[\bar{\lambda}_{c,N+1}^*, \bar{\lambda}_{c,N+1/2}^*, \bar{\lambda}_{c,N}; \bar{t}\right] & (k=1) \\ Q_{\bar{\lambda}_c}\left[\bar{\lambda}_{c,N+1}^*, \bar{\lambda}_{c,N+1/2}^*, \bar{\lambda}_{c,N}; \bar{t}\right] & (k=2) \end{cases} \tag{3.43}$$

yields the state variables at the macro-time point $\bar{T}_{N+1}$

$$
\begin{aligned}
\bar{x}^*_{1,N+1} &= \bar{x}^*_{1,N+1}\left(\bar{\lambda}^*_{c,N+1}, \bar{\lambda}^*_{c,N+1/2}, \bar{\lambda}_{c,N}, \boldsymbol{z}_N\right),\\
\bar{v}^*_{1,N+1} &= \bar{v}^*_{1,N+1}\left(\bar{\lambda}^*_{c,N+1}, \bar{\lambda}^*_{c,N+1/2}, \bar{\lambda}_{c,N}, \boldsymbol{z}_N\right),\\
\bar{x}^*_{2,N+1} &= \bar{x}^*_{2,N+1}\left(\bar{\lambda}^*_{c,N+1}, \bar{\lambda}^*_{c,N+1/2}, \bar{\lambda}_{c,N}, \boldsymbol{z}_N\right),\\
\bar{v}^*_{2,N+1} &= \bar{v}^*_{2,N+1}\left(\bar{\lambda}^*_{c,N+1}, \bar{\lambda}^*_{c,N+1/2}, \bar{\lambda}_{c,N}, \boldsymbol{z}_N\right).
\end{aligned}
\tag{3.44}
$$

It should be mentioned that $\bar{\lambda}^*_{c,N+1}$ and $\bar{\lambda}^*_{c,N+1/2}$ denote arbitrary coupling forces at the time points $\bar{T}_{N+1}$ and $\bar{T}_{N+1/2}$.

Differentiating the state variables of Eq. (3.44) and the corresponding acceleration variables $\bar{v}'^*_{1,N+1}$ and $\bar{v}'^*_{2,N+1}$ with respect to $\bar{\lambda}^*_{c,N+1}$, one gets the partial derivatives

$$
\begin{aligned}
&\frac{\partial \bar{x}^*_{1,N+1}}{\partial \bar{\lambda}^*_{c,N+1}} = \text{const.}, \qquad
\frac{\partial \bar{v}^*_{1,N+1}}{\partial \bar{\lambda}^*_{c,N+1}} = \text{const.}, \qquad
\frac{\partial \bar{v}'^*_{1,N+1}}{\partial \bar{\lambda}^*_{c,N+1}} = \text{const.},\\
&\frac{\partial \bar{x}^*_{2,N+1}}{\partial \bar{\lambda}^*_{c,N+1}} = \text{const.}, \qquad
\frac{\partial \bar{v}^*_{2,N+1}}{\partial \bar{\lambda}^*_{c,N+1}} = \text{const.}, \qquad
\frac{\partial \bar{v}'^*_{2,N+1}}{\partial \bar{\lambda}^*_{c,N+1}} = \text{const.}\ .
\end{aligned}
\tag{3.45}
$$

Similarly, the partial derivatives with respect to $\bar{\lambda}^*_{c,N+1/2}$ are calculated. It should be stressed that the partial derivatives are constant, since the state variables in Eq. (3.44) and the corresponding accelerations are linear functions of $\bar{\lambda}^*_{c,N+1}$ and $\bar{\lambda}^*_{c,N+1/2}$.

Making use of the partial derivatives, we can calculate corrected coupling forces $\bar{\lambda}_{c,N+1}$ and $\bar{\lambda}_{c,N+1/2}$ so that the coupling conditions $\bar{g}_{c\lambda}$ and $\bar{g}'_{c\lambda}$ are simultaneously fulfilled at the macro-time point $\bar{T}_{N+1}$. Regarding the fixed time point $\bar{T}_{N+1}$, $\bar{g}_{c\lambda,N+1}$ and $\bar{g}'_{c\lambda,N+1}$ can be considered as functions of the coupling forces $\bar{\lambda}^*_{c,N+1}$ and $\bar{\lambda}^*_{c,N+1/2}$, i.e.

$$
\begin{aligned}
&\bar{g}_{c\lambda,N+1}\left(\bar{\lambda}^*_{c,N+1}, \bar{\lambda}^*_{c,N+1/2}\right)\\
&\coloneqq \bar{\lambda}^*_{c,N+1} - \alpha_{cc1}\cdot\bar{c}_1\cdot\left(\bar{x}^*_{2,N+1}\left(\bar{\lambda}^*_{c,N+1}, \bar{\lambda}^*_{c,N+1/2}\right) - \bar{x}^*_{1,N+1}\left(\bar{\lambda}^*_{c,N+1}, \bar{\lambda}^*_{c,N+1/2}\right)\right)\\
&\qquad - \alpha_{dc1}\cdot\bar{d}_1\cdot\left(\bar{v}^*_{2,N+1}\left(\bar{\lambda}^*_{c,N+1}, \bar{\lambda}^*_{c,N+1/2}\right) - \bar{v}^*_{1,N+1}\left(\bar{\lambda}^*_{c,N+1}, \bar{\lambda}^*_{c,N+1/2}\right)\right),\\
&\bar{g}'_{c\lambda,N+1}\left(\bar{\lambda}^*_{c,N+1}, \bar{\lambda}^*_{c,N+1/2}\right)\\
&\coloneqq \bar{\lambda}'^*_{c,N+1} - \alpha_{cc1}\cdot\bar{c}_1\cdot\left(\bar{v}^*_{2,N+1}\left(\bar{\lambda}^*_{c,N+1}, \bar{\lambda}^*_{c,N+1/2}\right) - \bar{v}^*_{1,N+1}\left(\bar{\lambda}^*_{c,N+1}, \bar{\lambda}^*_{c,N+1/2}\right)\right)\\
&\qquad - \alpha_{dc1}\cdot\bar{d}_1\cdot\left(\bar{v}'^*_{2,N+1}\left(\bar{\lambda}^*_{c,N+1}, \bar{\lambda}^*_{c,N+1/2}\right) - \bar{v}'^*_{1,N+1}\left(\bar{\lambda}^*_{c,N+1}, \bar{\lambda}^*_{c,N+1/2}\right)\right).
\end{aligned}
\tag{3.46}
$$

Because the state variables $\bar{x}^*_{1,N+1}$, $\bar{x}^*_{2,N+1}$, $\bar{v}^*_{1,N+1}$, $\bar{v}^*_{2,N+1}$ and the accelerations $\bar{v}'^*_{1,N+1}$, $\bar{v}'^*_{2,N+1}$ are only linear functions of $\bar{\lambda}^*_{c,N+1}$ and $\bar{\lambda}^*_{c,N+1/2}$, Eq. (3.46) can be rewritten as

$$
\begin{aligned}
&\bar{g}_{c\lambda,N+1}\left(\bar{\lambda}^{*}_{c,N+1},\bar{\lambda}^{*}_{c,N+1/2}\right)\\
&\coloneqq \bar{g}_{c\lambda,N+1}(\boldsymbol{e}^{p})+\left.\frac{\partial \bar{g}_{c\lambda,N+1}}{\partial \bar{\lambda}^{*}_{c,N+1}}\right|_{\boldsymbol{e}^{p}}\cdot\left(\bar{\lambda}^{*}_{c,N+1}-\bar{\lambda}^{p}_{c,N+1}\right)+\left.\frac{\partial \bar{g}_{c\lambda,N+1}}{\partial \bar{\lambda}^{*}_{c,N+1/2}}\right|_{\boldsymbol{e}^{p}}\\
&\qquad\cdot\left(\bar{\lambda}^{*}_{c,N+1/2}-\bar{\lambda}^{p}_{c,N+1/2}\right)\\
&=\bar{\lambda}^{p}_{c,N+1}-\alpha_{cc1}\cdot\bar{c}_{1}\cdot\left(\bar{x}^{p}_{2,N+1}-\bar{x}^{p}_{1,N+1}\right)-\ \alpha_{dc1}\cdot\bar{d}_{1}\cdot\left(\bar{v}^{p}_{2,N+1}-\bar{v}^{p}_{1,N+1}\right)\\
&+\left[1-\alpha_{cc1}\cdot\bar{c}_{1}\cdot\left(\frac{\partial\bar{x}^{*}_{2,N+1}}{\partial\bar{\lambda}^{*}_{c,N+1}}-\frac{\partial\bar{x}^{*}_{1,N+1}}{\partial\bar{\lambda}^{*}_{c,N+1}}\right)-\alpha_{dc1}\cdot\bar{d}_{1}\cdot\left(\frac{\partial\bar{v}^{*}_{2,N+1}}{\partial\bar{\lambda}^{*}_{c,N+1}}-\frac{\partial\bar{v}^{*}_{1,N+1}}{\partial\bar{\lambda}^{*}_{c,N+1}}\right)\right]\\
&\quad\cdot\left(\bar{\lambda}^{*}_{c,N+1}-\bar{\lambda}^{p}_{c,N+1}\right)\\
&+\left[-\alpha_{cc1}\cdot\bar{c}_{1}\cdot\left(\frac{\partial\bar{x}^{*}_{2,N+1}}{\partial\bar{\lambda}^{*}_{c,N+1/2}}-\frac{\partial\bar{x}^{*}_{1,N+1}}{\partial\bar{\lambda}^{*}_{c,N+1/2}}\right)-\alpha_{dc1}\cdot\bar{d}_{1}\cdot\left(\frac{\partial\bar{v}^{*}_{2,N+1}}{\partial\bar{\lambda}^{*}_{c,N+1/2}}-\frac{\partial\bar{v}^{*}_{1,N+1}}{\partial\bar{\lambda}^{*}_{c,N+1/2}}\right)\right]\\
&\quad\cdot\left(\bar{\lambda}^{*}_{c,N+1/2}-\bar{\lambda}^{p}_{c,N+1/2}\right),
\end{aligned}
\tag{3.47}
$$

$$
\begin{aligned}
&\bar{g}'_{c\lambda,N+1}\left(\bar{\lambda}^{*}_{c,N+1},\bar{\lambda}^{*}_{c,N+1/2}\right)\\
&\coloneqq \bar{g}'_{c\lambda,N+1}(\boldsymbol{e}^{p})+\left.\frac{\partial \bar{g}'_{c\lambda,N+1}}{\partial \bar{\lambda}^{*}_{c,N+1}}\right|_{\boldsymbol{e}^{p}}\cdot\left(\bar{\lambda}^{*}_{c,N+1}-\bar{\lambda}^{p}_{c,N+1}\right)+\left.\frac{\partial \bar{g}'_{c\lambda,N+1}}{\partial \bar{\lambda}^{*}_{c,N+1/2}}\right|_{\boldsymbol{e}^{p}}\\
&\qquad\cdot\left(\bar{\lambda}^{*}_{c,N+1/2}-\bar{\lambda}^{p}_{c,N+1/2}\right)\\
&=\bar{\lambda}'^{p}_{c,N+1}-\alpha_{cc1}\cdot\bar{c}_{1}\cdot\left(\bar{v}^{p}_{2,N+1}-\bar{v}^{p}_{1,N+1}\right)-\ \alpha_{dc1}\cdot\bar{d}_{1}\cdot\left(\bar{v}'^{p}_{2,N+1}-\bar{v}'^{p}_{1,N+1}\right)\\
&+\left[\frac{\partial\bar{\lambda}'^{*}_{c,N+1}}{\partial\bar{\lambda}^{*}_{c,N+1}}-\alpha_{cc1}\cdot\bar{c}_{1}\cdot\left(\frac{\partial\bar{v}^{*}_{2,N+1}}{\partial\bar{\lambda}^{*}_{c,N+1}}-\frac{\partial\bar{v}^{*}_{1,N+1}}{\partial\bar{\lambda}^{*}_{c,N+1}}\right)-\alpha_{dc1}\cdot\bar{d}_{1}\cdot\left(\frac{\partial\bar{v}'^{*}_{2,N+1}}{\partial\bar{\lambda}^{*}_{c,N+1}}-\frac{\partial\bar{v}'^{*}_{1,N+1}}{\partial\bar{\lambda}^{*}_{c,N+1}}\right)\right]\\
&\quad\cdot\left(\bar{\lambda}^{*}_{c,N+1}-\bar{\lambda}^{p}_{c,N+1}\right)\\
&+\left[\frac{\partial\bar{\lambda}'^{*}_{c,N+1}}{\partial\bar{\lambda}^{*}_{c,N+1/2}}-\alpha_{cc1}\bar{c}_{1}\left(\frac{\partial\bar{v}^{*}_{2,N+1}}{\partial\bar{\lambda}^{*}_{c,N+1/2}}-\frac{\partial\bar{v}^{*}_{1,N+1}}{\partial\bar{\lambda}^{*}_{c,N+1/2}}\right)-\alpha_{dc1}\bar{d}_{1}\left(\frac{\partial\bar{v}'^{*}_{2,N+1}}{\partial\bar{\lambda}^{*}_{c,N+1/2}}-\frac{\partial\bar{v}'^{*}_{1,N+1}}{\partial\bar{\lambda}^{*}_{c,N+1/2}}\right)\right]\\
&\quad\cdot\left(\bar{\lambda}^{*}_{c,N+1/2}-\bar{\lambda}^{p}_{c,N+1/2}\right),
\end{aligned}
\tag{3.47}
$$

where the vector $\boldsymbol{e}^{p}=\left(\bar{\lambda}^{p}_{c,N+1}\ \bar{\lambda}^{p}_{c,N+1/2}\right)^{T}$ collects the predicted coupling variables at the time points $\bar{T}_{N+1}$ and $\bar{T}_{N+1/2}$. The derivatives $\bar{\lambda}'^{p}_{c,N+1}\left(\bar{\lambda}_{c,N},\bar{\lambda}_{c,N-1/2},\bar{\lambda}_{c,N-1}\right)$ and $\bar{\lambda}'^{*}_{c,N+1}\left(\bar{\lambda}^{*}_{c,N+1},\bar{\lambda}^{*}_{c,N+1/2},\bar{\lambda}_{c,N}\right)$ are defined by Eq. (3.41) and (3.43), respectively. For the case of $k=0$ the derivatives have to be approximated, e.g. by using $\bar{\lambda}'^{p}_{c,N+1}=2\cdot\left(\bar{\lambda}_{c,N}-\bar{\lambda}_{c,N-1/2}\right)$ and $\bar{\lambda}'^{*}_{c,N+1}=2\cdot\left(\bar{\lambda}^{*}_{c,N+1}-\bar{\lambda}^{*}_{c,N+1/2}\right)$, respectively.

Setting $\bar{g}_{c\lambda,N+1}\left(\bar{\lambda}^{*}_{c,N+1},\bar{\lambda}^{*}_{c,N+1/2}\right)=0$ and $\bar{g}'_{c\lambda,N+1}\left(\bar{\lambda}^{*}_{c,N+1},\bar{\lambda}^{*}_{c,N+1/2}\right)=0$, we obtain the corrected coupling forces

$$
\begin{aligned}
&\bar{g}_{c\lambda,N+1}\left(\bar{\lambda}^{*}_{c,N+1},\bar{\lambda}^{*}_{c,N+1/2}\right)=0\\
&\bar{g}'_{c\lambda,N+1}\left(\bar{\lambda}^{*}_{c,N+1},\bar{\lambda}^{*}_{c,N+1/2}\right)=0
\end{aligned}
\quad\Rightarrow\quad \bar{\lambda}_{c,N+1},\ \bar{\lambda}_{c,N+1/2}\quad .
\tag{3.48}
$$

Note that for the reason of a clear representation, different variables have been used for the general coupling forces $\bar{\lambda}^{*}_{c,N+1},\bar{\lambda}^{*}_{c,N+1/2}$ at the time points $\bar{T}_{N+1}$ and $\bar{T}_{N+1/2}$ and the corrected coupling forces $\bar{\lambda}_{c,N+1},\ \bar{\lambda}_{c,N+1/2}$, which represent the roots of Eq. (3.47).

Step 3 Corrector Steps

Applying the interpolation function

$$\bar{\lambda}_c\,(\bar{t}) = \begin{cases} C_{\bar{\lambda}_c}\left[\bar{\lambda}_{c,N+1}, \bar{\lambda}_{c,N+1/2}; \bar{t}\right] & (k=0) \\ L_{\bar{\lambda}_c}\left[\bar{\lambda}_{c,N+1}, \bar{\lambda}_{c,N+1/2}, \bar{\lambda}_{c,N}; \bar{t}\right] & (k=1) \\ Q_{\bar{\lambda}_c}\left[\bar{\lambda}_{c,N+1}, \bar{\lambda}_{c,N+1/2}, \bar{\lambda}_{c,N}; \bar{t}\right] & (k=2) \end{cases} \tag{3.49}$$

with the corrected coupling forces $\bar{\lambda}_{c,N+1}$, $\bar{\lambda}_{c,N+1/2}$ from Eq. (3.48), an analytical integration of subsystem 1 and subsystem 2 from $\bar{T}_N$ to $\bar{T}_{N+1}$ with initial conditions (3.40a) yields the corrected state variables

$$\begin{aligned} \bar{x}_{1,N+1} &= \bar{x}_{1,N+1}\left(\bar{\lambda}_{c,N+1}, \bar{\lambda}_{c,N+1/2}, \bar{\lambda}_{c,N}, \boldsymbol{z}_N\right), \\ \bar{v}_{1,N+1} &= \bar{v}_{1,N+1}\left(\bar{\lambda}_{c,N+1}, \bar{\lambda}_{c,N+1/2}, \bar{\lambda}_{c,N}, \boldsymbol{z}_N\right), \\ \bar{x}_{2,N+1} &= \bar{x}_{2,N+1}\left(\bar{\lambda}_{c,N+1}, \bar{\lambda}_{c,N+1/2}, \bar{\lambda}_{c,N}, \boldsymbol{z}_N\right), \\ \bar{v}_{2,N+1} &= \bar{v}_{2,N+1}\left(\bar{\lambda}_{c,N+1}, \bar{\lambda}_{c,N+1/2}, \bar{\lambda}_{c,N}, \boldsymbol{z}_N\right). \end{aligned} \tag{3.50}$$

Using the corrected state variables of Eq. (3.50), derivation of a recurrence equations system, which only contains the state variables at the current and the previous macro-time point is easily accomplished. Eliminating $\bar{\lambda}_{c,N+1}$ and $\bar{\lambda}_{c,N}$ with the help of $\bar{g}_{c\lambda,N+1}$ and $\bar{g}_{c\lambda,N}$ as well as $\bar{\lambda}_{c,N+1/2}$ with the help of $\bar{g}'_{c\lambda,N+1}$, we obtain relationships of the form

$$\begin{aligned} \bar{x}_{1,N+1} &= \bar{x}_{1,N+1}(\boldsymbol{z}_{N+1}, \boldsymbol{z}_N), \qquad \bar{v}_{1,N+1} = \bar{v}_{1,N+1}(\boldsymbol{z}_{N+1}, \boldsymbol{z}_N), \\ \bar{x}_{2,N+1} &= \bar{x}_{2,N+1}(\boldsymbol{z}_{N+1}, \boldsymbol{z}_N), \qquad \bar{v}_{2,N+1} = \bar{v}_{2,N+1}(\boldsymbol{z}_{N+1}, \boldsymbol{z}_N). \end{aligned} \tag{3.51}$$

Therefore, an eigenvalue analysis can be performed using (3.51) that represents a system of 4 coupled linear recurrence equations of order 1

$$\boldsymbol{A}_{N+1} \cdot \boldsymbol{z}_{N+1} + \boldsymbol{A}_N \cdot \boldsymbol{z}_N = \boldsymbol{0}. \tag{3.52}$$

The real-valued matrices $\boldsymbol{A}_{N+1}, \boldsymbol{A}_N \in \mathbb{R}^{4\times4}$ are constant and depend only on the 7 parameters of the co-simulation test model introduced before. The stability properties can be determined by the spectral radius of the corresponding linear recurrence equations system and can be displayed in 2D stability plots as shown before.

3.4.2. Implicit Force/Force Co-Simulation Approach: I-Extension

The idea of the I-extended co-simulation approach is to simultaneously take into account the coupling condition $\bar{g}_{c\lambda}$ and its integral $\bar{G}_{c\lambda}$. To calculate $\bar{G}_{c\lambda}$, integrals of the position variables over the time $\bar{t}$ are required. Therefore, it is useful to extend the equations of motion by introducing the integrated position variables $\bar{p}_1 = \int \bar{x}_1\, d\bar{t}$ and $\bar{p}_2 = \int \bar{x}_2\, d\bar{t}$. The equations of motion for the decomposed I-extended co-simulation test model are given by

Subsystem 1:

$$\begin{aligned} \bar{p}_1' &= \bar{x}_1 \\ \bar{x}_1' &= \bar{v}_1 \\ \bar{v}_1' &= -\bar{c}_1 \cdot \bar{x}_1 - \bar{d}_1 \cdot \bar{v}_1 + \bar{\lambda}_c \end{aligned} \tag{3.53a}$$

Subsystem 2:

$$\begin{aligned} \bar{p}_2' &= \bar{x}_2 \\ \bar{x}_2' &= \bar{v}_2 \\ \bar{v}_2' &= -\frac{\alpha_{c21}}{\alpha_{m21}} \cdot \bar{c}_1 \cdot \bar{x}_2 - \frac{\alpha_{d21}}{\alpha_{m21}} \cdot \bar{d}_1 \cdot \bar{v}_2 - \frac{1}{\alpha_{m21}} \bar{\lambda}_c \end{aligned} \tag{3.53b}$$

Coupling conditions:

$$\begin{aligned} \bar{g}_{c\lambda} &:= \bar{\lambda}_c - \alpha_{cc1} \cdot \bar{c}_1 \cdot (\bar{x}_2 - \bar{x}_1) - \alpha_{dc1} \cdot \bar{d}_1 \cdot (\bar{v}_2 - \bar{v}_1) = 0 \\ \bar{G}_{c\lambda} &:= \int \bar{\lambda}_c \, d\bar{t} - \alpha_{cc1} \cdot \bar{c}_1 \cdot \int (\bar{x}_2 - \bar{x}_1) \, d\bar{t} - \alpha_{dc1} \cdot \bar{d}_1 \cdot \int (\bar{v}_2 - \bar{v}_1) \, d\bar{t} = 0. \end{aligned} \tag{3.53c}$$

The initial conditions (3.40a) have to be complemented by the initial conditions for $\bar{p}_1$ and $\bar{p}_2$, namely by

$$\bar{p}_{1,N}(\bar{t} = \bar{T}_N) = 0\,, \qquad \bar{p}_{2,N}(\bar{t} = \bar{T}_N) = 0\,. \tag{3.54}$$

Step 1: Predictor Step

The predictor step is equivalent to Step 1 in Section 3.4.1. Using the extrapolation functions (3.41), subsystem integration with initial conditions (3.40a) and (3.54) yields the states and the integrated position variables at the macro-time point $\bar{T}_{N+1}$

$$\begin{aligned} \bar{x}^p_{1,N+1} &= \bar{x}^p_{1,N+1}\big(\bar{\lambda}_{c,N}, \bar{\lambda}_{c,N-1/2}, \bar{\lambda}_{c,N-1}, \boldsymbol{z}_N\big), \\ \bar{v}^p_{1,N+1} &= \bar{v}^p_{1,N+1}\big(\bar{\lambda}_{c,N}, \bar{\lambda}_{c,N-1/2}, \bar{\lambda}_{c,N-1}, \boldsymbol{z}_N\big), \\ \bar{p}^p_{1,N+1} &= \bar{p}^p_{1,N+1}\big(\bar{\lambda}_{c,N}, \bar{\lambda}_{c,N-1/2}, \bar{\lambda}_{c,N-1}, \boldsymbol{z}_N\big), \\ \bar{x}^p_{2,N+1} &= \bar{x}^p_{2,N+1}\big(\bar{\lambda}_{c,N}, \bar{\lambda}_{c,N-1/2}, \bar{\lambda}_{c,N-1}, \boldsymbol{z}_N\big), \\ \bar{v}^p_{2,N+1} &= \bar{v}^p_{2,N+1}\big(\bar{\lambda}_{c,N}, \bar{\lambda}_{c,N-1/2}, \bar{\lambda}_{c,N-1}, \boldsymbol{z}_N\big), \\ \bar{p}^p_{2,N+1} &= \bar{p}^p_{2,N+1}\big(\bar{\lambda}_{c,N}, \bar{\lambda}_{c,N-1/2}, \bar{\lambda}_{c,N-1}, \boldsymbol{z}_N\big). \end{aligned} \tag{3.55}$$

Step 2: Calculation of Corrected Coupling Forces

Applying the interpolated coupling variables defined in Eq. (3.43), subsystem integration from $\bar{T}_N$ to $\bar{T}_{N+1}$ with initial conditions (3.40a) and (3.54) gives the following state and integrated position variables at the macro-time point $\bar{T}_{N+1}$

$$\begin{aligned} \bar{x}^*_{1,N+1} &= \bar{x}^*_{1,N+1}\big(\bar{\lambda}^*_{c,N+1}, \bar{\lambda}^*_{c,N+1/2}, \bar{\lambda}_{c,N}, \boldsymbol{z}_N\big), \\ \bar{v}^*_{1,N+1} &= \bar{v}^*_{1,N+1}\big(\bar{\lambda}^*_{c,N+1}, \bar{\lambda}^*_{c,N+1/2}, \bar{\lambda}_{c,N}, \boldsymbol{z}_N\big), \\ \bar{p}^*_{1,N+1} &= \bar{p}^*_{1,N+1}\big(\bar{\lambda}^*_{c,N+1}, \bar{\lambda}^*_{c,N+1/2}, \bar{\lambda}_{c,N}, \boldsymbol{z}_N\big), \\ \bar{x}^*_{2,N+1} &= \bar{x}^*_{2,N+1}\big(\bar{\lambda}^*_{c,N+1}, \bar{\lambda}^*_{c,N+1/2}, \bar{\lambda}_{c,N}, \boldsymbol{z}_N\big), \\ \bar{v}^*_{2,N+1} &= \bar{v}^*_{2,N+1}\big(\bar{\lambda}^*_{c,N+1}, \bar{\lambda}^*_{c,N+1/2}, \bar{\lambda}_{c,N}, \boldsymbol{z}_N\big), \\ \bar{p}^*_{2,N+1} &= \bar{p}^*_{2,N+1}\big(\bar{\lambda}^*_{c,N+1}, \bar{\lambda}^*_{c,N+1/2}, \bar{\lambda}_{c,N}, \boldsymbol{z}_N\big). \end{aligned} \tag{3.56}$$

Differentiating the state and integrated position variables of Eq. (3.56) with respect to $\bar{\lambda}^*_{c,N+1}$ and $\bar{\lambda}^*_{c,N+1/2}$, we obtain partial derivatives similar to Eq. (3.45).

Making use of the partial derivatives, corrected coupling forces $\bar{\lambda}_{c,N+1}$ and $\bar{\lambda}_{c,N+1/2}$ can be computed so that the coupling conditions (3.53c) are satisfied at the macro-time point $\bar{T}_{N+1}$. Regarding the fixed time point $\bar{T}_{N+1}$, $\bar{g}_{c\lambda,N+1}$ and $\bar{G}_{c\lambda,N+1}$ may be considered as functions of the coupling forces $\bar{\lambda}^*_{c,N+1}$ and $\bar{\lambda}^*_{c,N+1/2}$

$$
\begin{aligned}
&\bar{g}_{c\lambda,N+1}\left(\bar{\lambda}^*_{c,N+1}, \bar{\lambda}^*_{c,N+1/2}\right) \\
&:= \bar{\lambda}^*_{c,N+1} - \alpha_{cc1} \cdot \bar{c}_1 \cdot \left(\bar{x}^*_{2,N+1}\left(\bar{\lambda}^*_{c,N+1}, \bar{\lambda}^*_{c,N+1/2}\right) - \bar{x}^*_{1,N+1}\left(\bar{\lambda}^*_{c,N+1}, \bar{\lambda}^*_{c,N+1/2}\right)\right) \\
&\qquad - \alpha_{dc1} \cdot \bar{d}_1 \cdot \left(\bar{v}^*_{2,N+1}\left(\bar{\lambda}^*_{c,N+1}, \bar{\lambda}^*_{c,N+1/2}\right) - \bar{v}^*_{1,N+1}\left(\bar{\lambda}^*_{c,N+1}, \bar{\lambda}^*_{c,N+1/2}\right)\right), \\
&\bar{G}_{c\lambda,N+1}\left(\bar{\lambda}^*_{c,N+1}, \bar{\lambda}^*_{c,N+1/2}\right) \\
&:= \int_{\bar{T}_N}^{\bar{T}_{N+1}} \bar{\lambda}^*_c \, d\bar{t} - \alpha_{cc1}\bar{c}_1 \left(\bar{p}^*_{2,N+1}\left(\bar{\lambda}^*_{c,N+1}, \bar{\lambda}^*_{c,N+1/2}\right) - \bar{p}^*_{1,N+1}\left(\bar{\lambda}^*_{c,N+1}, \bar{\lambda}^*_{c,N+1/2}\right)\right) \\
&-\alpha_{dc1}\bar{d}_1 \left(\left(\bar{x}^*_{2,N+1}\left(\bar{\lambda}^*_{c,N+1}, \bar{\lambda}^*_{c,N+1/2}\right) - x_{2,N}\right) - \left(\bar{x}^*_{1,N+1}\left(\bar{\lambda}^*_{c,N+1}, \bar{\lambda}^*_{c,N+1/2}\right) - x_{1,N}\right)\right).
\end{aligned}
\tag{3.57}
$$

Due to the fact that the state variables $\bar{x}^*_{1,N+1}$, $\bar{x}^*_{2,N+1}$, $\bar{v}^*_{1,N+1}$, $\bar{v}^*_{2,N+1}$ and the integrated position variables $\bar{p}^*_{1,N+1}$, $\bar{p}^*_{2,N+1}$ only depend linearly on $\bar{\lambda}^*_{c,N+1}, \bar{\lambda}^*_{c,N+1/2}$, Eq. (3.57) can be rewritten as

$$
\begin{aligned}
&\bar{g}_{c\lambda,N+1}\left(\bar{\lambda}^*_{c,N+1},\bar{\lambda}^*_{c,N+1/2}\right)\\
&\coloneqq \bar{g}_{c\lambda,N+1}(\boldsymbol{e}^p)+\left.\frac{\partial \bar{g}_{c\lambda,N+1}}{\partial \bar{\lambda}^*_{c,N+1}}\right|_{\boldsymbol{e}^p}\cdot\left(\bar{\lambda}^*_{c,N+1}-\bar{\lambda}^p_{c,N+1}\right)+\left.\frac{\partial \bar{g}_{c\lambda,N+1}}{\partial \bar{\lambda}^*_{c,N+1/2}}\right|_{\boldsymbol{e}^p}\\
&\qquad\cdot\left(\bar{\lambda}^*_{c,N+1/2}-\bar{\lambda}^p_{c,N+1/2}\right)\\
&=\bar{\lambda}^p_{c,N+1}-\alpha_{cc1}\cdot\bar{c}_1\cdot\left(\overline{x}^p_{2,N+1}-\overline{x}^p_{1,N+1}\right)-\alpha_{dc1}\cdot\bar{d}_1\cdot\left(\bar{v}^p_{2,N+1}-\bar{v}^p_{1,N+1}\right)\\
&\quad+\left[1-\alpha_{cc1}\cdot\bar{c}_1\cdot\left(\frac{\partial\overline{x}^*_{2,N+1}}{\partial\bar{\lambda}^*_{c,N+1}}-\frac{\partial\overline{x}^*_{1,N+1}}{\partial\bar{\lambda}^*_{c,N+1}}\right)-\alpha_{dc1}\cdot\bar{d}_1\cdot\left(\frac{\partial\bar{v}^*_{2,N+1}}{\partial\bar{\lambda}^*_{c,N+1}}-\frac{\partial\bar{v}^*_{1,N+1}}{\partial\bar{\lambda}^*_{c,N+1}}\right)\right]\\
&\quad\cdot\left(\bar{\lambda}^*_{c,N+1}-\bar{\lambda}^p_{c,N+1}\right)\\
&\quad+\left[-\alpha_{cc1}\cdot\bar{c}_1\cdot\left(\frac{\partial\overline{x}^*_{2,N+1}}{\partial\bar{\lambda}^*_{c,N+1/2}}-\frac{\partial\overline{x}^*_{1,N+1}}{\partial\bar{\lambda}^*_{c,N+1/2}}\right)-\alpha_{dc1}\cdot\bar{d}_1\cdot\left(\frac{\partial\bar{v}^*_{2,N+1}}{\partial\bar{\lambda}^*_{c,N+1/2}}-\frac{\partial\bar{v}^*_{1,N+1}}{\partial\bar{\lambda}^*_{c,N+1/2}}\right)\right]\\
&\quad\cdot\left(\bar{\lambda}^*_{c,N+1/2}-\bar{\lambda}^p_{c,N+1/2}\right),
\end{aligned}
$$

$$
\begin{aligned}
&\bar{G}_{c\lambda,N+1}\left(\bar{\lambda}^*_{c,N+1},\bar{\lambda}^*_{c,N+1/2}\right)\\
&\coloneqq \bar{G}_{c\lambda,N+1}(\boldsymbol{e}^p)+\left.\frac{\partial \bar{G}_{c\lambda,N+1}}{\partial \bar{\lambda}^*_{c,N+1}}\right|_{\boldsymbol{e}^p}\cdot\left(\bar{\lambda}^*_{c,N+1}-\bar{\lambda}^p_{c,N+1}\right)+\left.\frac{\partial \bar{G}_{c\lambda,N+1}}{\partial \bar{\lambda}^*_{c,N+1/2}}\right|_{\boldsymbol{e}^p}\\
&\qquad\cdot\left(\bar{\lambda}^*_{c,N+1/2}-\bar{\lambda}^p_{c,N+1/2}\right)\\
&=\int_{\bar{T}_N}^{\bar{T}_{N+1}}\bar{\lambda}^p_c\,d\bar{t}-\alpha_{cc1}\cdot\bar{c}_1\cdot\left(\bar{p}^p_{2,N+1}-\bar{p}^p_{1,N+1}\right)-\alpha_{dc1}\cdot\bar{d}_1\\
&\qquad\cdot\left(\left(\overline{x}^p_{2,N+1}-\overline{x}_{2,N}\right)-\left(\overline{x}^p_{1,N+1}-\overline{x}_{1,N}\right)\right)\\
&\quad+\left[\frac{\partial}{\partial\bar{\lambda}^*_{c,N+1}}\int_{\bar{T}_N}^{\bar{T}_{N+1}}\bar{\lambda}^*_c\,d\bar{t}-\alpha_{cc1}\bar{c}_1\left(\frac{\partial\bar{p}^*_{2,N+1}}{\partial\bar{\lambda}^*_{c,N+1}}-\frac{\partial\bar{p}^*_{1,N+1}}{\partial\bar{\lambda}^*_{c,N+1}}\right)-\alpha_{dc1}\bar{d}_1\right.\\
&\quad\left.\left(\frac{\partial\overline{x}^*_{2,N+1}}{\partial\bar{\lambda}^*_{c,N+1}}-\frac{\partial\overline{x}^*_{1,N+1}}{\partial\bar{\lambda}^*_{c,N+1}}\right)\right]\cdot\left(\bar{\lambda}^*_{c,N+1}-\bar{\lambda}^p_{c,N+1}\right)\\
&\quad+\left[\frac{\partial}{\partial\bar{\lambda}^*_{c,N+1/2}}\int_{\bar{T}_N}^{\bar{T}_{N+1}}\bar{\lambda}^*_c\,d\bar{t}-\alpha_{cc1}\cdot\bar{c}_1\cdot\left(\frac{\partial\bar{p}^*_{2,N+1}}{\partial\bar{\lambda}^*_{c,N+1/2}}-\frac{\partial\bar{p}^*_{1,N+1}}{\partial\bar{\lambda}^*_{c,N+1/2}}\right)\right.\\
&\quad\left.-\alpha_{dc1}\cdot\bar{d}_1\cdot\left(\frac{\partial\bar{x}^*_{2,N+1}}{\partial\bar{\lambda}^*_{c,N+1/2}}-\frac{\partial\bar{x}^*_{1,N+1}}{\partial\bar{\lambda}^*_{c,N+1/2}}\right)\right]\cdot\left(\bar{\lambda}^*_{c,N+1/2}-\bar{\lambda}^p_{c,N+1/2}\right).
\end{aligned}
\tag{3.58}
$$

By setting $\bar{g}_{c\lambda,N+1}\left(\bar{\lambda}^*_{c,N+1},\bar{\lambda}^*_{c,N+1/2}\right)=0$ and $\bar{G}_{c\lambda,N+1}\left(\bar{\lambda}^*_{c,N+1},\bar{\lambda}^*_{c,N+1/2}\right)=0$, we get the corrected coupling forces

$$
\begin{aligned}
&\bar{g}_{c\lambda,N+1}\left(\bar{\lambda}^*_{c,N+1},\bar{\lambda}^*_{c,N+1/2}\right)=0\\
&\bar{G}_{c\lambda,N+1}\left(\bar{\lambda}^*_{c,N+1},\bar{\lambda}^*_{c,N+1/2}\right)=0
\end{aligned}
\quad\Rightarrow\quad \bar{\lambda}_{c,N+1},\ \bar{\lambda}_{c,N+1/2}\,. \tag{3.59}
$$

Step 3: Corrector Step

Applying the interpolation functions of Eq. (3.49) with the corrected coupling forces of Eq. (3.59), subsystem integration from $\bar{T}_N$ to $\bar{T}_{N+1}$ with initial conditions (3.40a) and (3.54) yields the corrected states and integrated position variables

$$
\begin{aligned}
\bar{x}_{1,N+1} &= \bar{x}_{1,N+1}\left(\bar{\lambda}_{c,N+1}, \bar{\lambda}_{c,N+1/2}, \bar{\lambda}_{c,N}, \boldsymbol{z}_N\right),\\
\bar{v}_{1,N+1} &= \bar{v}_{1,N+1}\left(\bar{\lambda}_{c,N+1}, \bar{\lambda}_{c,N+1/2}, \bar{\lambda}_{c,N}, \boldsymbol{z}_N\right),\\
\bar{p}_{1,N+1} &= \bar{p}_{1,N+1}\left(\bar{\lambda}_{c,N+1}, \bar{\lambda}_{c,N+1/2}, \bar{\lambda}_{c,N}, \boldsymbol{z}_N\right),\\
\bar{x}_{2,N+1} &= \bar{x}_{2,N+1}\left(\bar{\lambda}_{c,N+1}, \bar{\lambda}_{c,N+1/2}, \bar{\lambda}_{c,N}, \boldsymbol{z}_N\right),\\
\bar{v}_{2,N+1} &= \bar{v}_{2,N+1}\left(\bar{\lambda}_{c,N+1}, \bar{\lambda}_{c,N+1/2}, \bar{\lambda}_{c,N}, \boldsymbol{z}_N\right),\\
\bar{p}_{2,N+1} &= \bar{p}_{2,N+1}\left(\bar{\lambda}_{c,N+1}, \bar{\lambda}_{c,N+1/2}, \bar{\lambda}_{c,N}, \boldsymbol{z}_N\right).
\end{aligned}
\tag{3.60}
$$

With the corrected variables from Eq. (3.60), it is simple to derive recurrence equations, which only contain the state variables at the current and the previous macro-time points. By eliminating $\bar{\lambda}_{c,N+1}$ and $\bar{\lambda}_{c,N}$ with the help of $\bar{g}_{c\lambda,N+1}$ and $\bar{g}_{c\lambda,N}$ as well as $\bar{\lambda}_{c,N+1/2}$ with the help of $\bar{G}_{c\lambda,N+1}$, we obtain again a recurrence equations system of form (3.51) and (3.52).

3.4.3. Implicit Force/Displacement Co-Simulation Approach: D-Extension

The second basic decomposition technique yields a force/displacement-coupling approach. Using this method, the co-simulation test model is split into two subsystems so that subsystem 1 is a force-driven and subsystem 2 a base-point excited single-mass oscillator as shown above. The decomposed D-extended system reads as

Subsystem 1:

$$
\begin{aligned}
\bar{x}_1' &= \bar{v}_1\\
\bar{v}_1' &= -\bar{c}_1 \cdot \bar{x}_1 - \bar{d}_1 \cdot \bar{v}_1 + \bar{\lambda}_c
\end{aligned}
\tag{3.61a}
$$

Subsystem 2:

$$
\begin{aligned}
\bar{x}_2' &= \bar{v}_2\\
\bar{v}_2' &= -\frac{\alpha_{c21}}{\alpha_{m21}}\bar{c}_1\bar{x}_2 - \frac{\alpha_{d21}}{\alpha_{m21}}\bar{d}_1\bar{v}_2 - \frac{\alpha_{cc1}}{\alpha_{m21}}\bar{c}_1(\bar{x}_2 - \tilde{\bar{x}}_1) - \frac{\alpha_{dc1}}{\alpha_{m21}}\bar{d}_1(\bar{v}_2 - \tilde{\bar{v}}_1)
\end{aligned}
\tag{3.61b}
$$

Coupling conditions:

$$
\begin{aligned}
\bar{g}_{c\lambda} &:= \bar{\lambda}_c - \alpha_{cc1} \cdot \bar{c}_1 \cdot (\bar{x}_2 - \bar{x}_1) - \alpha_{dc1} \cdot \bar{d}_1 \cdot (\bar{v}_2 - \bar{v}_1) = 0\\
\bar{g}_{c\lambda}' &:= \bar{\lambda}_c' - \alpha_{cc1} \cdot \bar{c}_1 \cdot (\bar{v}_2 - \bar{v}_1) - \alpha_{dc1} \cdot \bar{d}_1 \cdot (\bar{v}_2' - \bar{v}_1') = 0\\
\bar{g}_{cx_1} &:= \tilde{\bar{x}}_1 - \bar{x}_1 = 0\\
\bar{g}_{cv_1} &:= \tilde{\bar{v}}_1 - \bar{v}_1 = 0\\
\bar{g}_{cv_1}' &:= \tilde{\bar{v}}_1' - \bar{v}_1' = 0\ .
\end{aligned}
\tag{3.61c}
$$

Applying the original (non-extended) co-simulation technique, only the coupling conditions $\bar{g}_{c\lambda}, \bar{g}_{cx_1}$ and $\bar{g}_{cv_1}$ have to be taken into account and the coupling variables $\bar{\lambda}_c, \tilde{\bar{x}}_1$ and $\tilde{\bar{v}}_1$ are discretized only at the macro-time points $\bar{T}_N, \bar{T}_{N+1}$, etc.. In the framework of the D-extended co-simulation approach, the coupling conditions are extended by the time derivatives $\bar{g}_{c\lambda}'$ and $\bar{g}_{cv_1}'$. For that reason the additional variables $\bar{\lambda}_{c,N+1/2}, \bar{\lambda}_{c,N+3/2}$, etc. and $\tilde{\bar{v}}_{1,N+1/2}, \tilde{\bar{v}}_{1,N+3/2}$, etc. are introduced at the time points $\bar{T}_{N+1/2}, \bar{T}_{N+3/2}$, etc.. By introducing these additional variables, the five coupling

condition in Eq. (3.61c) can be enforced simultaneously at the macro-time points $\bar{T}_N, \bar{T}_{N+1}$, etc..

In order to derive the governing recurrence equations system, the general macro-step from $\bar{T}_N$ to $\bar{T}_{N+1}$ is considered again. It is assumed that the state and the coupling variables are known at the beginning of the macro-time step

$$\begin{aligned} \bar{x}_1(\bar{t}=\bar{T}_N) &= \bar{x}_{1,N}\,, \qquad \bar{v}_1(\bar{t}=\bar{T}_N) = \bar{v}_{1,N}\,, \\ \bar{x}_2(\bar{t}=\bar{T}_N) &= \bar{x}_{2,N}\,, \qquad \bar{v}_2(\bar{t}=\bar{T}_N) = \bar{v}_{2,N}\,, \end{aligned} \tag{3.62a}$$

$$\bar{\lambda}_c(\bar{t}=\bar{T}_N) = \bar{\lambda}_{c,N}\,, \qquad \tilde{\bar{x}}_1(\bar{t}=\bar{T}_N) = \tilde{\bar{x}}_{1,N}\,, \qquad \tilde{\bar{v}}_1(\bar{t}=\bar{T}_N) = \tilde{\bar{v}}_{1,N}. \tag{3.62b}$$

For higher order approximation $(k>0)$, the coupling variables at previous time points are also assumed to be known.

Step1: Predictor Step

Subsystem integration from $\bar{T}_N$ to $\bar{T}_{N+1}$ with the initial conditions (3.62a) and with the predictor (extrapolation) functions

$$\begin{aligned} \bar{\lambda}_c^p(\bar{t}) &= \begin{cases} \bar{\lambda}_{c,N} & (k=0) \\ P_{\bar{\lambda}_c}\left[\left(\bar{T}_N, \bar{\lambda}_{c,N}\right), \left(\bar{T}_{N-1/2}, \bar{\lambda}_{c,N-1/2}\right); \bar{t}\right] & (k=1) \\ Q_{\bar{\lambda}_c}\left[\bar{\lambda}_{c,N}, \bar{\lambda}_{c,N-1/2}, \bar{\lambda}_{c,N-1}; \bar{t}\right] & (k=2) \end{cases}, \\ \tilde{\bar{x}}_1^p(\bar{t}) &= \begin{cases} \tilde{\bar{x}}_{1,N} & (k=0) \\ P_{\tilde{\bar{x}}_1}\left[\left(\bar{T}_N, \tilde{\bar{x}}_{1,N}\right), \left(\bar{T}_{N-1}, \tilde{\bar{x}}_{1,N-1}\right); \bar{t}\right] & (k=1) \\ P_{\tilde{\bar{x}}_1}\left[\left(\bar{T}_N, \tilde{\bar{x}}_{1,N}\right), \left(\bar{T}_{N-1}, \tilde{\bar{x}}_{1,N-1}\right), \left(\bar{T}_{N-2}, \tilde{\bar{x}}_{1,N-2}\right); \bar{t}\right] & (k=2) \end{cases}, \\ \tilde{\bar{v}}_1^p(\bar{t}) &= \begin{cases} \tilde{\bar{v}}_{1,N} & (k=0) \\ P_{\tilde{\bar{v}}_1}\left[\left(\bar{T}_N, \tilde{\bar{v}}_{1,N}\right), \left(\bar{T}_{N-1/2}, \tilde{\bar{v}}_{1,N-1/2}\right); \bar{t}\right] & (k=1) \\ Q_{\tilde{\bar{v}}_1}\left[\tilde{\bar{v}}_{1,N}, \tilde{\bar{v}}_{1,N-1/2}, \tilde{\bar{v}}_{1,N-1}; \bar{t}\right] & (k=2) \end{cases}, \end{aligned} \tag{3.63}$$

we obtain the predicted state variables at the macro-time point $\bar{T}_{N+1}$

$$\begin{aligned} \bar{x}_{1,N+1}^p &= \bar{x}_{1,N+1}^p\left(\bar{\lambda}_{c,N}, \bar{\lambda}_{c,N-1/2}, \bar{\lambda}_{c,N-1}, \boldsymbol{z}_N\right), \\ \bar{v}_{1,N+1}^p &= \bar{v}_{1,N+1}^p\left(\bar{\lambda}_{c,N}, \bar{\lambda}_{c,N-1/2}, \bar{\lambda}_{c,N-1}, \boldsymbol{z}_N\right), \\ \bar{x}_{2,N+1}^p &= \bar{x}_{2,N+1}^p\left(\tilde{\boldsymbol{u}}_{2,N}, \tilde{\boldsymbol{u}}_{2,N-1/2}, \tilde{\boldsymbol{u}}_{2,N-1}, \tilde{\boldsymbol{u}}_{2,N-2}, \boldsymbol{z}_N\right), \\ \bar{v}_{2,N+1}^p &= \bar{v}_{2,N+1}^p\left(\tilde{\boldsymbol{u}}_{2,N}, \tilde{\boldsymbol{u}}_{2,N-1/2}, \tilde{\boldsymbol{u}}_{2,N-1}, \tilde{\boldsymbol{u}}_{2,N-2}, \boldsymbol{z}_N\right). \end{aligned} \tag{3.64}$$

The vectors $\tilde{\boldsymbol{u}}_{2,N} = (\tilde{x}_{1,N}\ \tilde{\bar{v}}_{1,N})^T$, $\tilde{\boldsymbol{u}}_{2,N-1/2} = (\tilde{x}_{1,N-1/2}\ \tilde{\bar{v}}_{1,N-1/2})^T$, etc. collect the coupling variables for subsystem 2 at the time points $\bar{T}_N, \bar{T}_{N-1/2}$, etc..

Step 2: Calculation of Corrected Coupling Variables

Integrating the subsystems from $\bar{T}_N$ to $\bar{T}_{N+1}$ with the initial conditions (3.62a) and using the interpolation functions

$$\bar{\lambda}_c^*(\bar{t}) = \begin{cases} C_{\bar{\lambda}_c}\left[\bar{\lambda}_{c,N+1}^*, \bar{\lambda}_{c,N+1/2}^*; \bar{t}\right] & (k=0) \\ L_{\bar{\lambda}_c}\left[\bar{\lambda}_{c,N+1}^*, \bar{\lambda}_{c,N+1/2}^*, \bar{\lambda}_{c,N}; \bar{t}\right] & (k=1) \\ Q_{\bar{\lambda}_c}\left[\bar{\lambda}_{c,N+1}^*, \bar{\lambda}_{c,N+1/2}^*, \bar{\lambda}_{c,N}; \bar{t}\right] & (k=2) \end{cases},$$

$$\tilde{\bar{x}}_1^*(\bar{t}) = \begin{cases} \tilde{\bar{x}}_{1,N+1}^* & (k=0) \\ P_{\tilde{\bar{x}}_1}\left[\left(\bar{T}_{N+1}, \tilde{\bar{x}}_{1,N+1}^*\right), \left(\bar{T}_N, \tilde{\bar{x}}_{1,N}\right); \bar{t}\right] & (k=1) \\ P_{\tilde{\bar{x}}_1}\left[\left(\bar{T}_{N+1}, \tilde{\bar{x}}_{1,N+1}^*\right), \left(\bar{T}_N, \tilde{\bar{x}}_{1,N}\right), \left(\bar{T}_{N-1}, \tilde{\bar{x}}_{1,N-1}\right); \bar{t}\right] & (k=2) \end{cases}, \qquad (3.65)$$

$$\tilde{\bar{v}}_1^*(\bar{t}) = \begin{cases} C_{\tilde{\bar{v}}_1}\left[\tilde{\bar{v}}_{1,N+1}^*, \tilde{\bar{v}}_{1,N+1/2}^*; \bar{t}\right] & (k=0) \\ L_{\tilde{\bar{v}}_1}\left[\tilde{\bar{v}}_{1,N+1}^*, \tilde{\bar{v}}_{1,N+1/2}^*, \tilde{\bar{v}}_{1,N}; \bar{t}\right] & (k=1) \\ Q_{\tilde{\bar{v}}_1}\left[\tilde{\bar{v}}_{1,N+1}^*, \tilde{\bar{v}}_{1,N+1/2}^*, \tilde{\bar{v}}_{1,N}; \bar{t}\right] & (k=2) \end{cases},$$

one gets the following state variables at the macro-time point $\bar{T}_{N+1}$

$$\begin{aligned} \bar{x}_{1,N+1}^* &= \bar{x}_{1,N+1}^*\left(\bar{\lambda}_{c,N+1}^*, \bar{\lambda}_{c,N+1/2}^*, \bar{\lambda}_{c,N}, \boldsymbol{z}_N\right), \\ \bar{v}_{1,N+1}^* &= \bar{v}_{1,N+1}^*\left(\bar{\lambda}_{c,N+1}^*, \bar{\lambda}_{c,N+1/2}^*, \bar{\lambda}_{c,N}, \boldsymbol{z}_N\right), \\ \bar{x}_{2,N+1}^* &= \bar{x}_{2,N+1}^*\left(\widetilde{\boldsymbol{u}}_{2,N+1}^*, \tilde{\bar{v}}_{1,N+1/2}^*, \widetilde{\boldsymbol{u}}_{2,N}, \widetilde{\boldsymbol{u}}_{2,N-1}, \boldsymbol{z}_N\right), \\ \bar{v}_{2,N+1}^* &= \bar{v}_{2,N+1}^*\left(\widetilde{\boldsymbol{u}}_{2,N+1}^*, \tilde{\bar{v}}_{1,N+1/2}^*, \widetilde{\boldsymbol{u}}_{2,N}, \widetilde{\boldsymbol{u}}_{2,N-1}, \boldsymbol{z}_N\right), \end{aligned} \qquad (3.66)$$

where $\bar{\lambda}_{c,N+1}^*, \bar{\lambda}_{c,N+1/2}^*, \widetilde{\boldsymbol{u}}_{2,N+1}^*$ and $\tilde{\bar{v}}_{1,N+1/2}^*$ denote arbitrary coupling variables at the time points $\bar{T}_{N+1}$ and $\bar{T}_{N+1/2}$.

Inserting the state variables from Eq. (3.66) into the coupling conditions (3.61c) results in a linear equations system for the coupling variables. Solving this system for the coupling variables yields the corrected variables $\bar{\lambda}_{c,N+1}, \bar{\lambda}_{c,N+1/2}, \widetilde{\boldsymbol{u}}_{2,N+1}$ and $\tilde{\bar{v}}_{1,N+1/2}$.

Step 3: Corrector Step

Making use of the interpolation functions

$$\bar{\lambda}_c(\bar{t}) = \begin{cases} C_{\bar{\lambda}_c}\left[\bar{\lambda}_{c,N+1}, \bar{\lambda}_{c,N+1/2}; \bar{t}\right] & (k=0) \\ L_{\bar{\lambda}_c}\left[\bar{\lambda}_{c,N+1}, \bar{\lambda}_{c,N+1/2}, \bar{\lambda}_{c,N}; \bar{t}\right] & (k=1) \\ Q_{\bar{\lambda}_c}\left[\bar{\lambda}_{c,N+1}, \bar{\lambda}_{c,N+1/2}, \bar{\lambda}_{c,N}; \bar{t}\right] & (k=2) \end{cases},$$

$$\tilde{\bar{x}}_1(\bar{t}) = \begin{cases} \tilde{\bar{x}}_{1,N+1} & (k=0) \\ P_{\tilde{\bar{x}}_1}\left[\left(\bar{T}_{N+1}, \tilde{\bar{x}}_{1,N+1}\right), \left(\bar{T}_N, \tilde{\bar{x}}_{1,N}\right); \bar{t}\right] & (k=1) \\ P_{\tilde{\bar{x}}_1}\left[\left(\bar{T}_{N+1}, \tilde{\bar{x}}_{1,N+1}\right), \left(\bar{T}_N, \tilde{\bar{x}}_{1,N}\right), \left(\bar{T}_{N-1}, \tilde{\bar{x}}_{1,N-1}\right); \bar{t}\right] & (k=2) \end{cases}, \qquad (3.67)$$

$$\tilde{\bar{v}}_1(\bar{t}) = \begin{cases} C_{\tilde{\bar{v}}_1}\left[\tilde{\bar{v}}_{1,N+1}, \tilde{\bar{v}}_{1,N+1/2}; \bar{t}\right] & (k=0) \\ L_{\tilde{\bar{v}}_1}\left[\tilde{\bar{v}}_{1,N+1}, \tilde{\bar{v}}_{1,N+1/2}, \tilde{\bar{v}}_{1,N}; \bar{t}\right] & (k=1) \\ Q_{\tilde{\bar{v}}_1}\left[\tilde{\bar{v}}_{1,N+1}, \tilde{\bar{v}}_{1,N+1/2}, \tilde{\bar{v}}_{1,N}; \bar{t}\right] & (k=2) \end{cases},$$

with the corrected coupling variables $\bar{\lambda}_{c,N+1}, \bar{\lambda}_{c,N+1/2}, \widetilde{\boldsymbol{u}}_{2,N+1}$ and $\tilde{\bar{v}}_{1,N+1/2}$, an analytical integration of subsystem 1 and subsystem 2 from $\bar{T}_N$ to $\bar{T}_{N+1}$ with initial conditions (3.62a) gives the corrected states

$$
\begin{aligned}
\bar{x}_{1,N+1} &= \bar{x}_{1,N+1}\left(\bar{\lambda}_{c,N+1}, \bar{\lambda}_{c,N+1/2}, \bar{\lambda}_{c,N}, \boldsymbol{z}_N\right),\\
\bar{v}_{1,N+1} &= \bar{v}_{1,N+1}\left(\bar{\lambda}_{c,N+1}, \bar{\lambda}_{c,N+1/2}, \bar{\lambda}_{c,N}, \boldsymbol{z}_N\right),\\
\bar{x}_{2,N+1} &= \bar{x}_{2,N+1}\left(\widetilde{\boldsymbol{u}}_{2,N+1}, \tilde{\bar{v}}_{1,N+1/2}, \widetilde{\boldsymbol{u}}_{2,N}, \widetilde{\boldsymbol{u}}_{2,N-1}, \boldsymbol{z}_N\right),\\
\bar{v}_{2,N+1} &= \bar{v}_{2,N+1}\left(\widetilde{\boldsymbol{u}}_{2,N+1}, \tilde{\bar{v}}_{1,N+1/2}, \widetilde{\boldsymbol{u}}_{2,N}, \widetilde{\boldsymbol{u}}_{2,N-1}, \boldsymbol{z}_N\right).
\end{aligned}
\tag{3.68}
$$

With the corrected coupling variables, recurrence equations can be derived, which only contain the state variables. Eliminating $\bar{\lambda}_{c,N+1}$, $\bar{\lambda}_{c,N}$, $\widetilde{\boldsymbol{u}}_{2,N+1}$, $\widetilde{\boldsymbol{u}}_{2,N}$ and $\widetilde{\boldsymbol{u}}_{2,N-1}$ with the help of $\bar{g}_{c\lambda,N+1}, \bar{g}_{c\lambda,N}, \bar{g}_{cx_1,N+1}, \bar{g}_{cx_1,N}, \bar{g}_{cv_1,N+1}, \bar{g}_{cv_1,N}, \bar{g}_{cx_1,N-1}$ and $\bar{g}_{cv_1,N-1}$ as well as $\bar{\lambda}_{c,N+1/2}$ and $\tilde{\bar{v}}_{1,N+1/2}$ with the help of $\bar{g}'_{c\lambda,N+1}$ and $\bar{g}'_{cv_1,N+1}$, one gets a linear recurrence equation system of the form

$$
\boldsymbol{A}_{N+1} \cdot \boldsymbol{z}_{N+1} + \boldsymbol{A}_N \cdot \boldsymbol{z}_N + \boldsymbol{A}_{N-1} \cdot \boldsymbol{z}_{N-1} = \boldsymbol{0}. \tag{3.69}
$$

The matrices $\boldsymbol{A}_{N+1}$, $\boldsymbol{A}_N$, $\boldsymbol{A}_{N-1} \in \mathbb{R}^{4\times4}$ are real-valued and constant; they only depend on the 7 test-model parameters. Note that $\boldsymbol{A}_{N-1} = \boldsymbol{0}$ for $k = 0$ and $k = 1$.

3.4.4. Implicit Force/Displacement Co-Simulation Approach: I-Extension

The equations of motion for the decomposed I-extended co-simulation system are given by

Subsystem 1:

$$
\begin{aligned}
\bar{p}_1' &= \bar{x}_1\\
\bar{x}_1' &= \bar{v}_1\\
\bar{v}_1' &= -\bar{c}_1 \cdot \bar{x}_1 - \bar{d}_1 \cdot \bar{v}_1 + \bar{\lambda}_c
\end{aligned}
\tag{3.70a}
$$

Subsystem 2:

$$
\begin{aligned}
\bar{p}_2' &= \bar{x}_2\\
\bar{x}_2' &= \bar{v}_2\\
\bar{v}_2' &= -\frac{\alpha_{c21}}{\alpha_{m21}}\bar{c}_1\bar{x}_2 - \frac{\alpha_{d21}}{\alpha_{m21}}\bar{d}_1\bar{v}_2 - \frac{\alpha_{cc1}}{\alpha_{m21}}\bar{c}_1(\bar{x}_2 - \tilde{\bar{x}}_1) - \frac{\alpha_{dc1}}{\alpha_{m21}}\bar{d}_1(\bar{v}_2 - \tilde{\bar{v}}_1)
\end{aligned}
\tag{3.70b}
$$

Coupling conditions:

$$
\begin{aligned}
\bar{g}_{c\lambda} &:= \bar{\lambda}_c - \alpha_{cc1} \cdot \bar{c}_1 \cdot (\bar{x}_2 - \bar{x}_1) - \alpha_{dc1} \cdot \bar{d}_1 \cdot (\bar{v}_2 - \bar{v}_1) = 0\\
\bar{G}_{c\lambda} &:= \int \bar{\lambda}_c \, d\bar{t} - \alpha_{cc1} \cdot \bar{c}_1 \cdot \int (\bar{x}_2 - \bar{x}_1) \, d\bar{t} - \alpha_{dc1} \cdot \bar{d}_1 \cdot \int (\bar{v}_2 - \bar{v}_1) \, d\bar{t} = 0\\
\bar{g}_{cx_1} &:= \tilde{\bar{x}}_1 - \bar{x}_1 = 0\\
\bar{g}_{cv_1} &:= \tilde{\bar{v}}_1 - \bar{v}_1 = 0\\
\bar{G}_{cx_1} &:= \int \tilde{\bar{x}}_1 \, d\bar{t} - \int \bar{x}_1 \, d\bar{t} = 0 \ .
\end{aligned}
\tag{3.70c}
$$

Compared with the original (non-extended) method, the integrated coupling conditions $\bar{G}_{c\lambda}$ and $\bar{G}_{cx_1}$ are also considered. Therefore, the additional coupling variables $\bar{\lambda}_{c,N+1/2}$, $\bar{\lambda}_{c,N+3/2}$, etc. and $\tilde{\bar{x}}_{1,N+1/2}, \tilde{\bar{x}}_{1,N+3/2}$, etc. are introduced. The initial conditions for the integrated position variables $\bar{p}_1$ and $\bar{p}_2$ read as

$$\bar{p}_{1,N}(\bar{t}=\bar{T}_N)=0\,,\qquad \bar{p}_{2,N}(\bar{t}=\bar{T}_N)=0\,. \tag{3.71}$$

Step 1: Predictor Step

Integration of both subsystems from $\bar{T}_N$ to $\bar{T}_{N+1}$ with initial conditions (3.62a) and (3.71) and with the predictor (extrapolation) functions

$$\begin{aligned}
\bar{\lambda}_c^p(\bar{t}) &= \begin{cases} \bar{\lambda}_{c,N} & (k=0) \\ P_{\bar{\lambda}_c}\left[\left(\bar{T}_N,\bar{\lambda}_{c,N}\right),\left(\bar{T}_{N-1/2},\bar{\lambda}_{c,N-1/2}\right);\bar{t}\right] & (k=1) \\ Q_{\bar{\lambda}_c}\left[\bar{\lambda}_{c,N},\bar{\lambda}_{c,N-1/2},\bar{\lambda}_{c,N-1};\bar{t}\right] & (k=2) \end{cases}, \\
\tilde{\bar{x}}_1^p(\bar{t}) &= \begin{cases} \tilde{\bar{x}}_{1,N} & (k=0) \\ P_{\tilde{\bar{x}}_1}\left[\left(\bar{T}_N,\tilde{\bar{x}}_{1,N}\right),\left(\bar{T}_{N-1},\tilde{\bar{x}}_{1,N-1}\right);\bar{t}\right] & (k=1) \\ Q_{\tilde{\bar{x}}_1}\left[\tilde{\bar{x}}_{1,N},\tilde{\bar{x}}_{1,N-1/2},\tilde{\bar{x}}_{1,N-1};\bar{t}\right] & (k=2) \end{cases}, \\
\tilde{\bar{v}}_1^p(\bar{t}) &= \begin{cases} \tilde{\bar{v}}_{1,N} & (k=0) \\ P_{\tilde{\bar{v}}_1}\left[\left(\bar{T}_N,\tilde{\bar{v}}_{1,N}\right),\left(\bar{T}_{N-1/2},\tilde{\bar{v}}_{1,N-1/2}\right);\bar{t}\right] & (k=1) \\ P_{\tilde{\bar{v}}_1}\left[\left(\bar{T}_N,\tilde{\bar{v}}_{1,N}\right),\left(\bar{T}_{N-1},\tilde{\bar{v}}_{1,N-1}\right),\left(\bar{T}_{N-2},\tilde{\bar{v}}_{1,N-2}\right);\bar{t}\right] & (k=2) \end{cases},
\end{aligned} \tag{3.72}$$

yields the predicted states and integrated position variables at the macro-time point $\bar{T}_{N+1}$

$$\begin{aligned}
\bar{x}_{1,N+1}^p &= \bar{x}_{1,N+1}^p\left(\bar{\lambda}_{c,N},\bar{\lambda}_{c,N-1/2},\bar{\lambda}_{c,N-1},\boldsymbol{z}_N\right), \\
\bar{v}_{1,N+1}^p &= \bar{v}_{1,N+1}^p\left(\bar{\lambda}_{c,N},\bar{\lambda}_{c,N-1/2},\bar{\lambda}_{c,N-1},\boldsymbol{z}_N\right), \\
\bar{p}_{1,N+1}^p &= \bar{p}_{1,N+1}^p\left(\bar{\lambda}_{c,N},\bar{\lambda}_{c,N-1/2},\bar{\lambda}_{c,N-1},\boldsymbol{z}_N\right), \\
\bar{x}_{2,N+1}^p &= \bar{x}_{2,N+1}^p\left(\tilde{\boldsymbol{u}}_{2,N},\tilde{\boldsymbol{u}}_{2,N-1/2},\tilde{\boldsymbol{u}}_{2,N-1},\tilde{\boldsymbol{u}}_{2,N-2},\boldsymbol{z}_N\right), \\
\bar{v}_{2,N+1}^p &= \bar{v}_{2,N+1}^p\left(\tilde{\boldsymbol{u}}_{2,N},\tilde{\boldsymbol{u}}_{2,N-1/2},\tilde{\boldsymbol{u}}_{2,N-1},\tilde{\boldsymbol{u}}_{2,N-2},\boldsymbol{z}_N\right), \\
\bar{p}_{2,N+1}^p &= \bar{p}_{2,N+1}^p\left(\tilde{\boldsymbol{u}}_{2,N},\tilde{\boldsymbol{u}}_{2,N-1/2},\tilde{\boldsymbol{u}}_{2,N-1},\tilde{\boldsymbol{u}}_{2,N-2},\boldsymbol{z}_N\right).
\end{aligned} \tag{3.73}$$

Step 2: Calculation of Corrected Coupling Variables

Subsystem integration from $\bar{T}_N$ to $\bar{T}_{N+1}$ with initial conditions (3.62a) and (3.71) and with interpolation functions

$$\begin{aligned}
\bar{\lambda}_c^*(\bar{t}) &= \begin{cases} C_{\bar{\lambda}_c}\left[\bar{\lambda}_{c,N+1}^*,\bar{\lambda}_{c,N+1/2}^*;\bar{t}\right] & (k=0) \\ L_{\bar{\lambda}_c}\left[\bar{\lambda}_{c,N+1}^*,\bar{\lambda}_{c,N+1/2}^*,\bar{\lambda}_{c,N};\bar{t}\right] & (k=1) \\ Q_{\bar{\lambda}_c}\left[\bar{\lambda}_{c,N+1}^*,\bar{\lambda}_{c,N+1/2}^*,\bar{\lambda}_{c,N};\bar{t}\right] & (k=2) \end{cases}, \\
\tilde{\bar{x}}_1^*(\bar{t}) &= \begin{cases} C_{\tilde{\bar{x}}_1}\left[\tilde{\bar{x}}_{1,N+1}^*,\tilde{\bar{x}}_{1,N+1/2}^*;\bar{t}\right] & (k=0) \\ L_{\tilde{\bar{x}}_1}\left[\tilde{\bar{x}}_{1,N+1}^*,\tilde{\bar{x}}_{1,N+1/2}^*,\tilde{\bar{x}}_{1,N};\bar{t}\right] & (k=1) \\ Q_{\tilde{\bar{x}}_1}\left[\tilde{\bar{x}}_{1,N+1}^*,\tilde{\bar{x}}_{1,N+1/2}^*,\tilde{\bar{x}}_{1,N};\bar{t}\right] & (k=2) \end{cases}, \\
\tilde{\bar{v}}_1^*(\bar{t}) &= \begin{cases} \tilde{\bar{v}}_{1,N+1}^* & (k=0) \\ P_{\tilde{\bar{v}}_1}\left[\left(\bar{T}_{N+1},\tilde{\bar{v}}_{1,N+1}^*\right),\left(\bar{T}_N,\tilde{\bar{v}}_{1,N}\right);\bar{t}\right] & (k=1) \\ P_{\tilde{\bar{v}}_1}\left[\left(\bar{T}_{N+1},\tilde{\bar{v}}_{1,N+1}^*\right),\left(\bar{T}_N,\tilde{\bar{v}}_{1,N}\right),\left(\bar{T}_{N-1},\tilde{\bar{v}}_{1,N-1}\right);\bar{t}\right] & (k=2) \end{cases},
\end{aligned} \tag{3.74}$$

provides the following state and integrated position variables at the macro-time point $\bar{T}_{N+1}$

$$
\begin{aligned}
\bar{x}^*_{1,N+1} &= \bar{x}^*_{1,N+1}\left(\bar{\lambda}^*_{c,N+1}, \bar{\lambda}^*_{c,N+1/2}, \bar{\lambda}_{c,N}, \boldsymbol{z}_N\right),\\
\bar{v}^*_{1,N+1} &= \bar{v}^*_{1,N+1}\left(\bar{\lambda}^*_{c,N+1}, \bar{\lambda}^*_{c,N+1/2}, \bar{\lambda}_{c,N}, \boldsymbol{z}_N\right),\\
\bar{p}^*_{1,N+1} &= \bar{p}^*_{1,N+1}\left(\bar{\lambda}^*_{c,N+1}, \bar{\lambda}^*_{c,N+1/2}, \bar{\lambda}_{c,N}, \boldsymbol{z}_N\right),\\
\bar{x}^*_{2,N+1} &= \bar{x}^*_{2,N+1}\left(\widetilde{\boldsymbol{u}}^*_{2,N+1}, \tilde{\bar{x}}^*_{1,N+1/2}, \widetilde{\boldsymbol{u}}_{2,N}, \widetilde{\boldsymbol{u}}_{2,N-1}, \boldsymbol{z}_N\right),\\
\bar{v}^*_{2,N+1} &= \bar{v}^*_{2,N+1}\left(\widetilde{\boldsymbol{u}}^*_{2,N+1}, \tilde{\bar{x}}^*_{1,N+1/2}, \widetilde{\boldsymbol{u}}_{2,N}, \widetilde{\boldsymbol{u}}_{2,N-1}, \boldsymbol{z}_N\right),\\
\bar{p}^*_{2,N+1} &= \bar{p}^*_{2,N+1}\left(\widetilde{\boldsymbol{u}}^*_{2,N+1}, \tilde{\bar{x}}^*_{1,N+1/2}, \widetilde{\boldsymbol{u}}_{2,N}, \widetilde{\boldsymbol{u}}_{2,N-1}, \boldsymbol{z}_N\right).
\end{aligned}
\tag{3.75}
$$

Inserting the state variables of Eq. (3.75) into the coupling conditions (3.70c) results in a linear equations system for the coupling variables. The solution of this system yields the corrected coupling variables $\bar{\lambda}_{c,N+1}$, $\bar{\lambda}_{c,N+1/2}$, $\tilde{\bar{x}}_{1,N+1}$, $\tilde{\bar{x}}_{1,N+1/2}$ and $\tilde{\bar{v}}_{1,N+1}$.

Step 3: Corrector Step

Applying the interpolation functions

$$
\bar{\lambda}_c(\bar{t}) = \begin{cases} C_{\bar{\lambda}_c}\left[\bar{\lambda}_{c,N+1}, \bar{\lambda}_{c,N+1/2}; \bar{t}\right] & (k=0)\\ L_{\bar{\lambda}_c}\left[\bar{\lambda}_{c,N+1}, \bar{\lambda}_{c,N+1/2}, \bar{\lambda}_{c,N}; \bar{t}\right] & (k=1)\\ Q_{\bar{\lambda}_c}\left[\bar{\lambda}_{c,N+1}, \bar{\lambda}_{c,N+1/2}, \bar{\lambda}_{c,N}; \bar{t}\right] & (k=2) \end{cases},
$$

$$
\tilde{\bar{x}}_1(\bar{t}) = \begin{cases} C_{\tilde{\bar{x}}_1}\left[\tilde{\bar{x}}_{1,N+1}, \tilde{\bar{x}}_{1,N+1/2}; \bar{t}\right] & (k=0)\\ L_{\tilde{\bar{x}}_1}\left[\tilde{\bar{x}}_{1,N+1}, \tilde{\bar{x}}_{1,N+1/2}, \tilde{\bar{x}}_{1,N}; \bar{t}\right] & (k=1)\\ Q_{\tilde{\bar{x}}_1}\left[\tilde{\bar{x}}_{1,N+1}, \tilde{\bar{x}}_{1,N+1/2}, \tilde{\bar{x}}_{1,N}; \bar{t}\right] & (k=2) \end{cases},
\tag{3.76}
$$

$$
\tilde{\bar{v}}_1(\bar{t}) = \begin{cases} \tilde{\bar{v}}_{1,N+1} & (k=0)\\ P_{\tilde{\bar{v}}_1}\left[\left(\bar{T}_{N+1}, \tilde{\bar{v}}_{1,N+1}\right), \left(\bar{T}_N, \tilde{\bar{v}}_{1,N}\right); \bar{t}\right] & (k=1)\\ P_{\tilde{\bar{v}}_1}\left[\left(\bar{T}_{N+1}, \tilde{\bar{v}}_{1,N+1}\right), \left(\bar{T}_N, \tilde{\bar{v}}_{1,N}\right), \left(\bar{T}_{N-1}, \tilde{\bar{v}}_{1,N-1}\right); \bar{t}\right] & (k=2) \end{cases}
$$

with the corrected coupling variables $\bar{\lambda}_{c,N+1}, \bar{\lambda}_{c,N+1/2}$, $\tilde{\bar{x}}_{1,N+1}, \tilde{\bar{x}}_{1,N+1/2}$ and $\tilde{\bar{v}}_{1,N+1}$, an integration of both subsystems from $\bar{T}_N$ to $\bar{T}_{N+1}$ with initial conditions (3.62a) and (3.71) gives the corrected states

$$
\begin{aligned}
\bar{x}_{1,N+1} &= \bar{x}_{1,N+1}\left(\bar{\lambda}_{c,N+1}, \bar{\lambda}_{c,N+1/2}, \bar{\lambda}_{c,N}, \boldsymbol{z}_N\right),\\
\bar{v}_{1,N+1} &= \bar{v}_{1,N+1}\left(\bar{\lambda}_{c,N+1}, \bar{\lambda}_{c,N+1/2}, \bar{\lambda}_{c,N}, \boldsymbol{z}_N\right),\\
\bar{p}_{1,N+1} &= \bar{p}_{1,N+1}\left(\bar{\lambda}_{c,N+1}, \bar{\lambda}_{c,N+1/2}, \bar{\lambda}_{c,N}, \boldsymbol{z}_N\right),\\
\bar{x}_{2,N+1} &= \bar{x}_{2,N+1}\left(\widetilde{\boldsymbol{u}}_{2,N+1}, \tilde{\bar{x}}_{1,N+1/2}, \widetilde{\boldsymbol{u}}_{2,N}, \widetilde{\boldsymbol{u}}_{2,N-1}, \boldsymbol{z}_N\right),\\
\bar{v}_{2,N+1} &= \bar{v}_{2,N+1}\left(\widetilde{\boldsymbol{u}}_{2,N+1}, \tilde{\bar{x}}_{1,N+1/2}, \widetilde{\boldsymbol{u}}_{2,N}, \widetilde{\boldsymbol{u}}_{2,N-1}, \boldsymbol{z}_N\right),\\
\bar{p}_{2,N+1} &= \bar{p}_{2,N+1}\left(\widetilde{\boldsymbol{u}}_{2,N+1}, \tilde{\bar{x}}_{1,N+1/2}, \widetilde{\boldsymbol{u}}_{2,N}, \widetilde{\boldsymbol{u}}_{2,N-1}, \boldsymbol{z}_N\right).
\end{aligned}
\tag{3.77}
$$

Eliminating the coupling variables with the help of the coupling conditions, results again in a recurrence equations system of the form (3.68) and (3.69), respectively.

3.4.5. Implicit Displacement/Displacement Co-Simulation Approach: D-Extension

Applying a displacement/displacement coupling approach to decompose the co-simulation model, two base-point excited single-mass oscillators are obtained. The decomposed D-extended system is mathematically represented by

Subsystem 1:

$$\begin{aligned} \bar{x}_1' &= \bar{v}_1 \\ \bar{v}_1' &= -\bar{c}_1 \cdot \bar{x}_1 - \bar{d}_1 \cdot \bar{v}_1 + \alpha_{cc1} \cdot \bar{c}_1 \cdot (\tilde{\bar{x}}_2 - \bar{x}_1) + \alpha_{dc1} \cdot \bar{d}_1 \cdot (\tilde{\bar{v}}_2 - \bar{v}_1) \end{aligned} \tag{3.78a}$$

Subsystem 2:

$$\begin{aligned} \bar{x}_2' &= \bar{v}_2 \\ \bar{v}_2' &= -\frac{\alpha_{c21}}{\alpha_{m21}} \bar{c}_1 \bar{x}_2 - \frac{\alpha_{d21}}{\alpha_{m21}} \bar{d}_1 \bar{v}_2 - \frac{\alpha_{cc1}}{\alpha_{m21}} \bar{c}_1 (\bar{x}_2 - \tilde{\bar{x}}_1) - \frac{\alpha_{dc1}}{\alpha_{m21}} \bar{d}_1 (\bar{v}_2 - \tilde{\bar{v}}_1) \end{aligned} \tag{3.78b}$$

Coupling conditions:

$$\begin{aligned} \bar{g}_{cx_1} &:= \tilde{\bar{x}}_1 - \bar{x}_1 = 0 \\ \bar{g}_{cv_1} &:= \tilde{\bar{v}}_1 - \bar{v}_1 = 0 \\ \bar{g}'_{cv_1} &:= \tilde{\bar{v}}_1' - \bar{v}_1' = 0 \\ \bar{g}_{cx_2} &:= \tilde{\bar{x}}_2 - \bar{x}_2 = 0 \\ \bar{g}_{cv_2} &:= \tilde{\bar{v}}_2 - \bar{v}_2 = 0 \\ \bar{g}'_{cv_2} &:= \tilde{\bar{v}}_2' - \bar{v}_2' = 0 \ . \end{aligned} \tag{3.78c}$$

In the framework of the original (non-extended) approach, only the 4 coupling conditions $\bar{g}_{cx_1}, \bar{g}_{cv_1}, \bar{g}_{cx_2}$ and $\bar{g}_{cv_2}$ are used and the coupling variables are only discretized at the macro-time points $\bar{T}_N$, $\bar{T}_{N+1}$, etc.. Making use of the D-extension approach, the coupling conditions are extended by $\bar{g}'_{cv_1}$ and $\bar{g}'_{cv_2}$. As a consequence, the coupling variables $\tilde{\bar{v}}_1$ and $\tilde{\bar{v}}_2$ are also discretized at the time points $\bar{T}_{N+1/2}$, $\bar{T}_{N+3/2}$, etc.. Once again, the general macro-time step from $\bar{T}_N$ to $\bar{T}_{N+1}$ is regarded to derive the governing recurrence equations system. The state and the coupling variables at the beginning of the macro-step are given by

$$\begin{aligned} \bar{x}_1(\bar{t} = \bar{T}_N) &= \bar{x}_{1,N}\,, \qquad \bar{v}_1(\bar{t} = \bar{T}_N) = \bar{v}_{1,N}\,, \\ \bar{x}_2(\bar{t} = \bar{T}_N) &= \bar{x}_{2,N}\,, \qquad \bar{v}_2(\bar{t} = \bar{T}_N) = \bar{v}_{2,N}\,, \end{aligned} \tag{3.79a}$$

$$\begin{aligned} \tilde{\bar{x}}_1(\bar{t} = \bar{T}_N) &= \tilde{\bar{x}}_{1,N}\,, \qquad \tilde{\bar{v}}_1(\bar{t} = \bar{T}_N) = \tilde{\bar{v}}_{1,N}\,, \\ \tilde{\bar{x}}_2(\bar{t} = \bar{T}_N) &= \tilde{\bar{x}}_{2,N}, \qquad \tilde{\bar{v}}_2(\bar{t} = \bar{T}_N) = \tilde{\bar{v}}_{2,N}. \end{aligned} \tag{3.79b}$$

Step 1: Predictor Step

An integration of the subsystems from $\bar{T}_N$ to $\bar{T}_{N+1}$ with initial conditions (3.79a) and with the predictor (extrapolation) functions

$$
\begin{aligned}
\tilde{\tilde{x}}_1^p(\bar{t}) &= \begin{cases} \tilde{\tilde{x}}_{1,N} & (k=0) \\ P_{\tilde{\tilde{x}}_1}\left[(\bar{T}_N, \tilde{\tilde{x}}_{1,N}), (\bar{T}_{N-1}, \tilde{\tilde{x}}_{1,N-1}); \bar{t}\right] & (k=1) \\ P_{\tilde{\tilde{x}}_1}\left[(\bar{T}_N, \tilde{\tilde{x}}_{1,N}), (\bar{T}_{N-1}, \tilde{\tilde{x}}_{1,N-1}), (\bar{T}_{N-2}, \tilde{\tilde{x}}_{1,N-2}); \bar{t}\right] & (k=2) \end{cases}, \\
\tilde{\tilde{v}}_1^p(\bar{t}) &= \begin{cases} \tilde{\tilde{v}}_{1,N} & (k=0) \\ P_{\tilde{\tilde{v}}_1}\left[(\bar{T}_N, \tilde{\tilde{v}}_{1,N}), (\bar{T}_{N-1/2}, \tilde{\tilde{v}}_{1,N-1/2}); \bar{t}\right] & (k=1) \\ Q_{\tilde{\tilde{v}}_1}\left[\tilde{\tilde{v}}_{1,N}, \tilde{\tilde{v}}_{1,N-1/2}, \tilde{\tilde{v}}_{1,N-1}; \bar{t}\right] & (k=2) \end{cases}, \\
\tilde{\tilde{x}}_2^p(\bar{t}) &= \begin{cases} \tilde{\tilde{x}}_{2,N} & (k=0) \\ P_{\tilde{\tilde{x}}_2}\left[(\bar{T}_N, \tilde{\tilde{x}}_{2,N}), (\bar{T}_{N-1}, \tilde{\tilde{x}}_{2,N-1}); \bar{t}\right] & (k=1) \\ P_{\tilde{\tilde{x}}_2}\left[(\bar{T}_N, \tilde{\tilde{x}}_{2,N}), (\bar{T}_{N-1}, \tilde{\tilde{x}}_{2,N-1}), (\bar{T}_{N-2}, \tilde{\tilde{x}}_{2,N-2}); \bar{t}\right] & (k=2) \end{cases}, \\
\tilde{\tilde{v}}_2^p(\bar{t}) &= \begin{cases} \tilde{\tilde{v}}_{2,N} & (k=0) \\ P_{\tilde{\tilde{v}}_2}\left[(\bar{T}_N, \tilde{\tilde{v}}_{2,N}), (\bar{T}_{N-1/2}, \tilde{\tilde{v}}_{2,N-1/2}); \bar{t}\right] & (k=1) \\ Q_{\tilde{\tilde{v}}_2}\left[\tilde{\tilde{v}}_{2,N}, \tilde{\tilde{v}}_{2,N-1/2}, \tilde{\tilde{v}}_{2,N-1}; \bar{t}\right] & (k=2) \end{cases}
\end{aligned}
\tag{3.80}
$$

yields the predicted state variables at the macro-time point $\bar{T}_{N+1}$

$$
\begin{aligned}
\bar{x}_{1,N+1}^p &= \bar{x}_{1,N+1}^p\left(\tilde{\boldsymbol{u}}_{1,N}, \tilde{\boldsymbol{u}}_{1,N-1/2}, \tilde{\boldsymbol{u}}_{1,N-1}, \tilde{\boldsymbol{u}}_{1,N-2}, \boldsymbol{z}_N\right), \\
\bar{v}_{1,N+1}^p &= \bar{v}_{1,N+1}^p\left(\tilde{\boldsymbol{u}}_{1,N}, \tilde{\boldsymbol{u}}_{1,N-1/2}, \tilde{\boldsymbol{u}}_{1,N-1}, \tilde{\boldsymbol{u}}_{1,N-2}, \boldsymbol{z}_N\right), \\
\bar{x}_{2,N+1}^p &= \bar{x}_{2,N+1}^p\left(\tilde{\boldsymbol{u}}_{2,N}, \tilde{\boldsymbol{u}}_{2,N-1/2}, \tilde{\boldsymbol{u}}_{2,N-1}, \tilde{\boldsymbol{u}}_{2,N-2}, \boldsymbol{z}_N\right), \\
\bar{v}_{2,N+1}^p &= \bar{v}_{2,N+1}^p\left(\tilde{\boldsymbol{u}}_{2,N}, \tilde{\boldsymbol{u}}_{2,N-1/2}, \tilde{\boldsymbol{u}}_{2,N-1}, \tilde{\boldsymbol{u}}_{2,N-2}, \boldsymbol{z}_N\right),
\end{aligned}
\tag{3.81}
$$

where the vectors $\tilde{\boldsymbol{u}}_{1,N} = (\tilde{x}_{2,N}\ \tilde{\tilde{v}}_{2,N})^T, \tilde{\boldsymbol{u}}_{1,N-1/2} = (\tilde{x}_{2,N-1/2}\ \tilde{\tilde{v}}_{2,N-1/2})^T$, etc. collect the coupling variables for subsystem 1 at the time points $\bar{T}_N$, $\bar{T}_{N-1/2}$, etc.

Step 2: Calculation of the Corrected Coupling Variables

Integrating the subsystems from $\bar{T}_N$ to $\bar{T}_{N+1}$ with initial conditions (3.79a) and using the interpolation functions

$$
\begin{aligned}
\tilde{\tilde{x}}_1^*(\bar{t}) &= \begin{cases} \tilde{\tilde{x}}_{1,N+1}^* & (k=0) \\ P_{\tilde{\tilde{x}}_1}\left[(\bar{T}_{N+1}, \tilde{\tilde{x}}_{1,N+1}^*), (\bar{T}_N, \tilde{\tilde{x}}_{1,N}); \bar{t}\right] & (k=1) \\ P_{\tilde{\tilde{x}}_1}\left[(\bar{T}_{N+1}, \tilde{\tilde{x}}_{1,N+1}^*), (\bar{T}_N, \tilde{\tilde{x}}_{1,N}), (\bar{T}_{N-1}, \tilde{\tilde{x}}_{1,N-1}); \bar{t}\right] & (k=2) \end{cases}, \\
\tilde{\tilde{v}}_1^*(\bar{t}) &= \begin{cases} C_{\tilde{\tilde{v}}_1}\left[\tilde{\tilde{v}}_{1,N+1}^*, \tilde{\tilde{v}}_{1,N+1/2}^*; \bar{t}\right] & (k=0) \\ L_{\tilde{\tilde{v}}_1}\left[\tilde{\tilde{v}}_{1,N+1}^*, \tilde{\tilde{v}}_{1,N+1/2}^*, \tilde{\tilde{v}}_{1,N}; \bar{t}\right] & (k=1) \\ Q_{\tilde{\tilde{v}}_1}\left[\tilde{\tilde{v}}_{1,N+1}^*, \tilde{\tilde{v}}_{1,N+1/2}^*, \tilde{\tilde{v}}_{1,N}; \bar{t}\right] & (k=2) \end{cases}, \\
\tilde{\tilde{x}}_2^*(\bar{t}) &= \begin{cases} \tilde{\tilde{x}}_{2,N+1}^* & (k=0) \\ P_{\tilde{\tilde{x}}_2}\left[(\bar{T}_{N+1}, \tilde{\tilde{x}}_{2,N+1}^*), (\bar{T}_N, \tilde{\tilde{x}}_{2,N}); \bar{t}\right] & (k=1) \\ P_{\tilde{\tilde{x}}_2}\left[(\bar{T}_{N+1}, \tilde{\tilde{x}}_{2,N+1}^*), (\bar{T}_N, \tilde{\tilde{x}}_{2,N}), (\bar{T}_{N-1}, \tilde{\tilde{x}}_{2,N-1}); \bar{t}\right] & (k=2) \end{cases}, \\
\tilde{\tilde{v}}_2^*(\bar{t}) &= \begin{cases} C_{\tilde{\tilde{v}}_2}\left[\tilde{\tilde{v}}_{2,N+1}^*, \tilde{\tilde{v}}_{2,N+1/2}^*; \bar{t}\right] & (k=0) \\ L_{\tilde{\tilde{v}}_2}\left[\tilde{\tilde{v}}_{2,N+1}^*, \tilde{\tilde{v}}_{2,N+1/2}^*, \tilde{\tilde{v}}_{2,N}; \bar{t}\right] & (k=1) \\ Q_{\tilde{\tilde{v}}_2}\left[\tilde{\tilde{v}}_{2,N+1}^*, \tilde{\tilde{v}}_{2,N+1/2}^*, \tilde{\tilde{v}}_{2,N}; \bar{t}\right] & (k=2) \end{cases}
\end{aligned}
\tag{3.82}
$$

we get the following state variables at the macro-time point $\bar{T}_{N+1}$

$$
\begin{aligned}
\bar{x}^*_{1,N+1} &= \bar{x}^*_{1,N+1}\big(\widetilde{\boldsymbol{u}}^*_{1,N+1}, \tilde{\bar{v}}^*_{2,N+1/2}, \widetilde{\boldsymbol{u}}_{1,N}, \widetilde{\boldsymbol{u}}_{1,N-1}, \boldsymbol{z}_N\big),\\
\bar{v}^*_{1,N+1} &= \bar{v}^*_{1,N+1}\big(\widetilde{\boldsymbol{u}}^*_{1,N+1}, \tilde{\bar{v}}^*_{2,N+1/2}, \widetilde{\boldsymbol{u}}_{1,N}, \widetilde{\boldsymbol{u}}_{1,N-1}, \boldsymbol{z}_N\big),\\
\bar{x}^*_{2,N+1} &= \bar{x}^*_{2,N+1}\big(\widetilde{\boldsymbol{u}}^*_{2,N+1}, \tilde{\bar{v}}^*_{1,N+1/2}, \widetilde{\boldsymbol{u}}_{2,N}, \widetilde{\boldsymbol{u}}_{2,N-1}, \boldsymbol{z}_N\big),\\
\bar{v}^*_{2,N+1} &= \bar{v}^*_{2,N+1}\big(\widetilde{\boldsymbol{u}}^*_{2,N+1}, \tilde{\bar{v}}^*_{1,N+1/2}, \widetilde{\boldsymbol{u}}_{2,N}, \widetilde{\boldsymbol{u}}_{2,N-1}, \boldsymbol{z}_N\big),
\end{aligned}
\tag{3.83}
$$

where $\widetilde{\boldsymbol{u}}^*_{1,N+1}, \tilde{\bar{v}}^*_{2,N+1/2}, \widetilde{\boldsymbol{u}}^*_{2,N+1}$ and $\tilde{\bar{v}}^*_{1,N+1/2}$ denote arbitrary coupling variables at the time points $\bar{T}_{N+1}$ and $\bar{T}_{N+1/2}$.

Substituting the state variables of Eq. (3.83) into the coupling conditions (3.78c) results in a linear equations system for the coupling variables. Solving this equations system for the coupling variables yields the corrected variables $\widetilde{\boldsymbol{u}}_{1,N+1}, \tilde{\bar{v}}_{2,N+1/2}, \widetilde{\boldsymbol{u}}_{2,N+1}$ and $\tilde{\bar{v}}_{1,N+1/2}$.

Step 3: Corrector Step

Making use of the interpolation functions

$$
\begin{aligned}
\tilde{\bar{x}}_1(\bar{t}) &= \begin{cases} \tilde{\bar{x}}_{1,N+1} & (k=0) \\ P_{\tilde{\bar{x}}_1}\big[(\bar{T}_{N+1}, \tilde{\bar{x}}_{1,N+1}), (\bar{T}_N, \tilde{\bar{x}}_{1,N}); \bar{t}\big] & (k=1) \\ P_{\tilde{\bar{x}}_1}\big[(\bar{T}_{N+1}, \tilde{\bar{x}}_{1,N+1}), (\bar{T}_N, \tilde{\bar{x}}_{1,N}), (\bar{T}_{N-1}, \tilde{\bar{x}}_{1,N-1}); \bar{t}\big] & (k=2) \end{cases},\\
\tilde{\bar{v}}_1(\bar{t}) &= \begin{cases} C_{\tilde{\bar{v}}_1}\big[\tilde{\bar{v}}_{1,N+1}, \tilde{\bar{v}}_{1,N+1/2}; \bar{t}\big] & (k=0) \\ L_{\tilde{\bar{v}}_1}\big[\tilde{\bar{v}}_{1,N+1}, \tilde{\bar{v}}_{1,N+1/2}, \tilde{\bar{v}}_{1,N}; \bar{t}\big] & (k=1) \\ Q_{\tilde{\bar{v}}_1}\big[\tilde{\bar{v}}_{1,N+1}, \tilde{\bar{v}}_{1,N+1/2}, \tilde{\bar{v}}_{1,N}; \bar{t}\big] & (k=2) \end{cases},\\
\tilde{\bar{x}}_2(\bar{t}) &= \begin{cases} \tilde{\bar{x}}_{2,N+1} & (k=0) \\ P_{\tilde{\bar{x}}_2}\big[(\bar{T}_{N+1}, \tilde{\bar{x}}_{2,N+1}), (\bar{T}_N, \tilde{\bar{x}}_{2,N}); \bar{t}\big] & (k=1) \\ P_{\tilde{\bar{x}}_2}\big[(\bar{T}_{N+1}, \tilde{\bar{x}}_{2,N+1}), (\bar{T}_N, \tilde{\bar{x}}_{2,N}), (\bar{T}_{N-1}, \tilde{\bar{x}}_{2,N-1}); \bar{t}\big] & (k=2) \end{cases},\\
\tilde{\bar{v}}_2(\bar{t}) &= \begin{cases} C_{\tilde{\bar{v}}_2}\big[\tilde{\bar{v}}_{2,N+1}, \tilde{\bar{v}}_{2,N+1/2}; \bar{t}\big] & (k=0) \\ L_{\tilde{\bar{v}}_2}\big[\tilde{\bar{v}}_{2,N+1}, \tilde{\bar{v}}_{2,N+1/2}, \tilde{\bar{v}}_{2,N}; \bar{t}\big] & (k=1) \\ Q_{\tilde{\bar{v}}_2}\big[\tilde{\bar{v}}_{2,N+1}, \tilde{\bar{v}}_{2,N+1/2}, \tilde{\bar{v}}_{2,N}; \bar{t}\big] & (k=2) \end{cases},
\end{aligned}
\tag{3.84}
$$

with the corrected coupling variables $\widetilde{\boldsymbol{u}}_{1,N+1}, \tilde{\bar{v}}_{2,N+1/2}, \widetilde{\boldsymbol{u}}_{2,N+1}$ and $\tilde{\bar{v}}_{1,N+1/2}$, an integration of the subsystems from $\bar{T}_N$ to $\bar{T}_{N+1}$ with initial conditions (3.79a) gives the corrected states

$$
\begin{aligned}
\bar{x}_{1,N+1} &= \bar{x}_{1,N+1}\big(\widetilde{\boldsymbol{u}}_{1,N+1}, \tilde{\bar{v}}_{2,N+1/2}, \widetilde{\boldsymbol{u}}_{1,N}, \widetilde{\boldsymbol{u}}_{1,N-1}, \boldsymbol{z}_N\big),\\
\bar{v}_{1,N+1} &= \bar{v}_{1,N+1}\big(\widetilde{\boldsymbol{u}}_{1,N+1}, \tilde{\bar{v}}_{2,N+1/2}, \widetilde{\boldsymbol{u}}_{1,N}, \widetilde{\boldsymbol{u}}_{1,N-1}, \boldsymbol{z}_N\big),\\
\bar{x}_{2,N+1} &= \bar{x}_{2,N+1}\big(\widetilde{\boldsymbol{u}}_{2,N+1}, \tilde{\bar{v}}_{1,N+1/2}, \widetilde{\boldsymbol{u}}_{2,N}, \widetilde{\boldsymbol{u}}_{2,N-1}, \boldsymbol{z}_N\big),\\
\bar{v}_{2,N+1} &= \bar{v}_{2,N+1}\big(\widetilde{\boldsymbol{u}}_{2,N+1}, \tilde{\bar{v}}_{1,N+1/2}, \widetilde{\boldsymbol{u}}_{2,N}, \widetilde{\boldsymbol{u}}_{2,N-1}, \boldsymbol{z}_N\big).
\end{aligned}
\tag{3.85}
$$

Eliminating the coupling variables with the help of the coupling conditions, results again in a recurrence equations system of the form (3.68) and (3.69), respectively.

3.4.6. Implicit Displacement/Displacement Co-Simulation Approach: I-Extension

Applying the I-extended co-simulation approach, the equations of motion for the decomposed system read as

Subsystem 1:

$$\begin{aligned}\bar{p}_1' &= \bar{x}_1 \\ \bar{x}_1' &= \bar{v}_1 \\ \bar{v}_1' &= -\bar{c}_1 \cdot \bar{x}_1 - \bar{d}_1 \cdot \bar{v}_1 + \alpha_{cc1} \cdot \bar{c}_1 \cdot (\tilde{\bar{x}}_2 - \bar{x}_1) + \alpha_{dc1} \cdot \bar{d}_1 \cdot (\tilde{\bar{v}}_2 - \bar{v}_1)\end{aligned} \tag{3.86a}$$

Subsystem 2:

$$\begin{aligned}\bar{p}_2' &= \bar{x}_2 \\ \bar{x}_2' &= \bar{v}_2 \\ \bar{v}_2' &= -\frac{\alpha_{c21}}{\alpha_{m21}} \bar{c}_1 \bar{x}_2 - \frac{\alpha_{d21}}{\alpha_{m21}} \bar{d}_1 \bar{v}_2 - \frac{\alpha_{cc1}}{\alpha_{m21}} \bar{c}_1 (\bar{x}_2 - \tilde{\bar{x}}_1) - \frac{\alpha_{dc1}}{\alpha_{m21}} \bar{d}_1 (\bar{v}_2 - \tilde{\bar{v}}_1)\end{aligned} \tag{3.86b}$$

Coupling conditions:

$$\begin{aligned}\bar{g}_{cx_1} &:= \tilde{\bar{x}}_1 - \bar{x}_1 = 0 \\ \bar{g}_{cv_1} &:= \tilde{\bar{v}}_1 - \bar{v}_1 = 0 \\ \bar{G}_{cx_1} &:= \int \tilde{\bar{x}}_1 \, d\bar{t} - \int \bar{x}_1 \, d\bar{t} = 0 \\ \bar{g}_{cx_2} &:= \tilde{\bar{x}}_2 - \bar{x}_2 = 0 \\ \bar{g}_{cv_2} &:= \tilde{\bar{v}}_2 - \bar{v}_2 = 0 \\ \bar{G}_{cx_2} &:= \int \tilde{\bar{x}}_2 \, d\bar{t} - \int \bar{x}_2 \, d\bar{t} = 0 \ .\end{aligned} \tag{3.86c}$$

In contrast to the original (non-extended) method, the integrated coupling conditions $\bar{G}_{cx_1}$ and $\bar{G}_{cx_2}$ are also taken into account. Hence, the additional coupling variables $\tilde{\bar{x}}_{1,N+1/2}, \tilde{\bar{x}}_{1,N+3/2}$, etc. and $\tilde{\bar{x}}_{2,N+1/2}, \tilde{\bar{x}}_{2,N+3/2}$, etc. are introduced. The initial conditions for the integrated position variables $\bar{p}_1$ and $\bar{p}_2$ are again

$$\bar{p}_{1,N}(\bar{t} = \bar{T}_N) = 0\,, \quad \bar{p}_{2,N}(\bar{t} = \bar{T}_N) = 0\,. \tag{3.87}$$

Step 1: Predictor Step

An integration of the subsystems from $\bar{T}_N$ to $\bar{T}_{N+1}$ with initial conditions (3.79a) and (3.87) and with the predictor (extrapolation) functions

$$
\begin{aligned}
\tilde{\bar{x}}_1^p(\bar{t}) &= \begin{cases} \tilde{\bar{x}}_{1,N} & (k=0) \\ P_{\tilde{\bar{x}}_1}\left[\left(\bar{T}_N, \tilde{\bar{x}}_{1,N}\right), \left(\bar{T}_{N-1/2}, \tilde{\bar{x}}_{1,N-1/2}\right); \bar{t}\right] & (k=1) \\ Q_{\tilde{\bar{x}}_1}\left[\tilde{\bar{x}}_{1,N}, \tilde{\bar{x}}_{1,N-1/2}, \tilde{\bar{x}}_{1,N-1}; \bar{t}\right] & (k=2) \end{cases}, \\
\tilde{\bar{v}}_1^p(\bar{t}) &= \begin{cases} \tilde{\bar{v}}_{1,N} & (k=0) \\ P_{\tilde{\bar{v}}_1}\left[\left(\bar{T}_N, \tilde{\bar{v}}_{1,N}\right), \left(\bar{T}_{N-1}, \tilde{\bar{v}}_{1,N-1}\right); \bar{t}\right] & (k=1) \\ P_{\tilde{\bar{v}}_1}\left[\left(\bar{T}_N, \tilde{\bar{v}}_{1,N}\right), \left(\bar{T}_{N-1}, \tilde{\bar{v}}_{1,N-1}\right), \left(\bar{T}_{N-2}, \tilde{\bar{v}}_{1,N-2}\right); \bar{t}\right] & (k=2) \end{cases}, \\
\tilde{\bar{x}}_2^p(\bar{t}) &= \begin{cases} \tilde{\bar{x}}_{2,N} & (k=0) \\ P_{\tilde{\bar{x}}_2}\left[\left(\bar{T}_N, \tilde{\bar{x}}_{2,N}\right), \left(\bar{T}_{N-1/2}, \tilde{\bar{x}}_{2,N-1/2}\right); \bar{t}\right] & (k=1) \\ Q_{\tilde{\bar{x}}_2}\left[\tilde{\bar{x}}_{2,N}, \tilde{\bar{x}}_{2,N-1/2}, \tilde{\bar{x}}_{2,N-1}; \bar{t}\right] & (k=2) \end{cases}, \\
\tilde{\bar{v}}_2^p(\bar{t}) &= \begin{cases} \tilde{\bar{v}}_{2,N} & (k=0) \\ P_{\tilde{\bar{v}}_2}\left[\left(\bar{T}_N, \tilde{\bar{v}}_{2,N}\right), \left(\bar{T}_{N-1}, \tilde{\bar{v}}_{2,N-1}\right); \bar{t}\right] & (k=1) \\ P_{\tilde{\bar{v}}_2}\left[\left(\bar{T}_N, \tilde{\bar{v}}_{2,N}\right), \left(\bar{T}_{N-1}, \tilde{\bar{v}}_{2,N-1}\right), \left(\bar{T}_{N-2}, \tilde{\bar{v}}_{2,N-2}\right); \bar{t}\right] & (k=2) \end{cases},
\end{aligned}
\tag{3.88}
$$

gives the predicted state variables at the macro-time point $\bar{T}_{N+1}$

$$
\begin{aligned}
\bar{x}_{1,N+1}^p &= \bar{x}_{1,N+1}^p\left(\tilde{\boldsymbol{u}}_{1,N}, \tilde{\boldsymbol{u}}_{1,N-1/2}, \tilde{\boldsymbol{u}}_{1,N-1}, \tilde{\boldsymbol{u}}_{1,N-2}, \boldsymbol{z}_N\right), \\
\bar{v}_{1,N+1}^p &= \bar{v}_{1,N+1}^p\left(\tilde{\boldsymbol{u}}_{1,N}, \tilde{\boldsymbol{u}}_{1,N-1/2}, \tilde{\boldsymbol{u}}_{1,N-1}, \tilde{\boldsymbol{u}}_{1,N-2}, \boldsymbol{z}_N\right), \\
\bar{p}_{1,N+1}^p &= \bar{p}_{1,N+1}^p\left(\tilde{\boldsymbol{u}}_{1,N}, \tilde{\boldsymbol{u}}_{1,N-1/2}, \tilde{\boldsymbol{u}}_{1,N-1}, \tilde{\boldsymbol{u}}_{1,N-2}, \boldsymbol{z}_N\right), \\
\bar{x}_{2,N+1}^p &= \bar{x}_{2,N+1}^p\left(\tilde{\boldsymbol{u}}_{2,N}, \tilde{\boldsymbol{u}}_{2,N-1/2}, \tilde{\boldsymbol{u}}_{2,N-1}, \tilde{\boldsymbol{u}}_{2,N-2}, \boldsymbol{z}_N\right), \\
\bar{v}_{2,N+1}^p &= \bar{v}_{2,N+1}^p\left(\tilde{\boldsymbol{u}}_{2,N}, \tilde{\boldsymbol{u}}_{2,N-1/2}, \tilde{\boldsymbol{u}}_{2,N-1}, \tilde{\boldsymbol{u}}_{2,N-2}, \boldsymbol{z}_N\right), \\
\bar{p}_{2,N+1}^p &= \bar{p}_{2,N+1}^p\left(\tilde{\boldsymbol{u}}_{2,N}, \tilde{\boldsymbol{u}}_{2,N-1/2}, \tilde{\boldsymbol{u}}_{2,N-1}, \tilde{\boldsymbol{u}}_{2,N-2}, \boldsymbol{z}_N\right).
\end{aligned}
\tag{3.89}
$$

Step 2: Calculation of Corrected Coupling Variables

By integrating the subsystems from $\bar{T}_N$ to $\bar{T}_{N+1}$ with initial conditions (3.79a) and (3.87) and by using the interpolation functions

$$
\begin{aligned}
\tilde{\bar{x}}_1^*(\bar{t}) &= \begin{cases} C_{\tilde{\bar{x}}_1}\left[\tilde{\bar{x}}_{1,N+1}^*, \tilde{\bar{x}}_{1,N+1/2}^*; \bar{t}\right] & (k=0) \\ L_{\tilde{\bar{x}}_1}\left[\tilde{\bar{x}}_{1,N+1}^*, \tilde{\bar{x}}_{1,N+1/2}^*, \tilde{\bar{x}}_{1,N}; \bar{t}\right] & (k=1) \\ Q_{\tilde{\bar{x}}_1}\left[\tilde{\bar{x}}_{1,N+1}^*, \tilde{\bar{x}}_{1,N+1/2}^*, \tilde{\bar{x}}_{1,N}; \bar{t}\right] & (k=2) \end{cases}, \\
\tilde{\bar{v}}_1^*(\bar{t}) &= \begin{cases} \tilde{\bar{v}}_{1,N+1}^* & (k=0) \\ P_{\tilde{\bar{v}}_1}\left[\left(\bar{T}_{N+1}, \tilde{\bar{v}}_{1,N+1}^*\right), \left(\bar{T}_N, \tilde{\bar{v}}_{1,N}\right); \bar{t}\right] & (k=1) \\ P_{\tilde{\bar{v}}_1}\left[\left(\bar{T}_{N+1}, \tilde{\bar{v}}_{1,N+1}^*\right), \left(\bar{T}_N, \tilde{\bar{v}}_{1,N}\right), \left(\bar{T}_{N-1}, \tilde{\bar{v}}_{1,N-1}\right); \bar{t}\right] & (k=2) \end{cases}, \\
\tilde{\bar{x}}_2^*(\bar{t}) &= \begin{cases} C_{\tilde{\bar{x}}_2}\left[\tilde{\bar{x}}_{2,N+1}^*, \tilde{\bar{x}}_{2,N+1/2}^*; \bar{t}\right] & (k=0) \\ L_{\tilde{\bar{x}}_2}\left[\tilde{\bar{x}}_{2,N+1}^*, \tilde{\bar{x}}_{2,N+1/2}^*, \tilde{\bar{x}}_{2,N}; \bar{t}\right] & (k=1) \\ Q_{\tilde{\bar{x}}_2}\left[\tilde{\bar{x}}_{2,N+1}^*, \tilde{\bar{x}}_{2,N+1/2}^*, \tilde{\bar{x}}_{2,N}; \bar{t}\right] & (k=2) \end{cases}, \\
\tilde{\bar{v}}_2^*(\bar{t}) &= \begin{cases} \tilde{\bar{v}}_{2,N+1} & (k=0) \\ P_{\tilde{\bar{v}}_2}\left[\left(\bar{T}_{N+1}, \tilde{\bar{v}}_{2,N+1}^*\right), \left(\bar{T}_N, \tilde{\bar{v}}_{2,N}\right); \bar{t}\right] & (k=1) \\ P_{\tilde{\bar{v}}_2}\left[\left(\bar{T}_{N+1}, \tilde{\bar{v}}_{2,N+1}^*\right), \left(\bar{T}_N, \tilde{\bar{v}}_{2,N}\right), \left(\bar{T}_{N-1}, \tilde{\bar{v}}_{2,N-1}\right); \bar{t}\right] & (k=2) \end{cases},
\end{aligned}
\tag{3.90}
$$

we obtain the following state and integrated position variables at the macro time point $\bar{T}_{N+1}$

$$
\begin{aligned}
\bar{x}^*_{1,N+1} &= \bar{x}^*_{1,N+1}\left(\widetilde{\boldsymbol{u}}^*_{1,N+1}, \tilde{\bar{x}}^*_{2,N+1/2}, \widetilde{\boldsymbol{u}}_{1,N}, \widetilde{\boldsymbol{u}}_{1,N-1}, \boldsymbol{z}_N\right),\\
\bar{v}^*_{1,N+1} &= \bar{v}^*_{1,N+1}\left(\widetilde{\boldsymbol{u}}^*_{1,N+1}, \tilde{\bar{x}}^*_{2,N+1/2}, \widetilde{\boldsymbol{u}}_{1,N}, \widetilde{\boldsymbol{u}}_{1,N-1}, \boldsymbol{z}_N\right),\\
\bar{p}^*_{1,N+1} &= \bar{p}^*_{1,N+1}\left(\widetilde{\boldsymbol{u}}^*_{1,N+1}, \tilde{\bar{x}}^*_{2,N+1/2}, \widetilde{\boldsymbol{u}}_{1,N}, \widetilde{\boldsymbol{u}}_{1,N-1}, \boldsymbol{z}_N\right),\\
\bar{x}^*_{2,N+1} &= \bar{x}^*_{2,N+1}\left(\widetilde{\boldsymbol{u}}^*_{2,N+1}, \tilde{\bar{x}}^*_{1,N+1/2}, \widetilde{\boldsymbol{u}}_{2,N}, \widetilde{\boldsymbol{u}}_{2,N-1}, \boldsymbol{z}_N\right),\\
\bar{v}^*_{2,N+1} &= \bar{v}^*_{2,N+1}\left(\widetilde{\boldsymbol{u}}^*_{2,N+1}, \tilde{\bar{x}}^*_{1,N+1/2}, \widetilde{\boldsymbol{u}}_{2,N}, \widetilde{\boldsymbol{u}}_{2,N-1}, \boldsymbol{z}_N\right),\\
\bar{p}^*_{2,N+1} &= \bar{p}^*_{2,N+1}\left(\widetilde{\boldsymbol{u}}^*_{2,N+1}, \tilde{\bar{x}}^*_{1,N+1/2}, \widetilde{\boldsymbol{u}}_{2,N}, \widetilde{\boldsymbol{u}}_{2,N-1}, \boldsymbol{z}_N\right).
\end{aligned}
\tag{3.91}
$$

Inserting the state variables of Eq. (3.91) into the coupling conditions (3.86c) results in a linear equation system for the coupling variables, the solution of which yields the corrected coupling variables $\widetilde{\boldsymbol{u}}_{1,N+1}, \tilde{\bar{x}}_{2,N+1/2}, \widetilde{\boldsymbol{u}}_{2,N+1}$ and $\tilde{\bar{x}}_{1,N+1/2}$.

Step 3: Corrector Step

Using the interpolation functions

$$
\begin{aligned}
\tilde{\bar{x}}_1(\bar{t}) &= \begin{cases} C_{\tilde{\bar{x}}_1}\left[\tilde{\bar{x}}_{1,N+1}, \tilde{\bar{x}}_{1,N+1/2}; \bar{t}\right] & (k=0)\\ L_{\tilde{\bar{x}}_1}\left[\tilde{\bar{x}}_{1,N+1}, \tilde{\bar{x}}_{1,N+1/2}, \tilde{\bar{x}}_{1,N}; \bar{t}\right] & (k=1)\\ Q_{\tilde{\bar{x}}_1}\left[\tilde{\bar{x}}_{1,N+1}, \tilde{\bar{x}}_{1,N+1/2}, \tilde{\bar{x}}_{1,N}; \bar{t}\right] & (k=2) \end{cases},\\
\tilde{\bar{v}}_1(\bar{t}) &= \begin{cases} \tilde{\bar{v}}_{1,N+1} & (k=0)\\ P_{\tilde{\bar{v}}_1}\left[\left(\bar{T}_{N+1}, \tilde{\bar{v}}_{1,N+1}\right), \left(\bar{T}_N, \tilde{\bar{v}}_{1,N}\right); \bar{t}\right] & (k=1)\\ P_{\tilde{\bar{v}}_1}\left[\left(\bar{T}_{N+1}, \tilde{\bar{v}}_{1,N+1}\right), \left(\bar{T}_N, \tilde{\bar{v}}_{1,N}\right), \left(\bar{T}_{N-1}, \tilde{\bar{v}}_{1,N-1}\right); \bar{t}\right] & (k=2) \end{cases},\\
\tilde{\bar{x}}_2(\bar{t}) &= \begin{cases} C_{\tilde{\bar{x}}_2}\left[\tilde{\bar{x}}_{2,N+1}, \tilde{\bar{x}}_{2,N+1/2}; \bar{t}\right] & (k=0)\\ L_{\tilde{\bar{x}}_2}\left[\tilde{\bar{x}}_{2,N+1}, \tilde{\bar{x}}_{2,N+1/2}, \tilde{\bar{x}}_{2,N}; \bar{t}\right] & (k=1)\\ Q_{\tilde{\bar{x}}_2}\left[\tilde{\bar{x}}_{2,N+1}, \tilde{\bar{x}}_{2,N+1/2}, \tilde{\bar{x}}_{2,N}; \bar{t}\right] & (k=2) \end{cases},\\
\tilde{\bar{v}}_2(\bar{t}) &= \begin{cases} \tilde{\bar{v}}_{2,N+1} & (k=0)\\ P_{\tilde{\bar{v}}_2}\left[\left(\bar{T}_{N+1}, \tilde{\bar{v}}_{2,N+1}\right), \left(\bar{T}_N, \tilde{\bar{v}}_{2,N}\right); \bar{t}\right] & (k=1)\\ P_{\tilde{\bar{v}}_2}\left[\left(\bar{T}_{N+1}, \tilde{\bar{v}}_{2,N+1}\right), \left(\bar{T}_N, \tilde{\bar{v}}_{2,N}\right), \left(\bar{T}_{N-1}, \tilde{\bar{v}}_{2,N-1}\right); \bar{t}\right] & (k=2) \end{cases}
\end{aligned}
\tag{3.92}
$$

with the corrected coupling variables $\widetilde{\boldsymbol{u}}_{1,N+1}, \tilde{\bar{x}}_{2,N+1/2}, \widetilde{\boldsymbol{u}}_{2,N+1}$ and $\tilde{\bar{x}}_{1,N+1/2}$, a subsystem integration from $\bar{T}_N$ to $\bar{T}_{N+1}$ with initial conditions (3.79a) and (3.87) gives the corrected variables

$$
\begin{aligned}
\bar{x}_{1,N+1} &= \bar{x}_{1,N+1}\left(\widetilde{\boldsymbol{u}}_{1,N+1}, \tilde{\bar{x}}_{2,N+1/2}, \widetilde{\boldsymbol{u}}_{1,N}, \widetilde{\boldsymbol{u}}_{1,N-1}, \boldsymbol{z}_N\right),\\
\bar{v}_{1,N+1} &= \bar{v}_{1,N+1}\left(\widetilde{\boldsymbol{u}}_{1,N+1}, \tilde{\bar{x}}_{2,N+1/2}, \widetilde{\boldsymbol{u}}_{1,N}, \widetilde{\boldsymbol{u}}_{1,N-1}, \boldsymbol{z}_N\right),\\
\bar{p}_{1,N+1} &= \bar{p}_{1,N+1}\left(\widetilde{\boldsymbol{u}}_{1,N+1}, \tilde{\bar{x}}_{2,N+1/2}, \widetilde{\boldsymbol{u}}_{1,N}, \widetilde{\boldsymbol{u}}_{1,N-1}, \boldsymbol{z}_N\right),\\
\bar{x}_{2,N+1} &= \bar{x}_{2,N+1}\left(\widetilde{\boldsymbol{u}}_{2,N+1}, \tilde{\bar{x}}_{1,N+1/2}, \widetilde{\boldsymbol{u}}_{2,N}, \widetilde{\boldsymbol{u}}_{2,N-1}, \boldsymbol{z}_N\right),\\
\bar{v}_{2,N+1} &= \bar{v}_{2,N+1}\left(\widetilde{\boldsymbol{u}}_{2,N+1}, \tilde{\bar{x}}_{1,N+1/2}, \widetilde{\boldsymbol{u}}_{2,N}, \widetilde{\boldsymbol{u}}_{2,N-1}, \boldsymbol{z}_N\right),\\
\bar{p}_{2,N+1} &= \bar{p}_{2,N+1}\left(\widetilde{\boldsymbol{u}}_{2,N+1}, \tilde{\bar{x}}_{1,N+1/2}, \widetilde{\boldsymbol{u}}_{2,N}, \widetilde{\boldsymbol{u}}_{2,N-1}, \boldsymbol{z}_N\right).
\end{aligned}
\tag{3.93}
$$

A recurrence equation system of the form (3.69) can easily be obtained by eliminating the coupling variables with the help of the coupling conditions.

3.5. Stability and Convergence Plots of Extended Co-Simulation Approaches

In the previous sections, the recurrence equations for the extended (D-Extension and I-Extension) co-simulation approaches have been derived. As a result, the stability of the corresponding co-simulation approaches can be analyzed by calculating the spectral radius of the governing system of recurrence equations.

3.5.1. Stability Plots for Force/Force Coupling

Figure 3.13 collects 2D stability plots for the implicit co-simulation approach based on force/force-coupling for the symmetrical co-simulation test model ($\alpha_{m21} = \alpha_{\Lambda r21} = \alpha_{\Lambda i21} = \alpha_{\Lambda rc1} = \alpha_{\Lambda ic1} = 1$). The first row shows stability plots for the original method, for the D-extended approach and for the I-extended approach for the case of constant approximation ($k = 0$). Plots for linear ($k = 1$) and quadratic ($k = 2$) approximation are collected in the second and third row. Corresponding plots for the unsymmetrical test model ($\alpha_{m21} = \alpha_{\Lambda r21} = \alpha_{\Lambda i21} = \alpha_{\Lambda rc1} = \alpha_{\Lambda ic1} = 10$) are depicted in Figure 3.14.

For the case of constant polynomials ($k = 0$) the original method is completely stable in the considered parameter range. The D- and I-extended methods, however, show some unstable points for $k = 0$. Hence, application of the extended methods may not be useful for $k = 0$. For higher order approximation with linear or quadratic approximation functions, a significantly increased stability behavior can be observed, especially for the important case that the subsystems have very different mechanical properties (unsymmetrical test model). The best numerical stability shows – at least for the considered parameters – the D-extended version for $k = 2$.

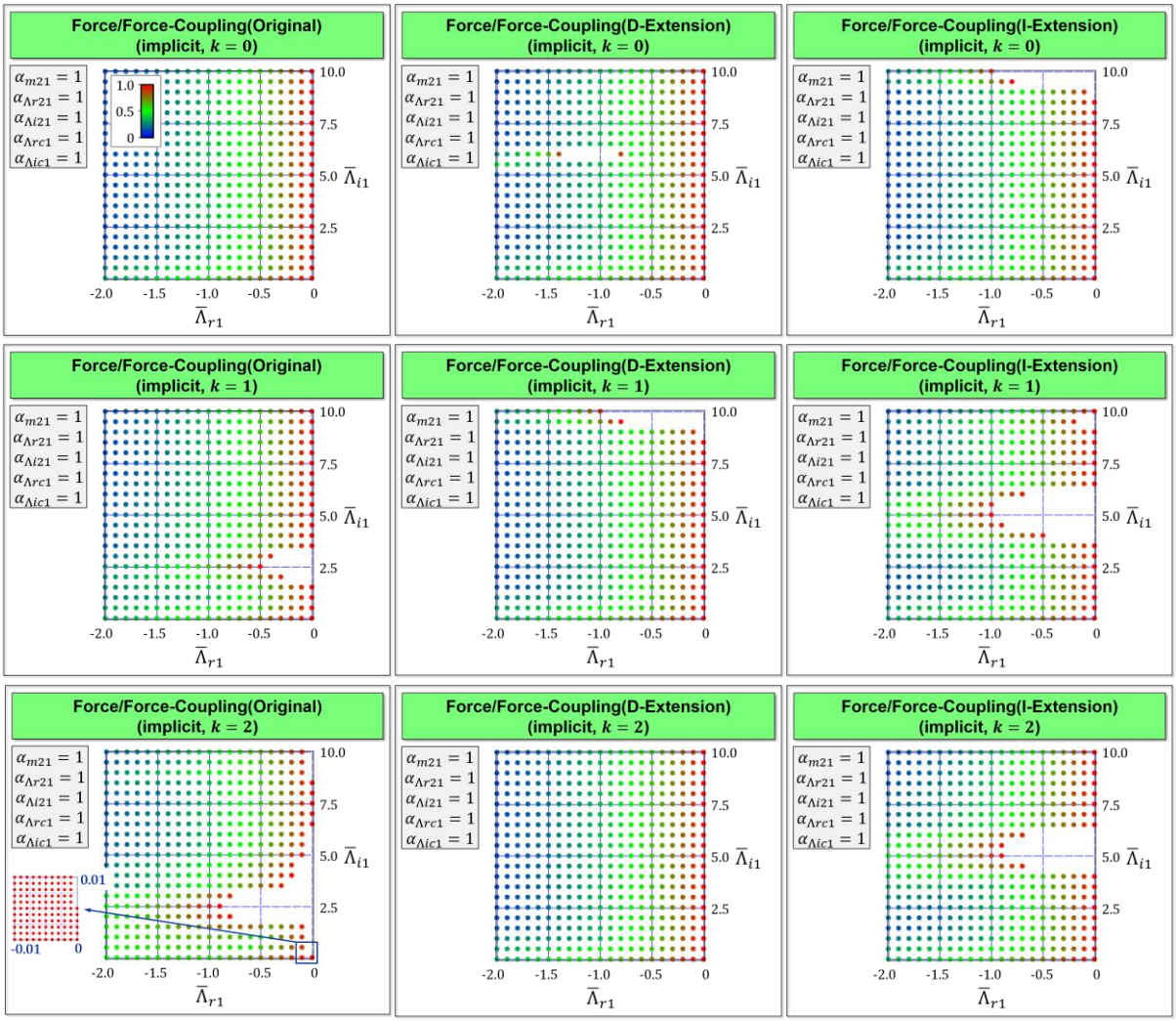

Figure 3.13 2D Stability plots for implicit co-simulation approaches using force/force decomposition: approximation order $k = 0, 1, 2$ for symmetrical test model

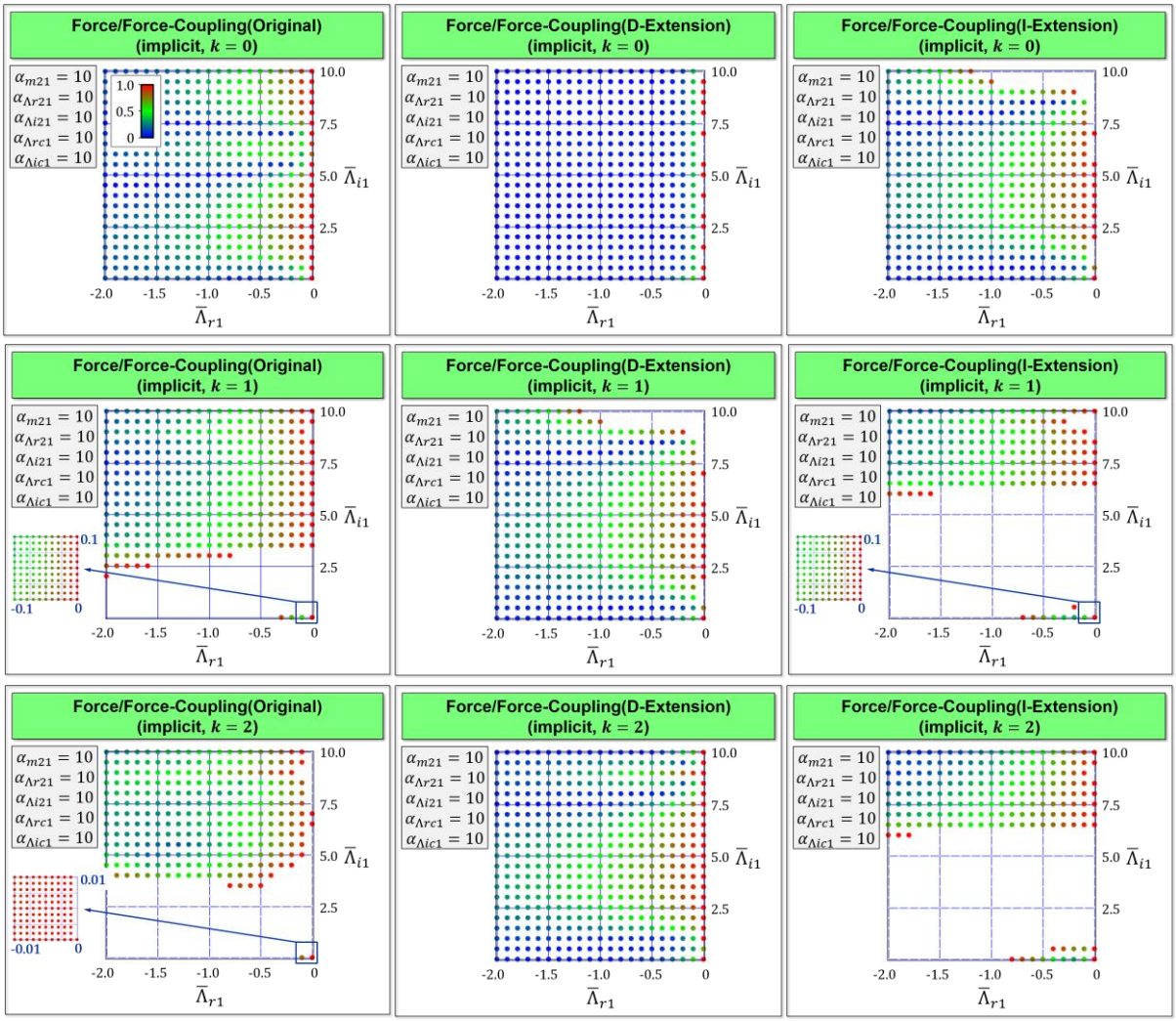

Figure 3.14 2D Stability plots for implicit co-simulation approaches using force/force decomposition: approximation order $k = 0, 1, 2$ for unsymmetrical test model

3.5.2. Stability Plots for Force/Displacement-Coupling

Stability plots for the symmetrical model are arranged in Figure 3.15 and for the unsymmetrical model in Figure 3.16. The results are similar to the case of force/force decomposition. The D-extended approach for $k = 2$ provides very good results for both the symmetrical and the unsymmetrical model.

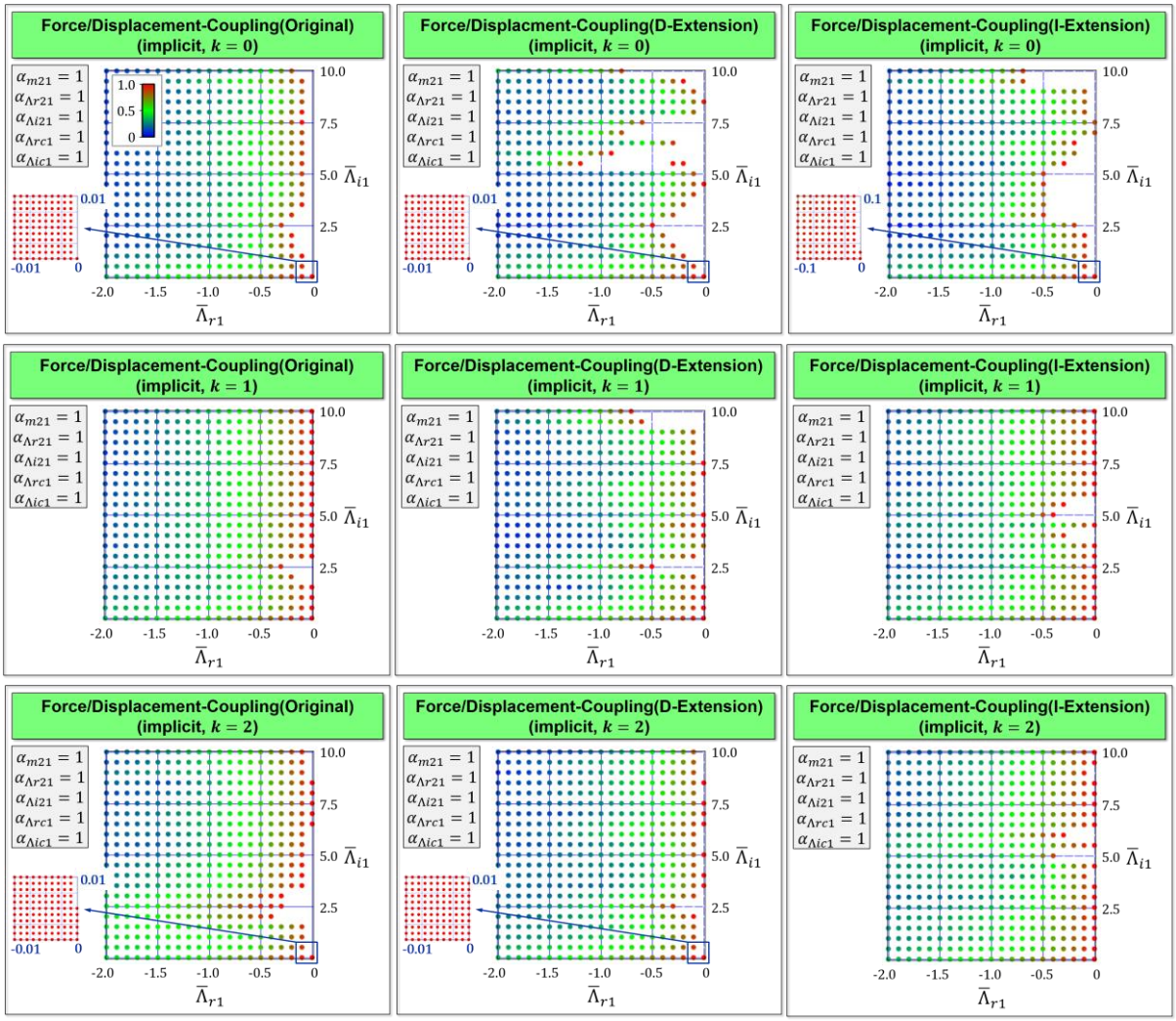

Figure 3.15 2D Stability plots for implicit co-simulation approaches using force/displacement decomposition: approximation order $k = 0, 1, 2$ for symmetrical test model

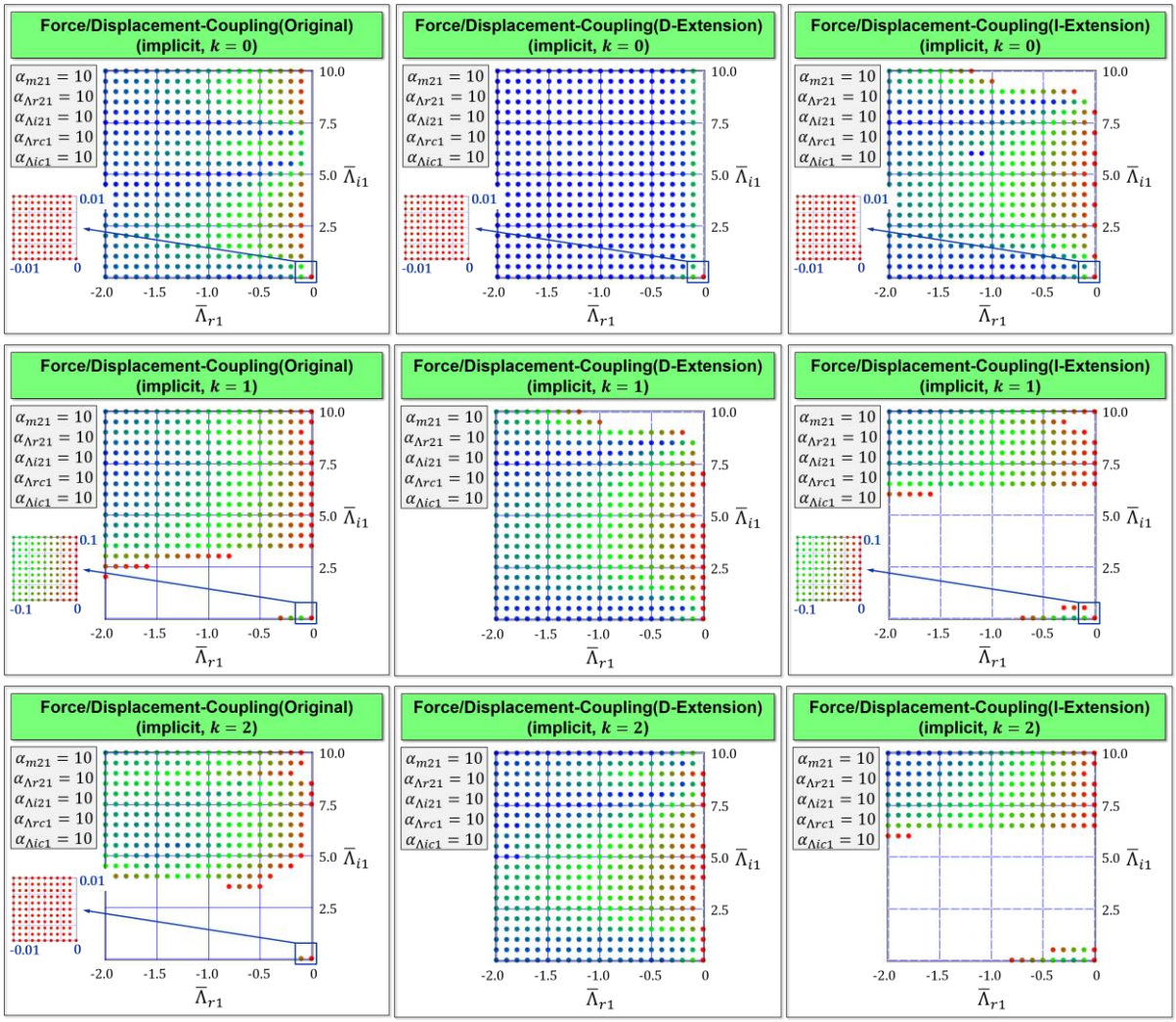

Figure 3.16 2D Stability plots for implicit co-simulation approaches using force/displacement decomposition: approximation order $k = 0, 1, 2$ for unsymmetrical test model

3.5.3. Stability Plots for Displacement/Displacement-Coupling

In Figure 3.17 and Figure 3.18, stability plots for the symmetrical and for the unsymmetrical model with displacement/displacement decomposition approach are collected. As can be seen, the original method as well as the D-extended and I-extended approach show a quite similar stability behavior. For the displacement/displacement-coupling approach, application of D- and I-extension may therefore not be beneficial.

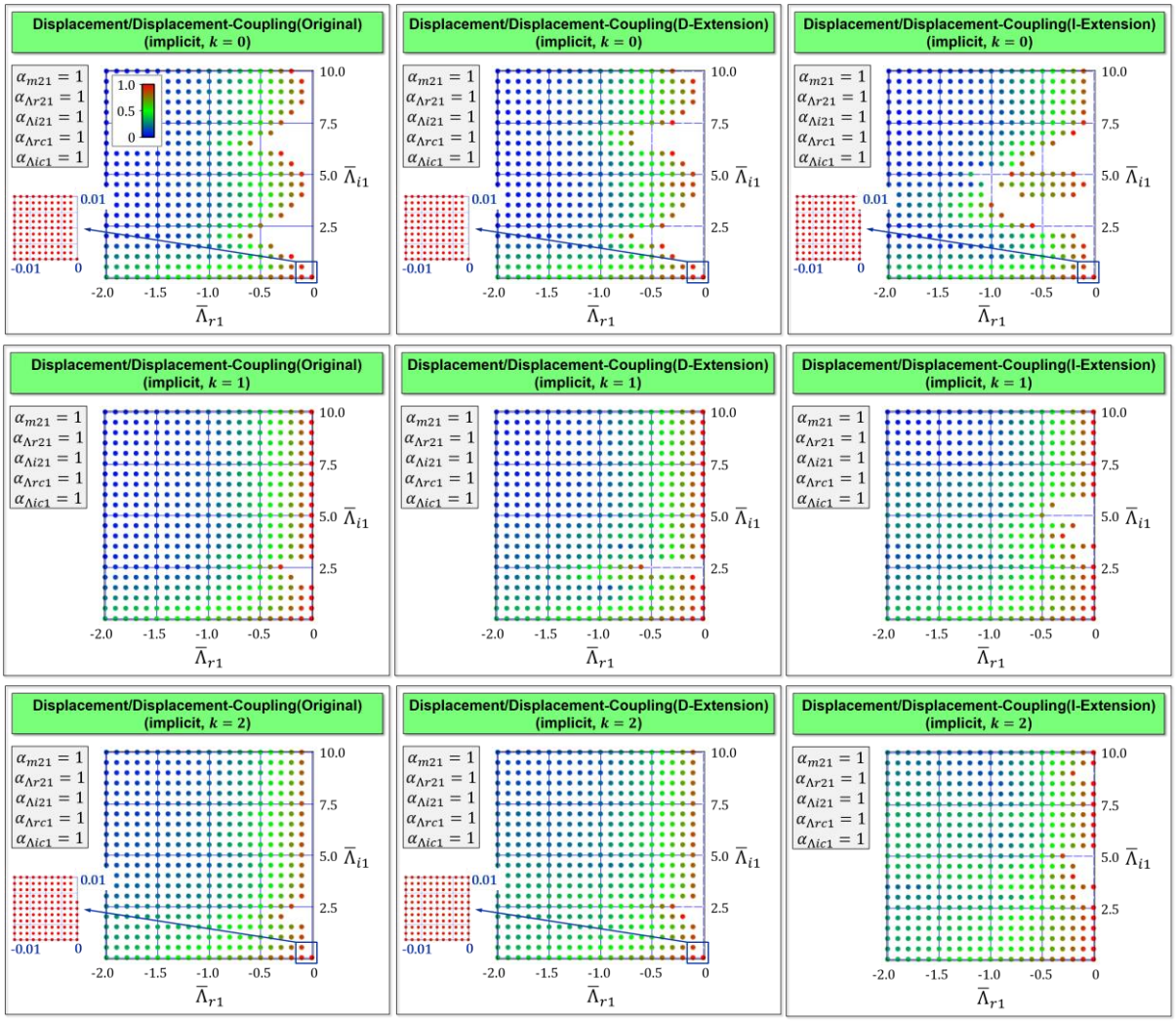

Figure 3.17 2D Stability plots for implicit co-simulation approaches using displacement/displacement decomposition: approximation order $k = 0, 1, 2$ for symmetrical test model

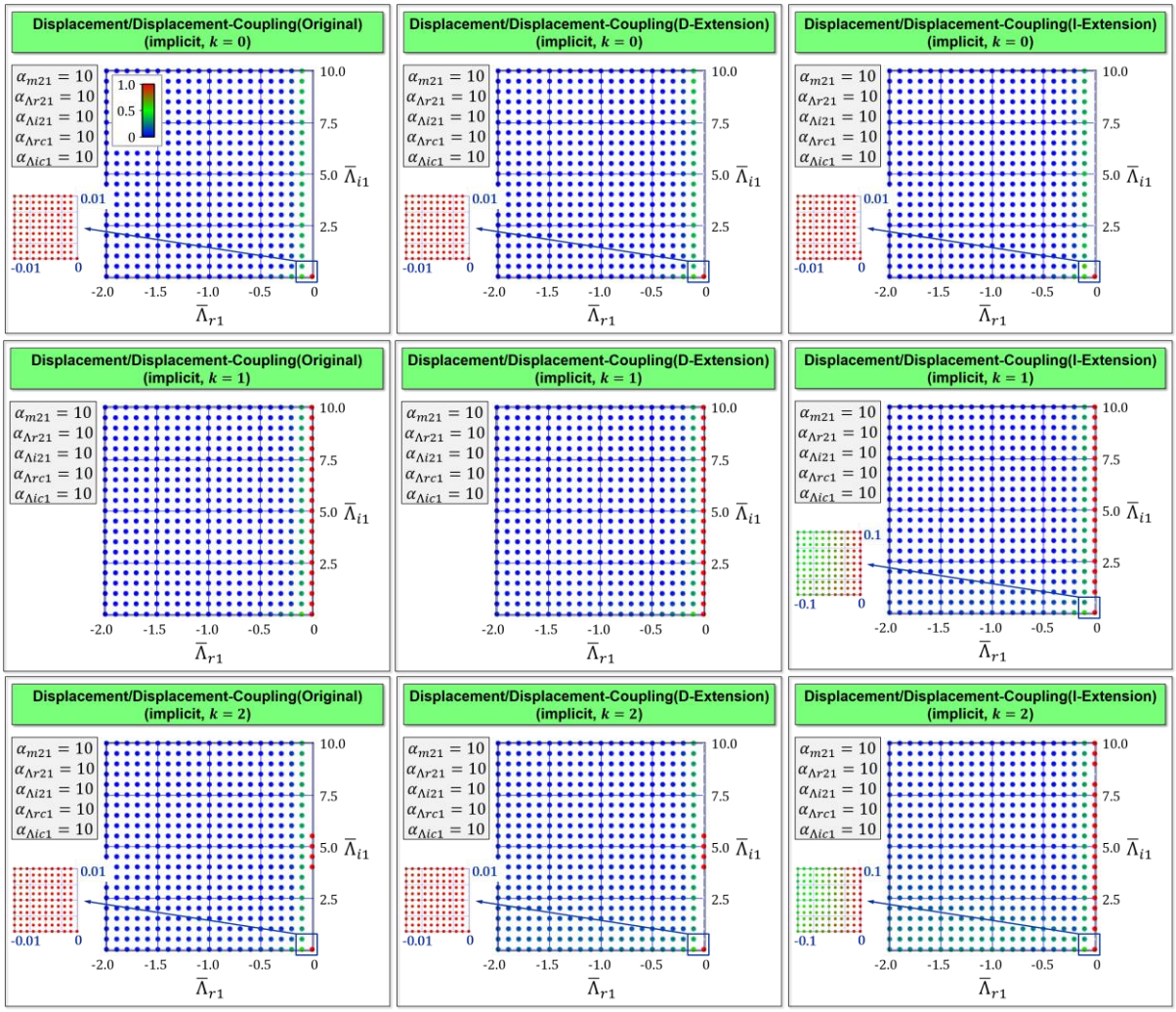

Figure 3.18 2D Stability plots for implicit co-simulation approaches using displacement/displacement decomposition: approximation order $k = 0, 1, 2$ for unsymmetrical test model

3.5.4. Convergence Plots

For the convergence analysis of the extended co-simulation approaches, the test model with force/force decomposition method is considered. The parameters $m_1 = 1, m_2 = 2,\ c_1 = c_2 = c_c = 1000,\ d_1 = d_2 = d_c = 10$ are used to calculate the global errors of the position and velocity variables as well as the local errors of the state variables according to the normalized root mean square error (NRMSE) in Eq. (3.34) and (3.35).

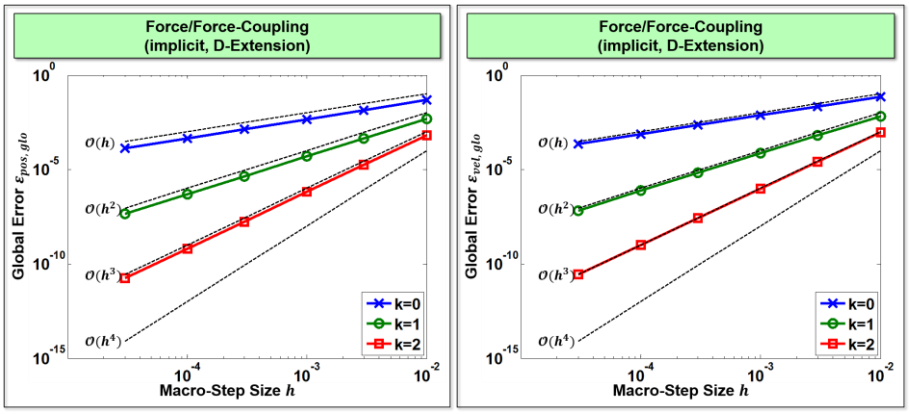

Figure 3.19 Global error plots for the D-Extension approach using force/force-decomposition

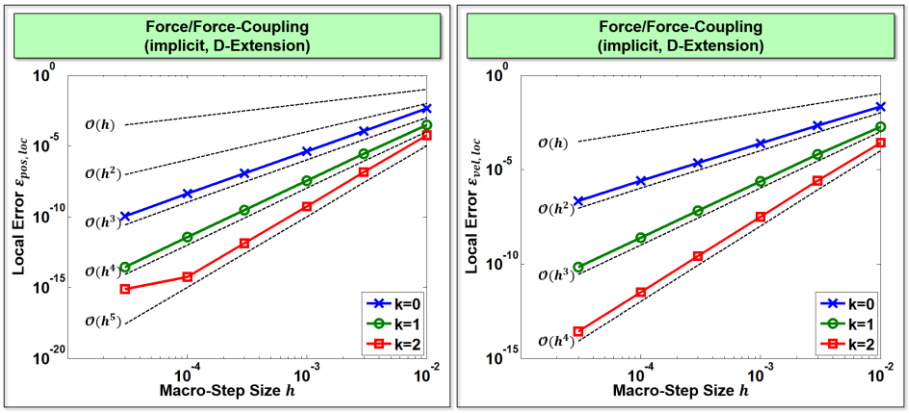

Figure 3.20 Local error plots for the D-Extension approach using force/force-decomposition

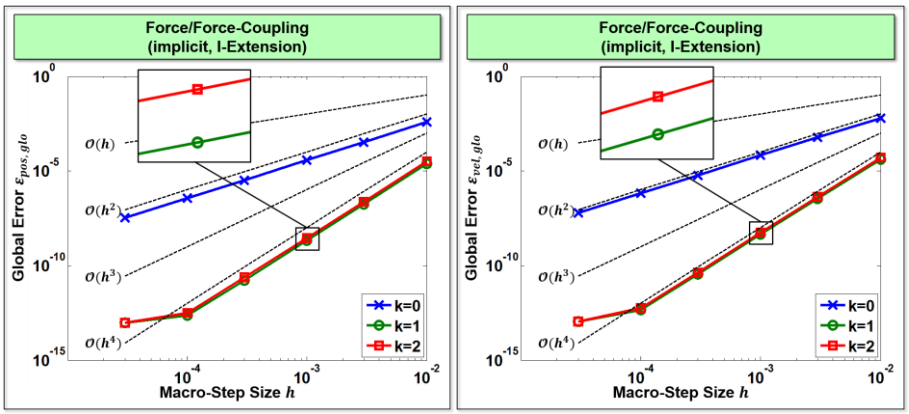

Figure 3.21 Global error plots for the I-Extension approach using force/force-decomposition

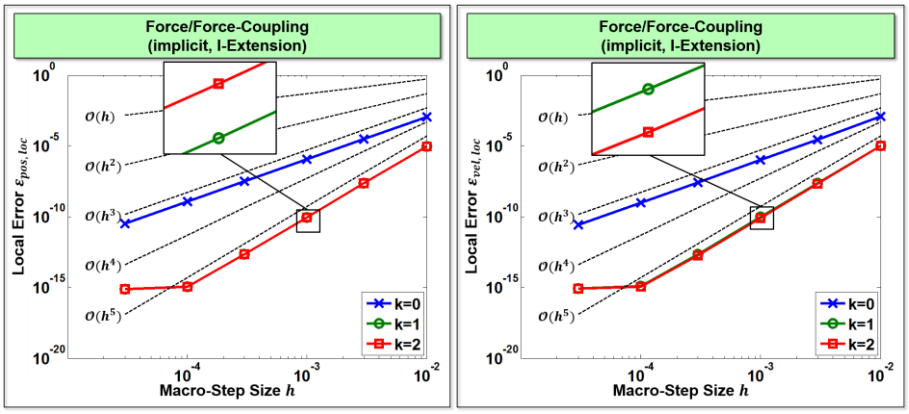

Figure 3.22 Local error plots for the I-Extension approach using force/force-decomposition

Convergence plots of the extended (D-Extension and I-Extension) force/force co-simulation approaches for the global errors $\varepsilon_{pos,glo}$, $\varepsilon_{vel,glo}$ and for the local errors $\varepsilon_{pos,loc}$, $\varepsilon_{vel,loc}$ are depicted in Figure 3.19-Figure 3.22.

As can be seen from Figure 3.19 and Figure 3.20, the global errors of D-Extension method in the position and velocity variables converge with $\mathcal{O}(H^{k+1})$ and the corresponding local errors with $\mathcal{O}(H^{k+3})$ and $\mathcal{O}(H^{k+2})$, respectively. For the I-Extension methods, see Figure 3.21 and Figure 3.22, the global errors for the position and velocity variables with respect to the constant approximation $(k = 0)$ converge with $\mathcal{O}(H^2)$ and with $\mathcal{O}(H^4)$ for linear and quadratic approximation. The corresponding local errors converge with $\mathcal{O}(H^3)$ for $k = 0$ and with $\mathcal{O}(H^5)$ for $k = 1$ and $k = 2$.

3.6. Nonlinear Example: Planar Four-Bar Mechanism

In order to demonstrate the improved numerical stability of the extended co-simulation approaches, the planar four-bar mechanism with the parameters of Section 3.3 is used again, see Figure 3.10.

Simulation results for the original (O-FF), the D-extended (D-FF) and the I-extended (I-FF) approach for constant $(k = 0)$, linear $(k = 1)$ and quadratic $(k = 2)$ approximation polynomials based on force/force decomposition are collected in Figure 3.23.

Depicted are the rotation angles $\varphi_2(t)$ and $\varphi_4(t)$ of bar 2 and bar 4, the corresponding angular velocities $\dot{\varphi}_2(t)$ and $\dot{\varphi}_4(t)$, the coupling force $\lambda_{cx}(t) = c_{cx} \cdot \big((x_3 - 0.5 \cdot l_3 \cdot cos\,\varphi_3) - (x_2 + 0.5 \cdot l_2 \cdot cos\,\varphi_2)\big) + d_{cx} \cdot \big((\dot{x}_3 + 0.5 \cdot l_3 \cdot sin\,\varphi_3 \cdot \dot{\varphi}_3) - (\dot{x}_2 - 0.5 \cdot l_2 \cdot sin\,\varphi_2 \cdot \dot{\varphi}_2)\big)$ acting in the bushing element in x-direction as well as the coupling torque $\lambda_{c\varphi}(t) = c_{c\varphi} \cdot (\varphi_3 - \varphi_2) + d_{c\varphi} \cdot (\dot{\varphi}_3 - \dot{\varphi}_2)$. It should be mentioned that the bushing stiffnesses have been set to $c_{cx} = c_{cy} = 1E3\ \mathrm{N/m}$ and $c_{c\varphi} = 1E3\ \mathrm{Nm/rad}$, the damping parameters of the bushing have assumed to be $d_{cx} = d_{cy} = 10\ \mathrm{Ns/m}$ and $d_{c\varphi} = 10\ \mathrm{Nms/rad}$. The co-simulations have been carried out with the constant macro-step size $H = 1E-3\ \mathrm{s}$. As can be seen, all coupling approaches yield stable and accurate simulation results.

Corresponding calculation results for the case of force/displacement-decomposition are collected in Figure 3.24. The coupling approaches yield stable and accurate results with two exceptions. The original and the D-extended method are unstable for the case that constant approximation polynomials are used.

In Figure 3.25, results are shown for the case that displacement/displacement-decomposition is applied. Results are similar to the force/displacement-approach: instabilities are detected for the original and for the D-extended method for $k = 0$.

Furthermore, a second case study is carried out to show the improved numerical stability of the D-extended approach in connection with force/force-decomposition. Therefore, the coupling stiffness parameters are successively increased. The coupling stiffness parameters are assumed to be equal ($c_{cx} = c_{cy} = c_{c\varphi} = c_c$), where c_c is set to $1E4, 1E5$ and $1E6$. The co-simulations have been carried out with the constant macro-step size $H = 5E-3$ s.

For $c_c = 1E4$, all coupling approaches are stable. For $c_c = 1E5$, the original approach becomes unstable for $k = 1$ and $k = 2$. For $c_c = 1E6$, also the I-extended approach gets unstable for $k = 1$ and $k = 2$. These results are in good correlation with the results of stability plots. The larger the coupling stiffness is chosen, the larger gets the asymmetry of the system described by the parameter $\alpha_{\lambda ic1}$. The stability plots in Figure 3.14, Figure 3.16 and Figure 3.18 represent the numerical stability for asymmetrical models. As can be seen, the basic trends obtained with the test model – very good stability behavior of the D-extended approach; slightly improved stability behavior of the I-extended approach compared to the original method – are also observed with the nonlinear model.

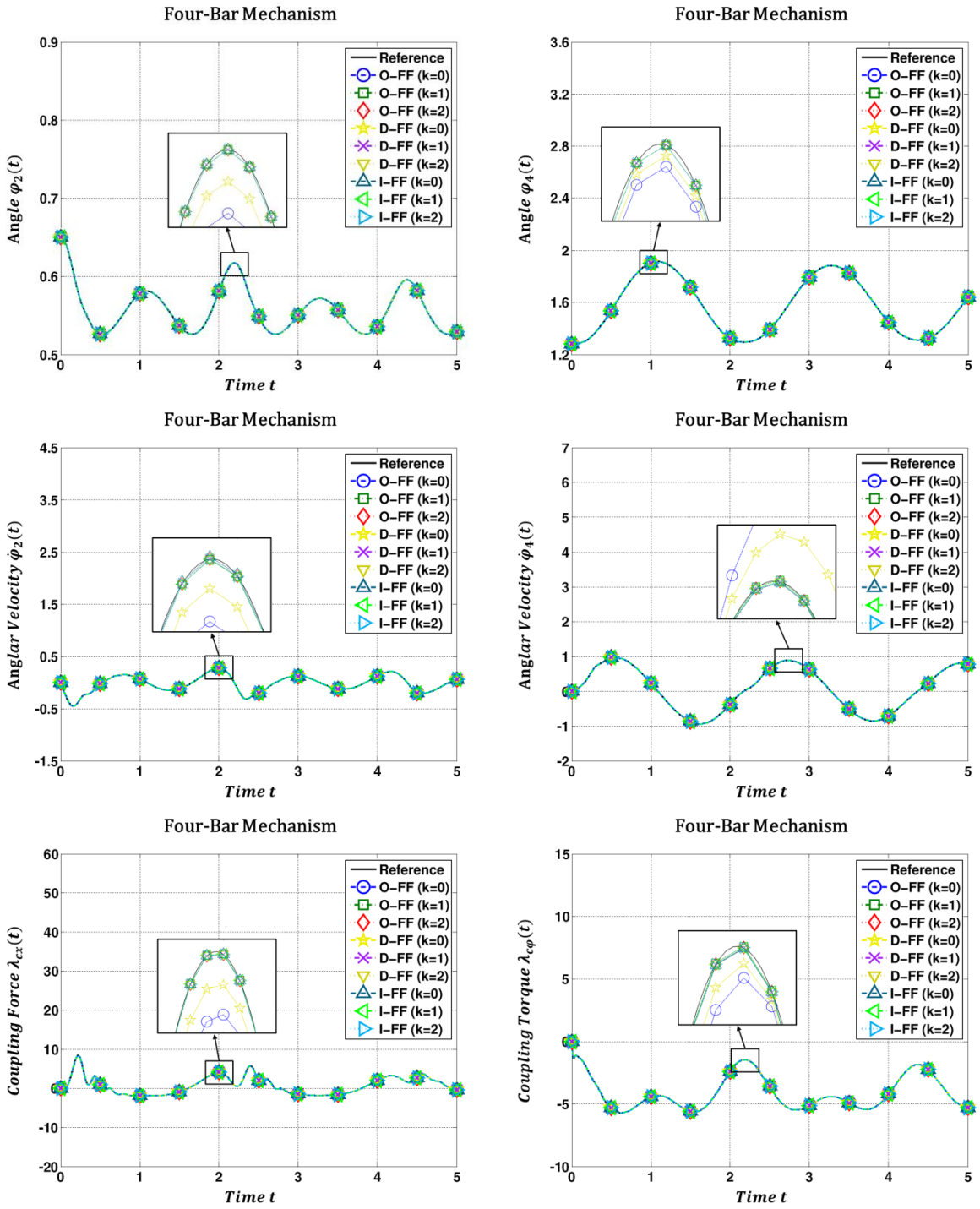

Figure 3.23 Simulation results for the four-bar mechanism based on force/force-decomposition: Rotation angles $\varphi_2(t), \varphi_4(t)$ and angular velocities $\dot{\varphi}_2(t), \dot{\varphi}_4(t)$; coupling force $\lambda_{cx}(t)$ and coupling torque $\lambda_{c\varphi}(t)$

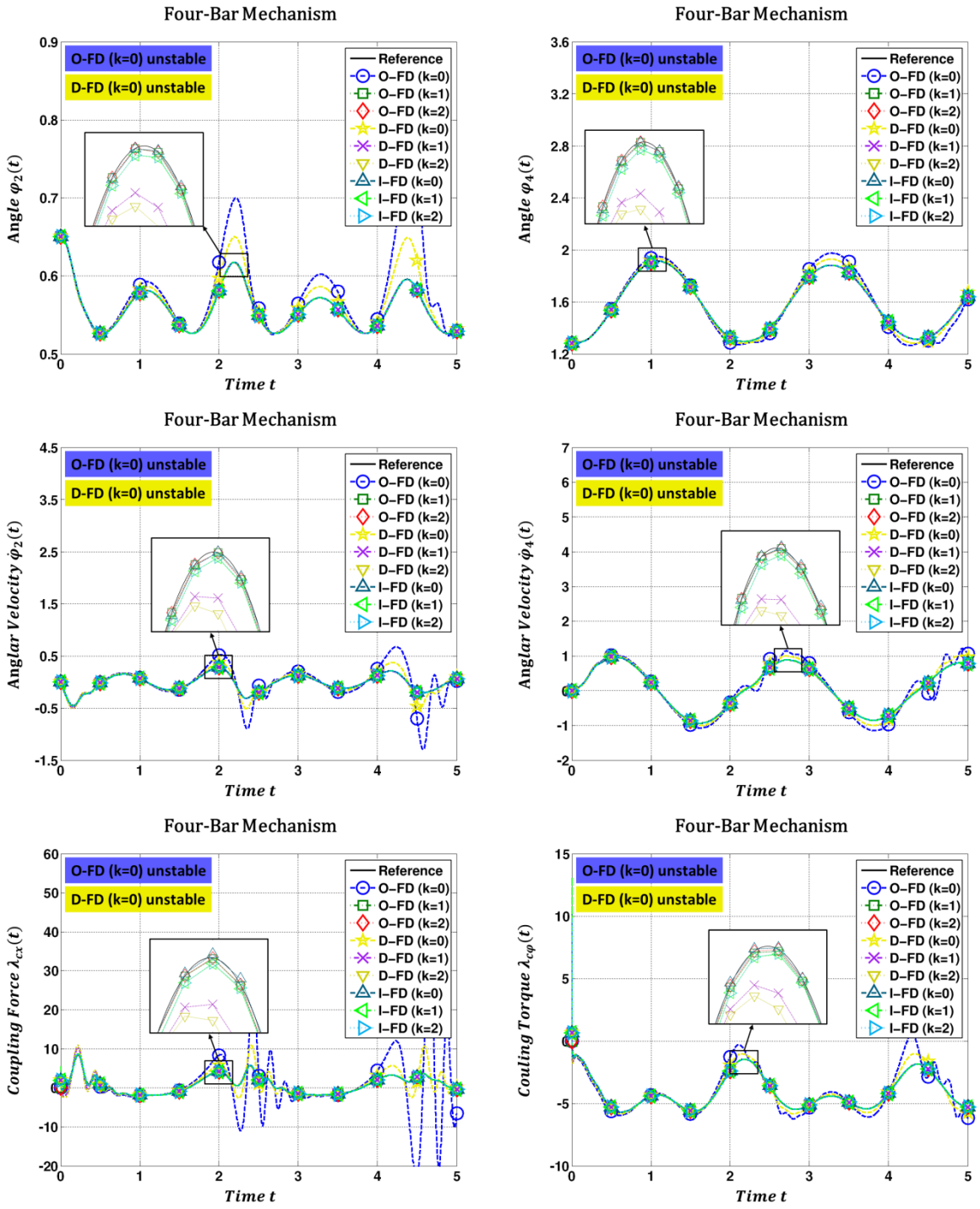

Figure 3.24 Simulation results for the four-bar mechanism based on force/displacement-decomposition: Rotation angles $\varphi_2(t), \varphi_4(t)$ and angular velocities $\dot{\varphi}_2(t), \dot{\varphi}_4(t)$; coupling force $\lambda_{cx}(t)$ and coupling torque $\lambda_{c\varphi}(t)$

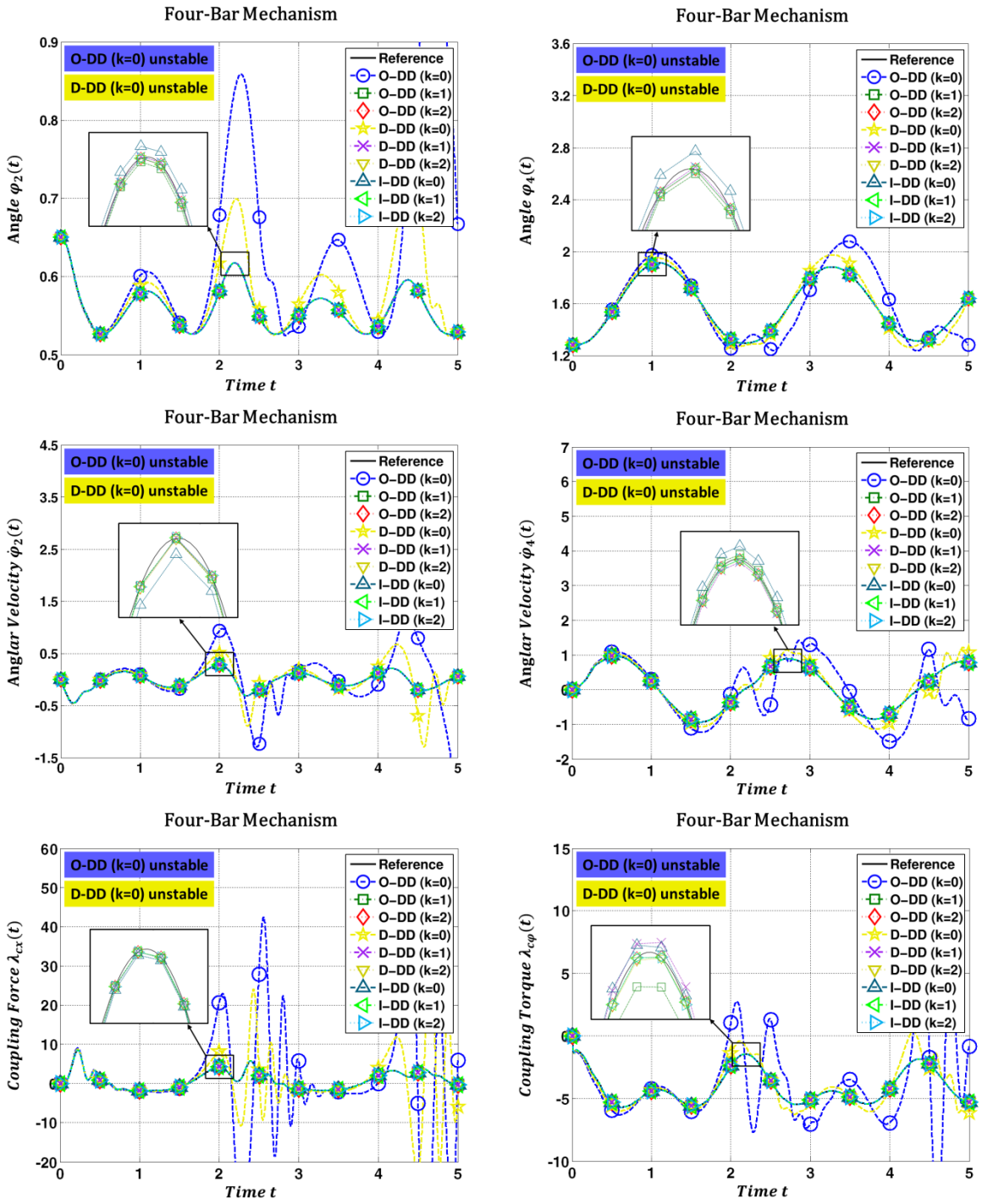

Figure 3.25 Simulation results for the four-bar mechanism based on displacement/displacement-decomposition: Rotation angles $\varphi_2(t), \varphi_4(t)$ and angular velocities $\dot{\varphi}_2(t), \dot{\varphi}_4(t)$; coupling force $\lambda_{cx}(t)$ and coupling torque $\lambda_{c\varphi}(t)$

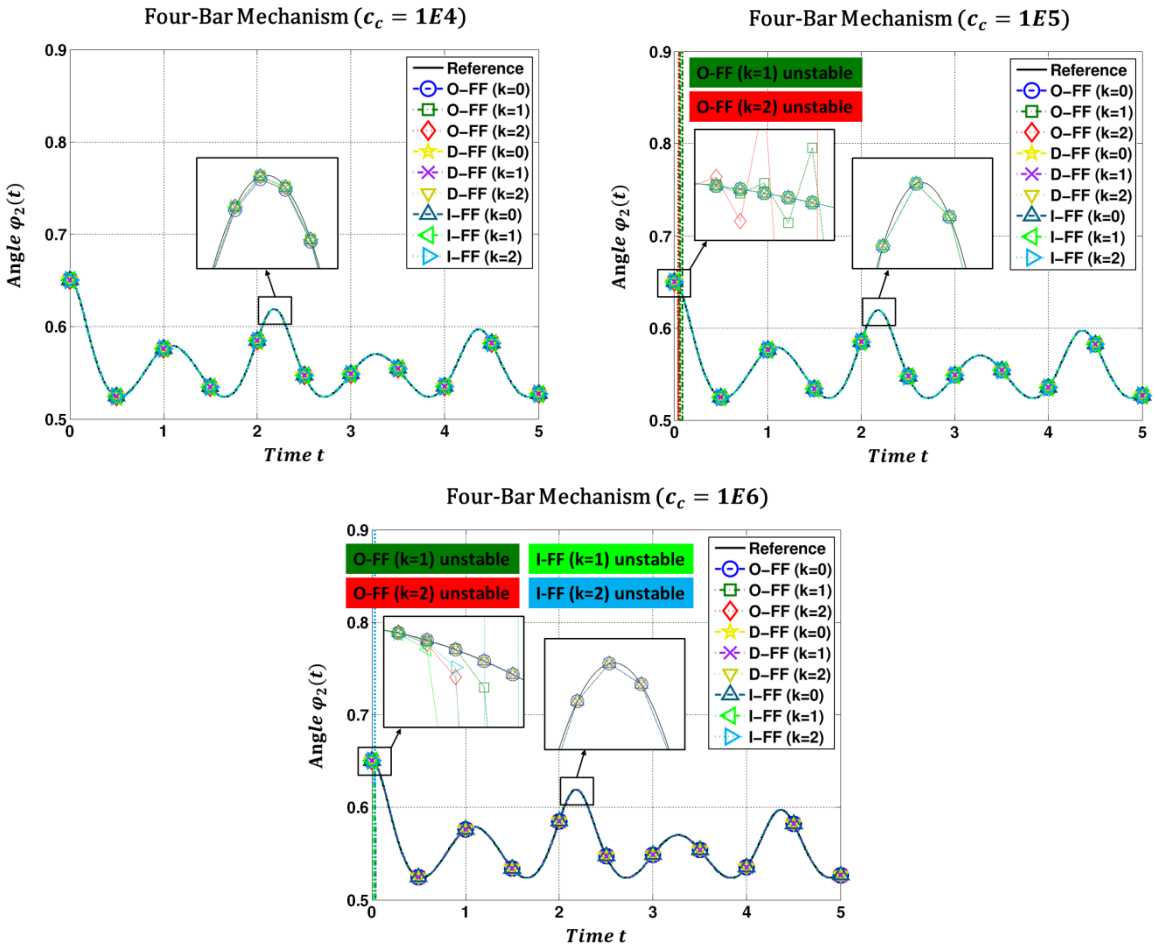

Figure 3.26 Simulation results for the four-bar mechanism based on force/force-decomposition for different coupling stiffness parameters: Rotation angle $\varphi_2(t)$

4. Stability Analysis of Co-Simulation Methods with Algebraic Constraints

The analysis of the numerical stability of co-simulation methods with algebraic constraints is subject of this chapter. Based on the test model introduced in section 2, (the two-mass oscillator connected by a rigid link), three different implicit coupling schemes are firstly investigated, namely a coupling approach based on Baumgarte stabilization, a weighted multiplier technique and a projection approach. We consider again the three decomposition methods, i.e. force/force-, force/displacement-, displacement/displacement decomposition. The stability of the co-simulation methods with algebraic constraints is again determined by calculating the spectral radius of the corresponding recurrence equations system resulting from the integration of the equations of motion of the test model. An improvement of the stability properties is possible by discretizing the Lagrange multipliers between the macro-time points (extended multiplier approach) so that the coupling conditions on position, velocity and acceleration level can be fulfilled simultaneously. Stability and convergence plots will be are presented for the different methods.

4.1. Recurrence Equations of Force/Force Coupling Approach

4.1.1. Co-Simulation Method Based on Baumgarte Stabilization

Applying a force/force decomposition technique to split the test model into two subsystems, one obtains two force-driven single-mass oscillators, see Figure 4.1. Both masses are driven by the coupling force λ_c.

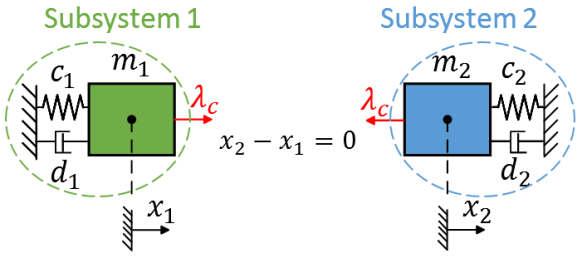

Figure 4.1 Co-simulation test model for force/force coupling approach

Using the modified variables $\bar{x}_1, \bar{x}_2, \bar{v}_1, \bar{v}_2$ and $\bar{\lambda}_c$ as well as the parameters from Eq. (2.10), the decomposed system is described by the following DAE system

Subsystem 1:

$$\begin{aligned} \bar{x}_1' &= \bar{v}_1 \\ \bar{v}_1' &= -\bar{c}_1 \cdot \bar{x}_1 - \bar{d}_1 \cdot \bar{v}_1 + \bar{\lambda}_c \end{aligned} \tag{4.1a}$$

Subsystem 2:

$$\begin{aligned} \bar{x}_2' &= \bar{v}_2 \\ \bar{v}_2' &= -\frac{\alpha_{c21}}{\alpha_{m21}} \cdot \bar{c}_1 \cdot \bar{x}_2 - \frac{\alpha_{d21}}{\alpha_{m21}} \cdot \bar{d}_1 \cdot \bar{v}_2 - \frac{1}{\alpha_{m21}} \bar{\lambda}_c \end{aligned} \tag{4.1b}$$

Coupling condition:

$$\bar{g}_{c\lambda}^{B} := (\bar{x}_2 - \bar{x}_1) + \bar{\beta} \cdot (\bar{v}_2 - \bar{v}_1) + \bar{\gamma} \cdot (\bar{v}_2' - \bar{v}_1') = 0\,. \tag{4.1c}$$

Note that the constraint equation $\bar{x}_2 - \bar{x}_1 = 0$ has been modified by using the well-known Baumgarte stabilization technique. $\bar{\beta} > 0$ and $\bar{\gamma} > 0$ are real-valued parameters, which have to be specified by the user. It should be mentioned that $\bar{\beta} = \beta/H$ and $\bar{\gamma} = \gamma/H^2$ denote modified (dimensionless) Baumgarte parameters.

Again, the general macro-time step from $\bar{T}_N$ to $\bar{T}_{N+1}$ is considered and the recurrence equations system for the discretized test-model is derived. In order to integrate the subsystems from $\bar{T}_N$ to $\bar{T}_{N+1}$, it is necessary to approximate the coupling variables $\bar{\lambda}_c$ in the time interval $[\bar{T}_N, \bar{T}_{N+1}]$. The approximation is accomplished with Lagrange polynomials of degree k. For the definition of the Lagrange polynomials, $k+1$ sampling points have to be specified. For instance, using the $k+1$ sampling points $(\bar{T}_N, \bar{\lambda}_{c,N}), (\bar{T}_{N-1}, \bar{\lambda}_{c,N-1}), \dots, (\bar{T}_{N-k}, \bar{\lambda}_{c,N-k})$, we get a polynomial of degree k, which we abbreviate by $P_{\bar{\lambda}_c}[(\bar{T}_N, \bar{\lambda}_{c,N}), (\bar{T}_{N-1}, \bar{\lambda}_{c,N-1}), \dots, (\bar{T}_{N-k}, \bar{\lambda}_{c,N-k}); \bar{t}]$.

At the beginning of the macro-time step, the state variables and the coupling variable are assumed to be known

$$\begin{aligned} \bar{x}_1(\bar{t} = \bar{T}_N) &= \bar{x}_{1,N}\,, \qquad \bar{v}_1(\bar{t} = \bar{T}_N) = \bar{v}_{1,N}\,, \\ \bar{x}_2(\bar{t} = \bar{T}_N) &= \bar{x}_{2,N}\,, \qquad \bar{v}_2(\bar{t} = \bar{T}_N) = \bar{v}_{2,N}\,, \end{aligned} \tag{4.2a}$$

$$\bar{\lambda}_c(\bar{t} = \bar{T}_N) = \bar{\lambda}_{c,N}\,. \tag{4.2b}$$

As in the previous sections, the implicit co-simulation approach considered is again a predictor/corrector approach and can be subdivided into 3 steps. Again, predicted variables are indicated with an upper index p (e.g.$\bar{x}_{1,N+1}^{p}$). Variables without upper index are assumed to be corrected variables (e.g. $\bar{x}_{1,N+1}$). For the following representation, we use the vectors $\boldsymbol{z}_N = \left(\bar{x}_{1,N}, \bar{v}_{1,N}, \bar{x}_{2,N}, \bar{v}_{2,N}\right)^T$, $\boldsymbol{z}_{N-1} = \left(\bar{x}_{1,N-1}, \bar{v}_{1,N-1}, \bar{x}_{2,N-1}, \bar{v}_{2,N-1}\right)^T$, …, $\boldsymbol{z}_{N-k} = \left(\bar{x}_{1,N-k}, \bar{v}_{1,N-k}, \bar{x}_{2,N-k}, \bar{v}_{2,N-k}\right)^T$, which collect the state variables of both subsystems at the macro-time points $\bar{T}_N$, $\bar{T}_{N-1}$, … , $\bar{T}_{N-k}$.

Step 1: Predictor Step

By analytically integrating subsystem 1 and subsystem 2 from $\bar{T}_N$ to $\bar{T}_{N+1}$ with the initial conditions (4.2a) and with the predictor (extrapolation) polynomial

$$\bar{\lambda}_c^p(\bar{t}) = P_{\bar{\lambda}_c}^p\left[\left(\bar{T}_N, \bar{\lambda}_{c,N}\right), \left(\bar{T}_{N-1}, \bar{\lambda}_{c,N-1}\right), \dots, \left(\bar{T}_{N-k}, \bar{\lambda}_{c,N-k}\right); \bar{t}\right], \tag{4.3}$$

one obtains the predicted state variables

$$\bar{x}_{1,N+1}^p, \quad \bar{v}_{1,N+1}^p \quad \text{and} \quad \bar{x}_{2,N+1}^p, \quad \bar{v}_{2,N+1}^p \tag{4.4}$$

at the macro-time point $\bar{T}_{N+1}$. It should be stressed that the predicted variables are depending on $\bar{\lambda}_{c,N}, \bar{\lambda}_{c,N-1}, \dots, \bar{\lambda}_{c,N-k}, \boldsymbol{z}_N$.

Step 2: Calculation of Corrected Coupling Force

An analytical integration of subsystem 1 and subsystem 2 from $\bar{T}_N$ to $\bar{T}_{N+1}$ with the initial conditions (4.2a) and with the interpolation polynomial

$$\bar{\lambda}_c^*(\bar{t}) = P_{\bar{\lambda}_c}^*\left[\left(\bar{T}_{N+1}, \bar{\lambda}_{c,N+1}^*\right), \left(\bar{T}_N, \bar{\lambda}_{c,N}\right), \dots, \left(\bar{T}_{N-k+1}, \bar{\lambda}_{c,N-k+1}\right); \bar{t}\right] \tag{4.5}$$

yields the state variables

$$\bar{x}_{1,N+1}^*, \quad \bar{v}_{1,N+1}^* \quad \text{and} \quad \bar{x}_{2,N+1}^*, \quad \bar{v}_{2,N+1}^* \tag{4.6}$$

at the macro-time point $\bar{T}_{N+1}$, which depend on $\bar{\lambda}_{c,N+1}^*, \bar{\lambda}_{c,N}, \dots, \bar{\lambda}_{c,N-k+1}, \boldsymbol{z}_N$. Note that $\bar{\lambda}_{c,N+1}^*$ represents an arbitrary coupling force at the macro-time point $\bar{T}_{N+1}$.

By differentiating the state variables of Eq. (4.6) and the corresponding acceleration variables $\bar{v}_{1,N+1}'^*$ and $\bar{v}_{2,N+1}'^*$ with respect to the arbitrary coupling force $\bar{\lambda}_{c,N+1}^*$, we get the partial derivatives

$$\begin{aligned} &\frac{\partial \bar{x}_{1,N+1}^*}{\partial \bar{\lambda}_{c,N+1}^*} = \text{const.}, \quad \frac{\partial \bar{v}_{1,N+1}^*}{\partial \bar{\lambda}_{c,N+1}^*} = \text{const.}, \quad \frac{\partial \bar{v}_{1,N+1}'^*}{\partial \bar{\lambda}_{c,N+1}^*} = \text{const.}, \\ &\frac{\partial \bar{x}_{2,N+1}^*}{\partial \bar{\lambda}_{c,N+1}^*} = \text{const.}, \quad \frac{\partial \bar{v}_{2,N+1}^*}{\partial \bar{\lambda}_{c,N+1}^*} = \text{const.}, \quad \frac{\partial \bar{v}_{2,N+1}'^*}{\partial \bar{\lambda}_{c,N+1}^*} = \text{const.}\ . \end{aligned} \tag{4.7}$$

It should be stressed that the partial derivatives are constant, because the state variables of Eq. (4.6) and the corresponding accelerations only depend linearly on $\bar{\lambda}_{c,N+1}^*$.

With the predicted variables and with the partial derivatives, a corrected coupling force $\bar{\lambda}_{c,N+1}$ can be computed, which fulfills the coupling condition (4.1c) at the macro-time point $\bar{T}_{N+1}$. Considering the fixed time point $\bar{T}_{N+1}$, $\bar{g}_{c\lambda,N+1}$ can be regarded as a function of the general coupling force $\bar{\lambda}_{c,N+1}^*$

$$\begin{aligned} &\bar{g}_{c\lambda,N+1}^B\left(\bar{\lambda}_{c,N+1}^*\right) \coloneqq \left(\bar{x}_{2,N+1}^*\left(\bar{\lambda}_{c,N+1}^*\right) - \bar{x}_{1,N+1}^*\left(\bar{\lambda}_{c,N+1}^*\right)\right) \\ &+ \bar{\beta} \cdot \left(\bar{v}_{2,N+1}^*\left(\bar{\lambda}_{c,N+1}^*\right) - \bar{v}_{1,N+1}^*\left(\bar{\lambda}_{c,N+1}^*\right)\right) + \bar{\gamma} \cdot \left(\bar{v}_{2,N+1}'^*\left(\bar{\lambda}_{c,N+1}^*\right) - \bar{v}_{1,N+1}'^*\left(\bar{\lambda}_{c,N+1}^*\right)\right). \end{aligned} \tag{4.8}$$

Note that the state variables $\bar{x}_{1,N+1}^*$, $\bar{x}_{2,N+1}^*$, $\bar{v}_{1,N+1}^*$, $\bar{v}_{2,N+1}^*$ and the accelerations $\bar{v}_{1,N+1}'^*$, $\bar{v}_{2,N+1}'^*$ depend only linearly on $\bar{\lambda}_{c,N+1}^*$. Thus, Eq. (4.8) can be rewritten as

$$
\begin{aligned}
&\bar{g}^{B}_{c\lambda,N+1}\left(\bar{\lambda}^{*}_{c,N+1}\right) \coloneqq \bar{g}^{B}_{c\lambda,N+1}\left(\bar{\lambda}^{p}_{c,N+1}\right) + \left.\frac{\partial \bar{g}^{B}_{c\lambda,N+1}}{\partial \bar{\lambda}^{*}_{c,N+1}}\right|_{\bar{\lambda}^{p}_{c,N+1}} \cdot \left(\bar{\lambda}^{*}_{c,N+1} - \bar{\lambda}^{p}_{c,N+1}\right) \\
&= \left(\bar{x}^{p}_{2,N+1} - \bar{x}^{p}_{1,N+1}\right) + \bar{\beta} \cdot \left(\bar{v}^{p}_{2,N+1} - \bar{v}^{p}_{1,N+1}\right) + \bar{\gamma} \cdot \left(\bar{v}'^{p}_{2,N+1} - \bar{v}'^{p}_{1,N+1}\right) \\
&+ \left[\left(\left.\frac{\partial \bar{x}^{*}_{2,N+1}}{\partial \bar{\lambda}^{*}_{c,N+1}}\right|_{\bar{\lambda}^{p}_{c,N+1}} - \left.\frac{\partial \bar{x}^{*}_{1,N+1}}{\partial \bar{\lambda}^{*}_{c,N+1}}\right|_{\bar{\lambda}^{p}_{c,N+1}}\right) + \bar{\beta} \cdot \left(\left.\frac{\partial \bar{v}^{*}_{2,N+1}}{\partial \bar{\lambda}^{*}_{c,N+1}}\right|_{\bar{\lambda}^{p}_{c,N+1}} - \left.\frac{\partial \bar{v}^{*}_{1,N+1}}{\partial \bar{\lambda}^{*}_{c,N+1}}\right|_{\bar{\lambda}^{p}_{c,N+1}}\right)\right. \\
&\left. + \bar{\gamma} \cdot \left(\left.\frac{\partial \bar{v}'^{*}_{2,N+1}}{\partial \bar{\lambda}^{*}_{c,N+1}}\right|_{\bar{\lambda}^{p}_{c,N+1}} - \left.\frac{\partial \bar{v}'^{*}_{1,N+1}}{\partial \bar{\lambda}^{*}_{c,N+1}}\right|_{\bar{\lambda}^{p}_{c,N+1}}\right)\right] \cdot \left(\bar{\lambda}^{*}_{c,N+1} - \bar{\lambda}^{p}_{c,N+1}\right) \ .
\end{aligned}
\tag{4.9}
$$

By setting $\bar{g}^{B}_{c\lambda,N+1}\left(\bar{\lambda}^{*}_{c,N+1}\right) = 0$, one obtains the corrected coupling force

$$
\begin{aligned}
&\bar{\lambda}_{c,N+1} = \bar{\lambda}^{p}_{c,N+1} \\
&- \frac{\left(\bar{x}^{p}_{2,N+1} - \bar{x}^{p}_{1,N+1}\right) + \bar{\beta} \cdot \left(\bar{v}^{p}_{2,N+1} - \bar{v}^{p}_{1,N+1}\right) + \cdots}{\left(\left.\frac{\partial \bar{x}^{*}_{2,N+1}}{\partial \bar{\lambda}^{*}_{c,N+1}}\right|_{\bar{\lambda}^{p}_{c,N+1}} - \left.\frac{\partial \bar{x}^{*}_{1,N+1}}{\partial \bar{\lambda}^{*}_{c,N+1}}\right|_{\bar{\lambda}^{p}_{c,N+1}}\right) + \bar{\beta}\left(\left.\frac{\partial \bar{v}^{*}_{2,N+1}}{\partial \bar{\lambda}^{*}_{c,N+1}}\right|_{\bar{\lambda}^{p}_{c,N+1}} - \left.\frac{\partial \bar{v}^{*}_{1,N+1}}{\partial \bar{\lambda}^{*}_{c,N+1}}\right|_{\bar{\lambda}^{p}_{c,N+1}}\right) + \cdots}
\end{aligned}
\tag{4.10}
$$

For the reason of a precise representation, we use different variables for the general coupling force $\bar{\lambda}^{*}_{c,N+1}$ at the time point $\bar{T}_{N+1}$ and the corrected coupling force $\bar{\lambda}_{c,N+1}$, which represents the root of Eq. (4.10).

Step 3: Corrector Step

Analytically integrating subsystem 1 and subsystem 2 from $\bar{T}_N$ to $\bar{T}_{N+1}$ and using the interpolated polynomial with the corrected coupling force $\bar{\lambda}_{c,N+1}$ from Eq. (4.10) yields the corrected states

$$
\bar{x}_{1,N+1}\,, \quad \bar{v}_{1,N+1} \quad \text{and} \quad \bar{x}_{2,N+1}\,, \quad \bar{v}_{2,N+1}\ , \tag{4.11}
$$

which are functions of $\bar{\lambda}_{c,N+1}, \bar{\lambda}_{c,N}, \ldots, \bar{\lambda}_{c,N-k+1}, \boldsymbol{z}_N$.

In Eq. (4.10), the predicted acceleration variables can be easily eliminated with the help of Equations (4.1a)-(4.1b) by means of

$$
\begin{aligned}
\bar{v}'^{p}_{1,N+1} &= -\bar{c}_1 \cdot \bar{x}^{p}_{1,N+1} - \bar{d}_1 \cdot \bar{v}^{p}_{1,N+1} + \bar{\lambda}^{p}_{c,N+1}\ , \\
\bar{v}'^{p}_{2,N+1} &= -\frac{\alpha_{c21}}{\alpha_{m21}} \cdot \bar{c}_1 \cdot \bar{x}^{p}_{2,N+1} - \frac{\alpha_{d21}}{\alpha_{m21}} \cdot \bar{d}_1 \cdot \bar{v}^{p}_{2,N+1} - \frac{1}{\alpha_{m21}} \bar{\lambda}^{p}_{c,N+1}\ .
\end{aligned}
\tag{4.12}
$$

Furthermore, the predicted position and velocity variables can be replaced with the help of Eq. (4.6) and the predicted Lagrange multiplier by means of Eq. (4.3) so that Eq. (4.11) finally results in a relationship of the form

$$
\bar{\lambda}_{c,N+1} = \bar{\lambda}_{c,N+1}\left(\bar{\lambda}_{c,N}, \bar{\lambda}_{c,N-1}, \ldots, \bar{\lambda}_{c,N-k}, \boldsymbol{z}_N\right) \tag{4.13}
$$

Combining Eq. (4.11) and Eq. (4.13) yields the governing system of recurrence equations

$$
\begin{aligned}
\bar{x}_{1,N+1} &= \bar{x}_{1,N+1}\left(\bar{\lambda}_{c,N+1}, \bar{\lambda}_{c,N}, \dots, \bar{\lambda}_{c,N-k+1}, \boldsymbol{z}_N\right), \\
\bar{v}_{1,N+1} &= \bar{v}_{1,N+1}\left(\bar{\lambda}_{c,N+1}, \bar{\lambda}_{c,N}, \dots, \bar{\lambda}_{c,N-k+1}, \boldsymbol{z}_N\right), \\
\bar{x}_{2,N+1} &= \bar{x}_{2,N+1}\left(\bar{\lambda}_{c,N+1}, \bar{\lambda}_{c,N}, \dots, \bar{\lambda}_{c,N-k+1}, \boldsymbol{z}_N\right), \\
\bar{v}_{2,N+1} &= \bar{v}_{2,N+1}\left(\bar{\lambda}_{c,N+1}, \bar{\lambda}_{c,N}, \dots, \bar{\lambda}_{c,N-k+1}, \boldsymbol{z}_N\right), \\
\bar{\lambda}_{c,N+1} &= \bar{\lambda}_{c,N+1}\left(\bar{\lambda}_{c,N}, \bar{\lambda}_{c,N-1}, \dots, \bar{\lambda}_{c,N-k}, \boldsymbol{z}_N\right).
\end{aligned}
\tag{4.14}
$$

Eq. (4.14) represents a system of 5 coupled linear recurrence equations of order $k+1$. Introducing the vectors $\hat{\boldsymbol{z}}_{N+1} = \left(\bar{x}_{1,N+1}, \bar{v}_{1,N+1}, \bar{x}_{2,N+1}, \bar{v}_{2,N+1}, \bar{\lambda}_{c,N+1}\right)^T \in \mathbb{R}^5$, $\hat{\boldsymbol{z}}_N$,etc., which collect the state variables of both subsystems and the Lagrange multiplier at the macro-time points. As a result, we obtain the recurrence equations in a compact form

$$
\widehat{\boldsymbol{A}}_{N+1} \cdot \hat{\boldsymbol{z}}_{N+1} + \widehat{\boldsymbol{A}}_N \cdot \hat{\boldsymbol{z}}_N + \cdots + \widehat{\boldsymbol{A}}_{N-k} \cdot \hat{\boldsymbol{z}}_{N-k} = \boldsymbol{0} \ . \tag{4.15}
$$

The real-valued matrices $\widehat{\boldsymbol{A}}_{N+1}$**,…,** $\widehat{\boldsymbol{A}}_{N-k} \in \mathbb{R}^{5\times5}$ are constant and depend only on the 5 dimensionless parameters of the co-simulation model defined in Eq. (2.10).

It should be stressed again that the subsystems are integrated analytically. This is possible, because the co-simulation test model is linear. Hence, the stability behavior of the system of recurrence equations (4.15) directly reflects (defines) the stability of the underlying co-simulation approach.

4.1.2. Co-Simulation Method based on Weighted Multiplier Approach

The second basic method analyzed in this chapter is called weighted multiplier approach, which makes use of the coupling equations on position, velocity and acceleration level in order to calculate corrected coupling variables for the corrector step. The weighted multiplier approach is almost identical with the Baumgarte co-simulation method of Section 4.1.1. Only step 2 has to be slightly modified.

Step 1: Predictor Step

Identical with Step 1 in Section 4.1.1.

Step 2: Calculation of Corrected Coupling Force

Instead of using Baumgarte stabilization technique to calculation the corrected coupling force shown in Eq. (4.10), the following corrected coupling force is applied

$$\bar{\lambda}_{c,N+1} = \bar{\lambda}^{p}_{c,N+1} - \frac{1}{1+a+b} \cdot \left[\frac{\left(\bar{x}^{p}_{2,N+1} - \bar{x}^{p}_{1,N+1}\right)}{\left(\left.\frac{\partial \bar{x}^{*}_{2,N+1}}{\partial \bar{\lambda}^{*}_{c,N+1}}\right|_{\bar{\lambda}^{p}_{c,N+1}} - \left.\frac{\partial \bar{x}^{*}_{1,N+1}}{\partial \bar{\lambda}^{*}_{c,N+1}}\right|_{\bar{\lambda}^{p}_{c,N+1}} \right)} \right.$$

$$\left. + a \cdot \frac{\left(\bar{v}^{p}_{2,N+1} - \bar{v}^{p}_{1,N+1}\right)}{\left(\left.\frac{\partial \bar{v}^{*}_{2,N+1}}{\partial \bar{\lambda}^{*}_{c,N+1}}\right|_{\bar{\lambda}^{p}_{c,N+1}} - \left.\frac{\partial \bar{v}^{*}_{1,N+1}}{\partial \bar{\lambda}^{*}_{c,N+1}}\right|_{\bar{\lambda}^{p}_{c,N+1}} \right)} + b \cdot \frac{\left(\bar{v}'^{p}_{2,N+1} - \bar{v}'^{p}_{1,N+1}\right)}{\left(\left.\frac{\partial \bar{v}'^{*}_{2,N+1}}{\partial \bar{\lambda}^{*}_{c,N+1}}\right|_{\bar{\lambda}^{p}_{c,N+1}} - \left.\frac{\partial \bar{v}'^{*}_{1,N+1}}{\partial \bar{\lambda}^{*}_{c,N+1}}\right|_{\bar{\lambda}^{p}_{c,N+1}} \right)} \right] \tag{4.16}$$

The real-valued parameters $a > 0$ and $b > 0$ have to be specified by the user (e.g. $a = b = 1$). The physical interpretation of the weighted multiplier approach is straightforward. Calculating a corrected coupling force based on the constraint equation $\bar{g}^{pos}_{c\lambda} := \bar{x}_2 - \bar{x}_1 = 0$ on position level yields the corrected coupling force

$$\bar{\lambda}^{pos}_{c,N+1} = \bar{\lambda}^{p}_{c,N+1} - \frac{\left(\bar{x}^{p}_{2,N+1} - \bar{x}^{p}_{1,N+1}\right)}{\left(\left.\frac{\partial \bar{x}^{*}_{2,N+1}}{\partial \bar{\lambda}^{*}_{c,N+1}}\right|_{\bar{\lambda}^{p}_{c,N+1}} - \left.\frac{\partial \bar{x}^{*}_{1,N+1}}{\partial \bar{\lambda}^{*}_{c,N+1}}\right|_{\bar{\lambda}^{p}_{c,N+1}} \right)}. \tag{4.17}$$

Analogously, by using the constraint equation $\bar{g}^{vel}_{c\lambda} := \bar{v}_2 - \bar{v}_1 = 0$ on velocity level, the corrected coupling force is given by

$$\bar{\lambda}^{vel}_{c,N+1} = \bar{\lambda}^{p}_{c,N+1} - \frac{\left(\bar{v}^{p}_{2,N+1} - \bar{v}^{p}_{1,N+1}\right)}{\left(\left.\frac{\partial \bar{v}^{*}_{2,N+1}}{\partial \bar{\lambda}^{*}_{c,N+1}}\right|_{\bar{\lambda}^{p}_{c,N+1}} - \left.\frac{\partial \bar{v}^{*}_{1,N+1}}{\partial \bar{\lambda}^{*}_{c,N+1}}\right|_{\bar{\lambda}^{p}_{c,N+1}} \right)}. \tag{4.18}$$

Applying the constraint equation $\bar{g}^{acc}_{c\lambda} := \bar{v}'_2 - \bar{v}'_1 = 0$ on acceleration level results in the corrected coupling force

$$\bar{\lambda}^{acc}_{c,N+1} = \bar{\lambda}^{p}_{c,N+1} - \frac{\left(\bar{v}'^{p}_{2,N+1} - \bar{v}'^{p}_{1,N+1}\right)}{\left(\left.\frac{\partial \bar{v}'^{*}_{2,N+1}}{\partial \bar{\lambda}^{*}_{c,N+1}}\right|_{\bar{\lambda}^{p}_{c,N+1}} - \left.\frac{\partial \bar{v}'^{*}_{1,N+1}}{\partial \bar{\lambda}^{*}_{c,N+1}}\right|_{\bar{\lambda}^{p}_{c,N+1}} \right)}. \tag{4.19}$$

Hence, the corrected coupling force $\bar{\lambda}_{c,N+1}$ defined in Eq. (4.16) is simply the weighted sum of $\bar{\lambda}^{pos}_{c,N+1}$, $\bar{\lambda}^{vel}_{c,N+1}$ and $\bar{\lambda}^{acc}_{c,N+1}$.

Step 3: Corrector Step

As step 3 in Section 4.1.1, however the corrected coupling force $\bar{\lambda}_{c,N+1}$ according to Eq. (4.16) is used to get the final corrected state variables.

Using the weighted multiplier approach also yields a linear system of recurrence equations of order $k+1$ with the same structure as Eq. (4.15). The matrices $\widehat{\boldsymbol{A}}_{N+1}$**,…,** $\widehat{\boldsymbol{A}}_{N-k} \in \mathbb{R}^{5\times5}$ for the weighted multiplier approach are, however, different from the corresponding matrices of the Baumgarte method.

4.1.3. Co-Simulation Method based on Projection Technique

The third method investigated here is based on a classical projection and carried out in four steps.

Step 1: Predictor Step

Identical with step 1 in Section 4.1.1.

Step 2: Calculation of Corrected Coupling Force

Identical with step 2 in Section 4.1.1 with one exception. Instead of calculating the corrected coupling force according to Eq. (4.10), the corrected coupling force $\bar{\lambda}_{c,N+1}^{acc}$ according to Eq. (4.19) is computed.

Step 3: Corrector Step

As step 3 in Section 4.1.1, however $\bar{\lambda}_{c,N+1} = \bar{\lambda}_{c,N+1}^{acc}$ is used as corrected coupling force. The results are the corrected state variables

$$\bar{x}_{1,N+1}\,,\quad \bar{v}_{1,N+1} \quad \text{and} \quad \bar{x}_{2,N+1}\,,\quad \bar{v}_{2,N+1}\,, \tag{4.20}$$

which depend on $\bar{\lambda}_{c,N+1}, \bar{\lambda}_{c,N}, \dots, \bar{\lambda}_{c,N-k+1}, \boldsymbol{z}_N$.

Eliminating the predicted acceleration variables in Eq. (4.19) with the help of Eq. (4.12) and making use of Eq. (4.3) and (4.4), Eq. (4.19) finally results in a relationship of the form

$$\bar{\lambda}_{c,N+1} = \bar{\lambda}_{c,N+1}\left(\bar{\lambda}_{c,N}, \bar{\lambda}_{c,N-1}, \dots, \bar{\lambda}_{c,N-k}, \boldsymbol{z}_N\right). \tag{4.21}$$

Step 4: Projection Step

Calculation of projected position and velocity variables gives

$$\bar{x}_{N+1} = \frac{\bar{x}_{1,N+1} + \alpha_{m21}\cdot\bar{x}_{2,N+1}}{1+\alpha_{m21}}\,,\quad \bar{v}_{N+1} = \frac{\bar{v}_{1,N+1} + \alpha_{m21}\cdot\bar{v}_{2,N+1}}{1+\alpha_{m21}}\,. \tag{4.22}$$

Eq. (4.21) together with (4.22) represent a system of 3 coupled linear recurrence equations of order $k+1$. Now it should be recognized again that the vector $\boldsymbol{z}_N$ represents the initial conditions for the macro-time step from $\bar{T}_N$ to $\bar{T}_{N+1}$. Since a projection step has also been carried out at the macro-time point $\bar{T}_N$, we have $\boldsymbol{z}_N = \left(\bar{x}_{1,N}, \bar{v}_{1,N}, \bar{x}_{2,N}, \bar{v}_{2,N}\right)^T = (\bar{x}_N, \bar{v}_N, \bar{x}_N, \bar{v}_N)^T$. Hence, the governing linear system of recurrence equations for the projected state variables $\bar{x}_{N+1}, \bar{v}_{N+1}$ and for the Lagrange multiplier $\bar{\lambda}_{c,N+1}$ can be described as follows

$$\begin{aligned}\bar{x}_{N+1} &= \bar{x}_{N+1}\left(\bar{\lambda}_{c,N+1}, \bar{\lambda}_{c,N}, \dots, \bar{\lambda}_{c,N-k+1}, \bar{x}_N, \bar{v}_N\right),\\ \bar{v}_{N+1} &= \bar{v}_{N+1}\left(\bar{\lambda}_{c,N+1}, \bar{\lambda}_{c,N}, \dots, \bar{\lambda}_{c,N-k+1}, \bar{x}_N, \bar{v}_N\right),\\ \bar{\lambda}_{c,N+1} &= \bar{\lambda}_{c,N+1}\left(\bar{\lambda}_{c,N}, \bar{\lambda}_{c,N-1}, \dots, \bar{\lambda}_{c,N-k}, \bar{x}_N, \bar{v}_N\right).\end{aligned} \tag{4.23}$$

Introducing the vectors $\hat{\boldsymbol{y}}_{N+1} = \left(\bar{x}_{N+1}, \bar{v}_{N+1}, \bar{\lambda}_{c,N+1}\right)^T$, $\hat{\boldsymbol{y}}_N = \left(\bar{x}_N, \bar{v}_N, \bar{\lambda}_{c,N}\right)^T$, etc. which collect the projected state variables and the Lagrange multiplier at the macro-time points, Eq. (4.23) can symbolically be rewritten as

$$\boldsymbol{B}_{N+1} \cdot \hat{\boldsymbol{y}}_{N+1} + \boldsymbol{B}_N \cdot \hat{\boldsymbol{y}}_N + \cdots + \boldsymbol{B}_{N-k} \cdot \hat{\boldsymbol{y}}_{N-k} = \boldsymbol{0}. \tag{4.24}$$

The real-valued matrices $\boldsymbol{B}_{N+1}, \dots, \boldsymbol{B}_{N-k} \in \mathbb{R}^{3\times 3}$ are constant and only depend on the 5 parameters of the co-simulation test model.

4.2. Recurrence Equations of Force/Displacement Coupling Approach

4.2.1. Co-Simulation Method based on Baumgarte Stabilization

If the co-simulation test model is decomposed with a force/displacement-coupling approach, subsystem 1 is a force-driven single-mass oscillator and subsystem 2 a kinematically driven single-mass oscillator, see Figure 4.2. The kinematical motion of the mass m_2 can be applied on position (index-3), velocity (index-2) or acceleration (index-1) level. Here, the motion is applied on index-1 level for stability reasons, i.e. the acceleration of the mass m_2 is prescribed by a rheonomic constraint equation. Since the two masses are coupled by a rigid link, the motion (acceleration) of both masses has to be identical. Consequently, the kinematical motion for the mass m_2 is defined by the motion of the mass m_1, i.e. the acceleration of m_2 is prescribed by the acceleration of m_1. Since the acceleration $\bar{v}_1'$ of mass m_1 is unknown in subsystem 2, the additional coupling variable $\tilde{\bar{a}}_1(t)$ is defined. Introducing an additional coupling variable requires the definition of an additional coupling condition, namely $\bar{g}_{c\mu} := \bar{\mu}_2 - \bar{\lambda}_c = 0$, which states that the coupling forces in both subsystems are equal.

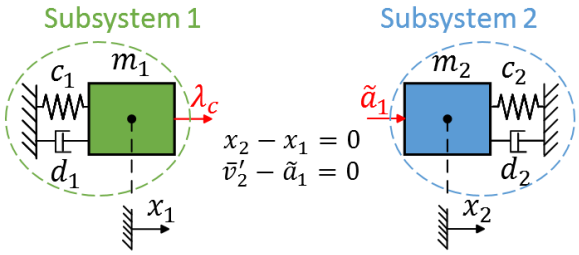

Figure 4.2 Co-simulation test model for force/displacement coupling approach

The decomposed system is described by the DAE system

Subsystem 1:

$$\begin{aligned} \bar{x}_1' &= \bar{v}_1 \\ \bar{v}_1' &= -\bar{c}_1 \cdot \bar{x}_1 - \bar{d}_1 \cdot \bar{v}_1 + \bar{\lambda}_c \end{aligned} \tag{4.25a}$$

Subsystem 2:

$$\begin{aligned} \bar{x}_2' &= \bar{v}_2 \\ \bar{v}_2' &= -\frac{\alpha_{c21}}{\alpha_{m21}} \cdot \bar{c}_1 \cdot \bar{x}_2 - \frac{\alpha_{d21}}{\alpha_{m21}} \cdot \bar{d}_1 \cdot \bar{v}_2 - \frac{1}{\alpha_{m21}} \cdot \bar{\mu}_2 \\ 0 &= \bar{v}_2' - \tilde{\bar{a}}_1 \end{aligned} \tag{4.25b}$$

Coupling conditions:

$$\begin{aligned} \bar{g}_{c\lambda}^B &:= (\bar{x}_2 - \bar{x}_1) + \bar{\beta} \cdot (\bar{v}_2 - \bar{v}_1) + \bar{\gamma} \cdot (\bar{v}_2' - \bar{v}_1') = 0 \\ \bar{g}_{c\mu} &:= \bar{\mu}_2 - \bar{\lambda}_c = 0\,. \end{aligned} \tag{4.25c}$$

Note that $\bar{\mu}_2$ terms a Lagrange multiplier, which is introduced to realize the rheonomic constraint equation $0 = \bar{v}_2' - \tilde{\bar{a}}_1$ in subsystem 2, where $\tilde{\bar{a}}_1(t)$ represents the applied motion for m_2. To derive the governing system of recurrence equations for the Baumgarte approach on the basis of a force/displacement-decomposition, we consider again the general macro-step from $\bar{T}_N$ to $\bar{T}_{N+1}$. We assume that at the beginning of the macro-time step, the state vectors, the Lagrange multiplier $\bar{\mu}_2$ and the coupling variables $\bar{\lambda}_c$, $\tilde{\bar{a}}_1$ are known

$$\begin{aligned} &\bar{x}_1(\bar{t} = \bar{T}_N) = \bar{x}_{1,N}\,, \qquad \bar{v}_1(\bar{t} = \bar{T}_N) = \bar{v}_{1,N}\,, \\ &\bar{x}_2(\bar{t} = \bar{T}_N) = \bar{x}_{2,N}\,, \qquad \bar{v}_2(\bar{t} = \bar{T}_N) = \bar{v}_{2,N}\,, \qquad \bar{\mu}_2(\bar{T}_N) = \bar{\mu}_{2,N}, \end{aligned} \tag{4.26a}$$

$$\bar{\lambda}_c(\bar{T}_N) = \bar{\lambda}_{c,N}\,, \qquad \tilde{\bar{a}}_1(\bar{T}_N) = \tilde{\bar{a}}_{1,N}\,. \tag{4.26b}$$

For higher order approximation $(k > 0)$, the corresponding variables at the previous macro-time points are also assumed to be known.

Step 1: Predictor Step

Analytically integrating subsystem 1 and subsystem 2 from $\bar{T}_N$ to $\bar{T}_{N+1}$ with the initial conditions (4.26a) and with the predictor (extrapolation) polynomials

$$\begin{aligned} \bar{\lambda}_c^p(\bar{t}) &= P_{\bar{\lambda}_c}^p\left[\left(\bar{T}_N, \bar{\lambda}_{c,N}\right), \left(\bar{T}_{N-1}, \bar{\lambda}_{c,N-1}\right), \ldots, \left(\bar{T}_{N-k}, \bar{\lambda}_{c,N-k}\right); \bar{t}\right], \\ \tilde{\bar{a}}_1^p(\bar{t}) &= P_{\tilde{\bar{a}}_1}^p\left[\left(\bar{T}_N, \tilde{\bar{a}}_{1,N}\right), \left(\bar{T}_{N-1}, \tilde{\bar{a}}_{1,N-1}\right), \ldots, \left(\bar{T}_{N-k}, \tilde{\bar{a}}_{1,N-k}\right); \bar{t}\right], \end{aligned} \tag{4.27}$$

yields the predicted state variables and the predicted Lagrange multiplier at the macro-time point $\bar{T}_{N+1}$, i.e.

$$\bar{x}_{1,N+1}^p\,, \quad \bar{v}_{1,N+1}^p \quad \text{and} \quad \bar{x}_{2,N+1}^p\,, \quad \bar{v}_{2,N+1}^p, \quad \bar{\mu}_{2,N+1}^p\,. \tag{4.28}$$

It should be pointed out that $\bar{x}_{1,N+1}^p$ and $\bar{v}_{1,N+1}^p$ are functions of $\bar{\lambda}_{c,N}, \bar{\lambda}_{c,N-1}, \ldots, \bar{\lambda}_{c,N-k}, \boldsymbol{z}_N$, whereas $\bar{x}_{2,N+1}^p, \bar{v}_{2,N+1}^p, \bar{\mu}_{2,N+1}^p$ depend on $\tilde{\bar{a}}_{1,N}, \tilde{\bar{a}}_{1,N-1}, \ldots, \tilde{\bar{a}}_{1,N-k}, \boldsymbol{z}_N$.

Step 2: Calculation of Corrected Coupling Variables

An analytical integration of subsystem 1 and subsystem 2 from $\bar{T}_N$ to $\bar{T}_{N+1}$ with the initial conditions (4.26a) and with the interpolation polynomials

$$\begin{aligned}\bar{\lambda}_c^*(\bar{t}) &= P_{\bar{\lambda}_c}^*\left[\left(\bar{T}_{N+1}, \bar{\lambda}_{c,N+1}^*\right), \left(\bar{T}_N, \bar{\lambda}_{c,N}\right), \dots, \left(\bar{T}_{N-k+1}, \bar{\lambda}_{c,N-k+1}\right); \bar{t}\right], \\ \tilde{\bar{a}}_1^*(\bar{t}) &= P_{\tilde{\bar{a}}_1}^*\left[\left(\bar{T}_{N+1}, \tilde{\bar{a}}_{1,N+1}^*\right), \left(\bar{T}_N, \tilde{\bar{a}}_{1,N}\right), \dots, \left(\bar{T}_{N-k+1}, \tilde{\bar{a}}_{1,N-k+1}\right); \bar{t}\right],\end{aligned} \tag{4.29}$$

gives the following state variables and Lagrange multiplier at the macro-time point $\bar{T}_{N+1}$

$$\bar{x}_{1,N+1}^*\,, \quad \bar{v}_{1,N+1}^* \quad \text{and} \quad \bar{x}_{2,N+1}^*\,, \quad \bar{v}_{2,N+1}^*, \quad \bar{\mu}_{2,N+1}^*\,. \tag{4.30}$$

Note that $\bar{x}_{1,N+1}^*$ and $\bar{v}_{1,N+1}^*$ are depending on $\bar{\lambda}_{c,N+1}^*, \bar{\lambda}_{c,N}, \dots, \bar{\lambda}_{c,N-k+1}, \boldsymbol{z}_N$, while $\bar{x}_{2,N+1}^*$, $\bar{v}_{2,N+1}^*$ and $\bar{\mu}_{2,N+1}^*$ are functions of $\tilde{\bar{a}}_{1,N+1}^*, \tilde{\bar{a}}_{1,N}, \dots, \tilde{\bar{a}}_{1,N-k+1}, \boldsymbol{z}_N$. It should be mentioned that $\bar{\lambda}_{c,N+1}^*$ and $\tilde{\bar{a}}_{1,N+1}^*$ represent arbitrary coupling variables at the macro-time point $\bar{T}_{N+1}$.

Differentiating the state variables and the Lagrange multiplier of Eq. (4.30) with respect to $\bar{\lambda}_{c,N+1}^*$ and $\tilde{\bar{a}}_{1,N+1}^*$, we get the following partial derivatives

$$\begin{aligned}&\frac{\partial \bar{x}_{1,N+1}^*}{\partial \bar{\lambda}_{c,N+1}^*} = const.\,, \frac{\partial \bar{v}_{1,N+1}^*}{\partial \bar{\lambda}_{c,N+1}^*} = const.\,, \frac{\partial \bar{v}_{1,N+1}'^*}{\partial \bar{\lambda}_{c,N+1}^*} = const.\,, \\ &\frac{\partial \bar{x}_{2,N+1}^*}{\partial \tilde{\bar{a}}_{1,N+1}^*} = const.\,, \frac{\partial \bar{v}_{2,N+1}^*}{\partial \tilde{\bar{a}}_{1,N+1}^*} = const.\,, \frac{\partial \bar{v}_{2,N+1}'^*}{\partial \tilde{\bar{a}}_{1,N+1}^*} = const.\,, \frac{\partial \bar{\mu}_{2,N+1}^*}{\partial \tilde{\bar{a}}_{1,N+1}^*} = const.\,.\end{aligned} \tag{4.31}$$

Regarding the fixed macro-time point $\bar{T}_{N+1}$, the coupling conditions $\bar{g}_{c\lambda,N+1}^B$ and $\bar{g}_{c\mu,N+1}$ can be considered as functions of the general coupling variables $\bar{\lambda}_{c,N+1}^*$ and $\tilde{\bar{a}}_{1,N+1}^*$, i.e.

$$\begin{aligned}&\bar{g}_{c\lambda,N+1}^B\left(\bar{\lambda}_{c,N+1}^*, \tilde{\bar{a}}_{1,N+1}^*\right) := \left(\bar{x}_{2,N+1}^*\left(\tilde{\bar{a}}_{1,N+1}^*\right) - \bar{x}_{1,N+1}^*\left(\bar{\lambda}_{c,N+1}^*\right)\right) \\ &+ \bar{\beta}\left(\bar{v}_{2,N+1}^*\left(\tilde{\bar{a}}_{1,N+1}^*\right) - \bar{v}_{1,N+1}^*\left(\bar{\lambda}_{c,N+1}^*\right)\right) + \bar{\gamma}\left(\bar{v}_{2,N+1}'^*\left(\tilde{\bar{a}}_{1,N+1}^*\right) - \bar{v}_{1,N+1}'^*\left(\bar{\lambda}_{c,N+1}^*\right)\right), \\ &\bar{g}_{c\mu,N+1}\left(\bar{\lambda}_{c,N+1}^*, \tilde{\bar{a}}_{1,N+1}^*\right) := \bar{\mu}_{2,N+1}^*\left(\tilde{\bar{a}}_{1,N+1}^*\right) - \bar{\lambda}_{c,N+1}^* = 0\,.\end{aligned} \tag{4.32}$$

Since the test-model is linear, the state variables $\bar{x}_{1,N+1}^*$, $\bar{x}_{2,N+1}^*$, $\bar{v}_{1,N+1}^*$, $\bar{v}_{2,N+1}^*$ the accelerations $\bar{v}_{1,N+1}'$, $\bar{v}_{2,N+1}'$ and the Lagrange multiplier $\bar{\mu}_{2,N+1}^*$ are linear functions of the coupling variables $\bar{\lambda}_{c,N+1}^*$ and $\tilde{\bar{a}}_{1,N+1}^*$. Hence, the coupling conditions can be expressed as

$$
\begin{aligned}
\bar{g}^B_{c\lambda,N+1}\left(\bar{\lambda}^*_{c,N+1},\tilde{\bar{a}}^*_{1,N+1}\right) &:= \bar{g}^B_{c\lambda,N+1}(\boldsymbol{e}^p) + \left.\frac{\partial \bar{g}^B_{c\lambda,N+1}}{\partial \bar{\lambda}^*_{c,N+1}}\right|_{\boldsymbol{e}^p} \cdot \left(\bar{\lambda}^*_{c,N+1} - \bar{\lambda}^p_{c,N+1}\right) \\
&\quad + \left.\frac{\partial \bar{g}^B_{c\lambda,N+1}}{\partial \tilde{\bar{a}}^*_{1,N+1}}\right|_{\boldsymbol{e}^p} \cdot \left(\tilde{\bar{a}}^*_{1,N+1} - \tilde{\bar{a}}^p_{1,N+1}\right) \\
&= \left(\bar{x}^p_{2,N+1} - \bar{x}^p_{1,N+1}\right) + \bar{\beta}\cdot\left(\bar{v}^p_{2,N+1} - \bar{v}^p_{1,N+1}\right) + \bar{\gamma}\cdot\left(\bar{v}'^p_{2,N+1} - \bar{v}'^p_{1,N+1}\right) \\
&\quad - \left[\left.\frac{\partial \bar{x}^*_{1,N+1}}{\partial \bar{\lambda}^*_{c,N+1}}\right|_{\boldsymbol{e}^p} + \bar{\beta}\cdot\left.\frac{\partial \bar{v}^*_{1,N+1}}{\partial \bar{\lambda}^*_{c,N+1}}\right|_{\boldsymbol{e}^p} + \bar{\gamma}\cdot\left.\frac{\partial \bar{v}'^*_{1,N+1}}{\partial \bar{\lambda}^*_{c,N+1}}\right|_{\boldsymbol{e}^p}\right]\cdot\left(\bar{\lambda}^*_{c,N+1} - \bar{\lambda}^p_{c,N+1}\right) \\
&\quad + \left[\left.\frac{\partial \bar{x}^*_{2,N+1}}{\partial \tilde{\bar{a}}^*_{1,N+1}}\right|_{\boldsymbol{e}^p} + \bar{\beta}\cdot\left.\frac{\partial \bar{v}^*_{2,N+1}}{\partial \tilde{\bar{a}}^*_{1,N+1}}\right|_{\boldsymbol{e}^p} + \bar{\gamma}\cdot\left.\frac{\partial \bar{v}'^*_{2,N+1}}{\partial \tilde{\bar{a}}^*_{1,N+1}}\right|_{\boldsymbol{e}^p}\right]\cdot\left(\tilde{\bar{a}}^*_{1,N+1} - \tilde{\bar{a}}^p_{1,N+1}\right),
\end{aligned}
\tag{4.33}
$$

$$
\begin{aligned}
\bar{g}_{c\mu,N+1}\left(\bar{\lambda}^*_{c,N+1},\tilde{\bar{a}}^*_{1,N+1}\right) &:= \bar{g}_{c\mu,N+1}(\boldsymbol{e}^p) + \left.\frac{\partial \bar{g}_{c\mu,N+1}}{\partial \bar{\lambda}^*_{c,N+1}}\right|_{\boldsymbol{e}^p} \cdot \left(\bar{\lambda}^*_{c,N+1} - \bar{\lambda}^p_{c,N+1}\right) \\
&\quad + \left.\frac{\partial \bar{g}_{c\mu,N+1}}{\partial \tilde{\bar{a}}^*_{1,N+1}}\right|_{\boldsymbol{e}^p} \cdot \left(\tilde{\bar{a}}^*_{1,N+1} - \tilde{\bar{a}}^p_{1,N+1}\right) \\
&= \bar{\mu}^p_{2,N+1} - \bar{\lambda}^p_{c,N+1} - 1\cdot\left(\bar{\lambda}^*_{c,N+1} - \bar{\lambda}^p_{c,N+1}\right) + \left.\frac{\partial \bar{\mu}^*_{2,N+1}}{\partial \tilde{\bar{a}}^*_{1,N+1}}\right|_{\boldsymbol{e}^p} \cdot \left(\tilde{\bar{a}}^*_{1,N+1} - \tilde{\bar{a}}^p_{1,N+1}\right),
\end{aligned}
\tag{4.34}
$$

where the vector $\boldsymbol{e}^p = \left(\bar{\lambda}^p_{c,N+1}\ \tilde{\bar{a}}^p_{1,N+1}\right)^T$ collects the predicted coupling variables at the macro-time point $\bar{T}_{N+1}$.

Corrected coupling variables, which fulfill the coupling conditions at the macro-time point $\bar{T}_{N+1}$, can be derived by calculating the roots of Equations (4.33) and (4.34)

$$
\begin{aligned}
&\bar{g}^B_{c\lambda,N+1}\left(\bar{\lambda}_{c,N+1},\tilde{\bar{a}}_{1,N+1}\right) = 0 \\
&\bar{g}_{c\mu,N+1}\left(\bar{\lambda}_{c,N+1},\tilde{\bar{a}}_{1,N+1}\right) = 0
\end{aligned}
\quad \Longrightarrow \quad \bar{\lambda}_{c,N+1},\tilde{\bar{a}}_{1,N+1}\,. \tag{4.35}
$$

Step 3: Corrector Step

Analytically integrating subsystem 1 and subsystem 2 from $\bar{T}_N$ to $\bar{T}_{N+1}$ with the initial conditions (4.26a) and with the interpolation polynomials with the corrected coupling variables $\bar{\lambda}_{c,N+1}$ and $\tilde{\bar{a}}_{1,N+1}$ from Eq. (4.35) gives the corrected states and the corrected Lagrange multiplier

$$
\bar{x}_{1,N+1}\,,\quad \bar{v}_{1,N+1} \quad \text{and} \quad \bar{x}_{2,N+1}\,,\quad \bar{v}_{2,N+1},\quad \bar{\mu}_{2,N+1}\,. \tag{4.36}
$$

Note that $\bar{x}_{1,N+1}$ and $\bar{v}_{1,N+1}$ are functions of $\bar{\lambda}_{c,N+1},\bar{\lambda}_{c,N},\ldots,\bar{\lambda}_{c,N-k+1},\boldsymbol{z}_N$ and $\bar{x}_{2,N+1}\,,\bar{v}_{2,N+1}$ and $\bar{\mu}_{2,N+1}$ are functions of $\tilde{\bar{a}}_{1,N+1},\tilde{\bar{a}}_{1,N},\ldots,\tilde{\bar{a}}_{1,N-k+1},\boldsymbol{z}_N$. It should be mentioned that $\bar{\lambda}^*_{c,N+1}$ and $\tilde{\bar{a}}^*_{1,N+1}$ represent arbitrary coupling variables at the macro-time point $\bar{T}_{N+1}$.

The corrected coupling variables of Eq. (4.35) are functions of the predicted states and accelerations and of the predicted coupling variables. In Eq. (4.35) the predicted acceleration variables can easily be eliminated with the help of Equations (4.25a) and (4.25b), i.e. by means of

$$\begin{aligned} \bar{v}'^{p}_{1,N+1} &= -\bar{c}_1 \cdot \bar{x}^{p}_{1,N+1} - \bar{d}_1 \cdot \bar{v}^{p}_{1,N+1} + \bar{\lambda}^{p}_{c,N+1} \ , \\ \bar{v}'^{p}_{2,N+1} &= \tilde{\bar{a}}^{p}_{1,N+1} \, . \end{aligned} \tag{4.37}$$

Furthermore, the predicted position and velocity variables as well as the predicted Lagrange multiplier can be replaced with the help of Eq. (4.28) and the predicted coupling variables by means of Eq. (4.27) so that the corrected coupling variables $\bar{\lambda}_{c,N+1}$ and $\tilde{\bar{a}}_{1,N+1}$ of Eq. (4.35) can be expressed as functions of $\bar{\lambda}_{c,N}, \bar{\lambda}_{c,N-1}, \dots, \bar{\lambda}_{c,N-k}$ as well as functions of $\tilde{\bar{a}}_{1,N}, \tilde{\bar{a}}_{1,N-1}, \dots, \tilde{\bar{a}}_{1,N-k}, \boldsymbol{z}_N$. The final system of recurrence equations for the state variables, the Lagrange multiplier and the coupling variables has therefore the following structure

$$\begin{aligned} \bar{x}_{1,N+1} &= \bar{x}_{1,N+1}\left(\bar{\lambda}_{c,N+1}, \bar{\lambda}_{c,N}, \dots, \bar{\lambda}_{c,N-k+1}, \boldsymbol{z}_N\right), \\ \bar{v}_{1,N+1} &= \bar{v}_{1,N+1}\left(\bar{\lambda}_{c,N+1}, \bar{\lambda}_{c,N}, \dots, \bar{\lambda}_{c,N-k+1}, \boldsymbol{z}_N\right), \\ \bar{x}_{2,N+1} &= \bar{x}_{2,N+1}\left(\tilde{\bar{a}}_{1,N+1}, \tilde{\bar{a}}_{1,N}, \dots, \tilde{\bar{a}}_{1,N-k+1}, \boldsymbol{z}_N\right), \\ \bar{v}_{2,N+1} &= \bar{v}_{2,N+1}\left(\tilde{\bar{a}}_{1,N+1}, \tilde{\bar{a}}_{1,N}, \dots, \tilde{\bar{a}}_{1,N-k+1}, \boldsymbol{z}_N\right), \\ \bar{\mu}_{2,N+1} &= \bar{\mu}_{2,N+1}\left(\tilde{\bar{a}}_{1,N+1}, \tilde{\bar{a}}_{1,N}, \dots, \tilde{\bar{a}}_{1,N-k+1}, \boldsymbol{z}_N\right), \\ \bar{\lambda}_{c,N+1} &= \bar{\lambda}_{c,N+1}\left(\bar{\lambda}_{c,N}, \bar{\lambda}_{c,N-1}, \dots, \bar{\lambda}_{c,N-k}, \tilde{\bar{a}}_{1,N}, \tilde{\bar{a}}_{1,N-1}, \dots, \tilde{\bar{a}}_{1,N-k}, \boldsymbol{z}_N\right), \\ \tilde{\bar{a}}_{1,N+1} &= \tilde{\bar{a}}_{1,N+1}\left(\bar{\lambda}_{c,N}, \bar{\lambda}_{c,N-1}, \dots, \bar{\lambda}_{c,N-k}, \tilde{\bar{a}}_{1,N}, \tilde{\bar{a}}_{1,N-1}, \dots, \tilde{\bar{a}}_{1,N-k}, \boldsymbol{z}_N\right). \end{aligned} \tag{4.38}$$

Eq. (4.38) represents 7 coupled linear recurrence equations of order $k+1$. The system only depends on the 5 parameters of the co-simulation test model.

4.2.2. Co-Simulation Method based on Weighted Multiplier Approach

Using the weighted multiplier approach, only step 2 where the corrected coupling variables are calculated, has to be modified.

Step 1: Predictor Step

Identical with step 1 in Section 4.2.1.

Step 2: Calculation of Corrected Coupling Variables

Instead of using the coupling condition $\bar{g}^{B}_{c\lambda,N+1}\left(\bar{\lambda}^{*}_{c,N+1}, \tilde{\bar{a}}^{*}_{1,N+1}\right)$ according to Eq. (4.33), we define the three coupling equations

$$\bar{g}_{c\lambda,N+1}^{pos}\left(\bar{\lambda}_{c,N+1}^{*},\tilde{\bar{a}}_{1,N+1}^{*}\right) := \bar{x}_{2,N+1}^{p} - \bar{x}_{1,N+1}^{p} - \left.\frac{\partial \bar{x}_{1,N+1}^{*}}{\partial \bar{\lambda}_{c,N+1}^{*}}\right|_{\boldsymbol{e}^{p}} \cdot \left(\bar{\lambda}_{c,N+1}^{*} - \bar{\lambda}_{c,N+1}^{p}\right) + \left.\frac{\partial \bar{x}_{2,N+1}^{*}}{\partial \tilde{\bar{a}}_{1,N+1}^{*}}\right|_{\boldsymbol{e}^{p}} \cdot \left(\tilde{\bar{a}}_{1,N+1}^{*} - \tilde{\bar{a}}_{1,N+1}^{p}\right) , \tag{4.39}$$

$$\bar{g}_{c\lambda,N+1}^{vel}\left(\bar{\lambda}_{c,N+1}^{*},\tilde{\bar{a}}_{1,N+1}^{*}\right) := \bar{v}_{2,N+1}^{p} - \bar{v}_{1,N+1}^{p} - \left.\frac{\partial \bar{v}_{1,N+1}^{*}}{\partial \bar{\lambda}_{c,N+1}^{*}}\right|_{\boldsymbol{e}^{p}} \cdot \left(\bar{\lambda}_{c,N+1}^{*} - \bar{\lambda}_{c,N+1}^{p}\right) + \left.\frac{\partial \bar{v}_{2,N+1}^{*}}{\partial \tilde{\bar{a}}_{1,N+1}^{*}}\right|_{\boldsymbol{e}^{p}} \cdot \left(\tilde{\bar{a}}_{1,N+1}^{*} - \tilde{\bar{a}}_{1,N+1}^{p}\right) , \tag{4.40}$$

$$\bar{g}_{c\lambda,N+1}^{acc}\left(\bar{\lambda}_{c,N+1}^{*},\tilde{\bar{a}}_{1,N+1}^{*}\right) := \bar{v}_{2,N+1}^{\prime p} - \bar{v}_{1,N+1}^{\prime p} - \left.\frac{\partial \bar{v}_{1,N+1}^{\prime *}}{\partial \bar{\lambda}_{c,N+1}^{*}}\right|_{\boldsymbol{e}^{p}} \cdot \left(\bar{\lambda}_{c,N+1}^{*} - \bar{\lambda}_{c,N+1}^{p}\right) + \left.\frac{\partial \bar{v}_{2,N+1}^{\prime *}}{\partial \tilde{\bar{a}}_{1,N+1}^{*}}\right|_{\boldsymbol{e}^{p}} \cdot \left(\tilde{\bar{a}}_{1,N+1}^{*} - \tilde{\bar{a}}_{1,N+1}^{p}\right) . \tag{4.41}$$

The coupling condition $\bar{g}_{c\mu,N+1}$ of Eq. (4.34) remains unchanged.

Combining Eq. (4.39) with Eq. (4.34) and solving this system for the coupling variables, yields

$$\begin{matrix} \bar{g}_{c\lambda,N+1}^{pos}\left(\bar{\lambda}_{c,N+1}^{pos},\tilde{\bar{a}}_{1,N+1}^{pos}\right) = 0 \\ \bar{g}_{c\mu,N+1}\left(\bar{\lambda}_{c,N+1}^{pos},\tilde{\bar{a}}_{1,N+1}^{pos}\right) = 0 \end{matrix} \quad \Longrightarrow \quad \bar{\lambda}_{c,N+1}^{pos},\tilde{\bar{a}}_{1,N+1}^{pos}. \tag{4.42}$$

Using Eq. (4.40) together with Eq. (4.34) and solving this system for the coupling variables gives

$$\begin{matrix} \bar{g}_{c\lambda,N+1}^{vel}\left(\bar{\lambda}_{c,N+1}^{vel},\tilde{\bar{a}}_{1,N+1}^{vel}\right) = 0 \\ \bar{g}_{c\mu,N+1}\left(\bar{\lambda}_{c,N+1}^{vel},\tilde{\bar{a}}_{1,N+1}^{vel}\right) = 0 \end{matrix} \quad \Longrightarrow \quad \bar{\lambda}_{c,N+1}^{vel},\tilde{\bar{a}}_{1,N+1}^{vel}. \tag{4.43}$$

By combining Eq. (4.41) with Eq. (4.34) and solving this system for the coupling variables, we get

$$\begin{matrix} \bar{g}_{c\lambda,N+1}^{acc}\left(\bar{\lambda}_{c,N+1}^{acc},\tilde{\bar{a}}_{1,N+1}^{acc}\right) = 0 \\ \bar{g}_{c\mu,N+1}\left(\bar{\lambda}_{c,N+1}^{acc},\tilde{\bar{a}}_{1,N+1}^{acc}\right) = 0 \end{matrix} \quad \Longrightarrow \quad \bar{\lambda}_{c,N+1}^{acc},\tilde{\bar{a}}_{1,N+1}^{acc}. \tag{4.44}$$

In the framework of the weighted multiplier approach, the corrected coupling variables are determined by

$$\begin{aligned} \bar{\lambda}_{c,N+1} &= \frac{1}{1+a+b}\left(\bar{\lambda}_{c,N+1}^{pos} + a\cdot\bar{\lambda}_{c,N+1}^{vel} + b\cdot\bar{\lambda}_{c,N+1}^{acc}\right) , \\ \tilde{\bar{a}}_{1,N+1} &= \frac{1}{1+a+b}\left(\tilde{\bar{a}}_{1,N+1}^{pos} + a\cdot\tilde{\bar{a}}_{1,N+1}^{vel} + b\cdot\tilde{\bar{a}}_{1,N+1}^{acc}\right) . \end{aligned} \tag{4.45}$$

Step 3: Corrector Step

As step 3 in Section 4.2.1. However, instead of using the corrected coupling variables from Eq. (4.35), the corrected coupling variables from Eq. (4.45) are used.

Applying the weighted multiplier approach also yields a linear system of 7 coupled recurrence equations of order $k+1$. This system has the same structure as Eq. (4.38).

4.2.3. Co-Simulation Method based on Projection Technique

Using the projection method in combination with a force/displacement coupling approach, the following four steps have to be carried out.

Step 1: Predictor Step

Identical with step 1 in Section 4.2.1.

Step 2: Calculation of Corrected Coupling Variables

Identical with step 2 in Section 4.2.1 with one exception: instead of calculating the corrected coupling variables from Eq. (4.35), the corrected coupling variables $\bar{\lambda}_{c,N+1}^{acc}, \tilde{\bar{a}}_{1,N+1}^{acc}$ according to Eq. (4.44) are computed.

Step 3: Corrector Step

As step 3 in Section 4.2.1, however $\bar{\lambda}_{c,N+1} = \bar{\lambda}_{c,N+1}^{acc}$ and $\tilde{\bar{a}}_{1,N+1} = \tilde{\bar{a}}_{1,N+1}^{acc}$ are used as corrected coupling variables. The result of the subsystem integration are the corrected state variables and the corrected Lagrange multiplier

$$\bar{x}_{1,N+1}\,, \quad \bar{v}_{1,N+1} \quad \text{and} \quad \bar{x}_{2,N+1}\,, \quad \bar{v}_{2,N+1}, \quad \bar{\mu}_{2,N+1}\,. \tag{4.46}$$

Note that $\bar{x}_{1,N+1}$ and $\bar{v}_{1,N+1}$ are depending on $\bar{\lambda}_{c,N+1}, \bar{\lambda}_{c,N}, \dots, \bar{\lambda}_{c,N-k+1}, \boldsymbol{z}_N$ while $\bar{x}_{2,N+1}\,, \bar{v}_{2,N+1}$ and $\bar{\mu}_{2,N+1}$ are functions of $\tilde{\bar{a}}_{1,N+1}, \tilde{\bar{a}}_{1,N}, \dots, \tilde{\bar{a}}_{1,N-k+1}, \boldsymbol{z}_N$.

The corrected coupling variables $\bar{\lambda}_{c,N+1} = \bar{\lambda}_{c,N+1}^{acc}$ and $\tilde{\bar{a}}_{1,N+1} = \tilde{\bar{a}}_{1,N+1}^{acc}$ according to Eq. (4.44) are functions of the predicted accelerations, the predicted Lagrange multiplier and of the predicted coupling variables. By eliminating the predicted variables with the help of Eq. (4.27), Eq. (4.28) and Eq. (4.37), the corrected coupling variables $\bar{\lambda}_{c,N+1}$ and $\tilde{\bar{a}}_{1,N+1}$ can finally be expressed as a function of $\bar{\lambda}_{c,N}, \bar{\lambda}_{c,N-1}, \dots, \bar{\lambda}_{c,N-k}, \tilde{\bar{a}}_{1,N}, \tilde{\bar{a}}_{1,N-1}, \dots, \tilde{\bar{a}}_{1,N-k}, \boldsymbol{z}_N$.

Step 4: Projection Step

Projected position and velocity variables are calculated by

$$\bar{x}_{N+1} = \frac{\bar{x}_{1,N+1} + \alpha_{m21} \cdot \bar{x}_{2,N+1}}{1+\alpha_{m21}}\,, \quad \bar{v}_{N+1} = \frac{\bar{v}_{1,N+1} + \alpha_{m21} \cdot \bar{v}_{2,N+1}}{1+\alpha_{m21}}\,. \tag{4.47}$$

Eq. (4.47) together with the corrected coupling variables $\bar{\lambda}_{c,N+1}$, $\tilde{\bar{a}}_{1,N+1}$ and the Lagrange multiplier $\bar{\mu}_{2,N+1}$ from Eq. (4.46) represent a system of five coupled linear recurrence equations of order $k+1$. Note that the vector z_N contains the initial conditions for the macro-time step from $\bar{T}_N$ to $\bar{T}_{N+1}$. Due to the fact that a projection step has also been accomplished at the macro-time point $\bar{T}_N$, we can conclude that $z_N = \left(\bar{x}_{1,N}, \bar{v}_{1,N}, \bar{x}_{2,N}, \bar{v}_{2,N}\right)^T = (\bar{x}_N, \bar{v}_N, \bar{x}_N, \bar{v}_N)^T$. Consequently, the governing

recurrence system consisting of 5 linear equations of order $k+1$ is structurally given by

$$\begin{aligned}
\bar{x}_{N+1} &= \bar{x}_{N+1}\left(\bar{\lambda}_{c,N+1}, \bar{\lambda}_{c,N}, \dots, \bar{\lambda}_{c,N-k+1}, \tilde{\bar{a}}_{1,N+1}, \tilde{\bar{a}}_{1,N}, \dots, \tilde{\bar{a}}_{1,N-k+1}, \bar{x}_N, \bar{v}_N\right) , \\
\bar{v}_{N+1} &= \bar{v}_{N+1}\left(\bar{\lambda}_{c,N+1}, \bar{\lambda}_{c,N}, \dots, \bar{\lambda}_{c,N-k+1}, \tilde{\bar{a}}_{1,N+1}, \tilde{\bar{a}}_{1,N}, \dots, \tilde{\bar{a}}_{1,N-k+1}, \bar{x}_N, \bar{v}_N\right) , \\
\bar{\mu}_{2,N+1} &= \bar{\mu}_{2,N+1}\left(\tilde{\bar{a}}_{1,N+1}, \tilde{\bar{a}}_{1,N}, \dots, \tilde{\bar{a}}_{1,N-k+1}, \bar{x}_N, \bar{v}_N\right) , \\
\bar{\lambda}_{c,N+1} &= \bar{\lambda}_{c,N+1}\left(\bar{\lambda}_{c,N}, \bar{\lambda}_{c,N-1}, \dots, \bar{\lambda}_{c,N-k}, \tilde{\bar{a}}_{1,N}, \tilde{\bar{a}}_{1,N-1}, \dots, \tilde{\bar{a}}_{1,N-k}, \bar{x}_N, \bar{v}_N\right) , \\
\tilde{\bar{a}}_{1,N+1} &= \tilde{\bar{a}}_{1,N+1}\left(\bar{\lambda}_{c,N}, \bar{\lambda}_{c,N-1}, \dots, \bar{\lambda}_{c,N-k}, \tilde{\bar{a}}_{1,N}, \tilde{\bar{a}}_{1,N-1}, \dots, \tilde{\bar{a}}_{1,N-k}, \bar{x}_N, \bar{v}_N\right) .
\end{aligned} \tag{4.48}$$

4.3. Recurrence Equations of Displacement/Displacement Coupling Approach

In connection with a displacement/displacement-decomposition approach, application of the Baumgarte and the weighted multiplier method is not treated here. Only the projection method is discussed in the following.

4.3.1. Co-Simulation Method based on Projection Technique

Applying a displacement/displacement-coupling approach, the two-mass oscillator is decomposed into two subsystems so that both subsystems are kinematically driven single-mass oscillators, see Figure 4.3. The kinematical motions are applied on acceleration (index-1) level, i.e. the accelerations of mass m_1 and mass m_2 are equal and in the following denoted by $\tilde{a}(t)$. Prescribing the acceleration $\tilde{a}(t)$ in subsystem 1 is accomplished by the rheonomic constraint equation $\bar{v}_1' - \tilde{\bar{a}} = 0$ and the corresponding Lagrange multiplier $\bar{\mu}_1$. Since the two masses are coupled by a rigid link, the coupling forces $\bar{\mu}_1$ and $\bar{\mu}_2$ must be equal. Hence, the coupling condition simply reads $\bar{g}_{c\mu} := \bar{\mu}_2 - \bar{\mu}_1 = 0$.

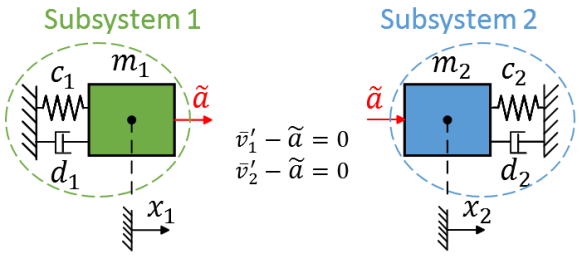

Figure 4.3 Co-simulation test model for displacement/displacement coupling approach

The DAE system characterizing the decomposed system reads as

Subsystem 1:

$$\begin{aligned}
\bar{x}_1' &= \bar{v}_1 \\
\bar{v}_1' &= -\bar{c}_1 \cdot \bar{x}_1 - \bar{d}_1 \cdot \bar{v}_1 + \bar{\mu}_1 \\
0 &= \bar{v}_1' - \tilde{\bar{a}}
\end{aligned} \tag{4.49a}$$

Subsystem 2: (4.49b)

$$\bar{x}_2' = \bar{v}_2$$
$$\bar{v}_2' = -\frac{\alpha_{c21}}{\alpha_{m21}} \cdot \bar{c}_1 \cdot \bar{x}_2 - \frac{\alpha_{d21}}{\alpha_{m21}} \cdot \bar{d}_1 \cdot \bar{v}_2 - \frac{1}{\alpha_{m21}} \cdot \bar{\mu}_2$$
$$0 = \bar{v}_2' - \tilde{\bar{a}}$$

Coupling condition:

$$\bar{g}_{c\mu} := \bar{\mu}_2 - \bar{\mu}_1 = 0 \ . \tag{4.49c}$$

In order to derive the governing system of recurrence equations, we once more analyze the general macro-time step from $\bar{T}_N$ to $\bar{T}_{N+1}$. At the beginning of the macro-step, the state variables, the Lagrange multipliers and the coupling variables are given by

$$\begin{aligned} &\bar{x}_1(\bar{t} = \bar{T}_N) = \bar{x}_{1,N}\,, \quad &&\bar{v}_1(\bar{t} = \bar{T}_N) = \bar{v}_{1,N}\,, \quad &&\bar{\mu}_1(\bar{T}_N) = \bar{\mu}_{1,N}, \\ &\bar{x}_2(\bar{t} = \bar{T}_N) = \bar{x}_{2,N}\,, \quad &&\bar{v}_2(\bar{t} = \bar{T}_N) = \bar{v}_{2,N}\,, \quad &&\bar{\mu}_2(\bar{T}_N) = \bar{\mu}_{2,N}, \end{aligned} \tag{4.50a}$$

$$\tilde{\bar{a}}(\bar{T}_N) = \tilde{\bar{a}}_N \ . \tag{4.50b}$$

Step 1: Predictor Step

With the initial conditions (4.50a) and the predictor (extrapolation) polynomial

$$\tilde{\bar{a}}^p(\bar{t}) = P^p_{\tilde{\bar{a}}}[(\bar{T}_N, \tilde{\bar{a}}_N), (\bar{T}_{N-1}, \tilde{\bar{a}}_{N-1}), \dots, (\bar{T}_{N-k}, \tilde{\bar{a}}_{N-k}); \bar{t}]\,, \tag{4.51}$$

an analytical integration of the two subsystems from $\bar{T}_N$ to $\bar{T}_{N+1}$ yields the predicted state variables and the predicted Lagrange multipliers at the macro-time point $\bar{T}_{N+1}$, i.e.

$$\bar{x}^p_{1,N+1}\,, \quad \bar{v}^p_{1,N+1}, \quad \bar{\mu}^p_{1,N+1} \quad \text{and} \quad \bar{x}^p_{2,N+1}\,, \quad \bar{v}^p_{2,N+1}, \quad \bar{\mu}^p_{2,N+1} \tag{4.52}$$

which are functions of $\tilde{\bar{a}}_N, \tilde{\bar{a}}_{N-1}, \dots, \tilde{\bar{a}}_{N-k}, \boldsymbol{z}_N$.

Step 2: Calculation of Corrected Coupling Variable

Making use of the interpolation polynomial

$$\tilde{\bar{a}}^*(\bar{t}) = P^*_{\tilde{\bar{a}}}[(\bar{T}_{N+1}, \tilde{\bar{a}}^*_{N+1}), (\bar{T}_N, \tilde{\bar{a}}_N), \dots, (\bar{T}_{N-k+1}, \tilde{\bar{a}}_{N-k+1}); \bar{t}]\ , \tag{4.53}$$

an integration from $\bar{T}_N$ to $\bar{T}_{N+1}$ with the initial conditions (4.50a) gives the state variables and Lagrange multipliers

$$\bar{x}^*_{1,N+1}\,, \quad \bar{v}^*_{1,N+1}, \quad \bar{\mu}^*_{1,N+1} \quad \text{and} \quad \bar{x}^*_{2,N+1}\,, \quad \bar{v}^*_{2,N+1}, \quad \bar{\mu}^*_{2,N+1} \tag{4.54}$$

at the macro-time point $\bar{T}_{N+1}$, which are depending on $\tilde{\bar{a}}^*_{N+1}, \tilde{\bar{a}}_N, \tilde{\bar{a}}_{N-1}, \dots, \tilde{\bar{a}}_{N-k+1}, \boldsymbol{z}_N$.

Differentiation with respect to $\tilde{\bar{a}}^*_{N+1}$, which denotes an arbitrary coupling variable at $\bar{T}_{N+1}$, yields

$$\begin{aligned}
\frac{\partial \bar{x}^*_{1,N+1}}{\partial \tilde{\bar{a}}^*_{N+1}} &= const.\,, \qquad \frac{\partial \bar{v}^*_{1,N+1}}{\partial \tilde{\bar{a}}^*_{N+1}} = const.\,, \\
\frac{\partial \bar{x}^*_{2,N+1}}{\partial \tilde{\bar{a}}^*_{N+1}} &= const.\,, \qquad \frac{\partial \bar{v}^*_{2,N+1}}{\partial \tilde{\bar{a}}^*_{N+1}} = const.\,, \\
\frac{\partial \bar{\mu}^*_{1,N+1}}{\partial \tilde{\bar{a}}^*_{N+1}} &= const.\,, \qquad \frac{\partial \bar{\mu}^*_{2,N+1}}{\partial \tilde{\bar{a}}^*_{N+1}} = const.\,.
\end{aligned} \tag{4.55}$$

At the fixed macro-time point $\bar{T}_{N+1}$, the coupling condition $\bar{g}_{c\mu,N+1}$ is regarded as a function of the general coupling variable $\tilde{\bar{a}}^*_{N+1}$

$$\bar{g}_{c\mu,N+1}(\tilde{\bar{a}}^*_{N+1}) \coloneqq \bar{\mu}^*_{2,N+1}(\tilde{\bar{a}}^*_{N+1}) - \bar{\mu}^*_{1,N+1}(\tilde{\bar{a}}^*_{N+1})\,. \tag{4.56}$$

Due to the linearity of the problem, the coupling condition can be rewritten as

$$\begin{aligned}
\bar{g}_{c\mu,N+1}(\tilde{\bar{a}}^*_{N+1}) &\coloneqq \bar{g}_{c\mu,N+1}\big(\tilde{\bar{a}}^p_{N+1}\big) + \left.\frac{\partial \bar{g}_{c\mu,N+1}}{\partial \tilde{\bar{a}}^*_{N+1}}\right|_{\tilde{\bar{a}}^p_{N+1}} \cdot \big(\tilde{\bar{a}}^*_{N+1} - \tilde{\bar{a}}^p_{N+1}\big) \\
&= \bar{\mu}^p_{2,N+1} - \bar{\mu}^p_{1,N+1} + \left(\frac{\partial \bar{\mu}^*_{2,N+1}}{\partial \tilde{\bar{a}}^*_{N+1}} - \frac{\partial \bar{\mu}^*_{1,N+1}}{\partial \tilde{\bar{a}}^*_{N+1}}\right) \cdot \big(\tilde{\bar{a}}^*_{N+1} - \tilde{\bar{a}}^p_{N+1}\big)\,.
\end{aligned} \tag{4.57}$$

A corrected coupling variable, which fulfills the coupling condition at the macro-time point $\bar{T}_{N+1}$, can be obtained by setting Eq. (4.57) equal to zero and by solving this equation for the coupling variable. One obtains

$$\tilde{\bar{a}}_{N+1} = \tilde{\bar{a}}^p_{N+1} - \frac{\bar{\mu}^p_{2,N+1} - \bar{\mu}^p_{1,N+1}}{\dfrac{\partial \bar{\mu}^*_{2,N+1}}{\partial \tilde{\bar{a}}^*_{N+1}} - \dfrac{\partial \bar{\mu}^*_{1,N+1}}{\partial \tilde{\bar{a}}^*_{N+1}}}\,. \tag{4.58}$$

Step 3: Corrector Step

Using the corrected coupling variable $\tilde{\bar{a}}_{N+1}$ from Eq. (4.58), subsystem integration from $\bar{T}_N$ to $\bar{T}_{N+1}$ with initial conditions (4.50a) yields the corrected states and Lagrange multipliers

$$\bar{x}_{1,N+1}\,,\quad \bar{v}_{1,N+1},\quad \bar{\mu}_{1,N+1} \quad \text{and} \quad \bar{x}_{2,N+1}\,,\quad \bar{v}_{2,N+1},\quad \bar{\mu}_{2,N+1}\,, \tag{4.59}$$

which are functions of $\tilde{\bar{a}}_{N+1}, \tilde{\bar{a}}_N, \tilde{\bar{a}}_{N-1}, \dots, \tilde{\bar{a}}_{N-k+1}, \boldsymbol{z}_N$.

In Eq. (4.58), the predicted variables can be replaced with the help of Equations (4.51) and (4.52). This results in a relationship of the form

$$\tilde{\bar{a}}_{N+1} = \tilde{\bar{a}}_{N+1}\,(\tilde{\bar{a}}_N, \tilde{\bar{a}}_{N-1}, \dots, \tilde{\bar{a}}_{N-k}, \boldsymbol{z}_N)\,. \tag{4.60}$$

Combining Eq. (4.59) and Eq. (4.60) yields a system of seven linear recurrence equations for the state variables, the Lagrange multipliers and the coupling variable.

Step 4: Projection Step

Projected position and velocity variables are calculated by

$$\bar{x}_{N+1} = \frac{\bar{x}_{1,N+1} + \alpha_{m21} \cdot \bar{x}_{2,N+1}}{1 + \alpha_{m21}}\,, \quad \bar{v}_{N+1} = \frac{\bar{v}_{1,N+1} + \alpha_{m21} \cdot \bar{v}_{2,N+1}}{1 + \alpha_{m21}}\,. \tag{4.61}$$

Thus, the governing recurrence system consisting of 5 linear equations of order $k+1$ for the projected state variables, the Lagrange multipliers and the coupling variable can finally be expressed as

$$\begin{aligned}
\bar{x}_{N+1} &= \bar{x}_{N+1}(\tilde{\bar{a}}_{N+1}, \tilde{\bar{a}}_N, \dots, \tilde{\bar{a}}_{N-k+1}, x_N, \bar{v}_N) \ , \\
\bar{v}_{N+1} &= \bar{v}_{N+1}(\tilde{\bar{a}}_{N+1}, \tilde{\bar{a}}_N, \dots, \tilde{\bar{a}}_{N-k+1}, x_N, \bar{v}_N) \ , \\
\bar{\mu}_{1,N+1} &= \bar{\mu}_{1,N+1}(\tilde{\bar{a}}_{N+1}, \tilde{\bar{a}}_N, \dots, \tilde{\bar{a}}_{N-k+1}, x_N, \bar{v}_N) \ , \\
\bar{\mu}_{2,N+1} &= \bar{\mu}_{2,N+1}(\tilde{\bar{a}}_{N+1}, \tilde{\bar{a}}_N, \dots, \tilde{\bar{a}}_{N-k+1}, x_N, \bar{v}_N) \ , \\
\tilde{\bar{a}}_{N+1} &= \tilde{\bar{a}}_{N+1}(\tilde{\bar{a}}_N, \tilde{\bar{a}}_{N-1}, \dots, \tilde{\bar{a}}_{N-k}, x_N, \bar{v}_N) \ .
\end{aligned} \tag{4.62}$$

For the linear co-simulation test model and in case of an analytical subsystem integration, the predicted and the corrected position and velocity variables of both subsystems are equal ($\bar{x}^p_{1,N+1} = \bar{x}^p_{2,N+1}$, $\bar{v}^p_{1,N+1} = \bar{v}^p_{2,N+1}$, $\bar{x}_{1,N+1} = \bar{x}_{2,N+1}$ and $\bar{v}^p_{1,N+1} = \bar{v}^p_{2,N+1}$), i.e. there is no drift effect. Thus, the projection step 4 is not necessary if displacement/displacement-decomposition is applied. In our representation, the projection step has been described in order to show the general procedure of the projection method in connection with a displacement/displacement-decomposition approach. For nonlinear problems or in case of a numerical subsystem integration, the projection step is required in order to avoid the drift effect.

Using the Baumgarte approach in connection with displacement/displacement-decomposition, the rheonomic constraint equations $0 = \bar{v}_1' - \tilde{\bar{a}}$ and $0 = \bar{v}_2' - \tilde{\bar{a}}$ in Eq. (4.49a) and Eq. (4.49b) have to be replaced by the Baumgarte functions $0 = (\bar{x}_1 - \tilde{\bar{x}}) + \bar{\beta} \cdot (\bar{v}_1 - \tilde{\bar{v}}) + \bar{\gamma} \cdot (\bar{v}_1' - \tilde{\bar{a}})$ and $0 = (\bar{x}_2 - \tilde{\bar{x}}) + \bar{\beta} \cdot (\bar{v}_2 - \tilde{\bar{v}}) + \bar{\gamma} \cdot (\bar{v}_2' - \tilde{\bar{a}})$, where $\tilde{\bar{x}}$, $\tilde{\bar{v}} = \frac{d}{d\bar{t}}\tilde{\bar{x}}$ and $\tilde{\bar{a}} = \frac{d}{d\bar{t}}\tilde{\bar{v}}$ represent the applied kinematical motion on position, velocity and acceleration level. Since motion has also to be applied on position level, $\tilde{\bar{x}}(\bar{t})$ has to be at least a quadratic function with respect to time $\bar{t}$ in order to obtain continuous state variables at the macro-time points. Since constant and linear approximation polynomials cannot be used, the Baumgarte and the weighted multiplier method are not discussed here for the case of displacement/displacement-decomposition.

4.4. Stability Plots for Implicit Co-Simulation Methods

The stability of the co-simulation test model depends on 5 independent parameters. Instead of using the 5 parameters defined in Eq. (2.10), it might be more useful to choose 5 other parameters. Bearing in mind the stability definition for numerical time integration schemes, where two parameters $h\Lambda_r$ and $h\Lambda_i$ are used to characterize the stability behavior, employing the following 5 independent parameters might be more convenient

$$\overline{\Lambda}_{r1} = -\frac{\bar{d}_1}{2}, \qquad \overline{\Lambda}_{i1} = \frac{1}{2}\sqrt{4\cdot\bar{c}_1 - \bar{d}_1^2}, \qquad \alpha_{m21} = \frac{m_2}{m_1},$$
$$\alpha_{\Lambda r21} = \frac{\overline{\Lambda}_{r2}}{\overline{\Lambda}_{r1}} = \frac{\alpha_{d21}}{\alpha_{m21}}, \quad \alpha_{\Lambda i21} = \frac{\overline{\Lambda}_{i2}}{\overline{\Lambda}_{i1}} = \frac{1}{\alpha_{m21}}\frac{\sqrt{4\cdot\alpha_{m21}\cdot\alpha_{c21}\cdot\bar{c}_1 - \alpha_{d21}^2\cdot\bar{d}_1^2}}{\sqrt{4\cdot\bar{c}_1 - \bar{d}_1^2}}. \tag{4.63}$$

The 5 parameters defined in Eq. (4.63) are easily explained. $\overline{\Lambda}_{r1}$ and $\overline{\Lambda}_{i1}$ characterize subsystem 1 and denote the real and imaginary part of the eigenvalue of subsystem 1. α_{m21} terms the mass ratio. The two parameters $\alpha_{\Lambda r21}$ and $\alpha_{\Lambda i21}$ specify subsystem 2 and describe the ratio of the real and the imaginary part of the eigenvalue of subsystem 2 with respect to $\overline{\Lambda}_{r1}$ and $\overline{\Lambda}_{i1}$. The stability of a co-simulation approach – i.e. the spectral radius of the corresponding recurrence equations system – is uniquely defined by the 5 independent parameters of Eq. (4.63). Thus, fixing three parameters, the spectral radius can be plotted as a function of the remaining two parameters in 2D stability plots according to the well-established 2D stability plots for time integration schemes.

In the following, the three parameters α_{m21}, $\alpha_{\Lambda r21}$ and $\alpha_{\Lambda i21}$ are fixed and 2D stability plots are presented as a function of $\overline{\Lambda}_{r1}$ and $\overline{\Lambda}_{i1}$. Therefore, the parameters $\overline{\Lambda}_{r1}$ and $\overline{\Lambda}_{i1}$ are varied in the range $[-2,0]$ and $[0,2]$. Specifying the 5 parameters of the co-simulation test model, the spectral radius ρ of the governing recurrence equations system can be calculated numerically. In the plots, stable parameter configurations are indicated be solid circles, i.e. points for which $\rho \leq 1$ holds. To reduce floating point errors, calculation of ρ has been carried out with 128 digits.

For the reason of a clear representation, all stability plots are collected in the Appendix. The discussion of the plots is carried out in the following sections.

4.4.1. Stability Plots: Force/Force-Coupling (Index-1)

Implicit Co-Simulation Method based on Baumgarte Stabilization ($\bar{\mu} = 1$)

Stability plots for the implicit co-simulation method based on the Baumgarte stabilization technique are collected in Figure A. 1. Applying the Baumgarte method, the two parameters $\bar{\beta}$ and $\bar{\gamma}$ have to be specified, see Eq. (4.1c). In literature, the two Baumgarte parameters are frequently replaced by one single parameter $\bar{\mu}$ by setting $\bar{\beta} = 2\bar{\mu}$ and $\bar{\gamma} = \bar{\mu}^2$. The plots were generated with $\bar{\mu} = 1$. In the left column, stability plots are collected for the case of constant approximation $(k = 0)$ for the four parameter sets $(\alpha_{m21} = 1, \alpha_{\Lambda r21} = 1, \alpha_{\Lambda i21} = 1)$, $(\alpha_{m21} = 10, \alpha_{\Lambda r21} = 1, \alpha_{\Lambda i21} = 1)$, $(\alpha_{m21} = 1, \alpha_{\Lambda r21} = 10, \alpha_{\Lambda i21} = 1)$ and $(\alpha_{m21} = 1, \alpha_{\Lambda r21} = 1, \alpha_{\Lambda i21} = 10)$. The column in the middle contains the plots for the case that linear approximation polynomials are used $(k = 1)$. The corresponding plots for quadratic approximation polynomials $(k = 2)$ are arranged in the right column. As can be seen, stable simulations are obtained in a wide range of the parameters $\overline{\Lambda}_{r1}$ and $\overline{\Lambda}_{i1}$ for constant, linear and quadratic approximation polynomials. The influence of the mass ratio coefficient α_{m21} and the

damping ratio coefficient $\alpha_{\Lambda r21}$ on the stability behavior is marginal. As can be seen in the fourth row, the crucial parameter for the stability is the frequency ratio coefficient $\alpha_{\Lambda i21}$. For $k = 0$, the region of stability is significantly reduced. For $k = 1$ and $k = 2$, most of the points remain stable.

Implicit Co-Simulation Method based on Weighted Multiplier Approach ($a = b = 1$)

Figure A. 2 collects the corresponding plots for the weighted multiplier approach. The plots have been generated with the parameters $a = b = 1$. Compared with the Baumgarte method, we observe a reduced stability for $k = 0$. For $k = 1$, the weighted multiplier approach shows almost the same stability behavior as the Baumgarte approach. For $k = 2$, however, the weighted multiplier approach shows an unstable region close the vertical axes as can be seen in the zoom plots. Hence, for $a = b = 1$ and for the case that quadratic approximation polynomials are used, the weighted multiplier method is not stable for $\overline{\Lambda}_{r1}, \overline{\Lambda}_{i1} \rightarrow 0$.

Implicit Co-Simulation Method based on Projection Technique

Results for the projection method are arranged in Figure A. 3. The plots indicate that the region of stability will notably be reduced if the damping ratio parameter $\alpha_{\Lambda r21}$ or the frequency ratio parameter $\alpha_{\Lambda i21}$ is increased.

4.4.2. Stability Plots: Force/Displacement-Coupling (Index-1)

Implicit Co-Simulation Method based on Baumgarte Stabilization ($\bar{\mu} = 1$)

Stability plots for the co-simulation method based on Baumgarte stabilization in connection with force/displacement-decomposition are collected in Figure A. 4. Compared with the results in Section 4.4.1, one observes an improved stability behavior for $k = 0$. For $k = 1$ and $k = 2$, however, the force/force-decomposition is more stable.

Implicit Co-Simulation Method based on Wighted Multiplier Approach ($a = b = 1$)

Applying a force/displacement-decomposition in combination with the weighted multiplier approach yields the stability plots depicted in Figure A. 5. Compared with the corresponding plots in Section 4.4.1, it can be noticed that the force/displacement-decomposition shows an improved stability behavior for $k = 0$. For $k = 1$ and $k = 2$ the force/force-decomposition yields better results.

Implicit Co-Simulation Method based on Projection Technique

Using the projection method in combination with a force/displacement-decomposition approach gives the stability plots collected in Figure A. 6. The stability plots are similar to the corresponding plots in Section 4.4.1 for the force/force-decomposition approach.

4.4.3. Stability Plots: Displacement/Displacement-Coupling

Implicit Co-Simulation Method based on Projection Technique

Figure A. 7 depicts the stability plots for the implicit co-simulation method based on the projection technique for the case that displacement/displacement-decomposition is applied. Compared with the results in Section 4.4.1 (force/force-decomposition) and Section 4.4.2 (force/displacement-decomposition), it can be observed that the displacement/displacement-decomposition shows the best stability behavior. For $k = 0$, we only detect stable points.

4.4.4. Stability Plots: Force/Force-Coupling (Index-2)

Implicit Co-Simulation Method based on Baumgarte Stabilization

Setting the Baumgarte parameters $\bar{\beta} = 2\bar{\mu}$ and $\bar{\gamma} = 0$ yields a co-simulation approach on index-2 level. Stability plots for $\bar{\mu} = 0.25, \bar{\mu} = 1$ and $\bar{\mu} = 5$ are collected in Figure A. 8 for constant $(k = 0)$, linear $(k = 1)$ and quadratic $(k = 2)$ approximation. For the reason of a concise representation, we only present stability plots for $\alpha_{m21} = 2, \alpha_{\Lambda r21} = 2, \alpha_{\Lambda i21} = 2$ based on a force/force-decomposition approach. For $k = 0$, the index-2 approach exhibits a good stability behavior. The plots exhibit that the influence of $\bar{\mu}$ on the stability behavior is small. Further simulations, which are not shown here, indicate that choosing smaller Baumgarte parameters may (slightly) improve the stability. For $k = 1$ and $k = 2$, the index-2 approach exhibits a bad performance (loss of stability for $\overline{\Lambda}_{r1}, \overline{\Lambda}_{i1} \to 0$) and may practically only be applied for larger values of $\bar{\mu}$ with the drawback of a reduced accuracy.

Implicit Co-Simulation Method based on Weighted Multiplier Approach

For $a > 0$ and $b = 0$, an index-2 approach is obtained. Figure A. 9 contains stability plots for $a = 0.5, a = 1$ and $a = 5$ for the case of constant $(k = 0)$, linear $(k = 1)$ and quadratic $(k = 2)$ approximation. The plots have been created with the parameters $\alpha_{m21} = 2, \alpha_{\Lambda r21} = 2, \alpha_{\Lambda i21} = 2$ using a force/force-decomposition approach. Good stability behavior is observed for $k = 0$. Additional simulations, which are not presented here, indicate that the stability for $k = 0$ may (slightly) be increased by choosing smaller values for the parameter a. A reduced stability behavior is detected for $k = 1$ and $k = 2$. Using linear and quadratic approximation, the parameter a has to be increased in order to obtain stable results, which however reduces the accuracy of the method so that – from the practical point of view – the cases $k = 1$ and $k = 2$ may only be of minor interest.

4.4.5. Stability Plots: Force/Force-Coupling (Index-3)

For $\bar{\beta} = \bar{\gamma} = 0$ and $a = b = 0$ the Baumgarte and the weighted multiplier method are identical and yield an index-3 approach. Results for the index-3 formulation with $\alpha_{m21} = 2, \alpha_{\Lambda r21} = 2, \alpha_{\Lambda i21} = 2$ based on a force/force-decomposition approach are arranged in Figure A. 10. Using constant approximation $(k = 0)$, a good stability behavior is

achieved, whereas only unstable points are observed for linear and quadratic approximation.

4.4.6. Influence of the Baumgarte and the Weighted Multiplier Parameters on the Stability Behavior (Index-1)

Implicit Co-Simulation Method based on Baumgarte Stabilization

In order to show the influence of the Baumgarte parameter $\bar{\mu}$ on the stability behavior, we consider an index-1 co-simulation approach based on force/force-decomposition with $\alpha_{m21} = 2, \alpha_{\Lambda r21} = 2, \alpha_{\Lambda i21} = 2$. Figure A. 11 depicts stability plots for $\bar{\mu} = 0.25, \bar{\mu} = 1$ and $\bar{\mu} = 5$. As can be seen, for $k = 0$ the stability can be improved by reducing $\bar{\mu}$. For $k = 1$ and $k = 2$, increasing the parameter $\bar{\mu}$ improves the stability behavior.

Implicit Co-Simulation Method based on Weighted Multiplier Approach

The influence of the parameters a and b on the stability behavior of the weighted multiplier approach with force/force-decomposition is illustrated in Figure A. 12. The plots have been generated with $\alpha_{m21} = 2, \alpha_{\Lambda r21} = 2, \alpha_{\Lambda i21} = 2$. Using constant approximation, the stability may be increased by using smaller values for a and b. In constrast, for $k = 1$ and $k = 2$ the stability can be increased by using larger values for a and b.

4.5. Convergence Plots: Force/Force Coupling (Index-1, Index-2 and Index-3)

In order to compare the three co-simulation approaches, besides the numerical stability there is also the convergence behavior and the numerical error of interest. Therefore, convergence plots have been generated using the co-simulation test model with the following parameters: $m_1 = 1,\ m_2 = 2,\ c_1 = c_2 = 1000,\ d_1 = d_2 = 10$. The relative global error ε_{glo} for the position and velocity variables is again computed by the normalized root mean square error (NRMSE) according to

$$\varepsilon_{glo} = \left[\frac{\sum_N \left(x_1(T_N) - x_{1,N}\right)^2}{\sum_N \left(x_1(T_N) - x_{1,mean}\right)^2} + \frac{\sum_N \left(x_2(T_N) - x_{2,N}\right)^2}{\sum_N \left(x_2(T_N) - x_{2,mean}\right)^2} + \frac{\sum_N \left(v_1(T_N) - v_{1,N}\right)^2}{\sum_N \left(v_1(T_N) - v_{1,mean}\right)^2} + \frac{\sum_N \left(v_2(T_N) - v_{2,N}\right)^2}{\sum_N \left(v_2(T_N) - v_{2,mean}\right)^2} \right]^{1/2} \tag{4.64}$$

$$\text{with} \quad x_{1,mean} = \sum_N \frac{x_1(T_N)}{N_{total}}, \qquad x_{2,mean} = \sum_N \frac{x_2(T_N)}{N_{total}},$$
$$v_{1,mean} = \sum_N \frac{v_1(T_N)}{N_{total}}, \qquad v_{2,mean} = \sum_N \frac{v_2(T_N)}{N_{total}}.$$

In the above equation, the values $x_{1,N}, x_{2,N}$ and $v_{1,N}, v_{2,N}$ denote the co-simulation results, i.e. the solution of the recurrence equations system. $x_1(T_N), x_2(T_N)$ and $v_1(T_N), v_2(T_N)$ term the values of the analytical solution at the macro-time point T_N. The

total number of macro-steps is indicated by N_{total}. The NRMSE is defined by the mean value of the squared difference between the reference and the numerical solution divided by the variance of the reference solution. Instead of using the variance in the denominator, the mean value $x_{1,mean}^2$ could also be used. Application of the NRMSE is, however, more appropriate for time series, where the mean value might become zero or close to zero. The solution of the co-simulation test model is an exponentially decaying oscillation (at least for small damping). Depending on the initial conditions, the simulation time and the subsystem parameters, the mean value may get close to zero. Therefore, the variance is used in the denominator and not the mean value.

4.5.1. Implicit Co-Simulation Method based on Baumgarte Stabilization

Figure A. 13 contains convergence plots for three different Baumgarte parameters, namely $\mu = 2.5E-4, \mu = 1E-3$ and $\mu = 5E-3$. The co-simulations were accomplished with a force/force-decomposition approach for $k = 0, k = 1$ and $k = 2$. The first row contains convergence plots for the index-1, the second row for the index-2 and the third row for the index-3 formulation. For the index-1 approach we observe that the numerical error becomes larger, if μ is increased. However, stability is increased, if μ is increased. The convergence order is also influenced by the Baumgarte parameter. For $\mu = 5E-3$, we observe a convergence behavior according to $\mathcal{O}(H^1), \mathcal{O}(H^2)$ and $\mathcal{O}(H^3)$ for the case of constant, linear and quadratic approximation polynomials. Decreasing μ, the convergence order is increased for $k = 0$ $\left(\mathcal{O}(H^1) \rightarrow \mathcal{O}(H^2)\right)$. In case of the index-2 formulation, only $k = 0$ yields stable results. The global error converges with $\mathcal{O}(H^2)$. The Baumgarte parameter μ has only little influence on the numerical error. Compared with the index-1 approach, the index-2 formulation yields a smaller numerical error. For the index-3 method, simulations for $k = 1$ and $k = 2$ are unstable. The numerical error is in the same range as in the index-2 case and converges with $\mathcal{O}(H^2)$. It should be mentioned that the straight dotted lines in the convergence plots are auxiliary lines, which indicate the convergence orders $\mathcal{O}(H), \mathcal{O}(H^1), \mathcal{O}(H^2)$, etc.

4.5.2. Implicit Co-Simulation Method based on Weighted Multiplier Approach

Convergence plots for the weighted multiplier approach are collected in Figure A. 14 for three different parameter sets, namely $a = 0.5, b = 0.25;$ $a = b = 1$ and $a = 2.5, b = 5$. The simulations were carried out with a force/force-decomposition approach for $k = 0, k = 1$ and $k = 2$. The first row contains convergence plots for the index-1 and the second row for the index-2 approach. It should be stressed again that the weighted multiplier and the Baumgarte approach have identical index-3 formulations. In the index-1 case, we observe that for $k = 0$ the global error is only slightly affected by the weighted multiplier parameters a and b. Interesting are the index-1 plots for $a = b = 1$ and $a = 2.5$ and $b = 5$: the numerical error for $k = 1$ is significantly smaller than for the Baumgarte approach. Hence, with respect to stability and accuracy the index-1 method with $a = b = 1$ in combination with linear approximation shows a good performance. The index-1 plots also exhibit that stability will be increased if the weighted multiplier

parameters a and b are increased. For $k = 0$, the global error converges with $\mathcal{O}(H^2)$. For $k = 1$ and $k = 2$, a convergence behavior with $\mathcal{O}(H^4)$ is observed. The results for the index-2 formulation are similar to the results obtained with the Baumgarte index-2 approach.

4.5.3. Implicit Co-Simulation Method based on Projection Technique

In Figure A. 15, a convergence plot is depicted for the projection method based on a force/force-coupling approach. Simulations have been carried out for $k = 0, k = 1$ and $k = 2$. We observe stable simulations for constant, linear and quadratic approximation. For $k = 0$, the magnitude of the global error is in the same range as for the weighted multiplier approach. For $k = 1$, the numerical error is larger compared with the index-1 weighted multiplier approach. For $k = 2$, the error is in the same range as for the index-1 weighted multiplier approach. The global error converges with $\mathcal{O}(H^2)$ for $k = 0$, with $\mathcal{O}(H^3)$ for $k = 1$ and with $\mathcal{O}(H^4)$ for $k = 2$.

4.6. Nonlinear Example: Double Pendulum

In the previous sections, three co-simulation methods have been investigated with respect to their numerical stability and convergence behavior. For analyzing the numerical stability, Dahlquist's stability theory based on a linear test model has been applied and extended to co-simulation approaches. In order to show the applicability of the presented co-simulation approaches to nonlinear problems, we consider the nonlinear double pendulum depicted in Figure 4.4. The pendulum consists of two rigid links. The system is decomposed into two subsystems and simulated by a co-simulation approach. The first link – representing subsystem 1 – is connected to ground by an atpoint joint. The second link – representing subsystem 2 – is coupled to the first link by an atpoint joint. Gravity is acting in negative y-direction ($g = 9.81\ m/s^2$). A linear viscous damping force is applied at the center of mass of both links (damping coefficients $d_x = d_y = 2\ Ns/m$). The simulations were accomplished with the subsequent parameters: masses $m_1 = m_2 = 1\ kg$, moments of inertia $J_1 = J_2 = 1/12\ kg\ m^2$, lengths $l_1 = l_2 = 1\ m$. As initial conditions, we chose $\varphi_{1,0} = \pi/4\ \mathrm{rad}$, $\varphi_{2,0} = -\pi/4\ \mathrm{rad}$, $\dot{\varphi}_{1,0} = \dot{\varphi}_{2,0} = 0\ \mathrm{rad/s}$. both subsystems were integrated with an implicit Runge-Kutta method (relative and absolute error tolerance $\varepsilon_{rel} = \varepsilon_{abs} = 1E-6$).

The nonlinear model is calculated with the three co-simulation approaches, e.g. Baumgarte, weighted multiplier and projection approach, using the three decomposition techniques (force/force-, force/displacement-, displacement/displacement-decomposition). In Figure 4.5, simulation results are collected for the case of constant approximation polynomials $(k = 0)$. The figure shows the angles $\varphi_1(t)$ and $\varphi_2(t)$. Moreover, the constraint equations $g_{cax}(t) = \left(x_{S1} + \frac{\ell_1}{2} \cdot \cos\varphi_1\right) - \left(x_{S2} - \frac{\ell_2}{2} \cdot \cos\varphi_2\right)$ and $g_{cay}(t) = \left(y_{S1} + \frac{\ell_1}{2} \cdot \sin\varphi_1\right) - \left(y_{S2} - \frac{\ell_2}{2} \cdot \sin\varphi_2\right)$ for the atpoint joint connecting the two links are plotted. Note that x_{s1}, y_{s1} as

well as x_{s2}, y_{s2} term the coordinates of the center of mass of the two links in horizontal and vertical direction. The figure also depicts the corresponding Lagrange multipliers (i.e. the reaction forces in horizontal and vertical direction) acting at the coupling joint. Corresponding simulation results for the case of linear and quadratic approximation polynomials are collected in Figure 4.6 and Figure 4.7. The simulations were carried out with the constant macro-step size $H = 1E-3$. It should be mentioned that the reference solution was calculated numerically with a monolithic model.

All co-simulation approaches are stable with two exceptions. The weighted multiplier approach (force/force- and force/displacement-decomposition) is unstable for the case that quadratic approximation polynomials are used, see Figure 4.7. This correlates very well with the stability plots in Appendix A.2 and B.2 (right column). Note, for instance, the zoom in the third plot in Figure A. 2, which illustrates that for small damping ($\bar{\lambda}_{r1} \approx -0.1$), the co-simulation gets unstable. For the two-mass oscillator, $\bar{\lambda}_{r1} = -\frac{\bar{d}_1}{2} = -\frac{d_1 \cdot H}{2m_1} < -0.1$ necessitates for $H = 1E-3$ and $m_1 = 1$ a damping parameter of $d_1 = 200$ for achieving stable results. The nonlinear model was integrated with a viscous damping parameter of 2 so that instability of the nonlinear model may easily be explained with the help of the stability plots.

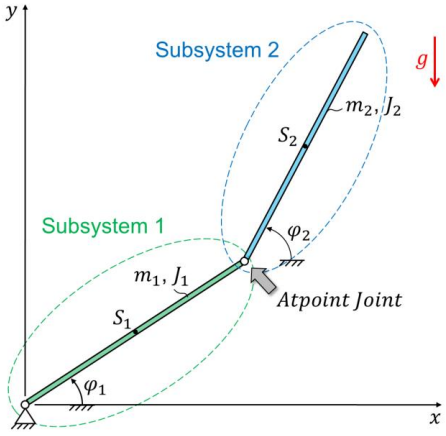

Figure 4.4 Double pendulum: interpretation as two coupled subsystems

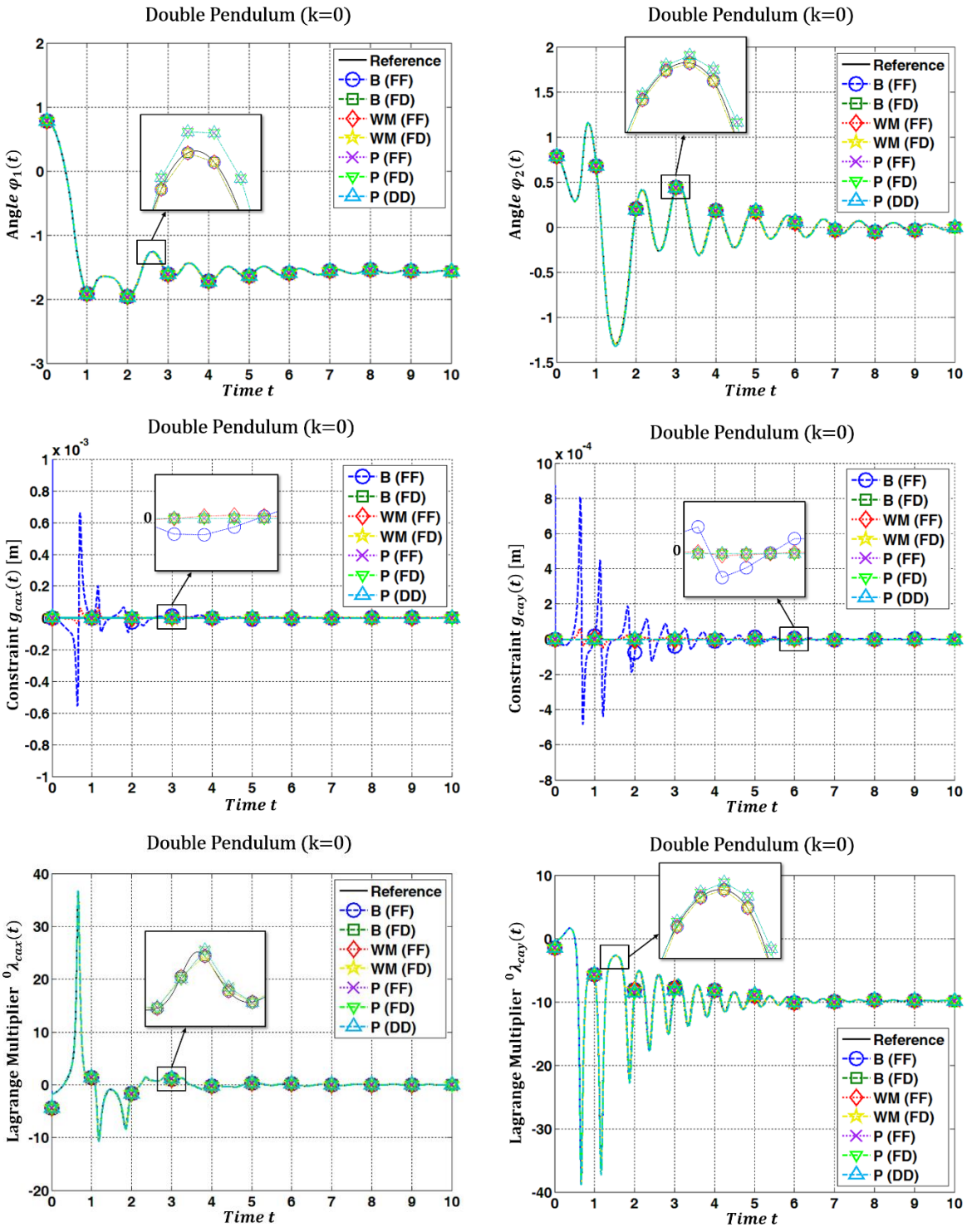

Figure 4.5 Simulation results for the double pendulum for different coupling approaches and decomposition techniques for the case of constant approximation ($k = 0$): angles $\varphi_1(t)$ and $\varphi_2(t)$, constraint equations $g_{cax}(t), g_{cay}(t)$ and Lagrange multipliers $\lambda_{cax}(t), \lambda_{cay}(t)$.

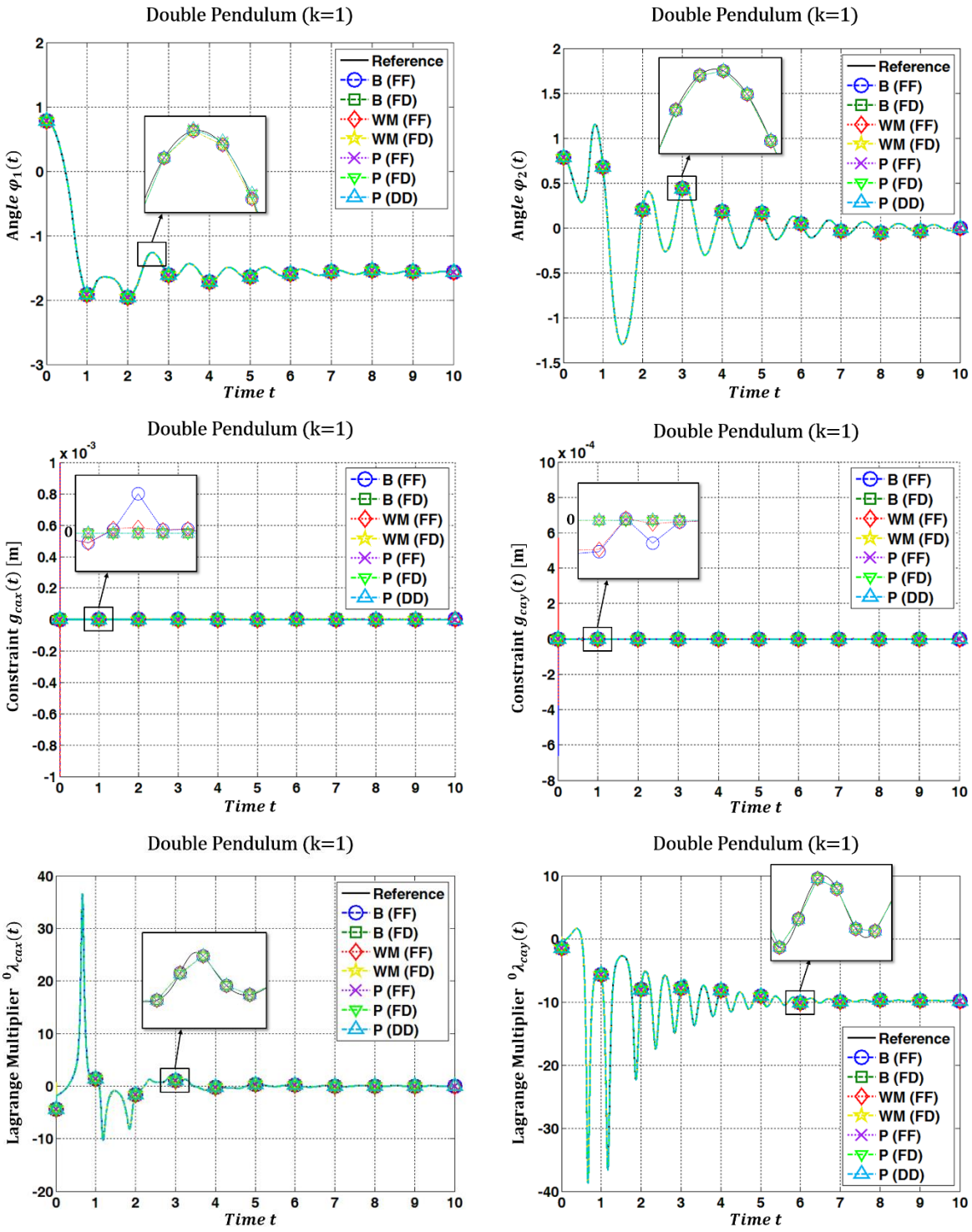

Figure 4.6 Simulation results for the double pendulum for different coupling approaches and decomposition techniques for the case of constant approximation ($k = 1$): angles $\varphi_1(t)$ and $\varphi_2(t)$, constraint equations $g_{cax}(t), g_{cay}(t)$ and Lagrange multipliers $\lambda_{cax}(t), \lambda_{cay}(t)$.

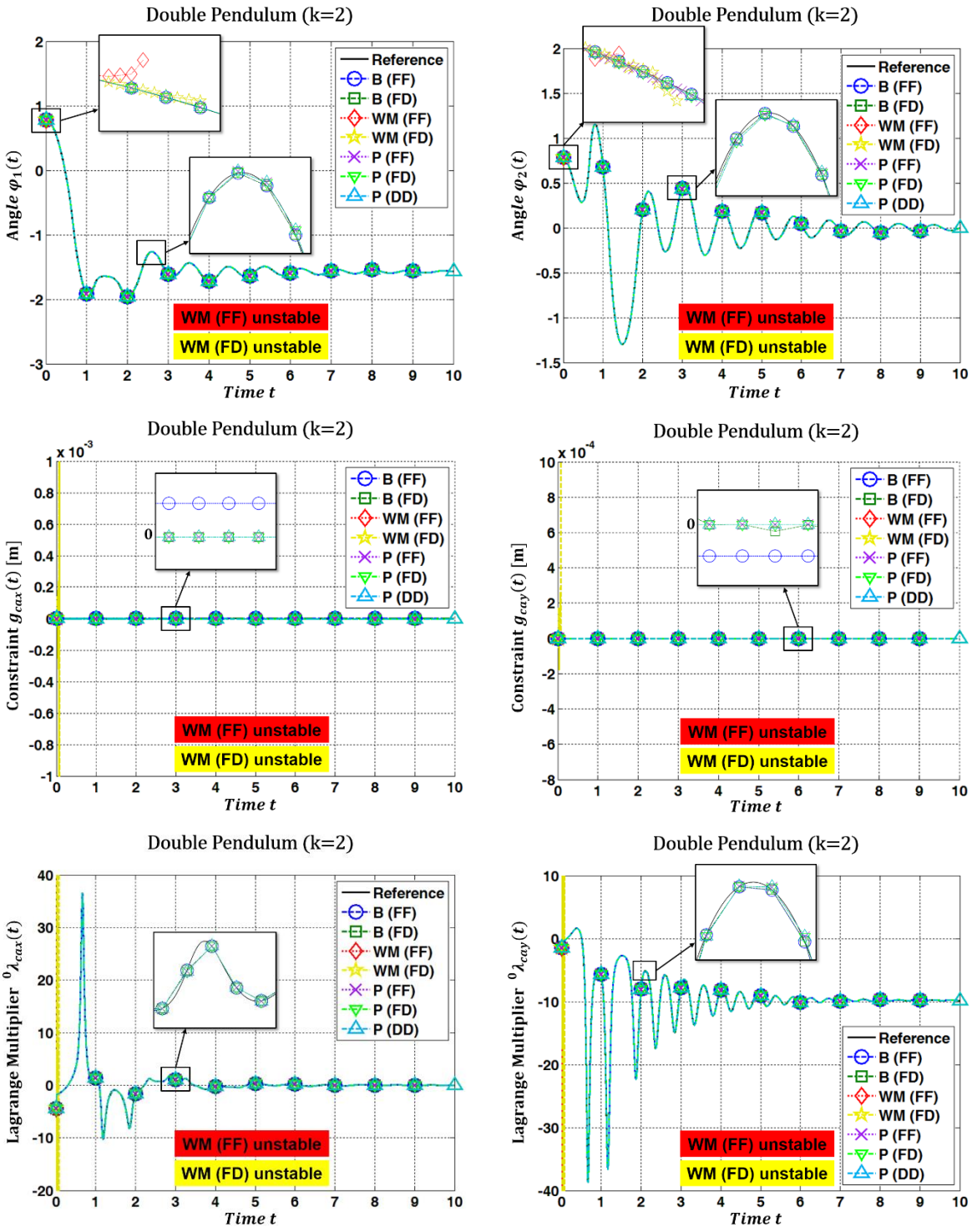

Figure 4.7 Simulation results for the double pendulum for different coupling approaches and decomposition techniques for the case of constant approximation ($k = 2$): angles $\varphi_1(t)$ and $\varphi_2(t)$, constraint equations $g_{cax}(t), g_{cay}(t)$ and Lagrange multipliers $\lambda_{cax}(t), \lambda_{cay}(t)$.

4.7. Stabilized Implicit Co-Simulation Method with Algebraic Constraints

Next, a stabilized implicit co-simulation method is analyzed. We discuss co-simulation approaches on index-2 and on index-1 level and investigate constant, linear and quadratic approximation functions for the coupling variables. The key idea of the method presented here is to discretize the Lagrange multiplier between the macro-time points (extended multiplier approach) so that the coupling equations and their time derivatives can simultaneously be fulfilled at the macro-time points. Stability and convergence of the method are investigated in detail.

4.7.1. Index-2 Co-Simulation Approach: Governing System of Recurrence Equations

The co-simulation test model is decomposed into two subsystems by means of a force/force-decomposition approach, therefore the test model is split into two single-mass oscillators. The two masses are both driven by the coupling force λ_c, see Figure 4.1.

Applying the index-2 co-simulation approach, the decomposed system is described by the subsequent equations of motion

Subsystem 1:

$$\begin{aligned} \bar{x}_1' &= \bar{v}_1 \\ \bar{v}_1' &= -\bar{c}_1 \cdot \bar{x}_1 - \bar{d}_1 \cdot \bar{v}_1 + \bar{\lambda}_c \end{aligned} \tag{4.65a}$$

Subsystem 2:

$$\begin{aligned} \bar{x}_2' &= \bar{v}_2 \\ \bar{v}_2' &= -\frac{\alpha_{c21}}{\alpha_{m21}} \cdot \bar{c}_1 \cdot \bar{x}_2 - \frac{\alpha_{d21}}{\alpha_{m21}} \cdot \bar{d}_1 \cdot \bar{v}_2 - \frac{1}{\alpha_{m21}} \bar{\lambda}_c \end{aligned} \tag{4.65b}$$

Coupling condition:

$$\begin{aligned} \bar{g}_{c\lambda} &:= \bar{x}_2 - \bar{x}_1 = 0 \\ \bar{g}_{c\lambda}' &:= \bar{v}_2 - \bar{v}_1 = 0 \quad . \end{aligned} \tag{4.65c}$$

Note that the coupling condition $\bar{x}_2 - \bar{x}_1 = 0$ has been complemented by its time derivative $\bar{v}_2 - \bar{v}_1 = 0$. In the framework of an index-3 co-simulation approach, only the coupling condition $\bar{g}_{c\lambda}$ is considered and the coupling force $\bar{\lambda}_c$ is only discretized at the macro-time points $\bar{T}_N, \bar{T}_{N+1}$, etc. Applying an index-2 co-simulation approach, not only the coupling condition $\bar{g}_{c\lambda}$, but also its time derivative $\bar{g}_{c\lambda}'$ has to be taken into account. Here, the basic idea to incorporate $\bar{g}_{c\lambda}$ and $\bar{g}_{c\lambda}'$ simultaneously is to discretize the coupling force $\bar{\lambda}_c$ not only at the macro-time points $\bar{T}_N, \bar{T}_{N+1}$, etc., but also at the time points $\bar{T}_{N+1/2}, \bar{T}_{N+3/2}$, etc.. Therefore, the additional coupling variables $\bar{\lambda}_{c,N+1/2}$, $\bar{\lambda}_{c,N+3/2}$, etc. are introduced. As a consequence of this approach, both the coupling condition and its derivative can be enforced at the macro-time points $\bar{T}_N, \bar{T}_{N+1}$, etc..

The governing system of recurrence equations, which describes the time discrete co-simulation simulation, is derived by considering the general macrostep from $\bar{T}_N$ to $\bar{T}_{N+1}$.

To integrate the subsystems from $\bar{T}_N$ to $\bar{T}_{N+1}$, the coupling variable $\bar{\lambda}_c(\bar{t})$ has to be approximated in the time interval $[\bar{T}_N,\ \bar{T}_{N+1}]$. For the index-2 co-simulation approach, we consider constant $(k=0)$, linear $(k=1)$, and quadratic $(k=2)$ approximation functions. For the reason of a concise representation, it is convenient to use the three auxiliary functions $C(\bar{t})$, $L(\bar{t})$ and $Q(\bar{t})$ introduced in Section 3.4.1.

We assume that the state variables and the coupling variable are known at the macro-time point $\bar{T}_N$, i.e.

$$\begin{aligned} \bar{x}_1(\bar{t}=\bar{T}_N) &= \bar{x}_{1,N}\,, \qquad \bar{v}_1(\bar{t}=\bar{T}_N) = \bar{v}_{1,N}\,, \\ \bar{x}_2(\bar{t}=\bar{T}_N) &= \bar{x}_{2,N}\,, \qquad \bar{v}_2(\bar{t}=\bar{T}_N) = \bar{v}_{2,N}\,, \end{aligned} \tag{4.66a}$$

$$\bar{\lambda}_c(\bar{t}=\bar{T}_N) = \bar{\lambda}_{c,N}\,. \tag{4.66b}$$

Step 1: Predictor Step

An analytical integration of subsystem 1 and subsystem 2 from $\bar{T}_N$ to $\bar{T}_{N+1}$ with the initial conditions (4.66a) and the predictor (extrapolation) function

$$\bar{\lambda}_c^p(\bar{t}) = \begin{cases} \bar{\lambda}_{c,N} & (k=0) \\ P_{\bar{\lambda}_c}\left[\left(\bar{T}_N, \bar{\lambda}_{c,N}\right), \left(\bar{T}_{N-1/2}, \bar{\lambda}_{c,N-1/2}\right); \bar{t}\right] & (k=1) \\ Q_{\bar{\lambda}_c}\left[\bar{\lambda}_{c,N}, \bar{\lambda}_{c,N-1/2}, \bar{\lambda}_{c,N-1}; \bar{t}\right] & (k=2) \end{cases} \tag{4.67}$$

yields the predicted state variables at the macro-time point $\bar{T}_{N+1}$

$$\begin{aligned} \bar{x}_{1,N+1}^p &= \bar{x}_{1,N+1}^p\left(\bar{\lambda}_{c,N}, \bar{\lambda}_{c,N-1/2}, \bar{\lambda}_{c,N-1}, \boldsymbol{z}_N\right), \\ \bar{v}_{1,N+1}^p &= \bar{v}_{1,N+1}^p\left(\bar{\lambda}_{c,N}, \bar{\lambda}_{c,N-1/2}, \bar{\lambda}_{c,N-1}, \boldsymbol{z}_N\right), \\ \bar{x}_{2,N+1}^p &= \bar{x}_{2,N+1}^p\left(\bar{\lambda}_{c,N}, \bar{\lambda}_{c,N-1/2}, \bar{\lambda}_{c,N-1}, \boldsymbol{z}_N\right), \\ \bar{v}_{2,N+1}^p &= \bar{v}_{2,N+1}^p\left(\bar{\lambda}_{c,N}, \bar{\lambda}_{c,N-1/2}, \bar{\lambda}_{c,N-1}, \boldsymbol{z}_N\right). \end{aligned} \tag{4.68}$$

It should be stressed that for $k=0$ the predicted states are only functions of $\bar{\lambda}_{c,N}$. For $k=1$ the predicted states depend on $\bar{\lambda}_{c,N}$ and $\bar{\lambda}_{c,N-1/2}$, only. In the subsequent representation, we generally use the arguments for the case of quadratic approximation $(k=2)$.

Step 2: Calculation of corrected coupling forces

By analytically integrating the two subsystems from $\bar{T}_N$ to $\bar{T}_{N+1}$ with the initial conditions (4.66a) and the interpolation function

$$\bar{\lambda}_c^*(\bar{t}) = \begin{cases} C_{\bar{\lambda}_c}\left[\bar{\lambda}_{c,N+1}^*, \bar{\lambda}_{c,N+1/2}^*; \bar{t}\right] & (k=0) \\ L_{\bar{\lambda}_c}\left[\bar{\lambda}_{c,N+1}^*, \bar{\lambda}_{c,N+1/2}^*, \bar{\lambda}_{c,N}; \bar{t}\right] & (k=1)\,, \\ Q_{\bar{\lambda}_c}\left[\bar{\lambda}_{c,N+1}^*, \bar{\lambda}_{c,N+1/2}^*, \bar{\lambda}_{c,N}; \bar{t}\right] & (k=2) \end{cases} \tag{4.69}$$

we get the subsequent state variables at the macro-time point $\bar{T}_{N+1}$

$$
\begin{aligned}
\bar{x}^*_{1,N+1} &= \bar{x}^*_{1,N+1}\left(\bar{\lambda}^*_{c,N+1}, \bar{\lambda}^*_{c,N+1/2}, \bar{\lambda}_{c,N}, \boldsymbol{z}_N\right), \\
\bar{v}^*_{1,N+1} &= \bar{v}^*_{1,N+1}\left(\bar{\lambda}^*_{c,N+1}, \bar{\lambda}^*_{c,N+1/2}, \bar{\lambda}_{c,N}, \boldsymbol{z}_N\right), \\
\bar{x}^*_{2,N+1} &= \bar{x}^*_{2,N+1}\left(\bar{\lambda}^*_{c,N+1}, \bar{\lambda}^*_{c,N+1/2}, \bar{\lambda}_{c,N}, \boldsymbol{z}_N\right), \\
\bar{v}^*_{2,N+1} &= \bar{v}^*_{2,N+1}\left(\bar{\lambda}^*_{c,N+1}, \bar{\lambda}^*_{c,N+1/2}, \bar{\lambda}_{c,N}, \boldsymbol{z}_N\right).
\end{aligned}
\tag{4.70}
$$

By differentiating the state variables of Eq. (4.70) with respect to $\bar{\lambda}^*_{c,N+1}$, one obtains the partial derivatives

$$
\begin{aligned}
\frac{\partial \bar{x}^*_{1,N+1}}{\partial \bar{\lambda}^*_{c,N+1}} &= const., \qquad & \frac{\partial \bar{v}^*_{1,N+1}}{\partial \bar{\lambda}^*_{c,N+1}} &= const., \\
\frac{\partial \bar{x}^*_{2,N+1}}{\partial \bar{\lambda}^*_{c,N+1}} &= const., \qquad & \frac{\partial \bar{v}^*_{2,N+1}}{\partial \bar{\lambda}^*_{c,N+1}} &= const..
\end{aligned}
\tag{4.71}
$$

In a similar manner, the partial derivatives with respect to $\bar{\lambda}^*_{c,N+1/2}$ are calculated. Note that the partial derivatives are constant, because the state variables in Eq. (4.70) depend only linearly on $\bar{\lambda}^*_{c,N+1}$ and $\bar{\lambda}^*_{c,N+1/2}$.

Using the partial derivatives, corrected coupling forces $\bar{\lambda}_{c,N+1}$ and $\bar{\lambda}_{c,N+1/2}$ can be derived so that the coupling conditions (4.65c) are both fulfilled at the macro-time point $\bar{T}_{N+1}$. Considering the fixed time point $\bar{T}_{N+1}$, $\bar{g}_{c\lambda,N+1}$ and $\bar{g}'_{c\lambda,N+1}$ can be regarded as functions of the coupling forces $\bar{\lambda}^*_{c,N+1}$ and $\bar{\lambda}^*_{c,N+1/2}$

$$
\begin{aligned}
\bar{g}_{c\lambda,N+1}\left(\bar{\lambda}^*_{c,N+1}, \bar{\lambda}^*_{c,N+1/2}\right) &:= \bar{x}^*_{2,N+1}\left(\bar{\lambda}^*_{c,N+1}, \bar{\lambda}^*_{c,N+1/2}\right) - \bar{x}^*_{1,N+1}\left(\bar{\lambda}^*_{c,N+1}, \bar{\lambda}^*_{c,N+1/2}\right), \\
\bar{g}'_{c\lambda,N+1}\left(\bar{\lambda}^*_{c,N+1}, \bar{\lambda}^*_{c,N+1/2}\right) &:= \bar{v}^*_{2,N+1}\left(\bar{\lambda}^*_{c,N+1}, \bar{\lambda}^*_{c,N+1/2}\right) - \bar{v}^*_{1,N+1}\left(\bar{\lambda}^*_{c,N+1}, \bar{\lambda}^*_{c,N+1/2}\right).
\end{aligned}
\tag{4.72}
$$

Due to the fact that the state variables $\bar{x}^*_{1,N+1}$, $\bar{x}^*_{2,N+1}$, $\bar{v}^*_{1,N+1}$ and $\bar{v}^*_{2,N+1}$ are only linear functions of $\bar{\lambda}^*_{c,N+1}$ and $\bar{\lambda}^*_{c,N+1/2}$, Eq. (4.72) may be rewritten as

$$
\begin{aligned}
&\bar{g}_{c\lambda,N+1}\left(\bar{\lambda}^{*}_{c,N+1},\bar{\lambda}^{*}_{c,N+1/2}\right)\\
&\coloneqq \bar{g}_{c\lambda,N+1}(\boldsymbol{e}^{p})+\left.\frac{\partial \bar{g}_{c\lambda,N+1}}{\partial \bar{\lambda}^{*}_{c,N+1}}\right|_{\boldsymbol{e}^{p}}\cdot\left(\bar{\lambda}^{*}_{c,N+1}-\bar{\lambda}^{p}_{c,N+1}\right)+\left.\frac{\partial \bar{g}_{c\lambda,N+1}}{\partial \bar{\lambda}^{*}_{c,N+1/2}}\right|_{\boldsymbol{e}^{p}}\\
&\qquad\qquad\cdot\left(\bar{\lambda}^{*}_{c,N+1/2}-\bar{\lambda}^{p}_{c,N+1/2}\right)\\
&=\bar{x}^{p}_{2,N+1}-\bar{x}^{p}_{1,N+1}+\left(\frac{\partial \bar{x}^{*}_{2,N+1}}{\partial \bar{\lambda}^{*}_{c,N+1}}-\frac{\partial \bar{x}^{*}_{1,N+1}}{\partial \bar{\lambda}^{*}_{c,N+1}}\right)\cdot\left(\bar{\lambda}^{*}_{c,N+1}-\bar{\lambda}^{p}_{c,N+1}\right)\\
&\quad+\left(\frac{\partial \bar{x}^{*}_{2,N+1}}{\partial \bar{\lambda}^{*}_{c,N+1/2}}-\frac{\partial \bar{x}^{*}_{1,N+1}}{\partial \bar{\lambda}^{*}_{c,N+1/2}}\right)\cdot\left(\bar{\lambda}^{*}_{c,N+1/2}-\bar{\lambda}^{p}_{c,N+1/2}\right),
\end{aligned}
\tag{4.73}
$$

$$
\begin{aligned}
&\bar{g}'_{c\lambda,N+1}\left(\bar{\lambda}^{*}_{c,N+1},\bar{\lambda}^{*}_{c,N+1/2}\right)\\
&\coloneqq \bar{g}'_{c\lambda,N+1}(\boldsymbol{e}^{p})+\left.\frac{\partial \bar{g}'_{c\lambda,N+1}}{\partial \bar{\lambda}^{*}_{c,N+1}}\right|_{\boldsymbol{e}^{p}}\cdot\left(\bar{\lambda}^{*}_{c,N+1}-\bar{\lambda}^{p}_{c,N+1}\right)+\left.\frac{\partial \bar{g}'_{c\lambda,N+1}}{\partial \bar{\lambda}^{*}_{c,N+1/2}}\right|_{\boldsymbol{e}^{p}}\\
&\qquad\qquad\cdot\left(\bar{\lambda}^{*}_{c,N+1/2}-\bar{\lambda}^{p}_{c,N+1/2}\right)\\
&=\bar{v}^{p}_{2,N+1}-\bar{v}^{p}_{1,N+1}+\left(\frac{\partial \bar{v}^{*}_{2,N+1}}{\partial \bar{\lambda}^{*}_{c,N+1}}-\frac{\partial \bar{v}^{*}_{1,N+1}}{\partial \bar{\lambda}^{*}_{c,N+1}}\right)\cdot\left(\bar{\lambda}^{*}_{c,N+1}-\bar{\lambda}^{p}_{c,N+1}\right)\\
&\quad+\left(\frac{\partial \bar{v}^{*}_{2,N+1}}{\partial \bar{\lambda}^{*}_{c,N+1/2}}-\frac{\partial \bar{v}^{*}_{1,N+1}}{\partial \bar{\lambda}^{*}_{c,N+1/2}}\right)\cdot\left(\bar{\lambda}^{*}_{c,N+1/2}-\bar{\lambda}^{p}_{c,N+1/2}\right),
\end{aligned}
$$

where the vector $\boldsymbol{e}^{p}=\left(\bar{\lambda}^{p}_{c,N+1}\;\bar{\lambda}^{p}_{c,N+1/2}\right)^{T}$ contains the predicted coupling variables at the time points $\bar{T}_{N+1}$ and $\bar{T}_{N+1/2}$.

By setting $\bar{g}_{c\lambda,N+1}\left(\bar{\lambda}^{*}_{c,N+1},\bar{\lambda}^{*}_{c,N+1/2}\right)=0$ and $\bar{g}'_{c\lambda,N+1}\left(\bar{\lambda}^{*}_{c,N+1},\bar{\lambda}^{*}_{c,N+1/2}\right)=0$, the corrected coupling forces can be determined

$$
\begin{aligned}
&\bar{g}_{c\lambda,N+1}\left(\bar{\lambda}^{*}_{c,N+1},\bar{\lambda}^{*}_{c,N+1/2}\right)=0\\
&\bar{g}'_{c\lambda,N+1}\left(\bar{\lambda}^{*}_{c,N+1},\bar{\lambda}^{*}_{c,N+1/2}\right)=0
\end{aligned}
\quad\Rightarrow\quad \bar{\lambda}_{c,N+1},\;\bar{\lambda}_{c,N+1/2}\;. \tag{4.74}
$$

Step 3: Corrector Step

By making use of the interpolation function

$$
\bar{\lambda}_{c}\left(\bar{t}\right)=\begin{cases}C_{\bar{\lambda}_{c}}\left[\bar{\lambda}_{c,N+1},\bar{\lambda}_{c,N+1/2};\bar{t}\right] & (k=0)\\ L_{\bar{\lambda}_{c}}\left[\bar{\lambda}_{c,N+1},\bar{\lambda}_{c,N+1/2},\bar{\lambda}_{c,N};\bar{t}\right] & (k=1)\\ Q_{\bar{\lambda}_{c}}\left[\bar{\lambda}_{c,N+1},\bar{\lambda}_{c,N+1/2},\bar{\lambda}_{c,N};\bar{t}\right] & (k=2)\end{cases} \tag{4.75}
$$

with the corrected coupling forces $\bar{\lambda}_{c,N+1},\bar{\lambda}_{c,N+1/2}$ from Eq. (4.74), an analytical integration of both subsystems from $\bar{T}_{N}$ to $\bar{T}_{N+1}$ with initial conditions (4.66a) provides the corrected state variables

$$
\begin{aligned}
\bar{x}_{1,N+1}&=\bar{x}_{1,N+1}\left(\bar{\lambda}_{c,N+1},\bar{\lambda}_{c,N+1/2},\bar{\lambda}_{c,N},\boldsymbol{z}_{N}\right),\\
\bar{v}_{1,N+1}&=\bar{v}_{1,N+1}\left(\bar{\lambda}_{c,N+1},\bar{\lambda}_{c,N+1/2},\bar{\lambda}_{c,N},\boldsymbol{z}_{N}\right),\\
\bar{x}_{2,N+1}&=\bar{x}_{2,N+1}\left(\bar{\lambda}_{c,N+1},\bar{\lambda}_{c,N+1/2},\bar{\lambda}_{c,N},\boldsymbol{z}_{N}\right),\\
\bar{v}_{2,N+1}&=\bar{v}_{2,N+1}\left(\bar{\lambda}_{c,N+1},\bar{\lambda}_{c,N+1/2},\bar{\lambda}_{c,N},\boldsymbol{z}_{N}\right).
\end{aligned}
\tag{4.76}
$$

The corrected coupling forces $\bar{\lambda}_{c,N+1}, \bar{\lambda}_{c,N+1/2}$ from Eq. (4.74) are functions of the predicted state variables and of the predicted coupling force. Eliminating in Eq. (4.74) the predicted variables with the help of Eq. (4.67) and Eq. (4.68) yields the relationships of the form

$$\begin{aligned} \bar{\lambda}_{c,N+1} &= \bar{\lambda}_{c,N+1}\left(\bar{\lambda}_{c,N}, \bar{\lambda}_{c,N-1/2}, \bar{\lambda}_{c,N-1}, \boldsymbol{z}_N\right), \\ \bar{\lambda}_{c,N+1/2} &= \bar{\lambda}_{c,N+1/2}\left(\bar{\lambda}_{c,N}, \bar{\lambda}_{c,N-1/2}, \bar{\lambda}_{c,N-1}, \boldsymbol{z}_N\right). \end{aligned} \tag{4.77}$$

Eq. (4.77) together with Eq. (4.76) represent a homogenous system of 6 coupled linear recurrence equations for the state variables $\bar{x}_{1,N+1}$, $\bar{v}_{1,N+1}$, $\bar{x}_{2,N+1}$, $\bar{v}_{2,N+1}$ and the Lagrange multipliers $\bar{\lambda}_{c,N+1}$, $\bar{\lambda}_{c,N+1/2}$. Introducing the vectors $\hat{\boldsymbol{z}}_{N+1} = \left(\bar{x}_{1,N+1}, \bar{v}_{1,N+1}, \bar{x}_{2,N+1}, \bar{v}_{2,N+1}, \bar{\lambda}_{c,N+1}, \bar{\lambda}_{c,N+1/2}\right)^T \in \mathbb{R}^6$, $\hat{\boldsymbol{z}}_N = \cdots$, etc., which collect the state variables of both subsystems and the Lagrange multipliers, Eq. (4.77) and Eq. (4.76) can symbolically be written as

$$\boldsymbol{A}_{N+1} \cdot \hat{\boldsymbol{z}}_{N+1} + \boldsymbol{A}_N \cdot \hat{\boldsymbol{z}}_N + \boldsymbol{A}_{N-1} \cdot \hat{\boldsymbol{z}}_{N-1} = \boldsymbol{0}. \tag{4.78}$$

The real-valued matrices $\boldsymbol{A}_{N+1}, \boldsymbol{A}_N, \boldsymbol{A}_{N-1} \in \mathbb{R}^{6\times 6}$ are constant and depend only on the 5 parameters of the co-simulation test model.

4.7.2. Index-1 Co-Simulation Approach: Governing System of Recurrence Equations

Applying the index-1 co-simulation approach, the decomposed system is given by

Subsystem 1:

$$\begin{aligned} \bar{x}_1' &= \bar{v}_1 \\ \bar{v}_1' &= -\bar{c}_1 \cdot \bar{x}_1 - \bar{d}_1 \cdot \bar{v}_1 + \bar{\lambda}_c \end{aligned} \tag{4.79a}$$

Subsystem 2:

$$\begin{aligned} \bar{x}_2' &= \bar{v}_2 \\ \bar{v}_2' &= -\frac{\alpha_{c21}}{\alpha_{m21}} \cdot \bar{c}_1 \cdot \bar{x}_2 - \frac{\alpha_{d21}}{\alpha_{m21}} \cdot \bar{d}_1 \cdot \bar{v}_2 - \frac{1}{\alpha_{m21}} \bar{\lambda}_c \end{aligned} \tag{4.79b}$$

Coupling conditions:

$$\begin{aligned} \bar{g}_{c\lambda} &:= \bar{x}_2 - \bar{x}_1 = 0 \\ \bar{g}_{c\lambda}' &:= \bar{v}_2 - \bar{v}_1 = 0 \\ \bar{g}_{c\lambda}'' &:= \bar{v}_2' - \bar{v}_1' = 0\,. \end{aligned} \tag{4.79c}$$

Note that for the index-1 formulation, the coupling condition $\bar{g}_{c\lambda}$ has been complemented by its first and its second derivatives, see Eq. (4.79c). In order to incorporate $\bar{g}_{c\lambda}$, $\bar{g}_{c\lambda}'$ and $\bar{g}_{c\lambda}''$ simultaneously, the coupling force $\bar{\lambda}_c$ is discretized at the macro-time points $\bar{T}_N$, $\bar{T}_{N+1}$, etc. and also at the intermediate points $\bar{\lambda}_{c,N+1/3}$, $\bar{\lambda}_{c,N+2/3}$, etc.. As a result, $\bar{g}_{c\lambda}$, $\bar{g}_{c\lambda}'$ and $\bar{g}_{c\lambda}''$ can be fulfilled simultaneously at the macro-time points $\bar{T}_N$, $\bar{T}_{N+1}$, etc..

In order to keep the representation concise, we only consider the case when the coupling variables are approximated by constant and linear functions. Higher order approximation may be treated in a similar manner. For the index-1 approach, the auxiliary functions $C(\bar{t})$ and $L(\bar{t})$ have to be modified. The piecewise constant function $C_{\bar{\lambda}_c}(\bar{t})$ is in the time interval $[\bar{T}_N,\ \bar{T}_{N+1}]$ defined by

$$C_{\bar{\lambda}_c}\left[\bar{\lambda}_{c,N+1}, \bar{\lambda}_{c,N+2/3}, \bar{\lambda}_{c,N+1/3}; \bar{t}\right] = \begin{cases} \bar{\lambda}_{c,N+1/3} & \text{for} \quad \bar{t} \in \left[\bar{T}_N, \bar{T}_{N+1/3}\right] \\ \bar{\lambda}_{c,N+2/3} & \text{for} \quad \bar{t} \in \left[\bar{T}_{N+1/3}, \bar{T}_{N+2/3}\right] \\ \bar{\lambda}_{c,N+1} & \text{for} \quad \bar{t} \in \left[\bar{T}_{N+2/3}, \bar{T}_{N+1}\right] \end{cases}, \tag{4.80}$$

where $\bar{\lambda}_{c,N+1}$, $\bar{\lambda}_{c,N+2/3}$ and $\bar{\lambda}_{c,N+1/3}$ represent the values of the coupling variable at the time points $\bar{T}_{N+1}$, $\bar{T}_{N+2/3}$, $\bar{T}_{N+1/3}$, see Figure 4.8. Correspondingly, we define the piecewise linear function $L_{\bar{\lambda}_c}(\bar{t})$ in the time interval $[\bar{T}_N,\ \bar{T}_{N+1}]$ according to

$$\begin{aligned} &L_{\bar{\lambda}_c}\left[\bar{\lambda}_{c,N+1}, \bar{\lambda}_{c,N+2/3}, \bar{\lambda}_{c,N+1/3}, \bar{\lambda}_{c,N}; \bar{t}\right] \\ &= \begin{cases} P_{\bar{\lambda}_c}\left[\left(\bar{T}_{N+1/3}, \bar{\lambda}_{c,N+1/3}\right), \left(\bar{T}_N, \bar{\lambda}_{c,N}\right); \bar{t}\right] & \text{for} \quad \bar{t} \in \left[\bar{T}_N, \bar{T}_{N+1/3}\right] \\ P_{\bar{\lambda}_c}\left[\left(\bar{T}_{N+2/3}, \bar{\lambda}_{c,N+2/3}\right), \left(\bar{T}_{N+1/3}, \bar{\lambda}_{c,N+1/3}\right); \bar{t}\right] & \text{for} \quad \bar{t} \in \left[\bar{T}_{N+1/3}, \bar{T}_{N+2/3}\right] \\ P_{\bar{\lambda}_c}\left[\left(\bar{T}_{N+1}, \bar{\lambda}_{c,N+1}\right), \left(\bar{T}_{N+2/3}, \bar{\lambda}_{c,N+2/3}\right); \bar{t}\right] & \text{for} \quad \bar{t} \in \left[\bar{T}_{N+2/3}, \bar{T}_{N+1}\right] \end{cases}, \end{aligned} \tag{4.81}$$

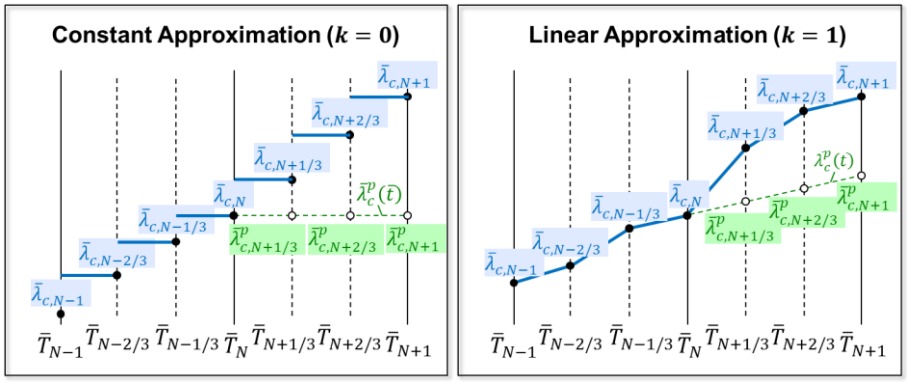

Figure 4.8 Extrapolation and interpolation functions for constant and linear approximation (index-1 co-simulation approach)

Again, we consider the general macro-time step from $\bar{T}_N$ to $\bar{T}_{N+1}$ in order to derive the governing recurrence equations system.

Step 1: Predictor Step

Integration of both subsystems from $\bar{T}_N$ to $\bar{T}_{N+1}$ with initial conditions (4.66a) and the predictor (extrapolation) function

$$\bar{\lambda}_c^p(\bar{t}) = \begin{cases} \bar{\lambda}_{c,N} & (k=0) \\ P_{\bar{\lambda}_c}\left[\left(\bar{T}_N, \bar{\lambda}_{c,N}\right), \left(\bar{T}_{N-1/3}, \bar{\lambda}_{c,N-1/3}\right); \bar{t}\right] & (k=1) \end{cases} \tag{4.82}$$

provides the predicted state variables at the macro-time point $\bar{T}_{N+1}$

$$\begin{aligned}
\bar{x}_{1,N+1}^{p} &= \bar{x}_{1,N+1}^{p}\left(\bar{\lambda}_{c,N}, \bar{\lambda}_{c,N-1/3}, \boldsymbol{z}_N\right),\\
\bar{v}_{1,N+1}^{p} &= \bar{v}_{1,N+1}^{p}\left(\bar{\lambda}_{c,N}, \bar{\lambda}_{c,N-1/3}, \boldsymbol{z}_N\right),\\
\bar{x}_{2,N+1}^{p} &= \bar{x}_{2,N+1}^{p}\left(\bar{\lambda}_{c,N}, \bar{\lambda}_{c,N-1/3}, \boldsymbol{z}_N\right),\\
\bar{v}_{2,N+1}^{p} &= \bar{v}_{2,N+1}^{p}\left(\bar{\lambda}_{c,N}, \bar{\lambda}_{c,N-1/3}, \boldsymbol{z}_N\right).
\end{aligned} \tag{4.83}$$

Note that for $k = 0$, the predicted states only depend on $\bar{\lambda}_{c,N}$. In the following representation, we generally use the arguments for the case of linear approximation $(k = 1)$.

Step 2: Calculation of Corrected Coupling Forces

An integration of the two subsystems from $\bar{T}_N$ to $\bar{T}_{N+1}$ with initial conditions (4.66a) and the interpolation function

$$\bar{\lambda}_c^*(\bar{t}) = \begin{cases} C_{\bar{\lambda}_c}\left[\bar{\lambda}_{c,N+1}^*, \bar{\lambda}_{c,N+2/3}^*, \bar{\lambda}_{c,N+1/3}^*; \bar{t}\right] & (k=0) \\ L_{\bar{\lambda}_c}\left[\bar{\lambda}_{c,N+1}^*, \bar{\lambda}_{c,N+2/3}^*, \bar{\lambda}_{c,N+1/3}^*, \bar{\lambda}_{c,N}; \bar{t}\right] & (k=1) \end{cases} \tag{4.84}$$

yields the subsequent state variables at the macro-time point $\bar{T}_{N+1}$

$$\begin{aligned}
\bar{x}_{1,N+1}^{*} &= \bar{x}_{1,N+1}^{*}\left(\bar{\lambda}_{c,N+1}^*, \bar{\lambda}_{c,N+2/3}^*, \bar{\lambda}_{c,N+1/3}^*, \bar{\lambda}_{c,N}, \boldsymbol{z}_N\right),\\
\bar{v}_{1,N+1}^{*} &= \bar{v}_{1,N+1}^{*}\left(\bar{\lambda}_{c,N+1}^*, \bar{\lambda}_{c,N+2/3}^*, \bar{\lambda}_{c,N+1/3}^*, \bar{\lambda}_{c,N}, \boldsymbol{z}_N\right),\\
\bar{x}_{2,N+1}^{*} &= \bar{x}_{2,N+1}^{*}\left(\bar{\lambda}_{c,N+1}^*, \bar{\lambda}_{c,N+2/3}^*, \bar{\lambda}_{c,N+1/3}^*, \bar{\lambda}_{c,N}, \boldsymbol{z}_N\right),\\
\bar{v}_{2,N+1}^{*} &= \bar{v}_{2,N+1}^{*}\left(\bar{\lambda}_{c,N+1}^*, \bar{\lambda}_{c,N+2/3}^*, \bar{\lambda}_{c,N+1/3}^*, \bar{\lambda}_{c,N}, \boldsymbol{z}_N\right).
\end{aligned} \tag{4.85}$$

Note that $\bar{\lambda}_{c,N+1}^*, \bar{\lambda}_{c,N+2/3}^*$ and $\bar{\lambda}_{c,N+1/3}^*$ denote arbitrary coupling forces at the time points $\bar{T}_{N+1}, \bar{T}_{N+2/3}$ and $\bar{T}_{N+1/3}$.

By differentiating the state variables of Eq. (4.85) and the corresponding accelerations with respect to $\bar{\lambda}_{c,N+1}^*$, one obtains the partial derivatives

$$\begin{aligned}
&\frac{\partial \bar{x}_{1,N+1}^*}{\partial \bar{\lambda}_{c,N+1}^*} = const., \quad &&\frac{\partial \bar{v}_{1,N+1}^*}{\partial \bar{\lambda}_{c,N+1}^*} = const., \quad &&\frac{\partial \bar{v}_{1,N+1}'^*}{\partial \bar{\lambda}_{c,N+1}^*} = const.,\\
&\frac{\partial \bar{x}_{2,N+1}^*}{\partial \bar{\lambda}_{c,N+1}^*} = const., \quad &&\frac{\partial \bar{v}_{2,N+1}^*}{\partial \bar{\lambda}_{c,N+1}^*} = const., \quad &&\frac{\partial \bar{v}_{2,N+1}'^*}{\partial \bar{\lambda}_{c,N+1}^*} = const. \ .
\end{aligned} \tag{4.86}$$

Similarly, the partial derivatives with respect to $\bar{\lambda}_{c,N+2/3}^*$ and $\bar{\lambda}_{c,N+1/3}^*$ are calculated. It should be stressed again that the partial derivatives are constant, because the state variables in Eq. (4.85) and the corresponding accelerations depend only linearly on $\bar{\lambda}_{c,N+1}^*$, $\bar{\lambda}_{c,N+2/3}^*$ and $\bar{\lambda}_{c,N+1/3}^*$.

Making use of the partial derivatives, corrected coupling forces $\bar{\lambda}_{c,N+1}$, $\bar{\lambda}_{c,N+2/3}$ and $\bar{\lambda}_{c,N+1/3}$ can be calculated so that the three coupling conditions (4.79c) are simultaneously fulfilled at the macro-time point $\bar{T}_{N+1}$. At the fixed time point $\bar{T}_{N+1}$, $\bar{g}_{c\lambda,N+1}$, $\bar{g}'_{c\lambda,N+1}$ and $\bar{g}''_{c\lambda,N+1}$ may be regarded as functions of the coupling forces $\bar{\lambda}_{c,N+1}^*$, $\bar{\lambda}_{c,N+2/3}^*$ and $\bar{\lambda}_{c,N+1/3}^*$, i.e.

$$
\begin{aligned}
&\bar{g}_{c\lambda,N+1}\left(\bar{\lambda}^*_{c,N+1},\bar{\lambda}^*_{c,N+2/3},\bar{\lambda}^*_{c,N+1/3}\right)\\
&\coloneqq \bar{x}^*_{2,N+1}\left(\bar{\lambda}^*_{c,N+1},\bar{\lambda}^*_{c,N+2/3},\bar{\lambda}^*_{c,N+1/3}\right)-\bar{x}^*_{1,N+1}\left(\bar{\lambda}^*_{c,N+1},\bar{\lambda}^*_{c,N+2/3},\bar{\lambda}^*_{c,N+1/3}\right)\ ,\\
&\bar{g}'_{c\lambda,N+1}\left(\bar{\lambda}^*_{c,N+1},\bar{\lambda}^*_{c,N+2/3},\bar{\lambda}^*_{c,N+1/3}\right)\\
&\coloneqq \bar{v}^*_{2,N+1}\left(\bar{\lambda}^*_{c,N+1},\bar{\lambda}^*_{c,N+2/3},\bar{\lambda}^*_{c,N+1/3}\right)-\bar{v}^*_{1,N+1}\left(\bar{\lambda}^*_{c,N+1},\bar{\lambda}^*_{c,N+2/3},\bar{\lambda}^*_{c,N+1/3}\right)\ ,\\
&\bar{g}''_{c\lambda,N+1}\left(\bar{\lambda}^*_{c,N+1},\bar{\lambda}^*_{c,N+2/3},\bar{\lambda}^*_{c,N+1/3}\right)\\
&\coloneqq \bar{v}'^*_{2,N+1}\left(\bar{\lambda}^*_{c,N+1},\bar{\lambda}^*_{c,N+2/3},\bar{\lambda}^*_{c,N+1/3}\right)-\bar{v}'^*_{1,N+1}\left(\bar{\lambda}^*_{c,N+1},\bar{\lambda}^*_{c,N+2/3},\bar{\lambda}^*_{c,N+1/3}\right)\ .
\end{aligned}
\tag{4.87}
$$

Due to the fact that the state variables $\bar{x}^*_{1,N+1}$, $\bar{x}^*_{2,N+1}$, $\bar{v}^*_{1,N+1}$, $\bar{v}^*_{2,N+1}$ and the corresponding accelerations $\bar{v}'^*_{1,N+1}$, $\bar{v}'^*_{2,N+1}$ are only functions of $\bar{\lambda}^*_{c,N+1}$, $\bar{\lambda}^*_{c,N+2/3}$ and $\bar{\lambda}^*_{c,N+1/3}$, Eq. (4.87) may be rewritten as

$$
\begin{aligned}
&\bar{g}_{c\lambda,N+1}\left(\bar{\lambda}^*_{c,N+1},\bar{\lambda}^*_{c,N+2/3},\bar{\lambda}^*_{c,N+1/3}\right)\\
&\coloneqq \bar{g}_{c\lambda,N+1}(\boldsymbol{e}^p)+\left.\frac{\partial \bar{g}_{c\lambda,N+1}}{\partial \bar{\lambda}^*_{c,N+1}}\right|_{\boldsymbol{e}^p}\cdot\left(\bar{\lambda}^*_{c,N+1}-\bar{\lambda}^p_{c,N+1}\right)\\
&\quad+\left.\frac{\partial \bar{g}_{c\lambda,N+1}}{\partial \bar{\lambda}^*_{c,N+2/3}}\right|_{\boldsymbol{e}^p}\left(\bar{\lambda}^*_{c,N+2/3}-\bar{\lambda}^p_{c,N+2/3}\right)+\left.\frac{\partial \bar{g}_{c\lambda,N+1}}{\partial \bar{\lambda}^*_{c,N+1/3}}\right|_{\boldsymbol{e}^p}\cdot\left(\bar{\lambda}^*_{c,N+1/3}-\bar{\lambda}^p_{c,N+1/3}\right)\\
&=\bar{x}^p_{2,N+1}-\bar{x}^p_{1,N+1}+\left(\frac{\partial \bar{x}^*_{2,N+1}}{\partial \bar{\lambda}^*_{c,N+1}}-\frac{\partial \bar{x}^*_{1,N+1}}{\partial \bar{\lambda}^*_{c,N+1}}\right)\cdot\left(\bar{\lambda}^*_{c,N+1}-\bar{\lambda}^p_{c,N+1}\right)\\
&\quad+\left(\frac{\partial \bar{x}^*_{2,N+1}}{\partial \bar{\lambda}^*_{c,N+2/3}}-\frac{\partial \bar{x}^*_{1,N+1}}{\partial \bar{\lambda}^*_{c,N+2/3}}\right)\cdot\left(\bar{\lambda}^*_{c,N+2/3}-\bar{\lambda}^p_{c,N+2/3}\right)\\
&\quad+\left(\frac{\partial \bar{x}^*_{2,N+1}}{\partial \bar{\lambda}^*_{c,N+1/3}}-\frac{\partial \bar{x}^*_{1,N+1}}{\partial \bar{\lambda}^*_{c,N+1/3}}\right)\cdot\left(\bar{\lambda}^*_{c,N+1/3}-\bar{\lambda}^p_{c,N+1/3}\right),
\end{aligned}
$$

$$
\begin{aligned}
&\bar{g}'_{c\lambda,N+1}\left(\bar{\lambda}^*_{c,N+1},\bar{\lambda}^*_{c,N+2/3},\bar{\lambda}^*_{c,N+1/3}\right)\\
&\coloneqq \bar{g}'_{c\lambda,N+1}(\boldsymbol{e}^p)+\left.\frac{\partial \bar{g}'_{c\lambda,N+1}}{\partial \bar{\lambda}^*_{c,N+1}}\right|_{\boldsymbol{e}^p}\cdot\left(\bar{\lambda}^*_{c,N+1}-\bar{\lambda}^p_{c,N+1}\right)\\
&\quad+\left.\frac{\partial \bar{g}'_{c\lambda,N+1}}{\partial \bar{\lambda}^*_{c,N+2/3}}\right|_{\boldsymbol{e}^p}\cdot\left(\bar{\lambda}^*_{c,N+2/3}-\bar{\lambda}^p_{c,N+2/3}\right)+\left.\frac{\partial \bar{g}'_{c\lambda,N+1}}{\partial \bar{\lambda}^*_{c,N+1/3}}\right|_{\boldsymbol{e}^p}\cdot\left(\bar{\lambda}^*_{c,N+1/3}-\bar{\lambda}^p_{c,N+1/3}\right)\\
&=\bar{v}^p_{2,N+1}-\bar{v}^p_{1,N+1}+\left(\frac{\partial \bar{v}^*_{2,N+1}}{\partial \bar{\lambda}^*_{c,N+1}}-\frac{\partial \bar{v}^*_{1,N+1}}{\partial \bar{\lambda}^*_{c,N+1}}\right)\cdot\left(\bar{\lambda}^*_{c,N+1}-\bar{\lambda}^p_{c,N+1}\right) \qquad (4.88)\\
&\quad+\left(\frac{\partial \bar{v}^*_{2,N+1}}{\partial \bar{\lambda}^*_{c,N+2/3}}-\frac{\partial \bar{v}^*_{1,N+1}}{\partial \bar{\lambda}^*_{c,N+2/3}}\right)\cdot\left(\bar{\lambda}^*_{c,N+2/3}-\bar{\lambda}^p_{c,N+2/3}\right)\\
&\quad+\left(\frac{\partial \bar{v}^*_{2,N+1}}{\partial \bar{\lambda}^*_{c,N+1/3}}-\frac{\partial \bar{v}^*_{1,N+1}}{\partial \bar{\lambda}^*_{c,N+1/3}}\right)\cdot\left(\bar{\lambda}^*_{c,N+1/3}-\bar{\lambda}^p_{c,N+1/3}\right),
\end{aligned}
$$

$$
\begin{aligned}
&\bar{g}''_{c\lambda,N+1}\left(\bar{\lambda}^*_{c,N+1},\bar{\lambda}^*_{c,N+2/3},\bar{\lambda}^*_{c,N+1/3}\right)\\
&\coloneqq \bar{g}''_{c\lambda,N+1}(\boldsymbol{e}^p)+\left.\frac{\partial \bar{g}''_{c\lambda,N+1}}{\partial \bar{\lambda}^*_{c,N+1}}\right|_{\boldsymbol{e}^p}\cdot\left(\bar{\lambda}^*_{c,N+1}-\bar{\lambda}^p_{c,N+1}\right)\\
&\quad+\left.\frac{\partial \bar{g}''_{c\lambda,N+1}}{\partial \bar{\lambda}^*_{c,N+2/3}}\right|_{\boldsymbol{e}^p}\cdot\left(\bar{\lambda}^*_{c,N+2/3}-\bar{\lambda}^p_{c,N+2/3}\right)+\left.\frac{\partial \bar{g}''_{c\lambda,N+1}}{\partial \bar{\lambda}^*_{c,N+1/3}}\right|_{\boldsymbol{e}^p}\cdot\left(\bar{\lambda}^*_{c,N+1/3}-\bar{\lambda}^p_{c,N+1/3}\right)\\
&=\bar{v}'^p_{2,N+1}-\bar{v}'^p_{1,N+1}+\left(\frac{\partial \bar{v}'^*_{2,N+1}}{\partial \bar{\lambda}^*_{c,N+1}}-\frac{\partial \bar{v}'^*_{1,N+1}}{\partial \bar{\lambda}^*_{c,N+1}}\right)\cdot\left(\bar{\lambda}^*_{c,N+1}-\bar{\lambda}^p_{c,N+1}\right)\\
&\quad+\left(\frac{\partial \bar{v}'^*_{2,N+1}}{\partial \bar{\lambda}^*_{c,N+2/3}}-\frac{\partial \bar{v}'^*_{1,N+1}}{\partial \bar{\lambda}^*_{c,N+2/3}}\right)\cdot\left(\bar{\lambda}^*_{c,N+2/3}-\bar{\lambda}^p_{c,N+2/3}\right)\\
&\quad+\left(\frac{\partial \bar{v}'^*_{2,N+1}}{\partial \bar{\lambda}^*_{c,N+1/3}}-\frac{\partial \bar{v}'^*_{1,N+1}}{\partial \bar{\lambda}^*_{c,N+1/3}}\right)\cdot\left(\bar{\lambda}^*_{c,N+1/3}-\bar{\lambda}^p_{c,N+1/3}\right),
\end{aligned}
$$

where the vector $\boldsymbol{e}^p=\left(\bar{\lambda}^p_{c,N+1}\;\bar{\lambda}^p_{c,N+2/3}\;\bar{\lambda}^p_{c,N+1/3}\right)^T$ collects the predicted coupling variables at the time points $\bar{T}_{N+1}$, $\bar{T}_{N+2/3}$ and $\bar{T}_{N+1/3}$.

Setting $\bar{g}_{c\lambda,N+1}\left(\bar{\lambda}^*_{c,N+1},\bar{\lambda}^*_{c,N+2/3},\bar{\lambda}^*_{c,N+1/3}\right)=0$, $\bar{g}'_{c\lambda,N+1}\left(\bar{\lambda}^*_{c,N+1},\bar{\lambda}^*_{c,N+2/3},\bar{\lambda}^*_{c,N+1/3}\right)=0$ and $\bar{g}''_{c\lambda,N+1}\left(\bar{\lambda}^*_{c,N+1},\bar{\lambda}^*_{c,N+2/3},\bar{\lambda}^*_{c,N+1/3}\right)=0$, the corrected coupling forces can be calculated

$$\begin{aligned}&\bar{g}_{c\lambda,N+1}\left(\bar{\lambda}^*_{c,N+1},\bar{\lambda}^*_{c,N+2/3},\bar{\lambda}^*_{c,N+1/3}\right)=0\\&\bar{g}'_{c\lambda,N+1}\left(\bar{\lambda}^*_{c,N+1},\bar{\lambda}^*_{c,N+2/3},\bar{\lambda}^*_{c,N+1/3}\right)=0\\&\bar{g}''_{c\lambda,N+1}\left(\bar{\lambda}^*_{c,N+1},\bar{\lambda}^*_{c,N+2/3},\bar{\lambda}^*_{c,N+1/3}\right)=0\end{aligned}\quad\Rightarrow\quad \bar{\lambda}_{c,N+1},\ \bar{\lambda}_{c,N+2/3},\ \bar{\lambda}_{c,N+1/3}\ . \tag{4.89}$$

For the reason of a clear representation, different variables have been used for general coupling forces $\bar{\lambda}^*_{c,N+1},\bar{\lambda}^*_{c,N+2/3}$ and $\bar{\lambda}^*_{c,N+1/3}$ at the time points $\bar{T}_{N+1}$, $\bar{T}_{N+2/3}$ and $\bar{T}_{N+1/3}$ and the corrected coupling forces $\bar{\lambda}_{c,N+1}$, $\bar{\lambda}_{c,N+2/3}$ and $\bar{\lambda}_{c,N+1/3}$ representing the roots of Eq. (4.89).

Step 3: Corrector Step

Applying the interpolation function

$$\bar{\lambda}_c(\bar{t})=\begin{cases}C_{\bar{\lambda}_c}\left[\bar{\lambda}_{c,N+1},\bar{\lambda}_{c,N+2/3},\bar{\lambda}_{c,N+1/3};\bar{t}\right] & (k=0)\\ L_{\bar{\lambda}_c}\left[\bar{\lambda}_{c,N+1},\bar{\lambda}_{c,N+2/3},\bar{\lambda}_{c,N+1/3},\bar{\lambda}_{c,N};\bar{t}\right] & (k=1)\end{cases} \tag{4.90}$$

with the corrected coupling forces $\bar{\lambda}_{c,N+1}$, $\bar{\lambda}_{c,N+2/3}$, $\bar{\lambda}_{c,N+1/3}$ from Eq. (4.89), an integration of both subsystems from $\bar{T}_N$ to $\bar{T}_{N+1}$ with initial conditions (4.66a) yields the corrected state variables

$$\begin{aligned}\bar{x}_{1,N+1}&=\bar{x}_{1,N+1}\left(\bar{\lambda}_{c,N+1},\bar{\lambda}_{c,N+2/3},\bar{\lambda}_{c,N+1/3},\bar{\lambda}_{c,N},\boldsymbol{z}_N\right),\\ \bar{v}_{1,N+1}&=\bar{v}_{1,N+1}\left(\bar{\lambda}_{c,N+1},\bar{\lambda}_{c,N+2/3},\bar{\lambda}_{c,N+1/3},\bar{\lambda}_{c,N},\boldsymbol{z}_N\right),\\ \bar{x}_{2,N+1}&=\bar{x}_{2,N+1}\left(\bar{\lambda}_{c,N+1},\bar{\lambda}_{c,N+2/3},\bar{\lambda}_{c,N+1/3},\bar{\lambda}_{c,N},\boldsymbol{z}_N\right),\\ \bar{v}_{2,N+1}&=\bar{v}_{2,N+1}\left(\bar{\lambda}_{c,N+1},\bar{\lambda}_{c,N+2/3},\bar{\lambda}_{c,N+1/3},\bar{\lambda}_{c,N},\boldsymbol{z}_N\right).\end{aligned} \tag{4.91}$$

The corrected coupling forces $\bar{\lambda}_{c,N+1},\bar{\lambda}_{c,N+2/3},\bar{\lambda}_{c,N+1/3}$ from Eq. (4.89) are functions of the predicted state variables and of the predicted coupling force. By replacing the predicted variables with the help of Eq. (4.82) and Eq. (4.83), we get relationships of the form

$$\begin{aligned}\bar{\lambda}_{c,N+1}&=\bar{\lambda}_{c,N+1}\ \left(\bar{\lambda}_{c,N},\bar{\lambda}_{c,N-1/3},\boldsymbol{z}_N\right),\\ \bar{\lambda}_{c,N+2/3}&=\bar{\lambda}_{c,N+2/3}\ \left(\bar{\lambda}_{c,N},\bar{\lambda}_{c,N-1/3},\boldsymbol{z}_N\right),\\ \bar{\lambda}_{c,N+1/3}&=\bar{\lambda}_{c,N+1/3}\ \left(\bar{\lambda}_{c,N},\bar{\lambda}_{c,N-1/3},\boldsymbol{z}_N\right).\end{aligned} \tag{4.92}$$

Eq. (4.91) and Eq. (4.92) represent a homogenous system of 7 coupled linear recurrence equations for the state variables $\bar{x}_{1,N+1}$, $\bar{v}_{1,N+1}$, $\bar{x}_{2,N+1}$, $\bar{v}_{2,N+1}$ and the Lagrange multipliers $\bar{\lambda}_{c,N+1},\bar{\lambda}_{c,N+2/3},\bar{\lambda}_{c,N+1/3}$. The solution of this system can simply be calculated by making use of an exponential approach. The recurrence equations system – and in consequence the underlying index-1 co-simulation approach - is stable, if the spectral radius of the system is smaller than 1.

Remark: Here, the macro-time interval has been split into two equidistant parts in case of the index-2 approach ($\bar{\lambda}_{c,N+1},\bar{\lambda}_{c,N+1/2}$) and into three equidistant parts in case of the

index-1 approach ($\bar{\lambda}_{c,N+1}, \bar{\lambda}_{c,N+2/3}, \bar{\lambda}_{c,N+1/3}$). Such a regular splitting is not mandatory. Using a non-equidistant grid, stability and numerical error of the method might be influenced advantageously. Probably, optimal grid points may be calculated in order to maximize the numerical stability and in order to minimize the numerical error of the co-simulation approach.

4.8. Stability Plots for the Stabilized Implicit Co-Simulation Method

The spectral radius of the governing recurrence equations systems for the index-2 and the index-1 method defines the numerical stability of the underlying co-simulation approach. According to Section 2.2, the spectral radius is a function of the five independent parameters of the co-simulation test model. For graphically illustrating the stability behavior of the presented co-simulation approaches, it is suitable to use the five independent parameters of Eq. (4.63).

4.8.1. Stability Plots for the Stabilized Index-2 Co-Simulation Method

2D stability plots for the implicit index-2 co-simulation approach based on the symmetrical co-simulation test model ($\alpha_{m21} = \alpha_{\Lambda r21} = \alpha_{\Lambda i21} = 1$) are collected in the first column of Figure 4.9 for constant ($k = 0$), linear ($k = 1$) and quadratic ($k = 2$) approximation. Corresponding plots generated with the explicit co-simulation method introduced in Ref. [46] (calculated with the dimensionless Baumgarte parameter $\bar{\mu} = \mu/H$) are arranged in the second column of Figure 4.9. The implicit approach shows – as expected – an improved stability behavior. Nevertheless, it should be pointed out that the numerical implementation of the implicit method is more involved, since the macro-step has to be repeated once. Solver reinitialization is, however, not required for the explicit method of Ref.[46]. For the symmetrical test model, the implicit method shows – except for a small unstable region close to the vertical axes at $\bar{\Lambda}_{i1} = 10$ for $k = 1$ – only stable points in the considered parameter range for $\bar{\Lambda}_{r1}$ and $\bar{\Lambda}_{i1}$. It should be stressed that points on the vertical axes ($\bar{\Lambda}_{r1} = 0$) represent stable co-simulations of the undamped test model. In Figure 4.10, plots are arranged for the unsymmetrical test model ($\alpha_{m21} = \alpha_{\Lambda r21} = \alpha_{\Lambda i21} = 10$). As can be seen, stability behavior for the symmetrical and unsymmetrical model are almost identical.

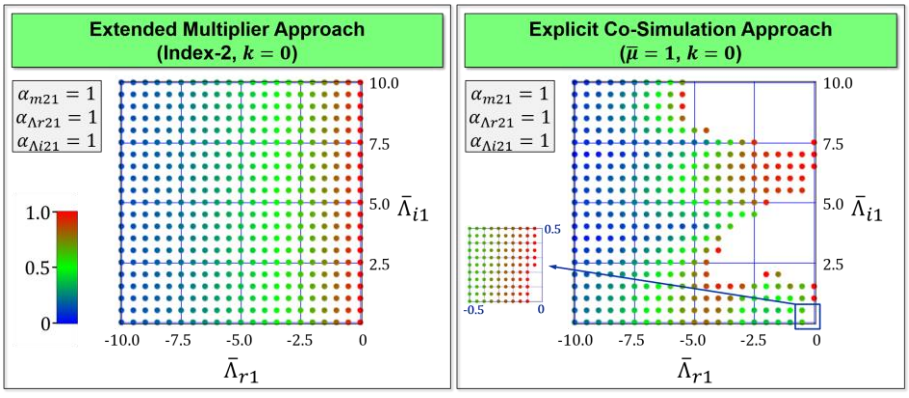

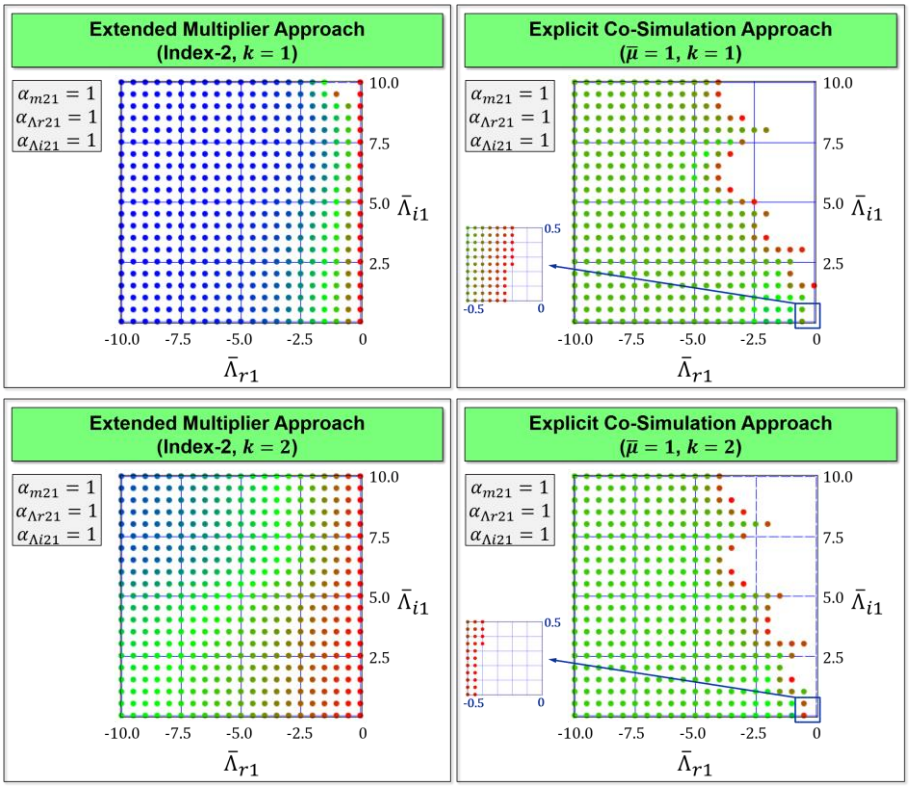

Figure 4.9 2D stability plots for the implicit index-2 co-simulation approach and the explicit co-simulation approach of Ref. [46] (approximation order $k = 0, 1, 2$) for the symmetrical test model ($\alpha_{m21} = \alpha_{\Lambda r21} = \alpha_{\Lambda i21} = 1$).

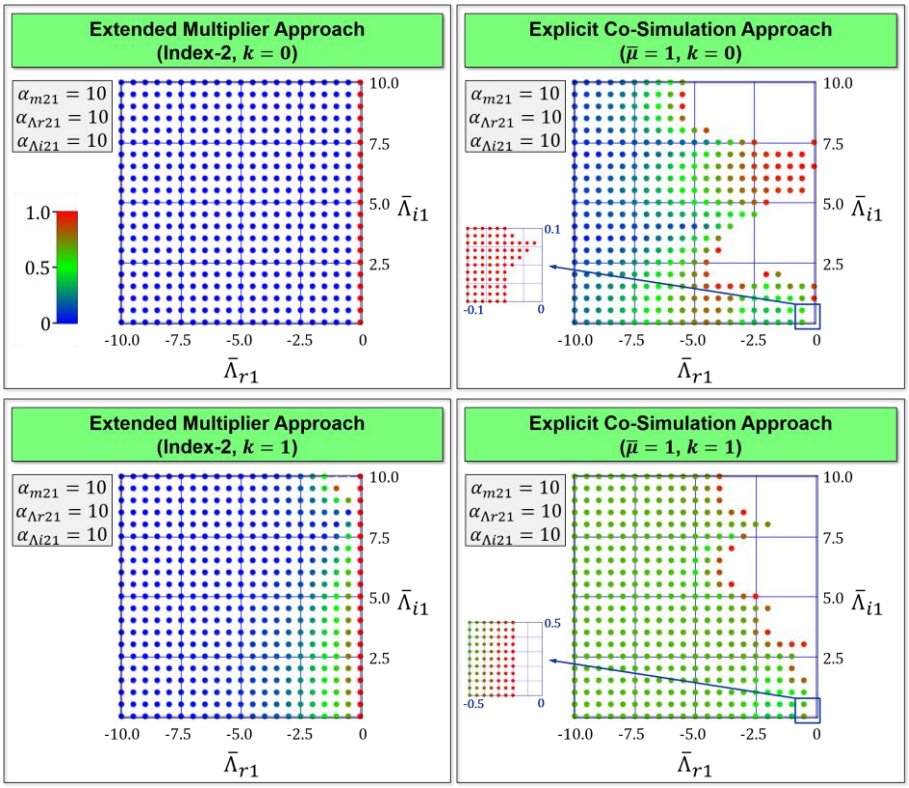

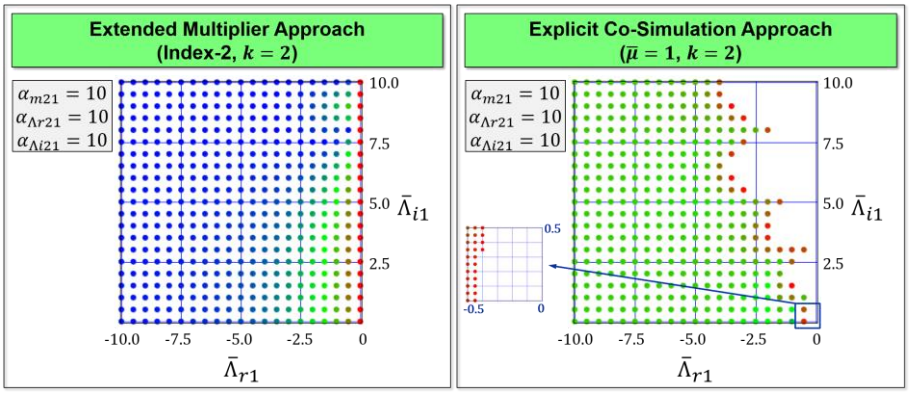

Figure 4.10 2D stability plots for the implicit index-2 co-simulation approach and the explicit co-simulation approach of Ref. [46] (approximation order $k = 0, 1, 2$) for the unsymmetrical test model ($\alpha_{m21} = \alpha_{\Lambda r21} = \alpha_{\Lambda i21} = 10$).

4.8.2. Stability Plots for the Stabilized Index-1 Co-Simulation Method

Stability plots for the implicit index-1 co-simulation method generated with the symmetrical co-simulation test model ($\alpha_{m21} = \alpha_{\Lambda r21} = \alpha_{\Lambda i21} = 1$) are shown in the first row of Figure 4.11 for constant ($k = 0$) and linear ($k = 1$) approximation order. Corresponding plots for the unsymmetrical test model ($\alpha_{m21} = \alpha_{\Lambda r21} = \alpha_{\Lambda i21} = 10$) are arranged in the second row.

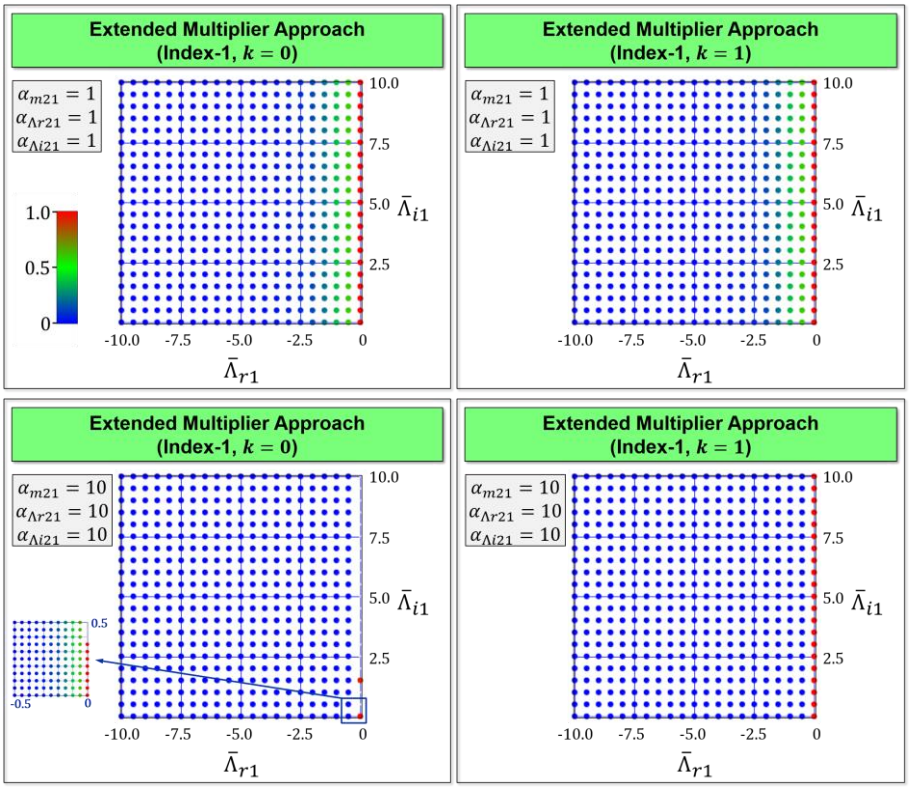

Figure 4.11 2D stability plots for the implicit index-1 co-simulation approach (approximation order $k = 0, 1, 2$) for the symmetrical ($\alpha_{m21} = \alpha_{\Lambda r21} = \alpha_{\Lambda i21} = 1$) and for the unsymmetrical test model ($\alpha_{m21} = \alpha_{\Lambda r21} = \alpha_{\Lambda i21} = 10$).

4.9. Convergence Plots for the Stabilized Implicit Co-Simulation Method

The convergence behavior of the implicit index-2 and index-1 co-simulation method is investigated by calculating the local and the global error for the position and velocity variables. Therefore, co-simulations are accomplished with the test model using the parameters $m_1 = 0.5 \cdot m_2 = 1,\ c_1 = c_2 = c_c = 1000,\ d_1 = d_2 = d_c = 10$. The relative global error ε_{glo} for the position and velocity variables is computed by the normalized root mean square error (NRMSE) according to Eq. (4.64).

In Figure 4.12, convergence plots of the global errors $\varepsilon_{pos,glo}$, $\varepsilon_{vel,glo}$ and of the local errors $\varepsilon_{pos,loc}$, $\varepsilon_{vel,loc}$ are depicted for the index-2 co-simulation approach using constant ($k = 0$), linear ($k = 1$) and quadratic ($k = 2$) approximation order. We observe that the global errors converge with $\mathcal{O}(H^4)$ and the local errors with $\mathcal{O}(H^5)$.

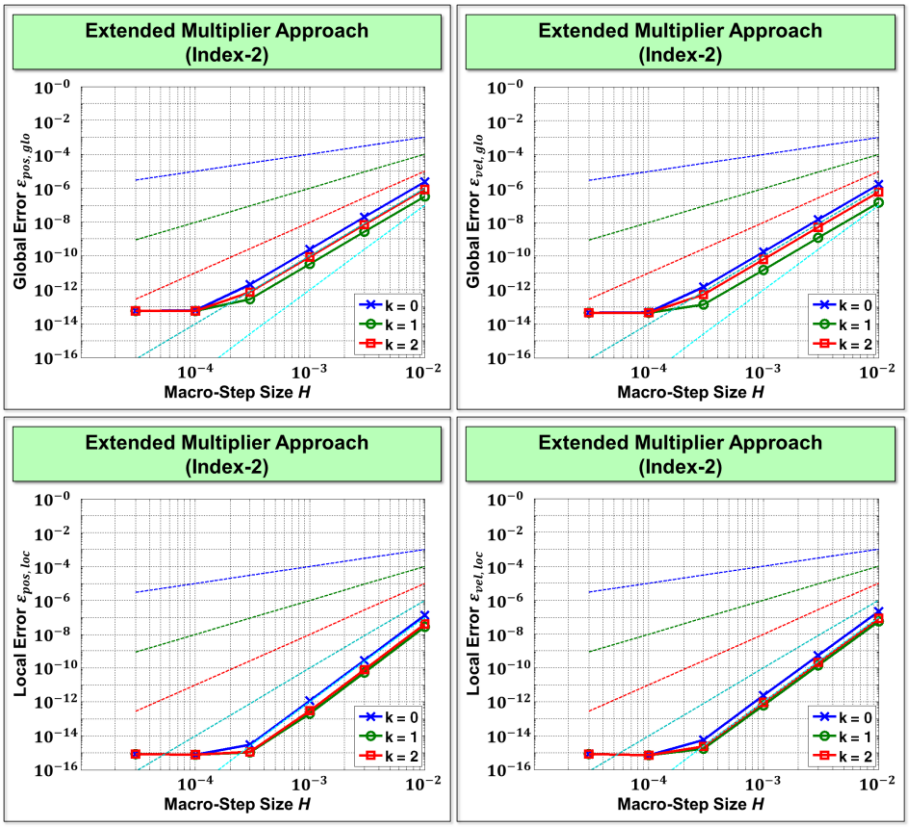

Figure 4.12 convergence plots for the stabilized implicit index-2 co-simulation approach (approximation order $k = 0, 1, 2$).

Figure 4.13 shows convergence plots of the global errors $\varepsilon_{pos,glo}$, $\varepsilon_{vel,glo}$ and of the local errors $\varepsilon_{pos,loc}$, $\varepsilon_{vel,loc}$ for the index-1 co-simulation approach for constant ($k = 0$) and linear ($k = 1$) approximation order. As can be seen, the global errors converge with $\mathcal{O}(H^3)$ for $k = 0$ and with $\mathcal{O}(H^4)$ for $k = 1$. The local errors converge with $\mathcal{O}(H^4)$ for $k = 0$ and with $\mathcal{O}(H^5)$ for $k = 1$.

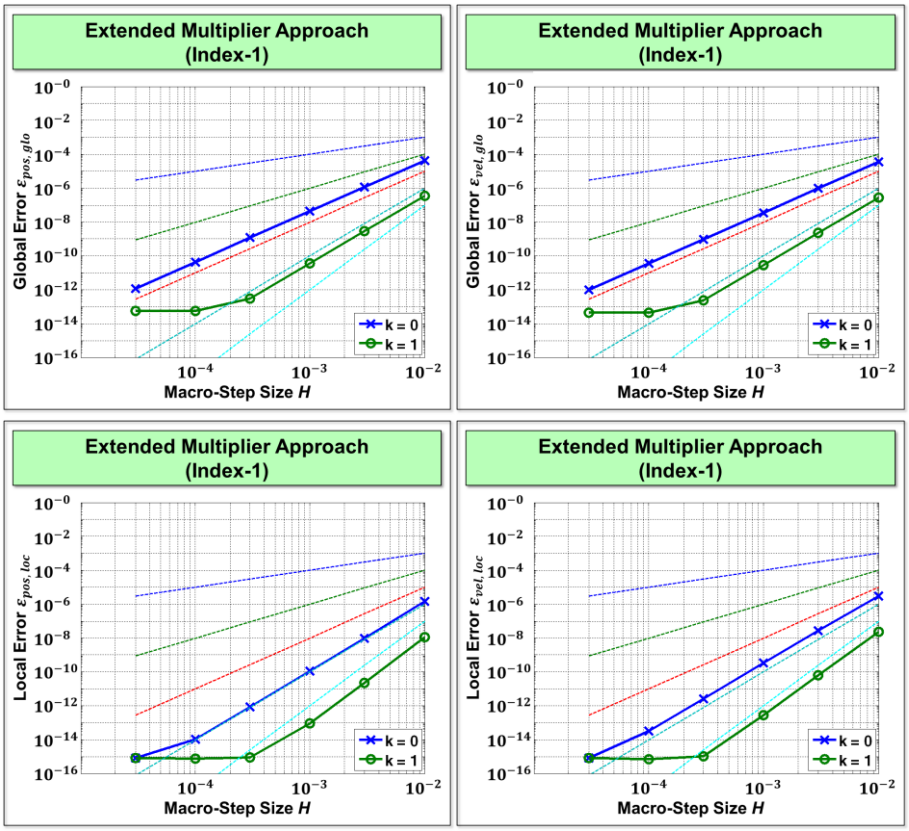

Figure 4.13 Convergence plots for the stabilized implicit index-1 co-simulation approach (approximation order $k = 0, 1$).

4.10. Numerical Examples

The applicability of the extended multiplier co-simulation approach to nonlinear models is demonstrated with two examples.

4.10.1. Nonlinear Two-Mass Oscillator

As a first example, we consider the two-mass oscillator of Section 2.2. Now, an additional nonlinear force $F_{nolin} = -0.01 \cdot e^{10\cdot(x_2-1)}$ is applied at the second mass, which may physically be interpreted as a kind of penalty force representing a soft contact at $x_2 = 1$. Consequently, the equation of motion for the second mass in Eq. (2.9) has to be replaced by $\dot{v}_2 = -\frac{c_2}{m_2}x_2 - \frac{d_2}{m_2}v_2 - \frac{1}{m_2}\lambda_c + \frac{1}{m_2}F_{nolin}$. Simulations have been carried out with the subsequent parameters: $m_1 = 1\,\mathrm{kg}, m_2 = 2\,\mathrm{kg}, c_1 = c_2 = 1E3\,\mathrm{N/m}$ and $d_1 = d_2 = 0\,\mathrm{Ns/m}$. As initial conditions, $x_{1,0} = x_{2,0} = 0\,\mathrm{m}$ and $v_{1,0} = v_{2,0} = 100\,\mathrm{m/s}$ have been chosen. The subsystems have been integrated numerically with an implicit Runge-Kutta solver. The co-simulations have been carried out with the constant macro-step size $H = 1E-4\,\mathrm{s}$.

Simulation results for the index-2 and index-1 co-simulation approaches are collected in Figure 4.14. The plots depict the displacement $x_1(t)$ and the velocity $v_1(t)$ of mass 1, the Lagrange multiplier $\lambda_c(t)$ as well as the constraint equation $g_c(t) = x_2(t) - x_1(t)$

and its time derivatives $\dot{g}_c(t), \ddot{g}_c(t)$. As can be seen, all coupling approaches yield stable results. As expected, the position constraint g_c and the velocity constraint $\dot{g}_c$ are enforced to be zero for the index-2 approaches. Applying the index-1 formulation, also the acceleration constraint $\ddot{g}_c$ is fulfilled. Convergence plots illustrating the global error for the position and for the velocity variables are collected in Figure 4.15.

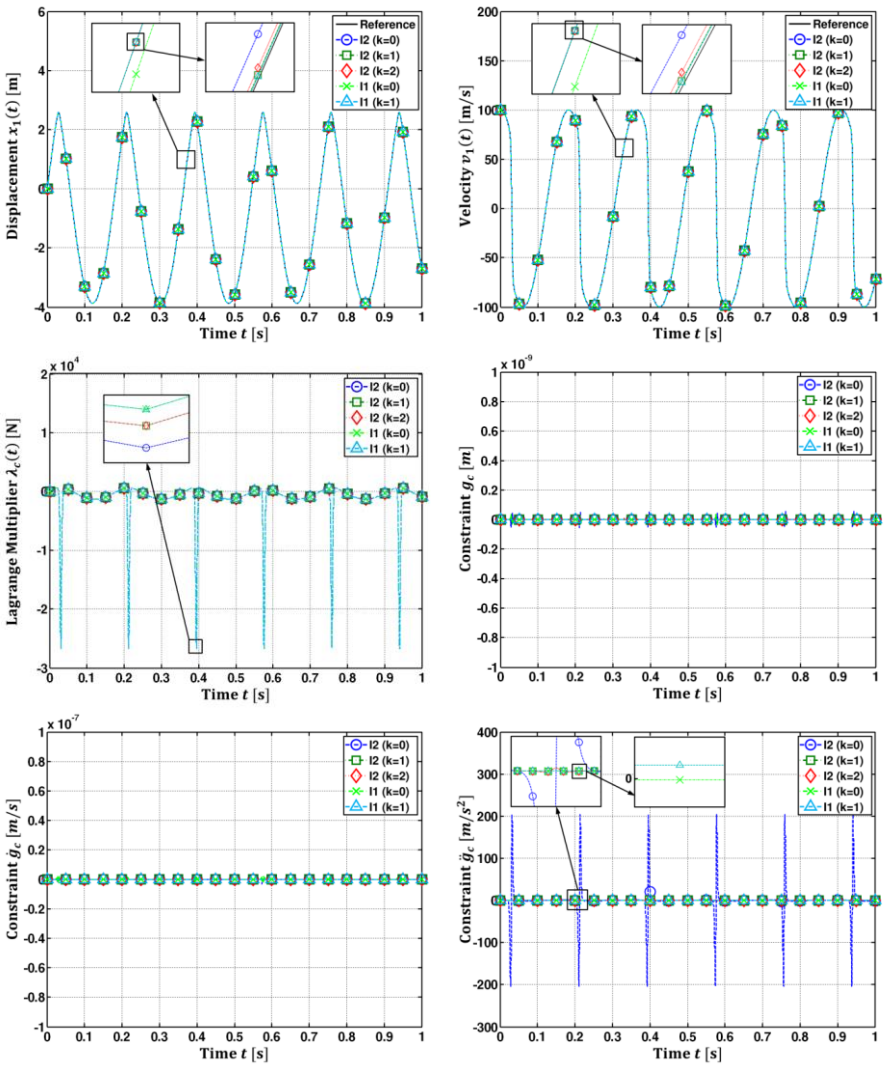

Figure 4.14 Co-simulation results for the nonlinear two-mass oscillator: Displacement $x_1(t)$ and velocity $v_1(t)$, Lagrange multiplier $\lambda_c(t)$, constraint equations $g_c(t)$, $\dot{g}_c(t)$ and $\ddot{g}_c(t)$.

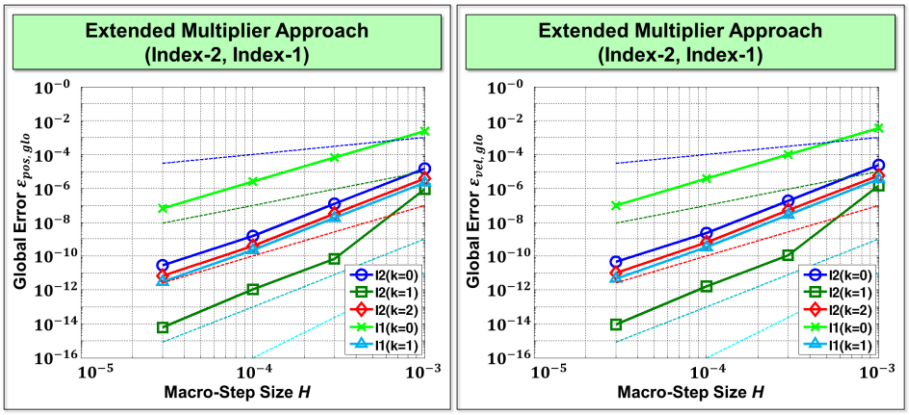

Figure 4.15 Convergence plots for the nonlinear two-mass oscillator: Global error of the position and velocity variables over the macro-step size H.

4.10.2. Four-Bar Mechanism

The planar four-bar mechanism, see Figure 4.16, is analyzed next. The system is decomposed into two subsystems by splitting the bar in the middle into two parts. Subsystem 1 contains bar 1 ($m_1 = 1\,\mathrm{kg}, J_1 = 1/12\,\mathrm{kg\,m^2}, l_1 = 1\,\mathrm{m}$) and bar 2 ($m_2 = 1\,\mathrm{kg}, J_2 = 1/12\,\mathrm{kg\,m^2}, l_2 = 1\,\mathrm{m}$); subsystem 2 consists of bar 3 ($m_3 = 1\,\mathrm{kg}, J_3 = 1/12\,\mathrm{kg\,m^2}, l_3 = 1\,\mathrm{m}$) and bar 4 ($m_4 = 2\,\mathrm{kg}, J_4 = 2/3\,\mathrm{kg\,m^2}, l_4 = 2\,\mathrm{m}$). Bar 2 and bar 3 are coupled by a fixed joint, i.e. by the constraint equations $g_{ca_x}(t) = (x_2 + 0.5 \cdot l_2 \cdot \cos\varphi_2) - (x_3 - 0.5 \cdot l_3 \cdot \cos\varphi_3) = 0, g_{ca_y}(t) = (y_2 + 0.5 \cdot l_2 \cdot \sin\varphi_2) - (y_3 - 0.5 \cdot l_3 \cdot \sin\varphi_3) = 0$ and $g_{cp}(t) = \varphi_3 - \varphi_2 = 0$. Gravity is acting in negative y-direction ($g = 9.81\,\mathrm{m/s^2}$). As initial conditions, $\varphi_{1,0} = \pi/4\,\mathrm{rad}$ and $\dot{\varphi}_{1,0} = 0\,\mathrm{rad/s}$ have been chosen. The subsystems have been integrated numerically with an implicit Runge-Kutta integrator. The co-simulations have been accomplished with the constant macro-step size $H = 1E-3$.

Numerical results for the index-2 and index-1 co-simulation approaches are collected in Figure 4.17. The plots show the displacements $x_2(t)$ and $y_2(t)$ of the center of mass S_2 and the rotation angle $\varphi_2(t)$ of bar 2. Furthermore, the coupling force $\lambda_{ca_x}(t)$ acting at the fixed joint in x-direction is depicted as well as the constraint equation $g_{ca_x}(t)$ and its time derivatives $\dot{g}_{ca_x}(t)$, $\ddot{g}_{ca_x}(t)$. As can be detected, all coupling approaches yield stable results. The constraints on position and velocity level are close to zero for the index-2 approaches. For the index-1 approaches, the constraints on acceleration level are also enforced to be zero.

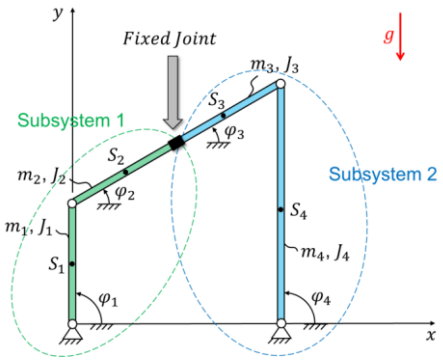

Figure 4.16 Planar four-bar mechanism: Interpretation as two double pendulums coupled by a fixed joint.

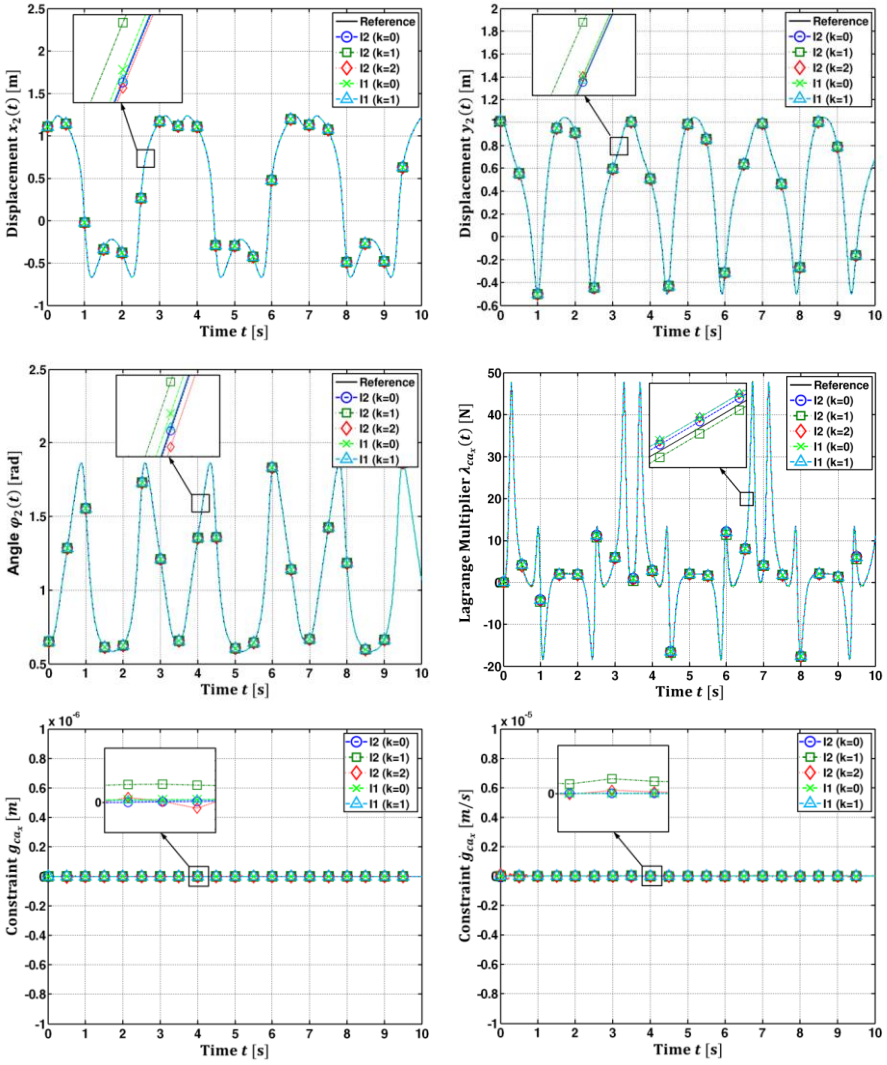

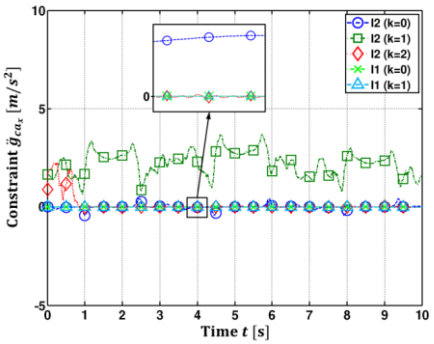

Figure 4.17 Co-simulation results for the four-bar mechanism: Displacements $x_2(t), y_2(t)$ and angle $\varphi_2(t)$, Lagrange multiplier $\lambda_{ca_x}(t)$, constraint equations $g_{ca_x}(t)$, $\dot{g}_{ca_x}(t)$ and $\ddot{g}_{ca_x}(t)$.

5. Conclusions and Outlook

5.1. Conclusions

In the work, the numerical stability of different co-simulation methods based on applied-force coupling and on constraint coupling approach has been analyzed. As co-simulation test model, the linear two-mass oscillator has been used. With the help of the test model, linear systems of recurrence equations have been derived, which characterize the numerical stability of the co-simulation approaches.

In the framework of the co-simulation method with applied-force coupling, the stability behavior is characterized by 7 independent parameters. Discretizing the test model with a co-simulation approach yields a linear homogenous system of recurrence equations. The spectral radius of this recurrence system characterizes the stability of the co-simulation method. In order to compare different co-simulation approaches, 2D stability plots are convenient. Therefore, 5 of the 7 parameters are fixed so that the spectral radius can be depicted as a function of the remaining 2 parameters. The results presented for the explicit co-simulation approaches show that the region of stability will successively be reduced if higher order approximation polynomials are used. Furthermore, it is shown that – at least for the chosen set of parameters – the displacement/displacement-decomposition approach exhibits a better stability behavior than co-simulation approaches based on force/displacement- and force/force-decomposition. As expected, implicit coupling schemes exhibit a significant better numerical stability than explicit schemes. Although $A(\alpha)$-stability cannot be proven, calculations show that the implicit approaches are stable for very large values of $\overline{\Lambda}_{r1}$ and $\overline{\Lambda}_{i1}$.

Furthermore, taking not only into account the constitutive equations, but also the derivative (D-extension) or the integral (I-extension) of the constitutive equations, the numerical stability of implicit (semi-implicit) co-simulation methods may considerably be improved for the case that higher order approximation functions are used. The original (non-extended) method exhibits a good stability behavior, if constant approximation is applied. For that case, the application of the extended formulations may not be useful. For linear and quadratic approximation functions, especially the D-extended co-simulation method may, however, be applied advantageously.

For analyzing the numerical stability of co-simulation methods based on algebraic constraint equations, a different test model has to be defined. The linear two-mass oscillator with one degree of freedom is the quite obvious choice. The stability of this co-simulation test model is characterized by 5 independent parameters ($\overline{\Lambda}_{r1}$, $\overline{\Lambda}_{i1}, \alpha_{m21}, \alpha_{\Lambda r21}$ and $\alpha_{\Lambda i21}$).

Making use of the extended multiplier approach, the key idea is to discretize the Lagrange multiplier between the macro-time points (extended multiplier approach) so that the coupling equations and their time derivatives can simultaneously be fulfilled at the macro-time points. An advantage of the proposed method is the good numerical stability; the convergence plots indicate small numerical errors. Compared with explicit approaches, the presented method has the drawback that the macro-step has to be

repeated once. Therefore, the subsystem solvers have to be reinitialized at the previous macro-time point.

5.2. Outlook

As mentioned in the introduction, co-simulation approaches have two main fields of application. Co-simulation may, on the one hand, be used in order to different simulation codes in time domain. On the other hand, co-simulation can be applied in order to parallelize dynamical systems in time domain.

Currently, application of co-simulation techniques for parallelizing multibody systems is not well established. One reason is that multibody systems normally have significantly smaller dimensions than finite element systems, so that parallelization is not mandatory for achieving practicable simulation times. A second reason is based on the fact that explicit co-simulation approach are, in contrast to finite element systems, often not appropriate in order to parallelize multibody systems. In future work, the potential of using co-simulation techniques to parallelize multibody systems should be investigated in detail.

In this work, only the case of equidistant communication-time grids has been considered. An interesting and important issue for future research is the realization of non-equidistant macro-grids by using appropriate error estimators for controlling the macro-step size.

Appendix A: Stability Plots for Force/Force-Coupling (Index-1)

A.1 Force/Force-Coupling based on Baumgarte Stabilization (Index-1)

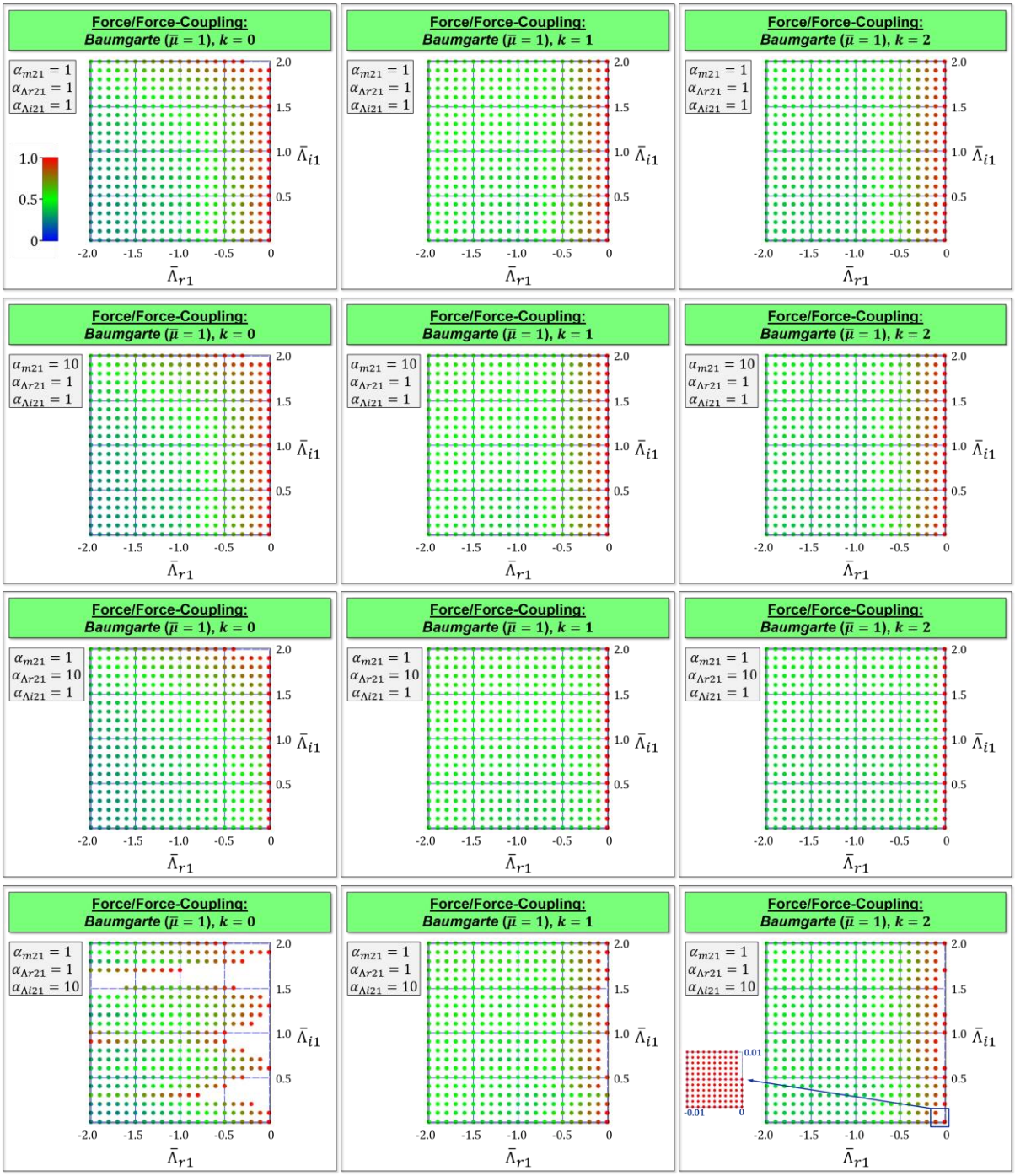

Figure A. 1 Stability plot for the implicit index-1 co-simulation method based on Baumgarte stabilization with force/force-decomposition: $\bar{\mu} = 1$, polynomial degrees $k = 0,1,2$.

A.2 Force/Force-Coupling based on Weighted Multiplier Approach (Index-1)

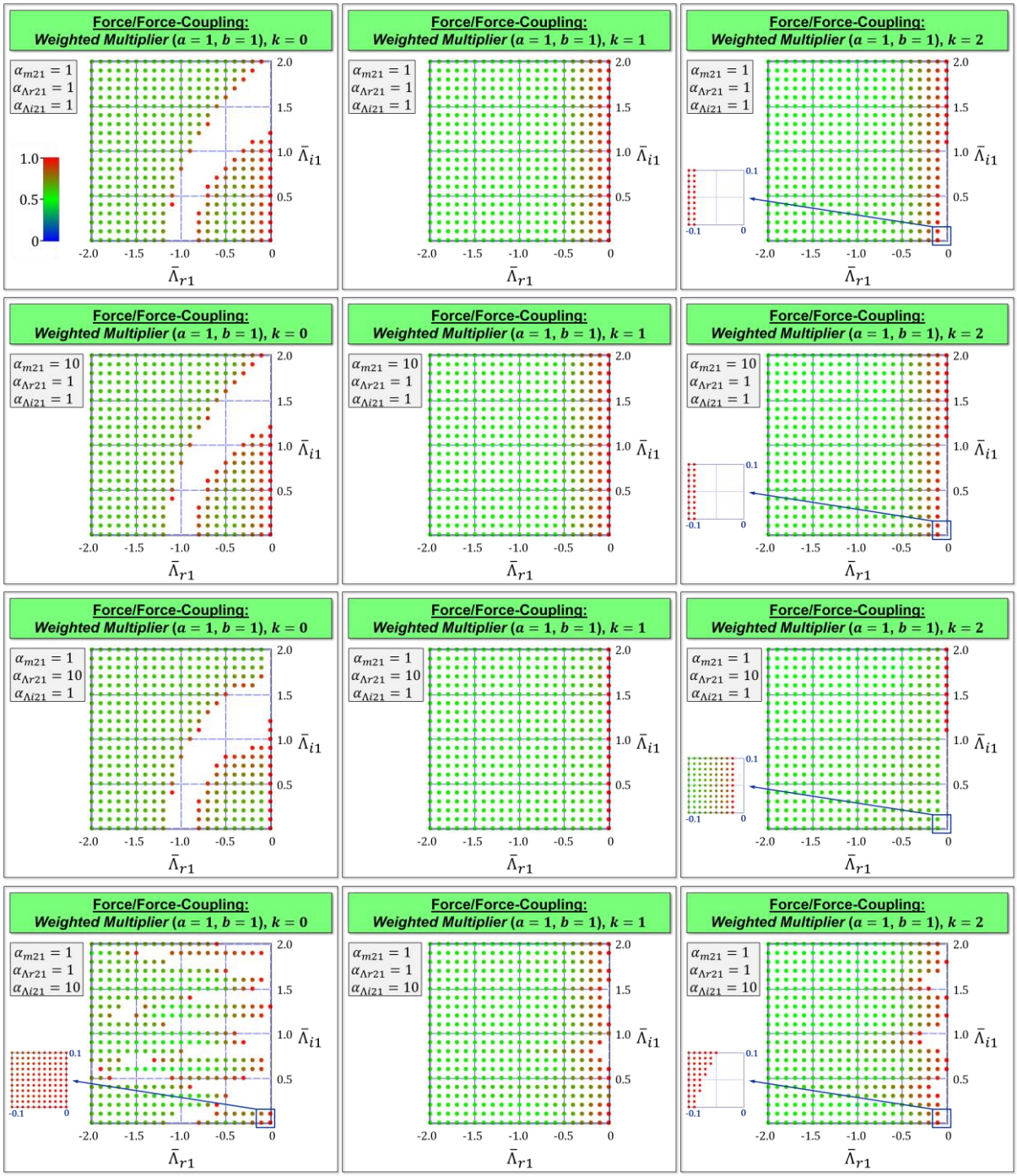

Figure A. 2 Stability plot for the implicit index-1 co-simulation method based on the weighted multiplier approach with force/force-decomposition: $a = b = 1$, polynomial degrees $k = 0,1,2$.

A.3 Force/Force-Coupling based on Projection Technique

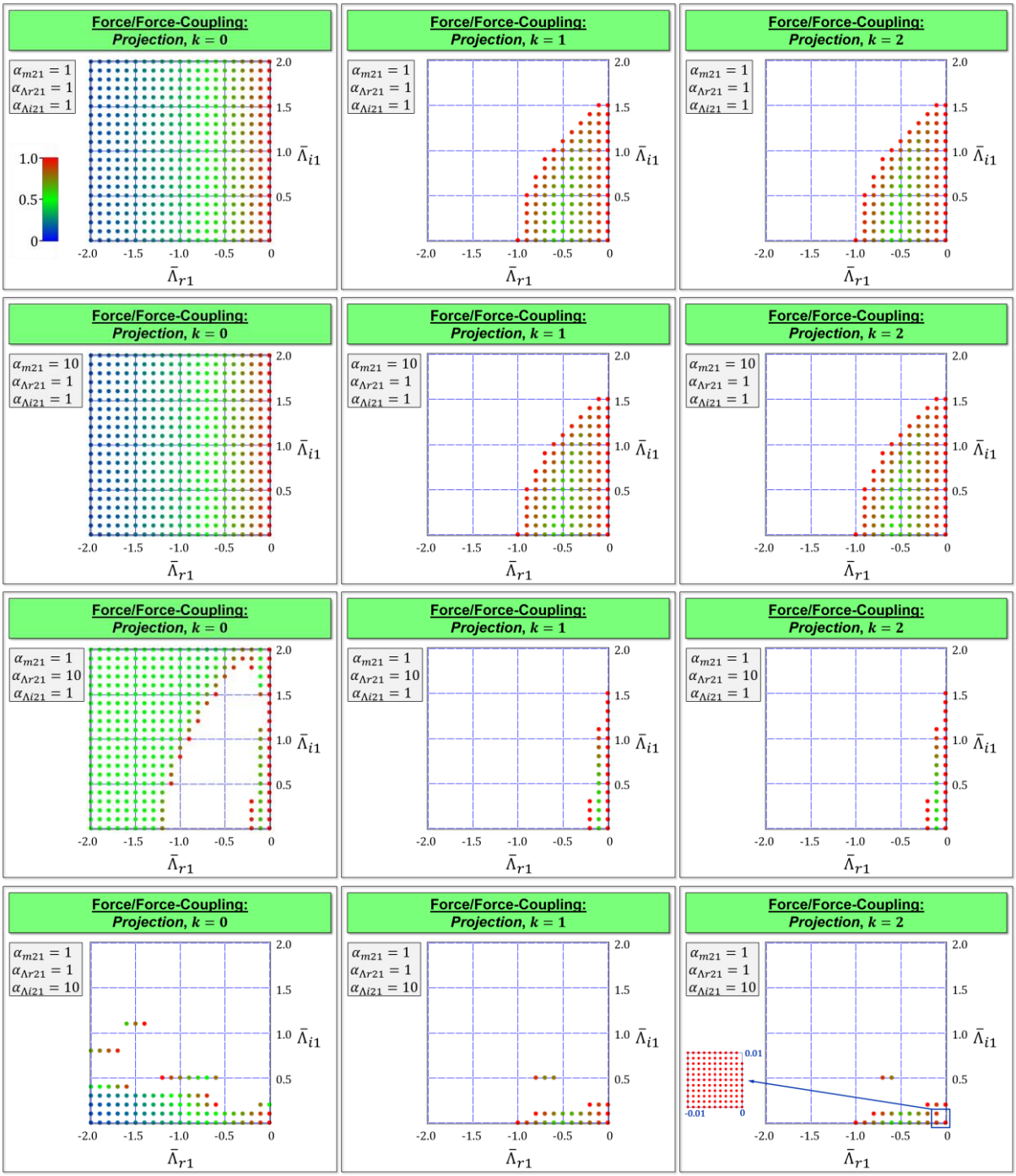

Figure A. 3 Stability plot for the implicit co-simulation method based on the projection technique with force/force-decomposition: polynomial degrees $k = 0,1,2$.

Appendix B: Stability Plots for Force/Displacement-Coupling (Index-1)

B.1 Force/Displacement-Coupling based on Baumgarte Stabilization (Index-1)

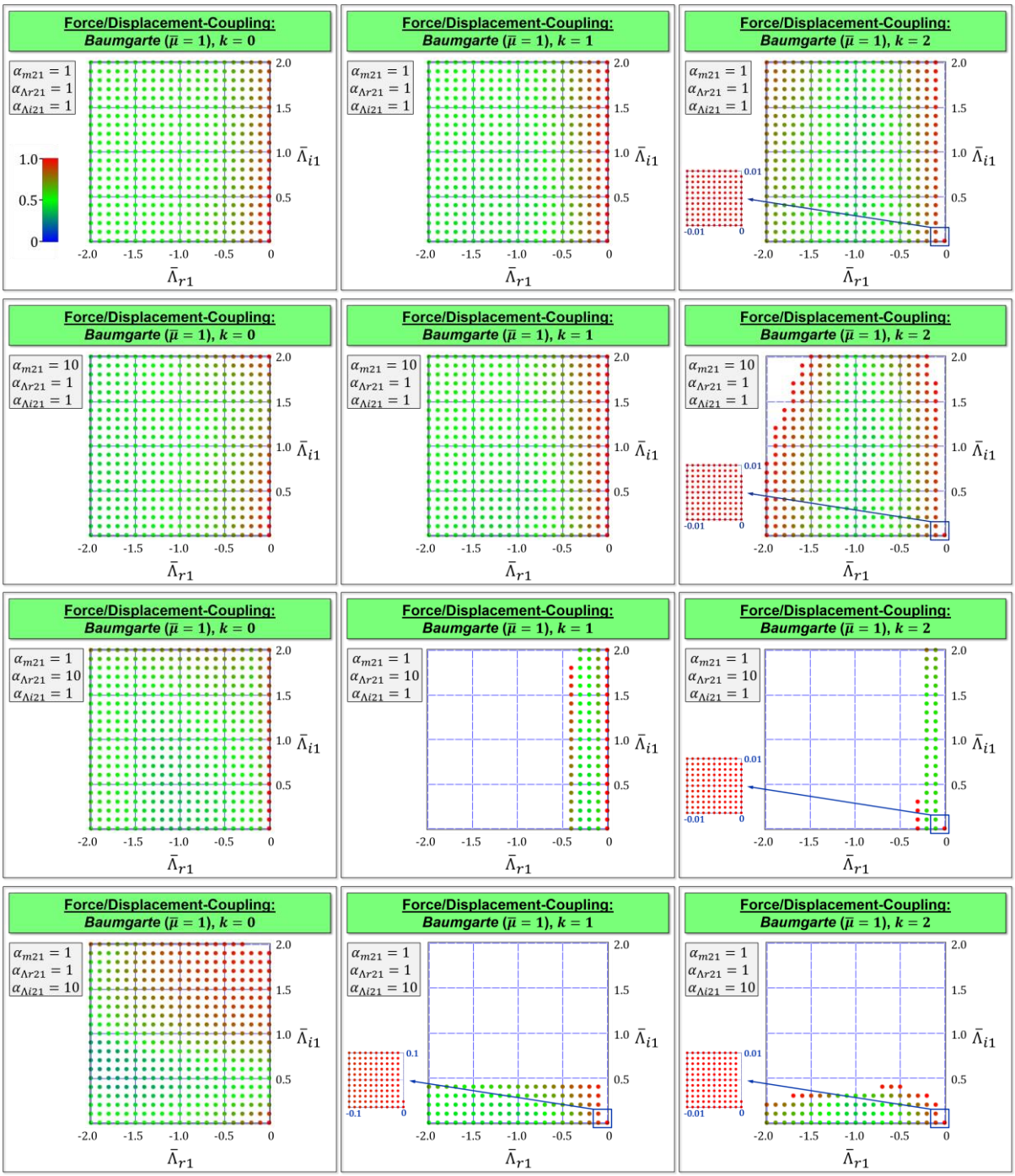

Figure A. 4 Stability plot for the implicit index-1 co-simulation method based on Baumgarte stabilization with force/displacement-decomposition: $\bar{\mu} = 1$, polynomial degrees $k = 0,1,2$.

B.2 Force/Displacement-Coupling based on Weighted Multiplier Approach (Index-1)

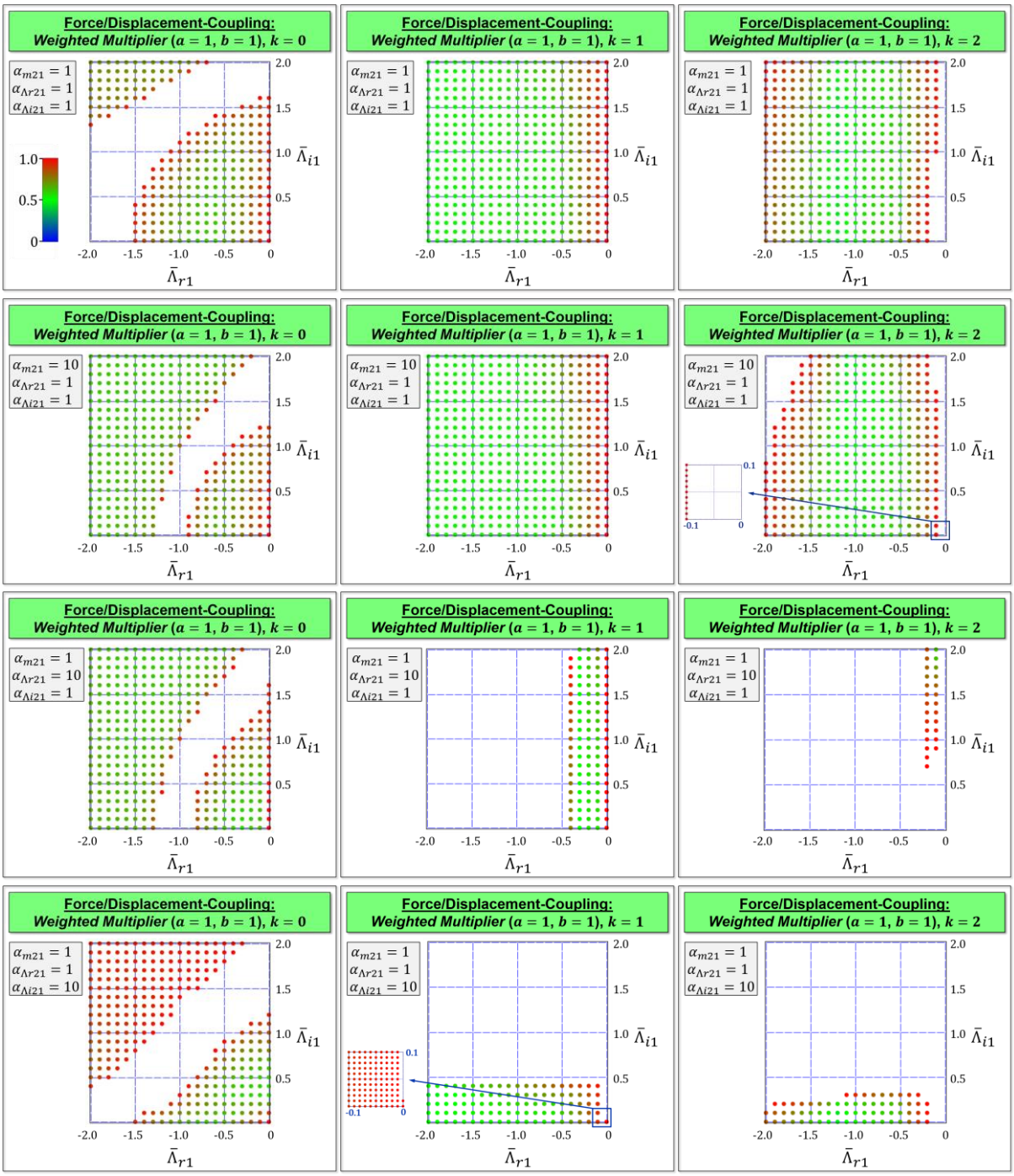

Figure A. 5 Stability plot for the implicit index-1 co-simulation method based on the weighted multiplier approach with force/displacement-decomposition: $a = b = 1$, polynomial degrees $k = 0,1,2$.

B.3 Force/Displacement-Coupling based on Projection Technique

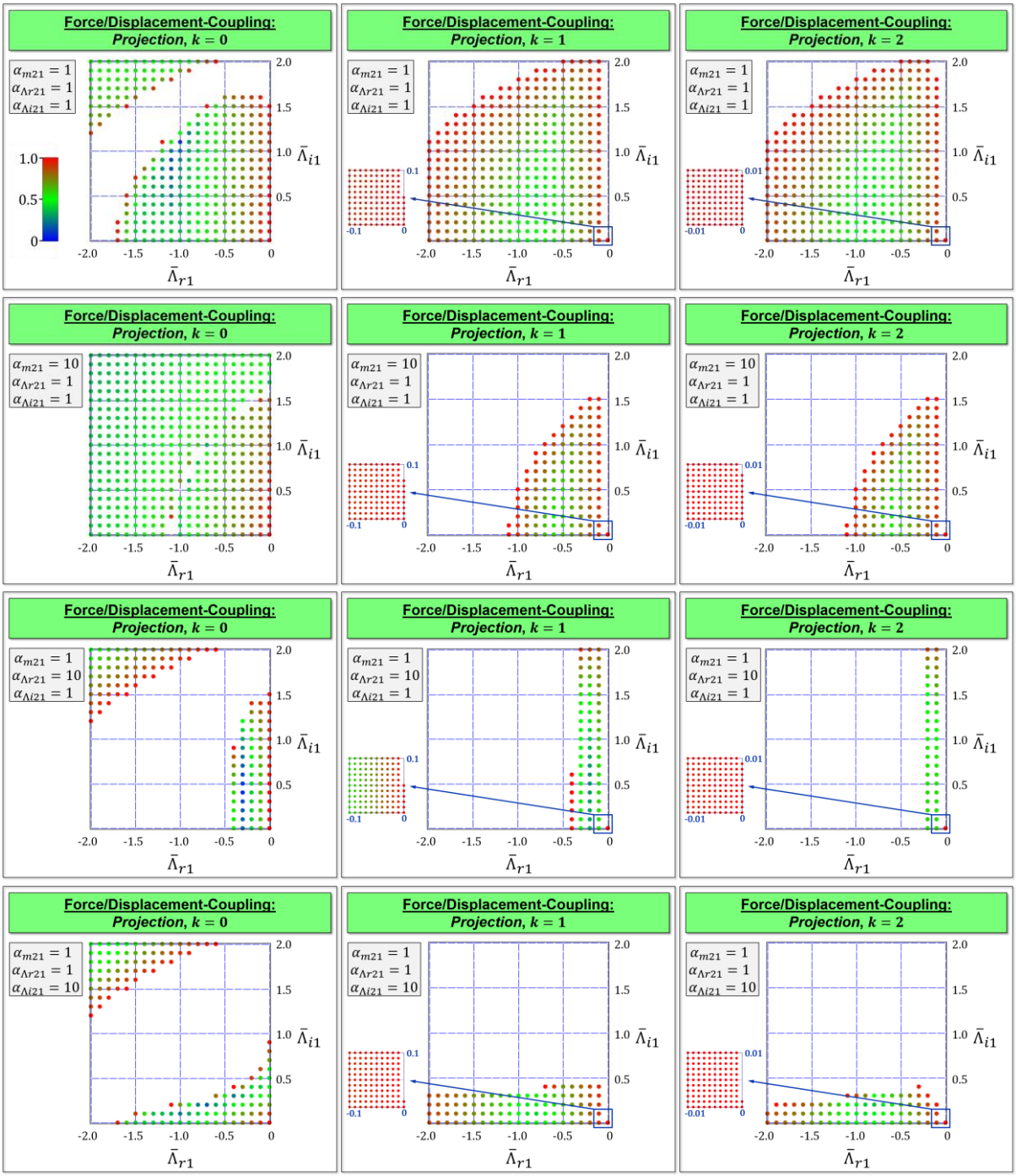

Figure A. 6 Stability plot for the implicit index-1 co-simulation method based on projection technique with force/displacement-decomposition: polynomial degrees $k = 0,1,2$.

Appendix C: Stability Plots for Displacement/Displacement-Coupling

C.1 Displacement/Displacement-Coupling based on Projection Technique

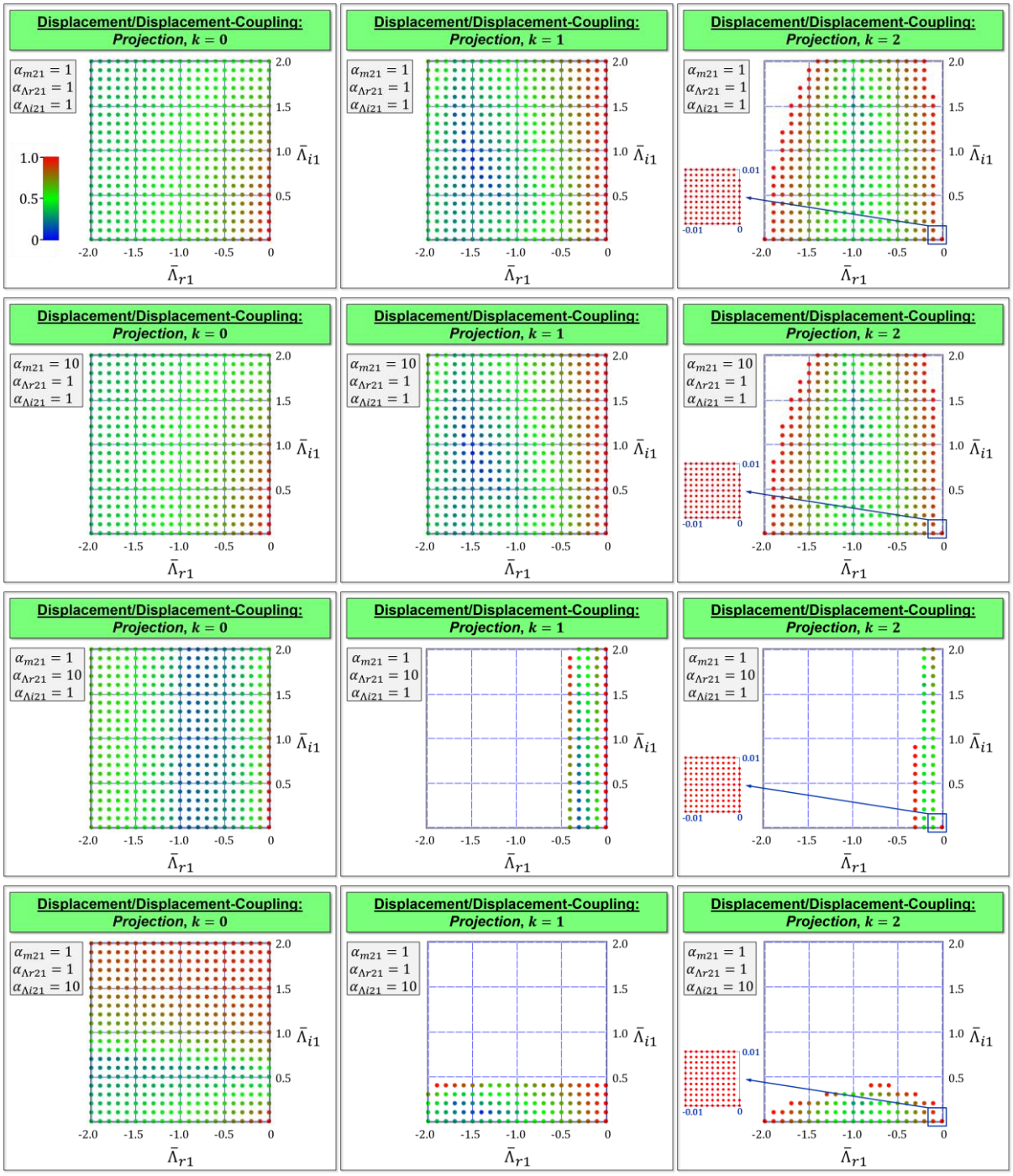

Figure A. 7 Stability plot for the implicit index-1 co-simulation method based on projection technique with displacement/displacement-decomposition: polynomial degrees $k = 0,1,2$.

Appendix D: Stability Plots for Force/Force-Coupling (Index-2)

D.1 Force/Force-Coupling based on Baumgarte Stabilization (Index-2)

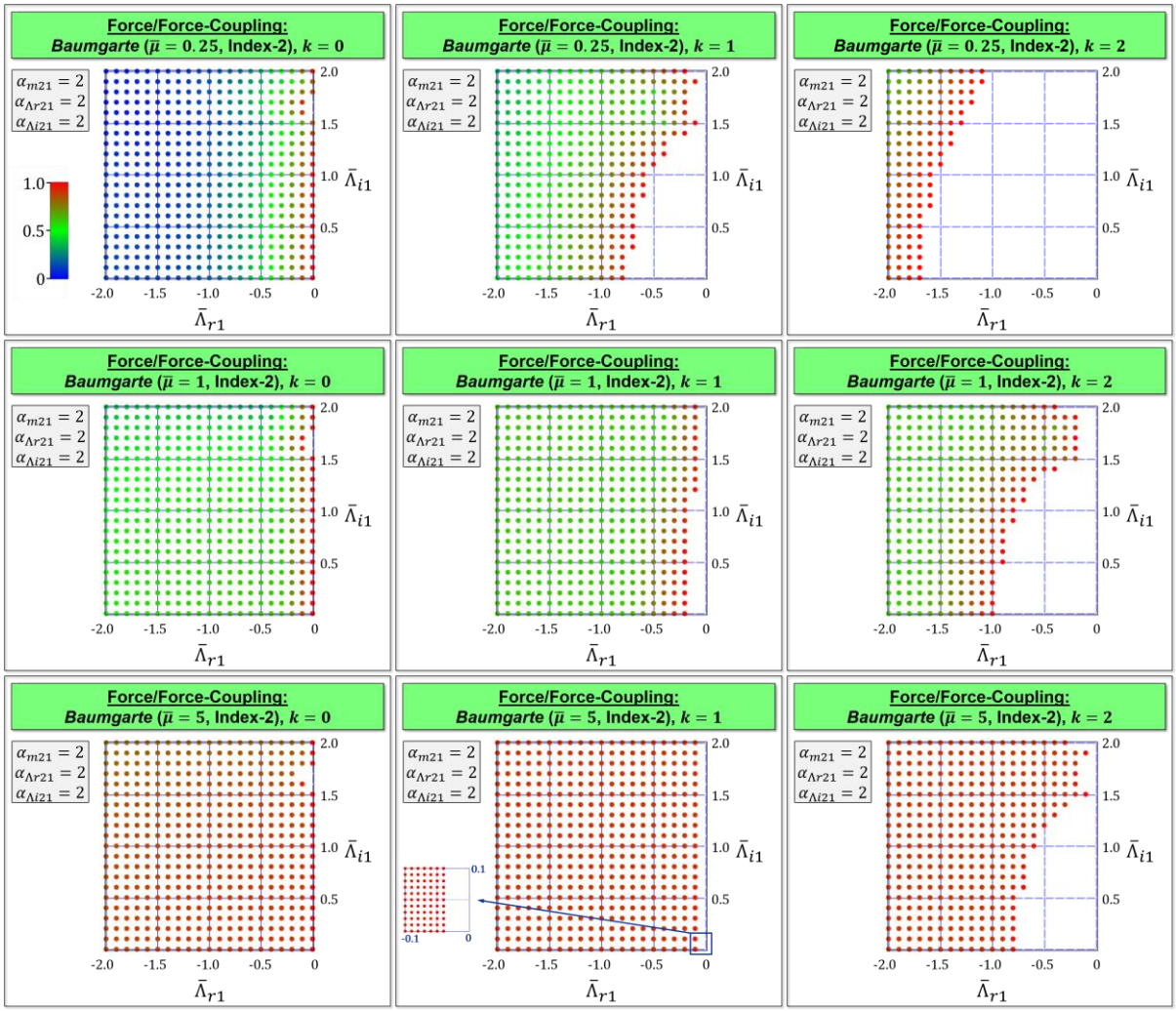

Figure A. 8 Stability plot for the implicit index-2 co-simulation method based on Baumgarte stabilization with force/force-decomposition (polynomial degrees $k = 0,1,2.$): Baumgarte parameters $\bar{\mu} = 0.25, \bar{\mu} = 0.1$ and $\bar{\mu} = 5$.

D.2 Force/Force-Coupling based on Weighted Multiplier Approach (Index-2)

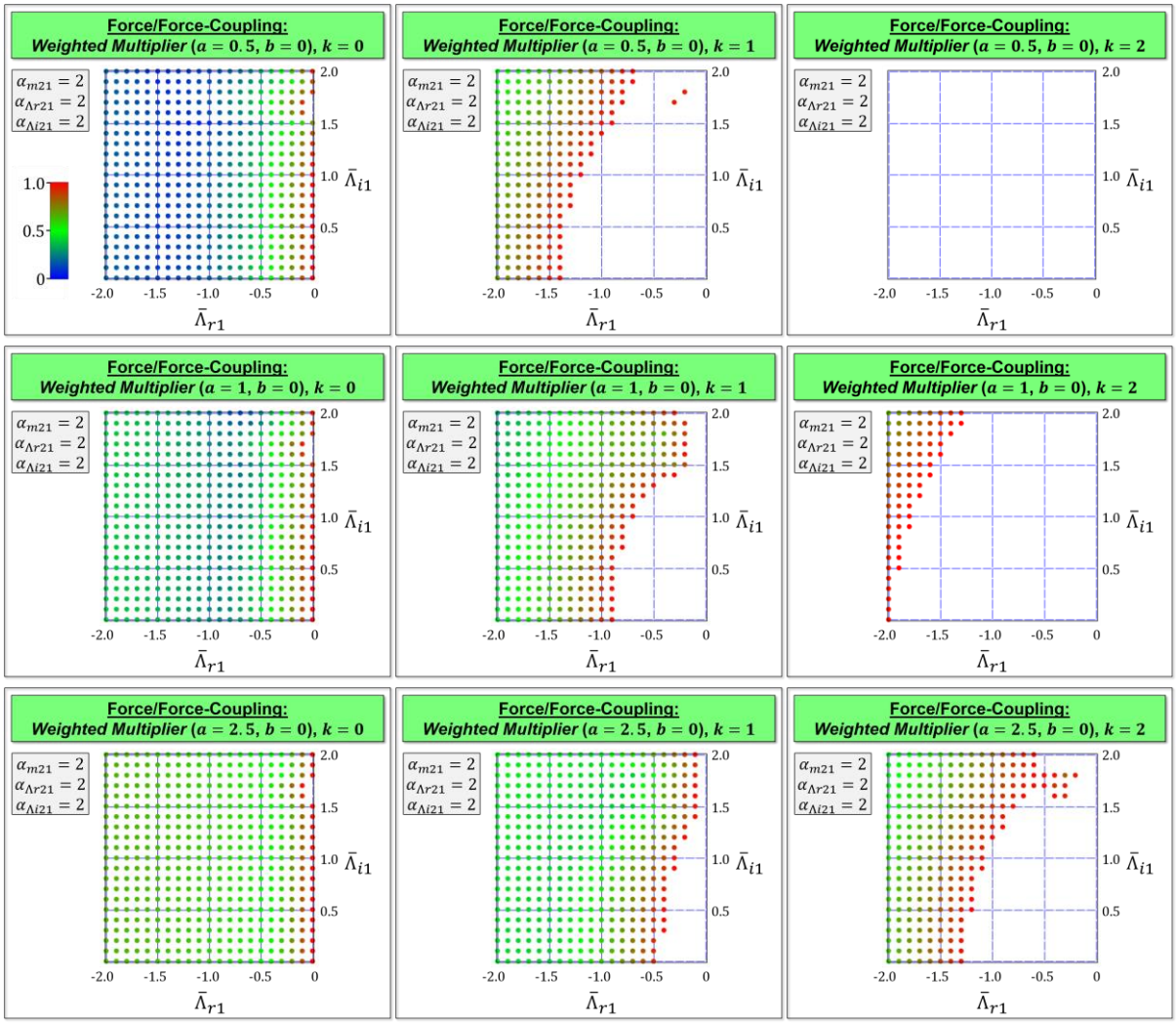

Figure A. 9 Stability plot for the implicit index-2 co-simulation method based on the weighted multiplier approach with force/force-decomposition (polynomial degrees $k = 0,1,2$): weighted multiplier parameters $a = 0.5, b = 0$; $a = 1, b = 0$ and $a = 2.5, b = 0$.

Appendix E: Stability Plots for Force/Force-Coupling (Index-3)

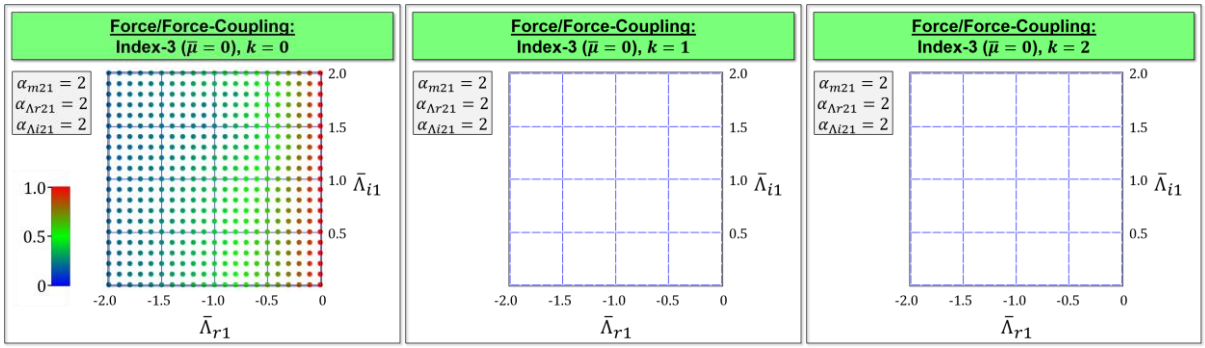

Figure A. 10 Stability plot for the implicit index-3 co-simulation method with force/force-decomposition (polynomial degrees $k = 0,1,2$).

Appendix F: Influence of the Baumgarte and the Weighted Multiplier Parameters on the Stability Behavior (Index-1)

F.1 Implicit Co-Simulation Method based on Baumgarte Stabilization (Index-1)

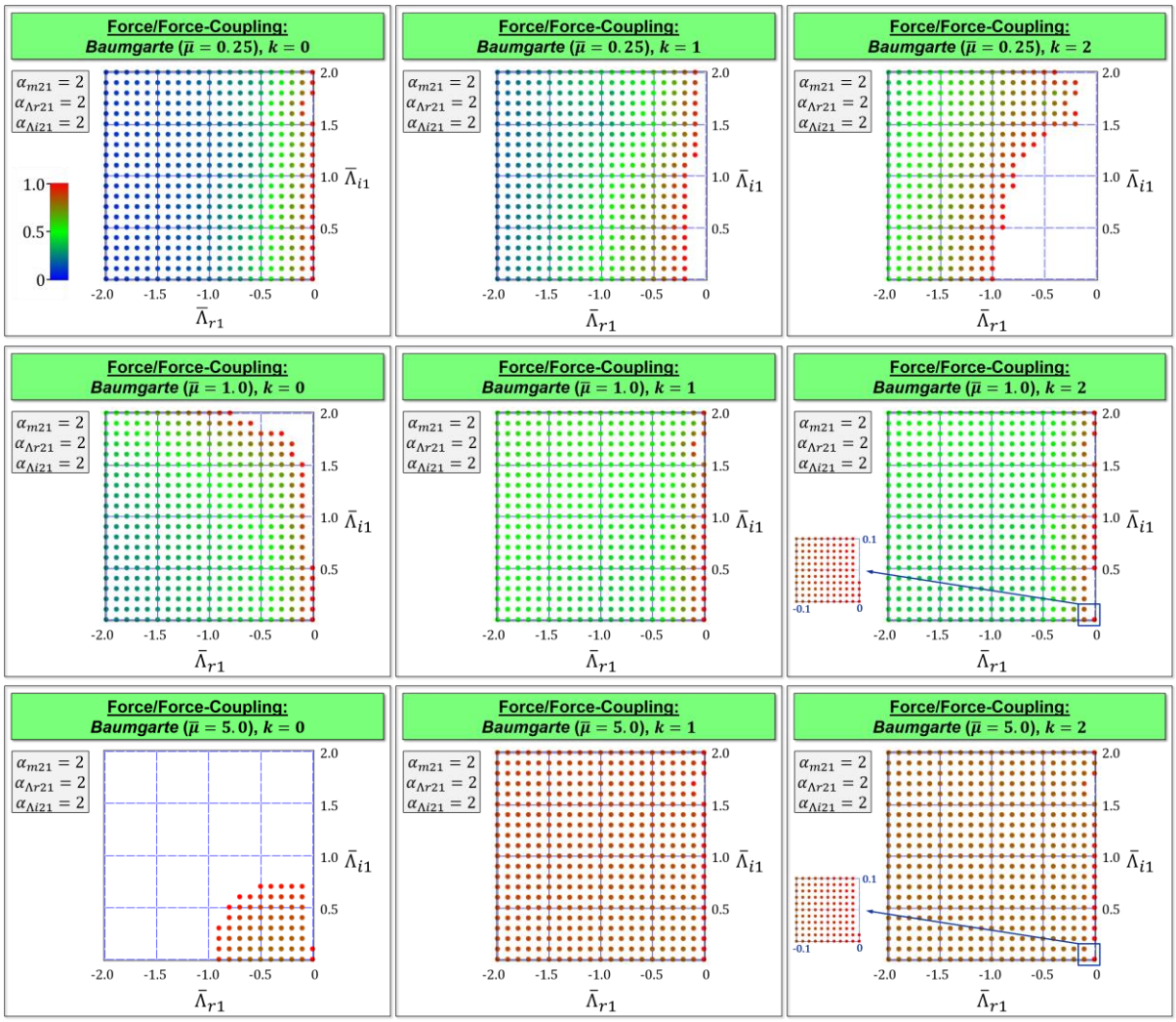

Figure A. 11 Stability plot for the implicit index-1 co-simulation method based on Baumgarte stabilization with force/force-decomposition (polynomial degrees $k = 0,1,2$): Baumgarte parameters $\bar{\mu} = 0.25, \bar{\mu} = 1$ and $\bar{\mu} = 5$.

F.2 Implicit Co-Simulation Method based on Weighted Multiplier Approach (Index-1)

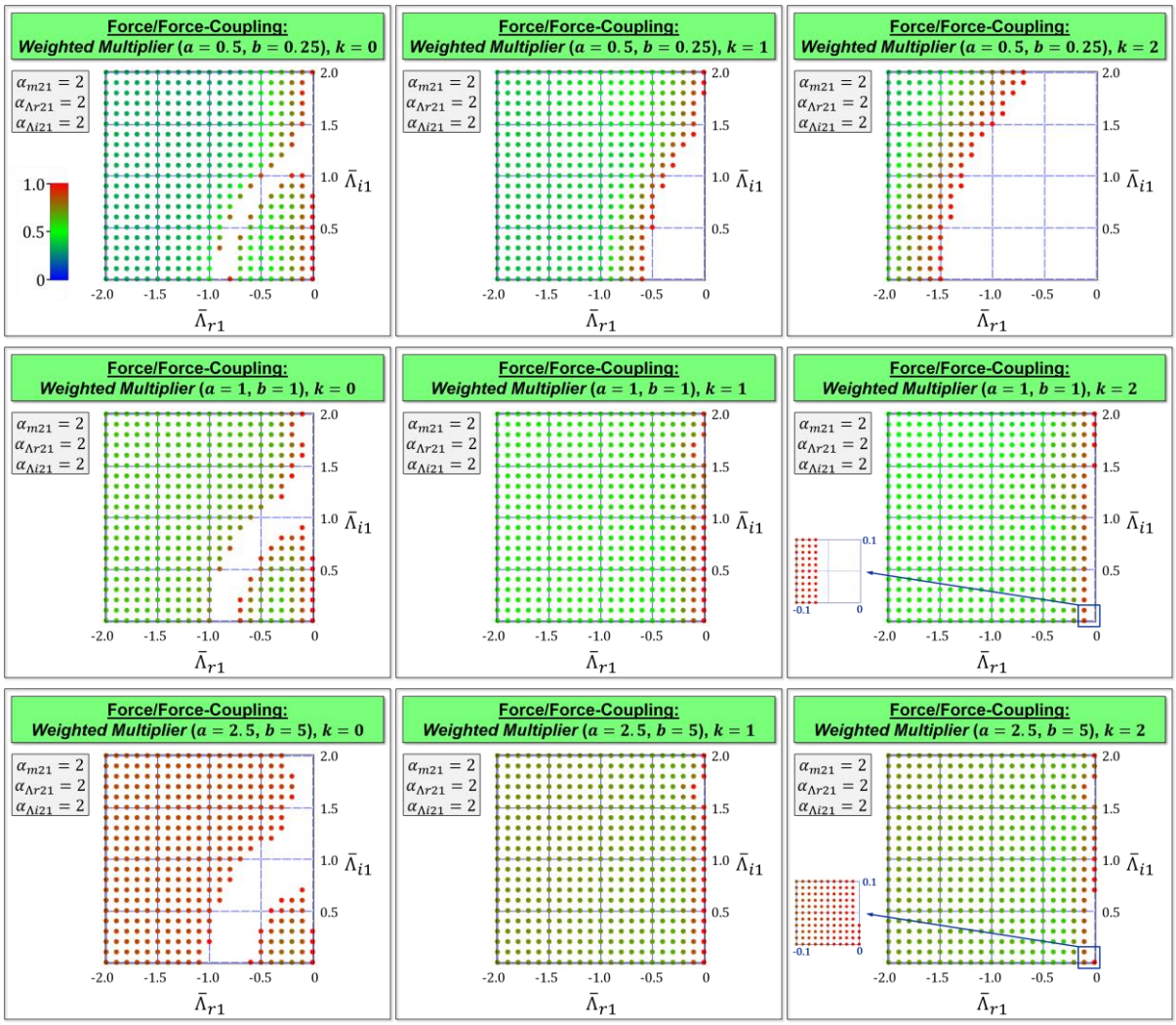

Figure A. 12 Stability plot for the implicit index-1 co-simulation method based on the weighted multiplier approach with force/force-decomposition (polynomial degrees $k = 0,1,2$): weighted multiplier parameters $a = 0.5, b = 0.25$; $a = b = 1$ and $a = 2.5, b = 5$.

Appendix G: Convergence Plots for Force/Force-Coupling

G.1 Implicit Co-Simulation Method based on Baumgarte Stabilization (Index-1, Index-2 and Index-3)

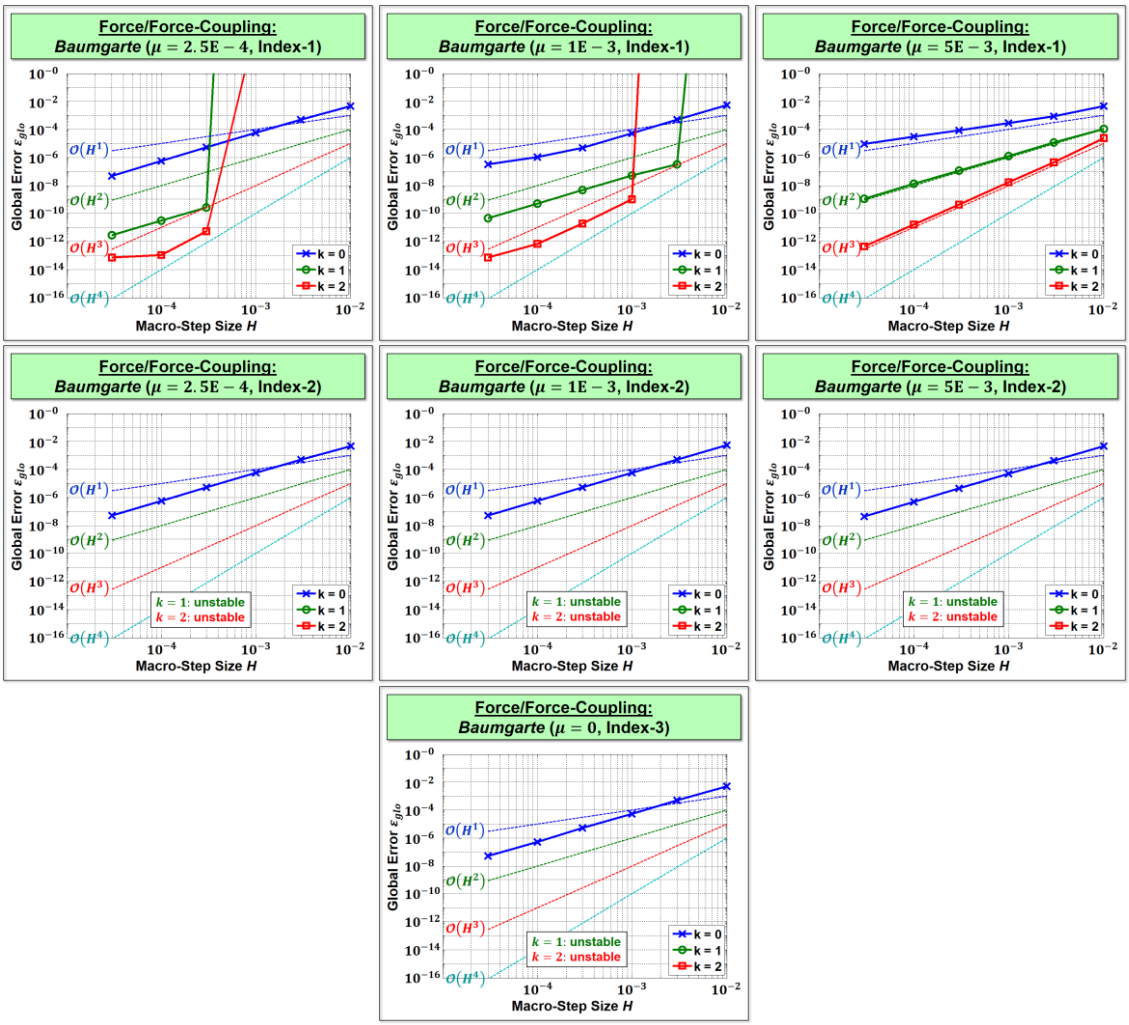

Figure A. 13 Convergence plots for the implicit co-simulation method based on Baumgarte stabilization (index-1, index-2 and index-3) using force/force-decomposition: Baumgarte parameters $\mu = 2.5E-4$, $\mu = 1E-3$ and $\mu = 5E-3$.

G.2 Implicit Co-Simulation Method based on Weighted Multiplier Approach (Index-1 and Index-2)

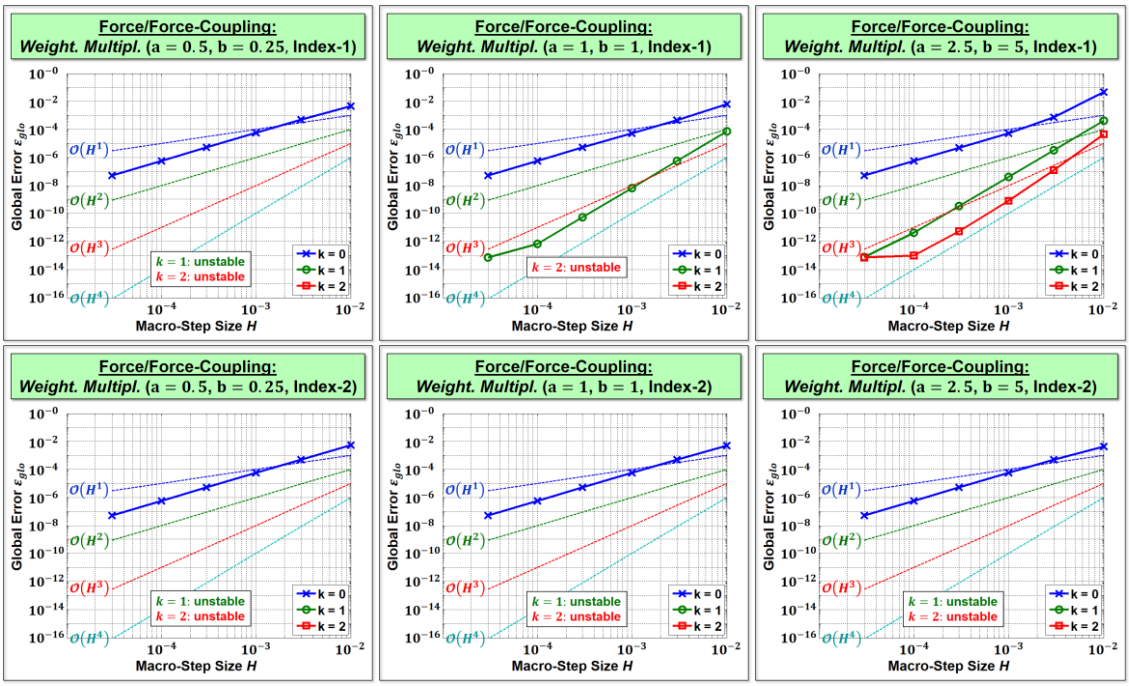

Figure A. 14 Convergence plots for the implicit co-simulation method based on the weighted multiplier approach (index-1 and index-2) using force/force-decomposition: weighted multiplier parameters $a = 0.5, b = 0.25$; $a = b = 1$ and $a = 0.25, b = 0.5$.

G.3 Implicit Co-Simulation Method based on Projection Technique

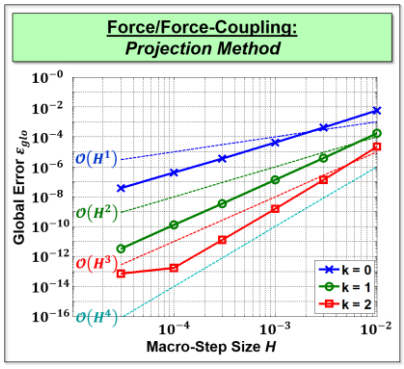

Figure A. 15 Convergence plots for the implicit co-simulation method based on the projection technique using force/force-decomposition.

Bibliography

[1] J. Ambrósio, J. Pombo, P. Antunes, and M. Pereira, “PantoCat statement of method”, *Vehicle System Dynamics,* vol. 53, pp. 314-328, 2015.

[2] J. Ambrósio, J. Pombo, M. Pereira, P. Antunes, and A. Mósca, “A computational procedure for the dynamic analysis of the catenary-pantograph interaction in high-speed trains”, *Journal of Theoretical and Applied Mechanics,* vol. 50, pp. 681-699, 2012.

[3] J. Ambrósio, J. Pombo, F. Rauter, and M. Pereira, “A Memory Based Communication in the Co-simulation of Multibody and Finite Element Codes for Pantograph-Catenary Interaction Simulation”, in *Multibody Dynamics*. vol. 12, C. Bottasso, Ed., ed: Springer Netherlands, 2009.

[4] M. Arnold, “Multi-rate time integration for large scale multibody system models”, in *IUTAM Symposium on Multiscale Problems in Multibody System Contacts*, pp. 1-10, 2007.

[5] M. Arnold, “Numerical methods for simulation in applied dynamics”, in *Simulation Techniques for Applied Dynamics*, M. Arnold and W. Schiehlen, Eds., ed Vienna: Springer Vienna, 2009.

[6] M. Arnold, “Stability of Sequential Modular Time Integration Methods for Coupled Multibody System Models”, *Journal of Computational and Nonlinear Dynamics,* vol. 5, pp. 1-9, 2010.

[7] M. Arnold and O. Brüls, “Convergence of the generalized-α scheme for constrained mechanical systems”, *Multibody System Dynamics,* vol. 18, pp. 185-202, 2007.

[8] U. M. Ascher, H. Chin, L. R. Petzold, and S. Reich, “Stabilization of Constrained Mechanical Systems with DAEs and Invariant Manifolds”, *Mechanics of Structures and Machines,* vol. 23, pp. 135-157, 1995.

[9] U. M. Ascher and L. R. Petzold, “Stability of Computational Methods for Constrained Dynamics Systems”, *SIAM Journal on Scientific Computing,* vol. 14, pp. 95-120, 1993.

[10] O. A. Bauchau and A. Laulusa, “Review of Contemporary Approaches for Constraint Enforcement in Multibody Systems”, *Journal of Computational and Nonlinear Dynamics,* vol. 3, pp. 011005-011005, 2007.

[11] J. Baumgarte, “Stabilization of constraints and integrals of motion in dynamical systems”, *Computer Methods in Applied Mechanics and Engineering,* vol. 1, pp. 1-16, 1972.

[12] T. Belytschko and R. Mullen, “Stability of explicit-implicit mesh partitions in time integration”, *International Journal for Numerical Methods in Engineering,* vol. 12, pp. 1575-1586, 1978.

[13] M. Benedikt, “Control-oriented Aspects of Non-Iterative Co-Simulation”, *At-Automatisierungstechnik,* vol. 62, pp. 598-606, 2014.

[14] M. Benedikt and F. R. Holzinger, “Automated configuration for non-iterative co-simulation”, in *2016 17th International Conference on Thermal, Mechanical and Multi-Physics Simulation and Experiments in Microelectronics and Microsystems (EuroSimE)*, pp. 1-7, 2016.

[15] M. Benedikt, G. Stettinger, and M. Horn, “Sliding mode control for constraint stabilization in multi-body system dynamic analysis”, in *Control Applications (CCA), 2014 IEEE Conference on*, pp. 1557-1562, 2014.

[16] M. Benedikt, D. Watzenig, and A. Hofer, “Modelling and analysis of the non-iterative coupling process for co-simulation”, *Mathematical and Computer Modelling of Dynamical Systems,* vol. 19, pp. 451-470, 2013.

[17] M. Benedikt, J. Zehetner, D. Watzenig, and J. Bernasch, “Moderne Kopplungsmethoden Ist Co-Simulation beherrschbar?”, *NAFEMS Magazin,* vol. 2, pp. 63-74, 2012.

[18] K. E. Brenan, S. L. Campbell, and L. R. Petzold, “Numerical Solution of Initial-Value Problems in Differential-Algebraic Equations”: SIAM, 1995.

[19] O. Brüls and M. Arnold, “The Generalized-α Scheme as a Linear Multistep Integrator: Toward a General Mechatronic Simulator”, *Journal of Computational and Nonlinear Dynamics,* vol. 3, pp. 041007-041007, 2008.

[20] M. Busch and B. Schweizer, “Coupled simulation of multibody and finite element systems: an efficient and robust semi-implicit coupling approach”, *Archive of Applied Mechanics,* vol. 82, pp. 723-741, 2012.

[21] M. Busch and B. Schweizer, “Stability of co-simulation methods using hermite and lagrange approximation techniques”, *Proceedings of ECCOMAS Thematic Conference on Multibody Dynamics, Brussels,* pp. 1-10, 2011.

[22] V. Carstens, R. Kemme, and S. Schmitt, “Coupled simulation of flow-structure interaction in turbomachinery”, *Aerospace Science and Technology,* vol. 7, pp. 298-306, 2003.

[23] K. Chadaj, P. Malczyk, and J. Frączek, “A parallel Hamiltonian formulation for forward dynamics of closed-loop multibody systems”, *Multibody System Dynamics,* vol. 39, pp. 51-77, 2016.

[24] J. Chung and G. M. Hulbert, “A Time Integration Algorithm for Structural Dynamics With Improved Numerical Dissipation: The Generalized-α Method”, *Journal of Applied Mechanics,* vol. 60, pp. 371-375, 1993.

[25] W. J. T. Daniel, “Analysis and implementation of a new constant acceleration subcycling algorithm”, *International Journal for Numerical Methods in Engineering,* vol. 40, pp. 2841-2855, 1997.

[26] W. J. T. Daniel, “A study of the stability of subcycling algorithms in structural dynamics”, *Computer Methods in Applied Mechanics and Engineering,* vol. 156, pp. 1-13, 1998.

[27] W. J. T. Daniel, “Subcycling first- and second-order generalizations of the trapezoidal rule”, *International Journal for Numerical Methods in Engineering,* vol. 42, pp. 1091-1119, 1998.

[28] M. Datar, I. Stanciulescu, and D. Negrut, “A co-simulation environment for high-fidelity virtual prototyping of vehicle systems”, *International Journal of Vehicle Systems Modelling and Testing,* vol. 7, pp. 54-72, 2012.

[29] M. Dörfel and B. Simeon, “Analysis and Acceleration of a Fluid-Structure Interaction Coupling Scheme”, in *Numerical Mathematics and Advanced Applications 2009*, G. Kreiss, P. Lötstedt, A. Målqvist, and M. Neytcheva, Eds., ed: Springer Berlin Heidelberg, 2010.

[30] E. Eich, “Convergence Results for a Coordinate Projection Method Applied to Mechanical Systems with Algebraic Constraints”, *SIAM Journal on Numerical Analysis,* vol. 30, pp. 1467-1482, 1993.

[31] C. Farhat and M. Lesoinne, “Two efficient staggered algorithms for the serial and parallel solution of three-dimensional nonlinear transient aeroelastic problems”, *Computer Methods in Applied Mechanics and Engineering,* vol. 182, pp. 499-515, 2000.

[32] C. Farhat and F.-X. Roux, “A method of finite element tearing and interconnecting and its parallel solution algorithm”, *International Journal for Numerical Methods in Engineering,* vol. 32, pp. 1205-1227, 1991.

[33] R. Featherstone, “A Divide-and-Conquer Articulated-Body Algorithm for Parallel O(log(n)) Calculation of Rigid-Body Dynamics. Part 1: Basic Algorithm”, *The International Journal of Robotics Research,* vol. 18, pp. 867-875, 1999.

[34] R. Featherstone, “A Divide-and-Conquer Articulated-Body Algorithm for Parallel O(log(n)) Calculation of Rigid-Body Dynamics. Part 2: Trees, Loops, and Accuracy”, *The International Journal of Robotics Research,* vol. 18, pp. 876-892, 1999.

[35] C. A. Felippa, K. Park, and C. Farhat, “Partitioned analysis of coupled mechanical systems”, *Computer methods in applied mechanics and engineering,* vol. 190, pp. 3247-3270, 2001.

[36] P. Fisette, O. Brüls, and J. Swevers, “Multiphysics modeling of mechatronic multibody systems”, *Proceedings of ISMA 2006,* pp. 41-68, 2006.

[37] M. Friedrich, “Parallel Co-Simulation for Mechatronic Systems”, PhD Thesis, Technische Universität München, 2011.

[38] C. Führer and B. J. Leimkuhler, “Numerical solution of differential-algebraic equations for constrained mechanical motion”, *Numerische Mathematik,* vol. 59, pp. 55-69, 1991.

[39] M. J. Gander, “50 Years of Time Parallel Time Integration”, in *Multiple Shooting and Time Domain Decomposition Methods*, T. Carraro, M. Geiger, S. Körkel, and R. Rannacher, Eds., ed: Springer International Publishing, 2015.

[40] C. W. Gear, “Differential-Algebraic Equation Index Transformations”, *SIAM Journal on Scientific and Statistical Computing,* vol. 9, pp. 39-47, 1988.

[41] C. W. Gear, B. Leimkuhler, and G. K. Gupta, “Automatic integration of Euler-Lagrange equations with constraints”, *Journal of Computational and Applied Mathematics,* vol. 12–13, pp. 77-90, 1985.

[42] C. W. Gear and D. R. Wells, “Multirate linear multistep methods”, *BIT Numerical Mathematics,* vol. 24, pp. 484-502, 1984.

[43] A. Gravouil and A. Combescure, “Multi-time-step explicit–implicit method for non-linear structural dynamics”, *International Journal for Numerical Methods in Engineering,* vol. 50, pp. 199-225, 2001.

[44] A. Gravouil, A. Combescure, and M. Brun, “Heterogeneous asynchronous time integrators for computational structural dynamics”, *International Journal for Numerical Methods in Engineering,* vol. 102, pp. 202-232, 2015.

[45] B. Gu, “Co-simulation of algebraically coupled dynamic subsystems”, PhD Thesis, Massachusetts Institute of Technology., 2001.

[46] B. Gu and H. H. Asada, “Co-simulation of algebraically coupled dynamic subsystems without disclosure of proprietary subsystem models”, *Journal of Dynamic Systems Measurement and Control-Transactions of the Asme,* vol. 126, pp. 1-13, 2004.

[47] G. Hippmann, M. Arnold, and M. Schittenhelm, “Efficient simulation of bush and roller chain drives”, in *Proceedings of ECCOMAS Thematic Conference on Advances in Computational Multibody Dynamics, Madrid*, pp. 1-18, 2005.

[48] R. Kubler and W. Schiehlen, “Modular simulation in multibody system dynamics”, *Multibody System Dynamics,* vol. 4, pp. 107-127, 2000.

[49] R. Kübler and W. Schiehlen, “Two methods of simulator coupling”, *Mathematical and Computer Modelling of Dynamical Systems,* vol. 6, pp. 93-113, 2000.

[50] J. J. Laflin, K. S. Anderson, I. M. Khan, and M. Poursina, “Advances in the Application of the Divide-and-Conquer Algorithm to Multibody System Dynamics”, *Journal of Computational and Nonlinear Dynamics,* vol. 9, pp. 041003-041003, 2014.

[51] E. Lelarasmee, A. E. Ruehli, and A. L. Sangiovanni-Vincentelli, “The Waveform Relaxation Method for Time-Domain Analysis of Large Scale Integrated Circuits”, *IEEE*

Transactions on Computer-Aided Design of Integrated Circuits and Systems, vol. 1, pp. 131-145, 1982.

[52] C. Lubich, “Extrapolation integrators for constrained multibody systems”, *IMPACT of Computing in Science and Engineering,* vol. 3, pp. 213-234, 1991.

[53] P. Malczyk and J. Fraczek, “A divide and conquer algorithm for constrained multibody system dynamics based on augmented Lagrangian method with projections-based error correction”, *Nonlinear Dynamics,* vol. 70, pp. 871-889, 2012.

[54] F. Marques, A. P. Souto, and P. Flores, “On the constraints violation in forward dynamics of multibody systems”, *Multibody System Dynamics,* pp. 1-35, 2016.

[55] P. Masarati, “Adding kinematic constraints to purely differential dynamics”, *Computational Mechanics,* vol. 47, pp. 187-203, 2010.

[56] P. Masarati, “Constraint Stabilization of Mechanical Systems in Ordinary Differential Equations Form”, *Proceedings of the Institution of Mechanical Engineers, Part K: Journal of Multi-body Dynamics,* vol. 225, pp. 12-33, 2011.

[57] S. Meynen, J. Mayer, and M. Schäfer, “Coupling algorithms for the numerical simulation of fluid-structure-interaction problems”, in *ECCOMAS 2000: European Congress on Computational Methods in Applied Sciences and Engineering*, pp. 11-14, September 11 - September 14, Barcelona, Spain, 2000.

[58] J. Miao, P. Zhu, G. Shi, and G. Chen, “Study on sub-cycling algorithm for flexible multi-body system—integral theory and implementation flow chart”, *Computational Mechanics,* vol. 41, pp. 257-268, 2008.

[59] J. Miao, P. Zhu, G. Shi, and G. Chen, “Study on sub-cycling algorithm for flexible multi-body system: stability analysis and numerical examples”, *Computational Mechanics,* vol. 41, pp. 269-277, 2008.

[60] Modelica Association. (2016). Available: https://www.modelica.org/

[61] D. Negrut, D. Melanz, H. Mazhar, D. Lamb, P. Jayakumar, and M. Letherwood, “Investigating through simulation the mobility of light tracked vehicles operating on discrete granular terrain”, *SAE Int. J. Passeng. Cars - Mech. Syst.,* vol. 6, pp. 369-381, 2013.

[62] J. Nievergelt, “Parallel methods for integrating ordinary differential equations”, *Commun. ACM,* vol. 7, pp. 731-733, 1964.

[63] G. Nowald, A. Boyaci, R. Schmoll, P. Koutsovasilis, and B. Schweizer, “Influence of Circumferential Grooves on the Non-Linear Oscillations of Turbocharger Rotors in Floating Ring Bearings”, presented at the 2015 IFToMM World Congress, Taipei, 2015.

[64] G. S. Ryu, “Integration of heterogeneous simulation models for network-distributed simulation”, PhD Thesis, The University of Michigan, 2009.

[65] T. Schierz and M. Arnold, “Stabilized overlapping modular time integration of coupled differential-algebraic equations”, *Applied Numerical Mathematics,* vol. 62, pp. 1491-1502, 2012.

[66] R. Schmoll, “Co-Simulation und Solverkopplung : Analyse komplexer multiphysikalischer Systeme”, in *Berichte des Instituts für Mechanik* vol. 2015,3, ed. Kassel: Kassel Univ. Press, 2015.

[67] R. Schmoll and B. Schweizer, “Convergence Study of Explicit Co-Simulation Approaches with Respect to Subsystem Solver Settings”, *PAMM,* vol. 12, pp. 81-82, 2012.

[68] S. Schoeps, H. De Gersem, and A. Bartel, “A Cosimulation Framework for Multirate Time Integration of Field/Circuit Coupled Problems”, *IEEE Transactions on Magnetics,* vol. 46, pp. 3233-3236, 2010.

[69] B. Schweizer and P. Li, “Solving Differential-Algebraic Equation Systems: Alternative Index-2 and Index-1 Approaches for Constrained Mechanical Systems”, *Journal of Computational and Nonlinear Dynamics,* vol. 11, pp. 044501-044501, 2015.

[70] B. Schweizer, P. Li, and D. Lu, “Explicit and Implicit Cosimulation Methods: Stability and Convergence Analysis for Different Solver Coupling Approaches”, *Journal of Computational and Nonlinear Dynamics,* vol. 10, pp. 051007-051007, 2015.

[71] B. Schweizer, P. Li, and D. Lu, “Implicit co-simulation methods: Stability and convergence analysis for solver coupling approaches with algebraic constraints”, *Journal of Applied Mathematics and Mechanics,* vol. 96, pp. 986-1012, 2015.

[72] B. Schweizer and D. Lu, “Predictor/corrector co-simulation approaches for solver coupling with algebraic constraints”, *Journal of Applied Mathematics and Mechanics,* vol. 95, pp. 911-938, 2014.

[73] B. Schweizer and D. Lu, “Semi-implicit co-simulation approach for solver coupling”, *Archive of Applied Mechanics,* vol. 86, pp. 1739-1769, 2014.

[74] B. Schweizer and D. Lu, “Stabilized index-2 co-simulation approach for solver coupling with algebraic constraints”, *Multibody System Dynamics,* vol. 34, pp. 129-161, 2014.

[75] A. A. Shabana, “Dynamics of multibody systems”: Cambridge university press, 2013.

[76] A. A. Shabana, O. A. Bauchau, and G. M. Hulbert, “Integration of Large Deformation Finite Element and Multibody System Algorithms”, *Journal of Computational and Nonlinear Dynamics,* vol. 2, pp. 351-359, 2007.

[77] S. A. Sicklinger, “Stabilized Co-Simulation of Coupled Problems Including Fields and Signals”, PhD Thesis, Technische Universität München, München, 2014.

[78] B. Simeon, “Computational flexible multibody dynamics”, in *A Differential-Algebraic Approach. Differential-Algebraic Equations Forum. Springer, Heidelberg*, 2013.

[79] B. Simeon, “Numerical Analysis of Flexible Multibody Systems”, *Multibody System Dynamics,* vol. 6, pp. 305-325, 2001.

[80] G. Stettinger, M. Horn, M. Benedikt, and J. Zehetner, “Model-based coupling approach for non-iterative real-time co-simulation”, in *Control Conference (ECC), 2014 European*, pp. 2084-2089, 2014.

[81] P. Tomulik and J. Fraczek, “Simulation of multibody systems with the use of coupling techniques: a case study”, *Multibody System Dynamics,* vol. 25, pp. 145-165, 2011.

[82] F. C. Tseng and G. M. Hulbert, “A gluing algorithm for network-distributed multibody dynamics simulation”, *Multibody System Dynamics,* vol. 6, pp. 377-396, 2001.

[83] L. Völker, “Untersuchung des Kommunikationsintervalls bei der gekoppelten Simulation”, PhD Thesis, Karlsruher Institut für Technologie, 2011.

[84] J. Wang, C. M. Gosselin, and L. Cheng, “Modeling and simulation of robotic systems with closed kinematic chains using the virtual spring approach”, *Multibody System Dynamics,* vol. 7, pp. 145-170, 2002.

[85] J. Z. Wang, Z. D. Ma, and G. M. Hulbert, “A gluing algorithm for distributed simulation of multibody systems”, *Nonlinear Dynamics,* vol. 34, pp. 159-188, 2003.

[86] T. Wang, “Development of Co-Simulation Environment and Mapping Algorithms”, PhD Thesis, Technische Universität München, 2016.

[87] G. Wanner and E. Hairer, “Solving ordinary differential equations II: Stiff and Differential-Algebraic Problems”, 2nd ed. Berlin: Springer, 1991.

[88] C. Woernle, “Mehrkörpersysteme: Eine Einführung in die Kinematik und Dynamik von Systemen starrer Körper”: Springer-Verlag, 2011.